Designing, Building, and Testing the Spin, Strip, and Stomp Mechanism for Pharmaceutical Tableting

by

Shahd Hassan Labib

B.S. Mechanical Engineering, The American University in Cairo (2015)

Submitted to the Department of Mechanical on May 19, 2017 in partial fulfillment of the requirements for the degree of

Master of Science in Mechanical Engineering

at the

MASSACHUSETTS INSTITUTE OF TECHNOLOGY

May 2017 [June 2017]

Author .... Signature redacted .....
Department of Mechanical Engineering
May 19, 2017

Certified by Signature redacted .....
Alexander Slocum
Pappalardo Professor of Mechanical Engineering
Thesis Supervisor

Accepted by..... Signature redacted ....
Rohan Abeyaratne
Quentin Berg Professor of Mechanical Engineering
Graduate Officer

[Left Blank]

Designing, Building, and Testing the Spin, Strip, and Stomp Mechanism for Pharmaceutical Tableting

by

Shahd Hassan Labib

Submitted to the Department of Mechanical Engineering
on May 19, 2017 in partial fulfillment of the requirements
for the degree of Master Science in Mechanical Engineering

Abstract

Nanofiber fabrication of pharmaceutical pills creates significant advantages over conventional techniques such as shorter pill dissolution times, airborne drug particulate matter elimination, and shorter liquid drying time, among many others. Therefore, the Novartis MIT Center for Continuous Manufacturing is prioritizing development of electrospinning techniques for producing nanofibrous pills. However, electrospinning pills still has a very low production rate compared to that of the current pharmaceutical techniques. Motivated by the need for an efficient and effective elecrospinning technique, we developed the "Spin, Strip, and Stomp Mechanism." This technique has successfully made pills of the required quality, designed with the goal of reducing the gap between the low production rates of nanofibrous pills and the high rates of the current pill making techniques.

Thesis Supervisor: Alexander Slocum

Title: Pappalardo Professor of Mechanical Engineering

Acknowledgements

Working on this thesis at MIT for the past two years has been the most enlightening, challenging, and rewarding period of my life that I would not have survived without my people. Mom and dad, thank you for supporting me endlessly, believing in me, and sending me overseas to get the education that I have always dreamt of. Prof. Slocum, the world's greatest role model, thank you for not only being my mentor, but my dad, my friend, and my sports buddy. I have not just learnt from you endless machine design skills, but I have learnt how the greatest people are the most humble, how any serious work could be a lot of fun, how ideal people function for this word to be a better place. Prof. Rutledge, thank you for giving me the opportunity to work on this project and the courage to dive deep into the chemical engineering field. Prof. Ghoneim, thank you for giving me the first opportunity of coming to MIT in 2014, and supporting me in following my bigger dreams of applying and coming back to MIT. Rana El Kahwagy, thank you for being my home away from home, my sister, my best friend, and my whole family here, I could not imagine my MIT experience without your support from day one. Thank you for listening to all my challenges in and out of school, believing that I could do it, proof-reading most of my work, and even teaching me how to adult and run my own house. Nour El Raghy, I am blessed to have had you as my best friend during my MIT journey, thank you for the support in growing the MIT Belly Dancing Club, and for always making my tough days at work a hundred times happier. Eddy, Qasim, Radwan, and Chika, thank you for being such great friends and for always being there for me during my time at MIT.

Table of Contents

List of Figures

List of Tables

List of Variables

Variable	Unit	Description
F_{sl}	N	Sliding force of the rod collector
T_{sl}	N.m	Torque of the driving motor
R_{py}	m	Radius of the belt's pulley
$M_{tipping}$	N.m	Stand's tipping moment
H_{rod}	m	Height of rod collector above the ground
k	N/m	Stiffness
E	N/m2	Modulus of elasticity
I	m4	Moment of inertia
L	m	Length of the beam
F	N	Applied force
K_s	N/m	Axial rigidity of screw shaft
K_N	N/m	Axial rigidity of nut
K_b	N/m	Axial rigidity of support bearing
K_H	N/m	Acial rigidity of support housing
w_n	rad/s	natural frequency
m	kg	mass
W_{sl}	N	Weight of sliding parts
F_{poly}	N	The frictional force between the polymer and the rod
F_{str}	N	Force by the strippers on the rod
μ_{slb}	unitless	Sliding bearings' coefficient of friction
☹	Sadness	Regular Setup
☺	Happiness	Flipped Setup
T_{sp}	N.m	Spinning torque needed to spin the polymer rod
F_{sp}	N	Spinning force required to spin the polymer rod
R_{driven}	m	Radius of driven gear
W_{gr}	N	Weight of drivern gears
W_{rod}	N	Weight of the rod collector
W_{cp}	N	Weight of rod collector coupling
W_{poly}	N	Weight of the polymer collected
σ	N/m2	Stress
A	m2	Applied area
D	m	Diameter
L_{cavity}	m	Length of the die cavity
L_{pr}	m	Length of polymer collected on the rod
L_{punch}	m	Length of the punch
L_{eject}	m	Additional length that the punch travels beyond the cavity

		to eject the pill
$L_{piston.cavity}$	m	Distance between the piston and the cavity
L_{gap}	m	Distance between punch and die cavity
$L_{press\ total}$	m	Total vertical length of the press assembly
L_{piston}	m	Length of the press's piston
$L_{side\ supports}$	m	Length of the side supports
$L_{strippers}$	m	Length of the strippers' assembly
y	rpm	Spinneret motor's rpm
x	V	Spinneret motor's applied voltage

Chapter One: Introduction

"My interest is the problems that people say it is hard & can't be done, I say Oh! Opportunity!"
Alexander Slocum

1.1 Motivation

Since the development of the pharmaceutical industry in the mid-1800s in Germany [long history paper reference] up through the mid-1900s, long drug development timelines and relatively few varieties of drugs allowed manufacturers to create set manufacturing processes. Now, in stark contrast, with many new and unique drugs discovered daily, pharmaceutical manufacturers must upgrade their traditional facilities' layout to agile layouts, which accommodate large spectrums of formulations and batch sizes. This agile layout is known as "continuous manufacturing". Current pharmaceutical research, including the MIT Novartis Center of Continuous Manufacturing, is thus concerned with re-designing current pharmaceutical machinery and changing it from "batch" to "continuous" manufacturing. Continuous manufacturing is easer to scale up, more consistent, and more reproducible than batch processing [1].

1.2 Prior Art

The current technologies on the mechanical design side are the rotary tablet presses and the hot melt extrusion systems. The rotary tablet presses have a very high throughput, but they have many challenges as the tablets stickiness on the punch and lack of flexibility in changing the drug ingredients. It is thus hard to adapt the rotary tableting mechanism in a continuous manufacturing layout. The second technology, the hot melt extrusion, can be better integrated into a continuous manufacturing system, but it has different challenges such as high temperature requirements among others.

On the chemical design side, electrospinning was initiated using the needle technology, but it had a very low throughput. Many other technologies were patented afterwards, like the multiple needle, ferromagnetic, and bubble electrospinning [2, 3, 4, 5, 6]. Also many different spinneret shapes were experimented with higher productivities, like the wire and the stepped pyramid spinnerets [7, 8].

1.3 Current Work

This work is about the novel machine designed here at the MIT Novartis Center, the "Spin Strip and Stomp" unique tableting mechanism. This machine is not just part of the continuous manufacturing system, but it is a solution to various problems in current machinery. Some of its numerous advantages are making pills with shorter dissolution times, reducing the number of processes to reach the final product, eliminating airborne drug particulate matter, and shortening the liquid drying time, among many others [9]. This mechanism is unique in its quick and smooth flow from the electrospinning processing to the tablet pressing. The free-surface electrospinning design by the Rutledge group [8] will be adapted to a mechanism that pulls the mixture and presses it into a tablet form with the least operations in between.

Chapter Two: Literature Review

"Think before you speak. Read before you think."
Fran Lebowitz

2.1 Tablet Pressing Background

2.1.1 Tablet Pressing History

The word "Drug" originally derives from the Dutch/German word "droog" which means "dry". This is because medicines were historically obtained from dry substances. Drug research started in Europe during the second half of the 19th century. It evolved after the development of chemistry, biology, and immunology. Also the development of transportation (coal locomotion) and communication (telephones) facilitated its growth. Germany and England took the lead in the drug industry. "Merck and Bayer" was the first pharmaceutical company in Germany; it was founded in 1863 [10].

The use of tablets was introduced in 1884 by Burroghs Wellcome, under the tabloid trademark. Before then, medicine was sold in liquid or powder forms. The first pharmaceutical factory was built by Beecham Group in 1859. The first pill-making machine was made by a physicist in Michigan in 1885. This machine allowed for precision, mixed dosage, and standardization of large-scale production. The first patent for the "process of making pills" was filed by William Erastus Upjohn. The patent number in the US was 312041A. He started a company called "Upjohn pill and granule Company", which is today called Pfizer [10].

2.1.2 Tablet Pressing Fundamentals

Tablets are the most common form of dosage because of their stability, ease of manufacture, convenience for patients, and flexible dosing [11, 12].
In addition to the tablet's active pharmaceutical ingredient (API), excipients are needed to bulk it, facilitate its compression, or modify its biopharmaceutical properties. According to Sinka, there are many types of excipients used for various purposes like [13]:

1- **Binders**: to assist granule and compact formation
2- **Disintegrants**: to assist the tablet breakdown in the body's fluids.
3- **Wetting agents**: to assist with the dissolution of hydrophobic APIs.
4- **Lubricants**: to reduce friction between powder and die.
5- **Glidants**: to assist with the powder flow.
6- **Fillers**: to provide controlled release of the API
7- **Anti-oxidants**: to stabilize the API chemically.

According to Rybski, the manufacturing process of the tablets consists of four main steps [14]:

1- **Weighing**: where the input materials are weighed.
2- **Mixing**: where there are three different mixing stations: dry-mix, wet-mix, and granulation.
3- **Compression**: where the granules and powders are pressed into tablet forms.
4- **Packaging**: where the tablets are blistered and packaged.

This thesis studies the third step in the manufacturing processes above, which is the tablet compression process. At this step, the API and the excipients are already mixed and ready for compression. Historically, tablets have been pressed using the rotary tablet press, seen in Figure 1 below.

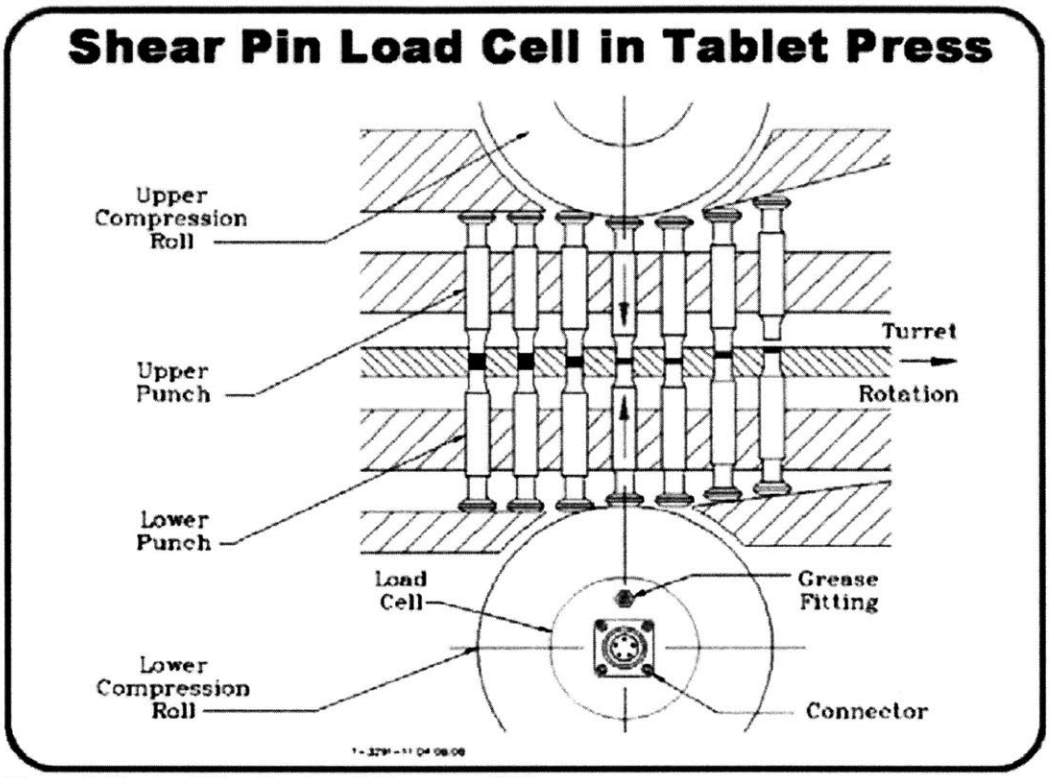

Figure 1: the traditional rotary tablet press [15]

As seen in Figure 1, the mixtures move from the left to the right side, the lower and upper compression rolls push the lower and upper punches towards each other to compress the powder mixture in between. The four main steps are: (1) the feed, (2) the pre-compression, (3) the main compression, and finally (4) the ejection [13].

Zooming into the contact area between the compression roll and the punch head, they would look as follows:

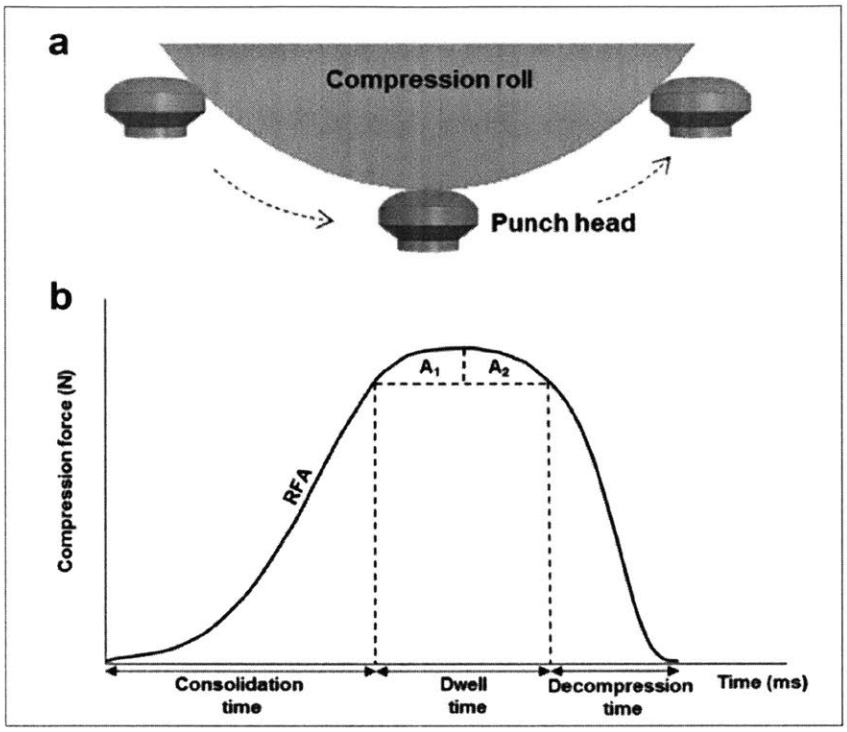

Figure 2: Schematic diagrams depicting the motion of punch head in relation with compression roll (a) and the graphical representation of compression profile with the associated compression parameters (b) [16, Figure 1].

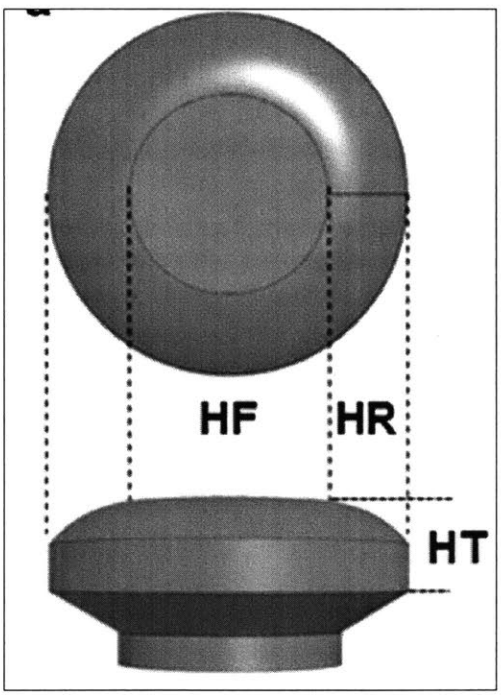

Figure 3: punch geometry with head flat (HF) and head radius (HR) [16, Figure 2].

The geometrical profile of the punch, shown in Figure 3, consists of the head flat (HF) and the head radius (HR). The head flat (HF) is the flat part of the punch, it makes contact with the compression roll and determines the dwell time. The head radius (HR) is the radius of the curved surface that blends middle section (HF) to the head thickness (HT), it allows for

smoother transition from the moving punch head to the compression cycle. The size of the compression roll affects the tablet pressing process by determining the rate and duration of applying the compression force [16].

The geometry of the punch determines the compression profile of the tablet, as seen in Figure 2. The compression profile is the variation of the compression force when the punch is in contact with the compression roll (contact time). It consists of three parts [16]:

1- **Consolidation time**: when the punch head starts to contact the mixture with an increasing compression force.
2- **Dwell time**: when the compression force is more than 90% of its peak value.
3- **Decompression time**: when the punch head starts moving away from the pressed mixture and the compression force decreases.

Other than the compression profile, the crucial machine settings were: (1) compression and pre-compresison forces, (2) press (turret) speed, (3) die feed frame speed, and (4) compression position in the die [16].

2.1.3 Tablet Pressing Parameters

The final properties of a tablet depend on the ingredients used, the mixing details, and the selection of pressing parameters [13, 17]. This work is primarily concerned with the pressing parameters, because they would need to be incorporated in the machine's design. The two main tablet properties are: the strength and the disintegration of the tablet. The pressing parameters give different internal density distributions [18]. These density distributions give different strengths and disintegrations. The lower the density, the lower the strength and the higher the disintegration and vice versa. The process is a compromise between the two main goals, which are having a tablet that has: (1) high strength for long shelf life, and (2) quick disintegration to release the API according to the patient's needs.

The mechanical strength is the pill's ability to resist breakdown and remain intact, while being soft enough for the API release [17]. The strength primarily depends on the pill's density. This density depends on two factors: the particle size, and the pressing parameters [19]. The particle size is determined in earlier manufacturing processes, but the pressing parameters could be controlled in this process. The higher the compression forces and the longer the dwell times give higher strength [16]. Having a head flat punch increases the dwell time and thus gives higher strength [16]. The compressing speed also affects the strength of the tablet [13]. The standard diameteral loading test is carried out to determine the tensile strength, but in the case of chewable tablets, the bending test is also needed [20].

On the other hand, when the compression force increases, the disintegration time increases [18,19]. The disintegration time also depends on the particle size distribution, internal density distribution, and the surface characteristics of the tablets [11,13,18]. The compression force causes a reduction in porosity, and thus a linear increase in disintegration time [11, 18].

2.1.4 Challenges in current tablet pressing mechanisms

The most common problem observed during the rotary tableting operation is the punch sticking. During the powder processing process, they come into contact with each other and with the wall of the equipment, so they become electrostatically charged, or in other words, "Triboelectrified". This causes loss of time and money because of stopping the machine, sorting, and disposing incomplete tablets. The selection of powders with fast charge decay kinetics and tight control of environmental conditions helps reduce punch sticking problems, but APIs get more electrostatically charged than tableting excipients, and they are the main component that cannot be replaced [12].

2.1.5 Other Tablet Compression Designs

The other major tablet manufacturing technique beside the rotary tablet press is the hot melt extrusion. Its eight process steps are: (1) weighing, (2) blending, (3) hot melt extrusion, (4) cooling, (5) cutting, (6) forming, (7) coating, and (8) packaging. The solid molecular dispersions are made by a melt blending process, where the API and the polymeric excipient are melted, mixed, discharged, and cooled to form tablets or capsules, as seen in Figure 4.

Some of its benefits are: (1) the absence of solvents, (2) fewer processing steps, (3) and low manufacturing cost compared to the standard tablet production methods. It is also seen as a great candidate for continuous manufacturing because it is very efficient for tamper resistant formulations [1].

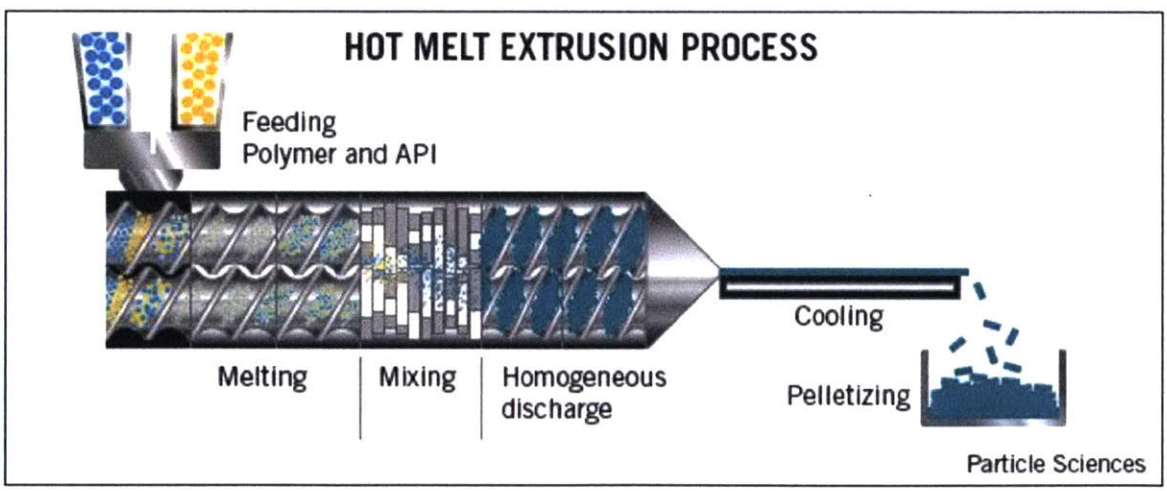

Figure 4: Hot melt extrusion process schematic [20, Figure 1].

2.2 Electrospinning Background

2.2.1 History

The phenomenon of electrospinning was first observed by William Gilbert in the 16th century. At that time, he found out that when water is bought close to electrically charged wood, water will form a cone shape, and then droplets will start being ejected from this cone's tip [21].

The second major step in electrospinning discovery was by the physicist Charles Vernon Boys. In 1888, Boys was designing a machine to measure the universal gravitational constant, and this machine apparatus needed a strong supporting fiber. He looked into existing fiber drawing techniques, and there were none at that time. So he designed his own setup where he was able to draw fibers from different melts to fulfill his experiment's requirements. At this time, he wrote the first worldwide paper describing the process of "nano-fiber manufacture" [21].

In 1902, The first patent in electrospinning was filed by William James Morton (US Patent 705691) under the name of "Method of Dispersing fluids". Some other major patents in the field is Formhals' 1934 and 1938 patents (US 1975504 A and US 2116942 A) with titles of "Process and Apparatus for preparing artificial threads" and "Method an Apparatus for the Production of fibers".

In 1964, Sir Geoffrey Ingram Taylor has worked on formulating the mathematical models for the shapes of the fluid droplets formed by electrical fields. This cone's shape is now known as a "Taylor cone" [21]. Afterwards, the electrospinning studies and its applications have grown exponentially starting with Reneker, Yarin, Wnek, Rutledge, and many others laying its fundamentals in the 1990s [22, 23, 24, 25, 26, 27].

2.2.2 Electrospinning Fundamentals

Electrospinning is the process of drawing fibers from a solution or melt phase to dry fibrous phase by electric forces. The process in controlled by "Electro-hydrodynamics"; which is the dynamics of electrically charged liquids. Firstly, velocity builds up under Coulomb drive, increasing the strain rate and building up stress. Secondly, viscoelastic relaxation reduces this stress, leaving more coulomb repulsion than viscoelastic drag forces. Thirdly, the motion of particles is dominated by the electric field, forming stretched jets pulled by this electric field's force minus the fluid's viscoelastic drag and surface tension [28]. This Taylor cone, discovered by Sir Geoffrey Taylor in 1964, looks as seen in the figure below:

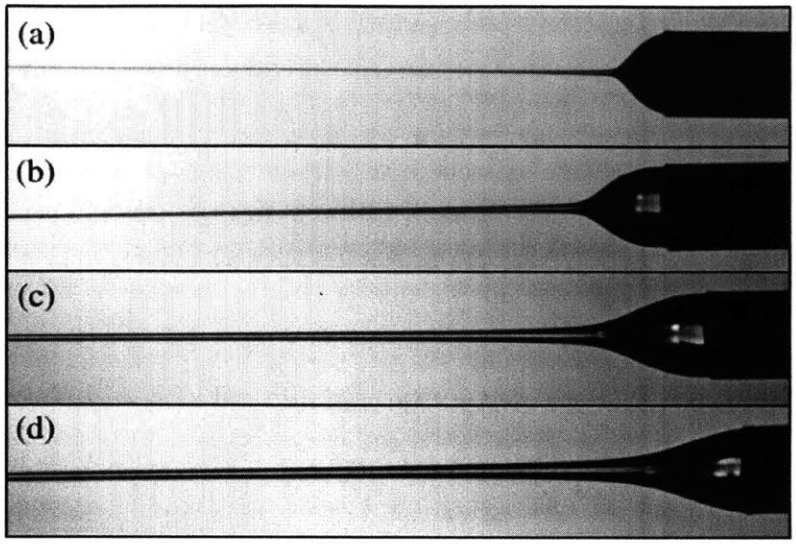

Figure 5: Taylor cones of polyethylene oxide at different flow rates [29, Figure 2].

The second phase in electrospinning is the instability phase; where the fibers experience bending and whipping due to the repulsive forces between them. The solvent evaporates leaving solid fibers due to the high surface area of the thinning jet. These fibers finally land on the grounded surface to form mats or other shapes and surfaces required [30].

In other words, if we want to sum up the electrospinning process in 5 points [29], these points will be:

1- Fluid Charging
2- Formation of the cone jet
3- Thinning of the study jet
4- Jet instabilities (caused by whipping)
5- Collection of fibers.

This process is similar to the well-known process of electro-spraying, but the main difference between them is that the jet breaks down into droplets in electro-spraying and micro or nano-fibers in electro-spinning. This is due to the fact that electro-spinning starts from a much more dilute solution than that of electrospraying, so the polymer solute stops the breaking out of jets into droplets[31].

2.2.3 Electrospinning Fluid Parameters

The first fluid parameter affecting the electrospinning process is *the* ***solution's concentration***. At a very low concentration, the result is beads not fibers due to insufficient entanglements [32]. While at the correct concentration, round fibers could be drawn from the solution. After exceeding a specific concentration, these rounds fibers turn into flat ribbons [32].

The second governing parameter is *the* ***solution's viscosity***. If it is too low, the fiber will not be continuous, and if it is too high, the jet shape will fail to eject. The spinning viscosities range from 1 to 215 poise, and the most successful range is between 1 and 20 poise according to Bhardwaj [34].

Thirdly, a high ***molecular weight*** is crucial to provide sufficient inter-chain connectivity and chain entanglements. Low molecular weight polymers are usually spun with a very low percentage of a high molecular weight polymer to engineer the desired shear thinning and reach the process's required elasticity [27]. The molecular weight dispersion together with the solution's concentration (parameter 1) will result in the process's required viscosity (parameter 2).

Fourthly, by reducing the ***surface tension***, the fibers can be obtained with no beads. Having surface tension does not have any strict requirements or preferred values, but it determines the required range of electro-spinning parameters like the needed voltage and spinneret collector distance [34].

Conductivity of the polymer solution is the fifth parameter that is determined from the polymer's type and the solvent used. High electrical conductivity was found to decrease the fibers' diameter, and low values resulted in beads due to unsufficient elongation (paper 13).

2.2.4 Electrospinning Process Parameters

The ***electric field*** is the driving force that moves the polymer solution from its source to the collecting surface. So the higher the electric field, the more the mass output. Since the equation of electric field is:

$$Electric\ Field = \frac{Voltage}{Distance}$$

Equation 1

Thus, either varying the voltage, the distance between the source and the collecting surface, or both, can change the electric field.

Figure 6 shows the relationship between ***voltage*** and percentage conversion of dope to nanofiber.

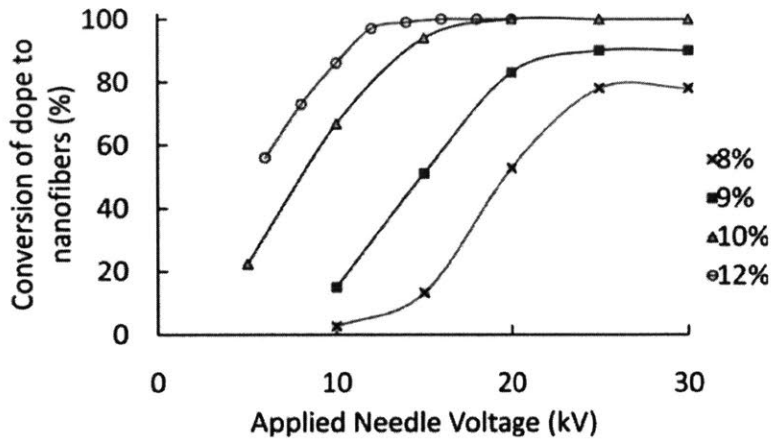

Figure 6: voltage versus fibers conversion rate [35, Figure 2].

According to this graph, the fiber conversion rate increases as the applied voltage increases until it reaches a certain point. After this point, the polymer dope has already had all the electrical driving force it needs to travel between its 2 points, so increasing the voltage more results in higher mass output in a certain time.

As stated in [34], researchers have argued whether higher voltage results in bigger or smaller fiber diameters, but the majority agreed that higher voltage would lead result in smaller diameter and quick evaporation [34]. Various setups give different relationships between voltage and mass output, so the direct relationship cannot be generalized, but it is certain that increasing the voltage increases the mass output.

Increasing the ***distance*** between the solution and the collecting surface results in a lower electric field and thus less fiber collected. Distance is also critical because if it is too close, the solvent would not have enough time to completely evaporate. Thus, the distance should be more than the minimal distance required for evaporation and less than the maximum distance that would result in the minimal electric field required.

Chakraborty's study on polycaprolactone (PCL) showed that the electrospinning process started at an ***electric field*** value of 0.3 kV/cm, then fiber diameter keeps decreasing until the field is 1.2 kV/cm. Higher electrical fields will add fiber size variability due to instabilities [31]. But we have to note that these specific electric field values are for the materials that Chakraborty tested in his specific setup, these values would differ from one study to the other according to the materials and surrounding conditions.

Operating ***temperature*** is another important factor because as the temperature increases, the viscosity decreases, and thus the fiber diameter decreases [34].

The last parameter to be discussed is the operating ***humidity***. At low humidity values, the volatile solvent will dry up very quickly [34]. Higher humidity will help

discharge the polymer until the acceptable humidity range is exceeded. Then higher values will result in larger fiber diameters and low evaporation rates (12).

2.3 Electrospinning Setups

There are various configurations for electrospinning, they all have the same general components that could be run at many setups.

2.3.1 Electrospinning setup components

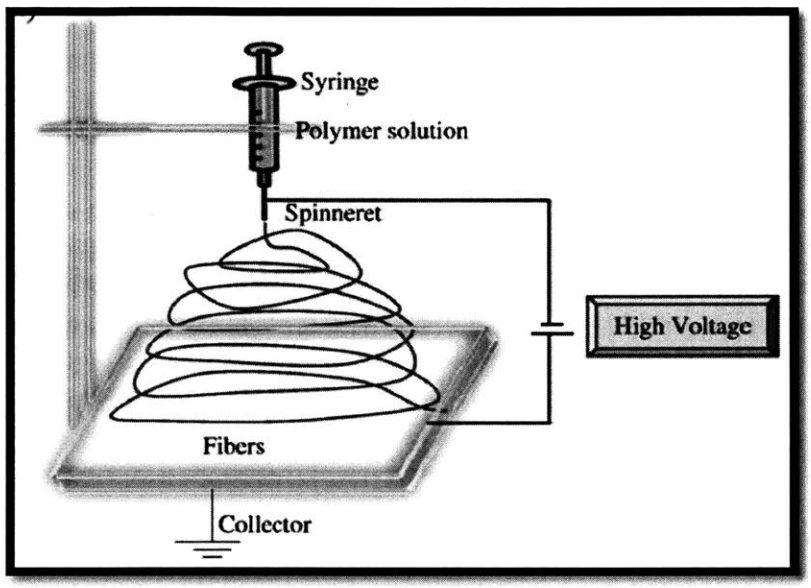

Figure 7: schematic diagram of the electrospinning setup [34, Figure 1]

The schematic shown above highlights the 3 basic components of the electrospinning setup. These 3 components are:

1) ***High voltage Source***: the big gap in electrical potential between the 2 points is the driving force that pulls the polymer from the solution to the fiber form.

2) ***Spinneret***: this is the source of the fiber jets, and where the polymer solution starts forming Taylor cones and becomes fibers. Spinnerets exist in many different forms. The most basic form is the syringe shown above for the original needle electrospinning, but many other designs will be discussed later.

3) ***Collector***: this is the medium where the fibers are collected. It may be in the form of fiber mats or many other shapes. It is usually grounded so that the fibers will gets attracted to it because it is the lowest potential in the area.

2.3.2 Latest Innovations in Electrospinning setups

The basic electrospinning technique is the needle setup shown in the previous section. However, this single needle setup has a very low productivity rate and some

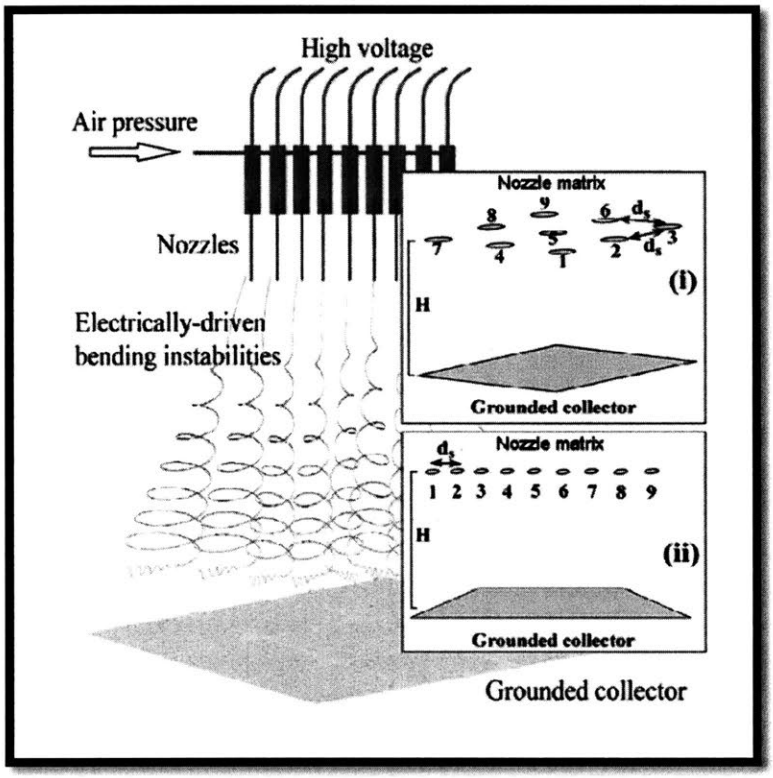

other restrictions. A lot of research has been done on more creative setups as using the multiple jets, pressured tubes and pyramid spinnerets, or performing coaxial, alternating current, melt, and bubble electrospinning.

Figure 8: chematic Diagram for multiple nozzle electrospinning (i) nozzles are in a 3x3 matrix (ii) nozzles are in a 9x1 matrix [2, Figure 1]

Theron has analyzed the multi-nozzle electrospinning shown in Figure 8 above. These multi-nozzles can be organized in different matrices as shown in the figure in order to increase the electrospinning rate or make multi-component blends of nano-fibrous mats. The main drawback of this technique is the repulsion between nozzles. But Theron's studies showed that the inter-nozzle distance should be at least 1 cm and studied repulsion patterns of different configurations [31].

Llorens studied co-axial electrospinning, which could be classified as a branch of the Theron's multi-nozzle electrospinning using only 2 nozzles. where an outer nozzle forms the shell while the inner nozzle forms the core. Physiochemical reactions, flow rates, concentrations, and hydrophilic-hydrophobic properties are coordinated to reach the required encapsulation [3].

Balogh tried out another setup using alternating current rather than direct current voltage source. He has prepared some poorly water-soluble drug (carvedilol), and claimed that using 25 kV AC rather than DC increased the specific productivity and double the average thickness of the fibers [4].

Nagy has worked on solvent free melt electrospinning, which combines the advantages of solvent free and solution electrospinning. It was made for chemicals that have low solubility and cannot be spun in solution form. Its main advantages are having 100% yield, being safer than organic solvent based solutions, avoiding solvent explosion, solvent residuals in fiber, and expensive solvent recovery. Its disadvantages is having a much bigger fiber size (250 compared to 0.7 micrometers) and high operating temperature (around 150 degrees Celsius) [5].

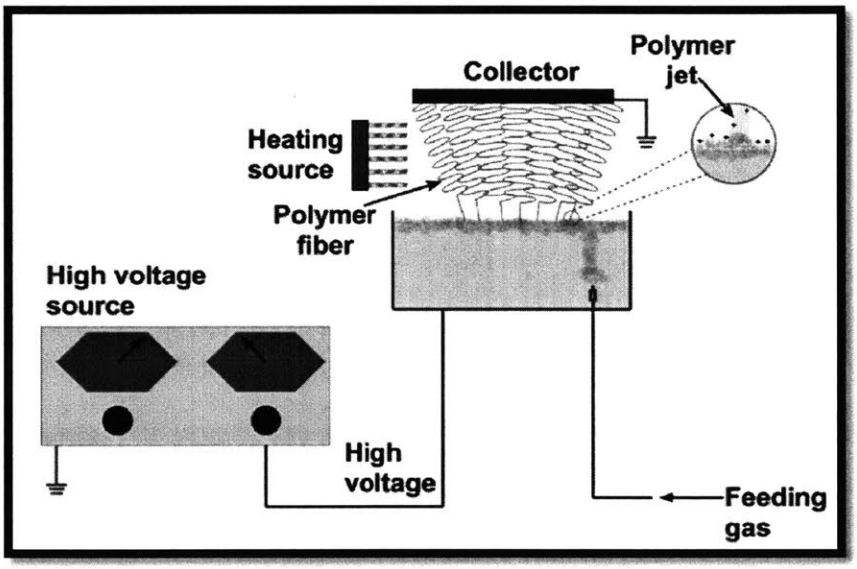

Figure 9: schematic diagram for the bubble electrospinning setup [7, Figure 3]

Another interesting setup is the bubble electrospinning. Navarro has carried out this analysis by placing an electrode inside the polymer solution and a gas tube feeding the reservoir from the bottom. Some polymer like Polyvinylidene fluoride (PVDF) would spin at higher speeds in this setup. Its regular spinning is too slow due to its insolubility and highly hydrophobic nature [7].

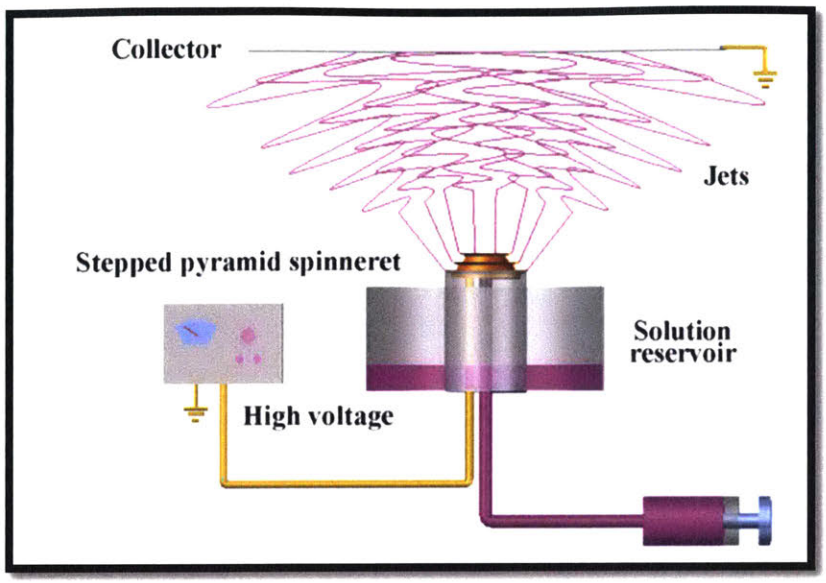

Figure 10: schematic of the pyramid spinneret free-surface electrospinning [7, Figure 2].

Jiang has discussed another novel setup using the stepped pyramid spinneret to perform free surface electrospinning [26]. A schematic of the setup is shown in Figure 10 above. This technology forms core-sheath fiber by feeding the solution from the syringe pump into the pyramid's center. The centrifugal force of the spinning pyramid assists the electrical force in forming jets of fibers. Some close up images of this pyramid spinneret can be seen in Figure 11below.

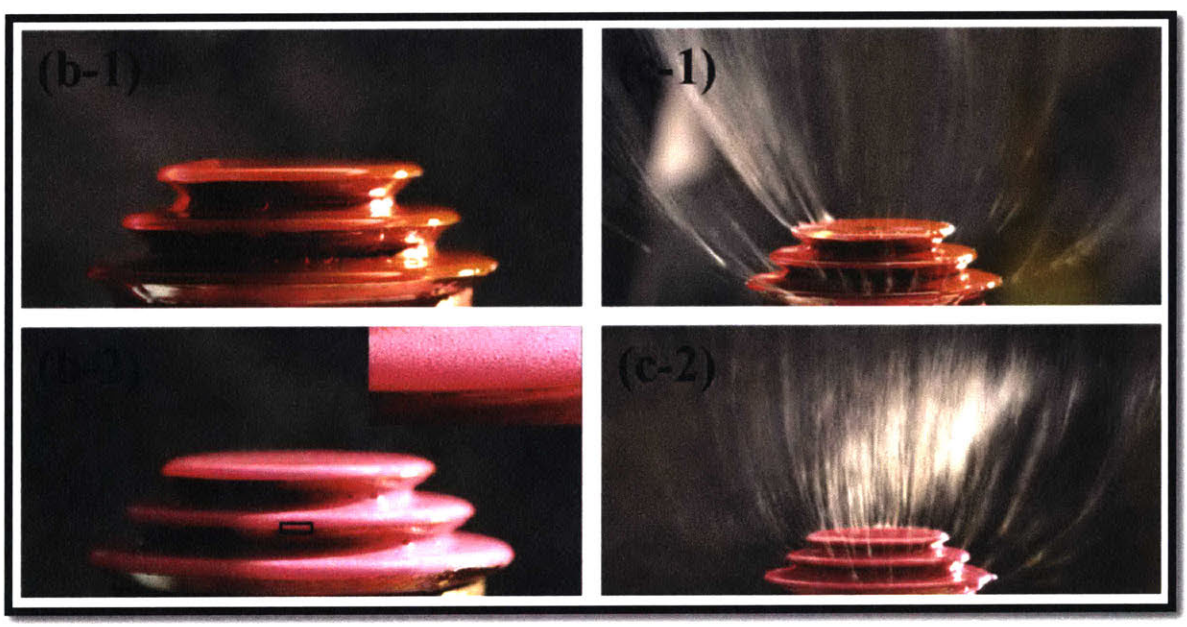

Figure 11: close up images of the stepped pyramid spinneret [7, Figure 2].

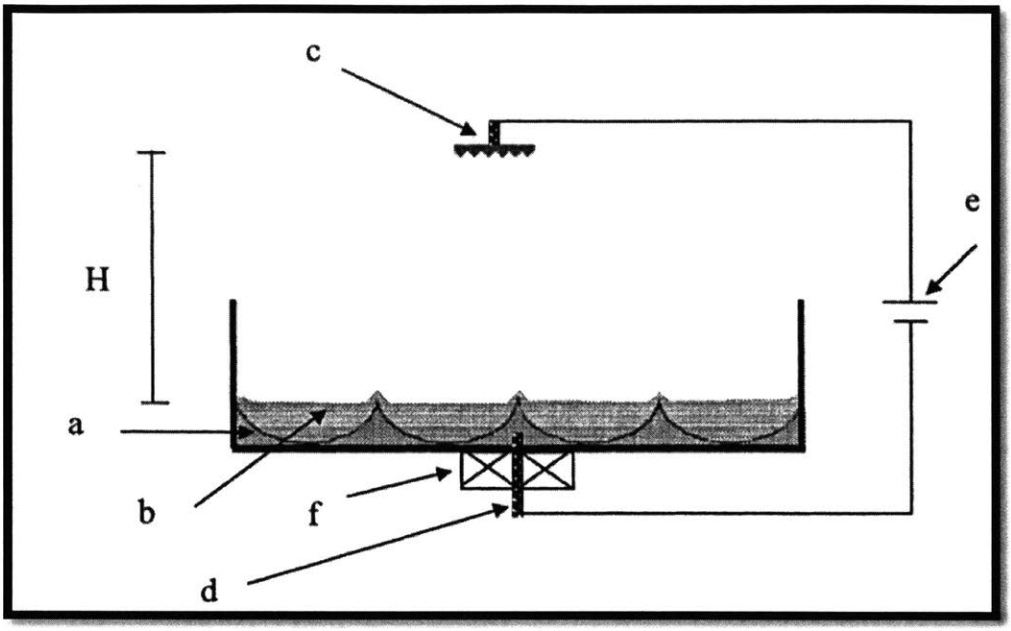

Figure 12: schematic of the ferromagnetic electrospinning setup (a)magnetic liquid layer, (b) polymer solution layer, (c)collector surface, (d) submerged electrode, (e) high voltage source, (f) strong permanent magnet [36, Figure 1].

Adding ferromagnetic suspensions to the polymer solution is another way of supporting the Taylor cone formation and enhancing the spinning output. Yarin has discussed this 2-layer setup shown in Figure 12, the lower one is a ferromagnetic suspension and the upper is the polymer solution. Under his experimental conditions, he claimed that it avoid clogging problems and was twelve times more efficient than needle electrospinning [36].

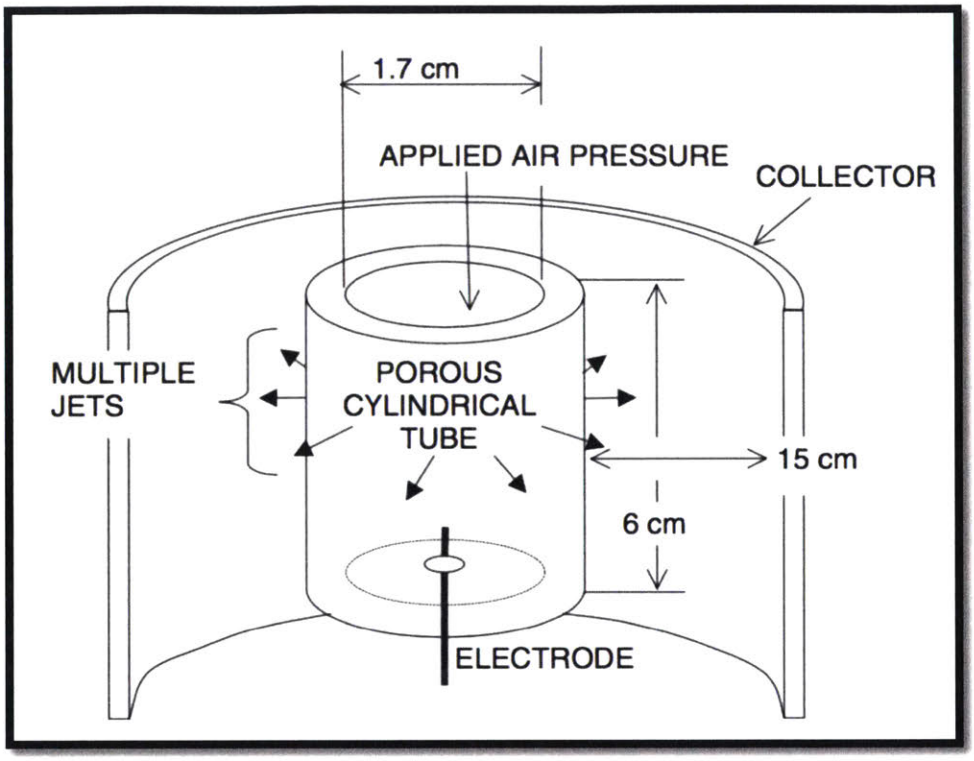

Figure 13: schematic of the porous pressurized tube electrospinning setup [37, Figure 3]

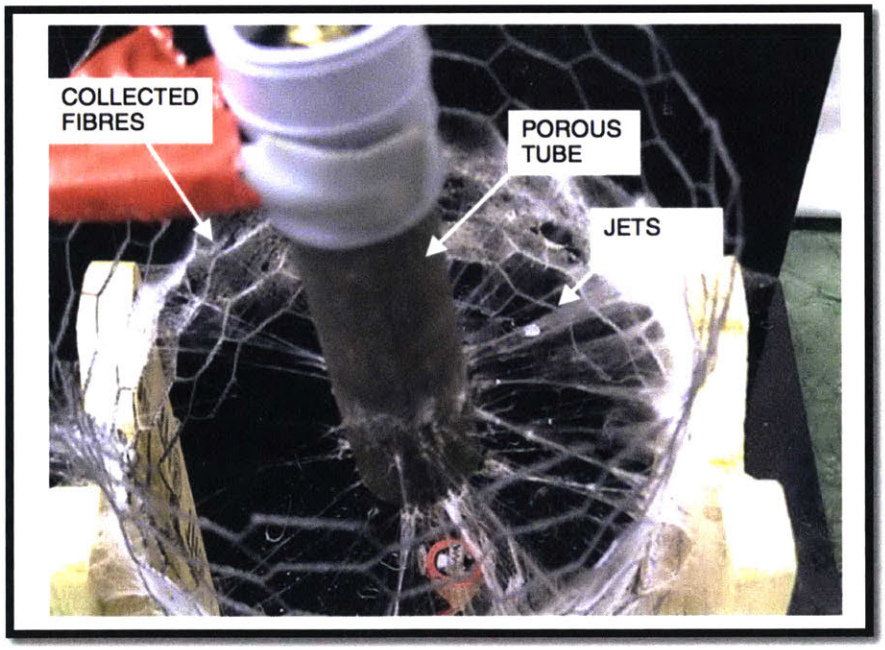

Figure 14: view of ceramic porous tube from above [33, Figure 5]

Another spinneret design studied by Donsunmu was the porous pressurized tube, shown in Figure 13 and Figure 14 above. These tubes were made of either polyethylene or ceramic, pressurized at 0.4-0.8 kPa to spin a polyvinylpyrrolidone (PVP) solution in ethanol. He found out that the mass production from the pressurized tubes was 250 times that of a single jet, and he claims that this is due to higher number of jets and larger fiber diameters [37].

2.3.3 Free-Surface Electrospinning

In our laboratory, the Rutledge group has done a lot of research on free-surface electrospinning, using another distinctive spinneret design. This spinneret is made of a set of thin wires wrapped around a spindle, as shown in Figure 15 below.

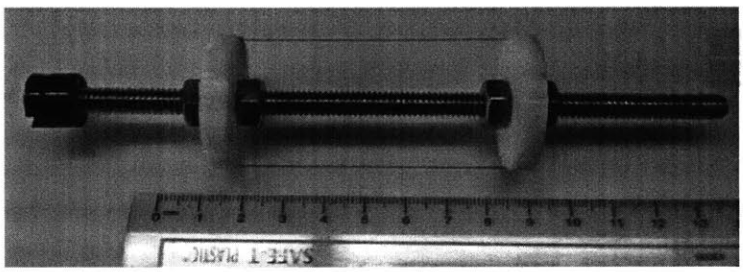

Figure 15: the spindle electrode with 2 wires [8, Figure 4].

This spinneret is placed in a polymer solution bath, where it rotates and the thin wires keep dipping in and out of the bath. The schematic of the whole system can be seen in Figure 15; where the wire spindle is placed at the bottom, and the collection plate at the top. A small DC motor rotates, and a belt drive transmits this rotation to the wire spindle electrode. The wire electrode is connected to the high voltage power supply and the collection plate is grounded to receive the fibers.

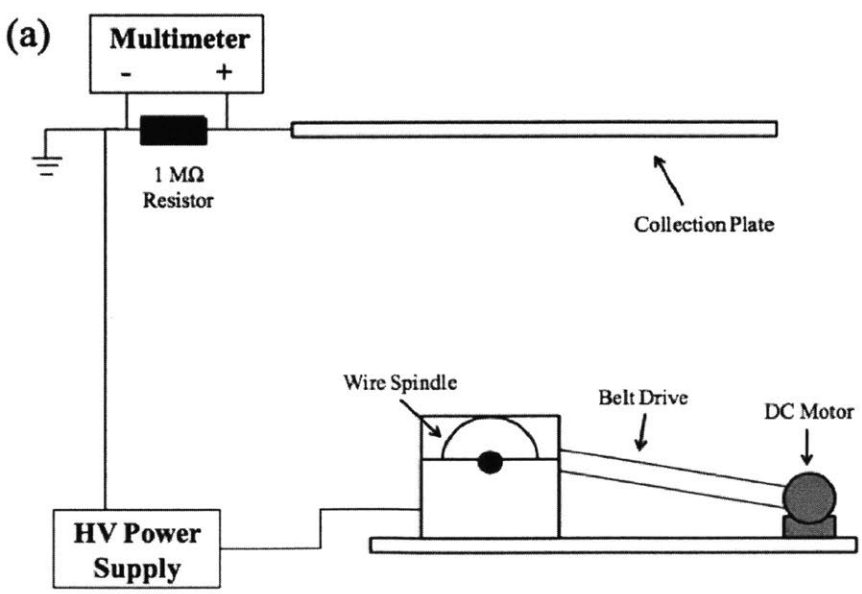

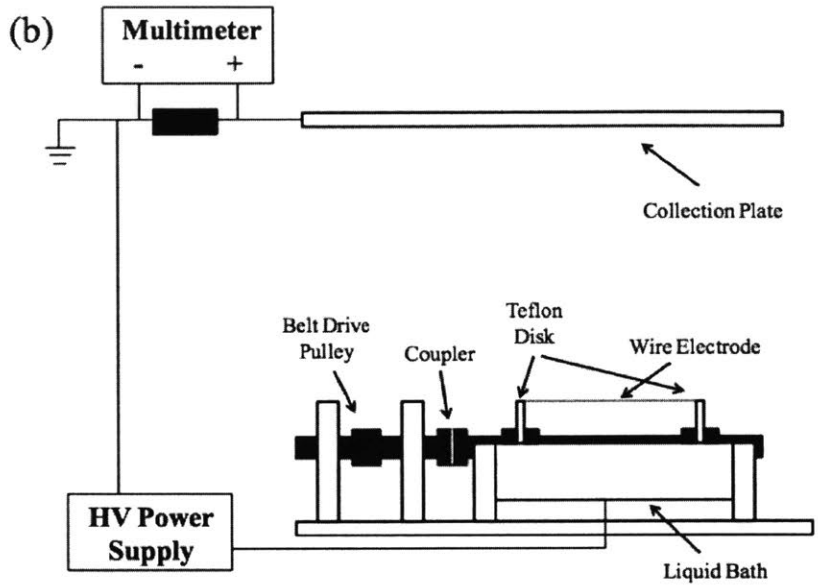

Figure 16: schematic of the free-surface electrospinning apparatus (a) side view, parallel to spindle axis (b) front view, perpendicular to spindle axis [8, Figure 3].

In this setup, the liquid is subjected to gravity, surface tension, viscosity, and inertial forces. The gravitational force pulls down and the viscous force pulls up, resulting in a thin film of liquid entrained, as seen in the schematic in figure (x) below. In the figure part (a), the large circle is the wire end-on, the line is the fluid-air interface, and the small dots are micro-particles that are a little enlarged in this figure. This figure part (a) goes with the setup side view (a) in the previous figure. While the view of fluid jetting from the wire electrode in part (b) aligns with the setup's schematic front view, part (b).

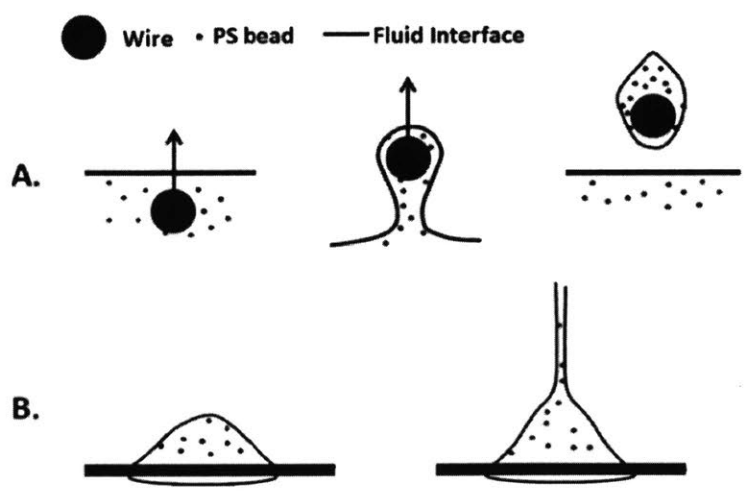

Figure 17: evolution of the surface profile (a) from the solution to the wire electrode (b) from the wire electrode to fiber formation [38, Figure 3].

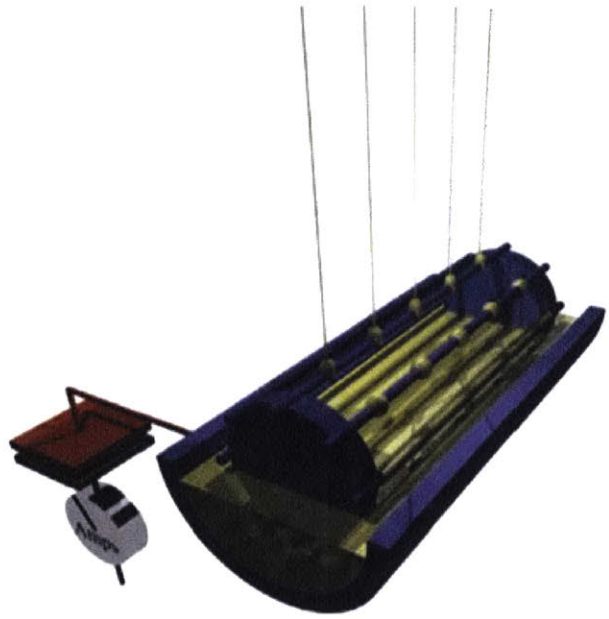

Figure 18: an isometric view of the wire electrode in the polymer bath [39, Figure 1].

As seen in Figure 18, the polymer solution is in yellow (light print) and the bath and spinneret are in purple (dark print). As the spinneret rotates, we can observe the yellow droplets forming on the wires, then the jet thinning turns these droplets into fibers. These fibers are attracted to the ground collector on top, this why the fibers travel vertically upwards.

2.3.4 Application of Free- Surface electrospinning in this work

After reading in the literature about the electrospinning history, basics, and different setups, I have adapted the Rutledge group' s setup of free-surface electrospinning using a wire spindle electrode to fit my needs, and integrated it into my machine's full setup. More details about my electrospinning setup will be covered in the next chapter.

Chapter Three: Designing The Machine

"Precision Machine Design isn't about finding the low hanging fruit, it is about finding the low hanging rabbit, because you get the rabbit and the fruit!"
Alexander Slocum

3.1 General Design of the Machine

3.1.1 Main Functional Requirements

The main functional requirement of our machine is to provide an automated pressing mechanism that extracts the pill's material from the electrospinning process and presses it into a pill shape with the fewest operations in between. The current nanofibers' pressing mechanisms have such a low production rate, while traditional pill pressing machines can produce up to 30 pills per second [41]. Therefore, our main requirement is to close the gap between these 2 production rates.

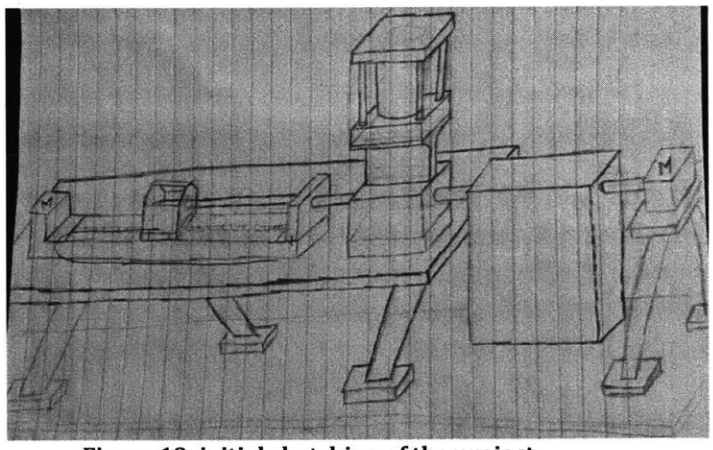

Figure 19: initial sketching of the project

This problem was approached by sketching the initial electrospinning setup with the final pill pressing setup, then coming up with different designs to connect these two mechanisms, as seen in Figure 19. The functional requirements table of the whole spin, strip, and stomp mechanism was as follows:

No.	Functional Requirements	Design Parameters	Analysis	References	Risks	Counter Measures
1	Design a simple and quick connecting mechanism between spinning and pressing	1- Pneumatic slider 2- Electrical Slider 3- Hydraulic slider	1- Speed of sliding 2- Electrical conductivity & safety 3- Quick feedback 4- Precision with nanofibers applications 5- Ease of control and adaptation to changes	1- Slocum's book 2- Manufacturer's catalogue of available sliders 3- Industries that currently use these kinds of sliders	1- Speed control problems 2- Contamination of pills 3- Interference with electrospinning's voltage and current	1- Isolation of the slider from the electrospinning chambers 2- Including variable speed control in the initial design 3- Ease of assembly/disassembly of speed control parts to change them if needed
2	Connecting mechanism needs to slide the polymer rod, and spin it during electrospinning	1- Sliding motor & setup 2- Spinning motor & setup	1- Torque needed by each motor. 2- Speed needed by each motor 3- Electrical control options 4- Electrical safety with high voltage in electrospinnin	1- Available motors & controls 2- Slocum's book 3- SparkFun	1- Motors' torque/speed is not enough 2- Resonance of the rod at specific frequencies 3- Rod deflection affecting the	1- Make quick tests to try torque & speed 2- Calculate natural frequency and consider all possible frequencies of the motion

			g		sliding process	3- Add supports along the way to reduce bending
3	Electrospinning adaptation to new design	1- Design stand to support spinning rod 2- Dynamic grounding for the spinning rod collector 3- Make all parts out other than the ground out of an insulating material	1- Sizing of the rod collector to size its hole 2- Possible deflection to size its receiving mechanism 3- Analyzing electrical conductivity of different materials 4- Forces generated by the rod, to design its stand support accordingly	Beam bending analysis and material properties from Slocum's book & others	1- Stand is not stiff enough 2- Polymer attracts to other conductive spots 3- Wear of the rod support from continuous spinning	1- Geometrical, materials changes for the stand 2- Insulate/change materials of the parts that attract the polymer to it 3- Increase tolerance between spinning rod and hole to decrease wear & frictional properties
4	Design press according to current electrospinning setup	1- Die cavity sizing according to rod collector size & length 2- Length of punch more than die	1- Die cavity length from collector length, from current spinneret length 2- Punch, die,	1- Pneumatics handbook 2- Pharmaceutical standards	1- High pressures & forces vibrating the rod too much 2- Some of the polymer does not get into	1- Increase stiffness to reduce vibrations 2- Make polymer hole conical 3- Tight tolerances for

Table 1: general functional requirements of the mechanism

3.1.2 Machine Components

This machine consists of three mechanisms with the following functions:

1- The electro-spinning chamber:
→ Spins nanofibers from the polymer solution.
2- The Mechanical press:
→ Presses the nanofibers into a pill shape.
3- The sliding spinner:
→ Slides nanofibers from mechanism (1) to mechanism (2).

As seen in Figure 20 below, the arrows show the material flow and the three boxes represent the three main mechanisms mentioned above.

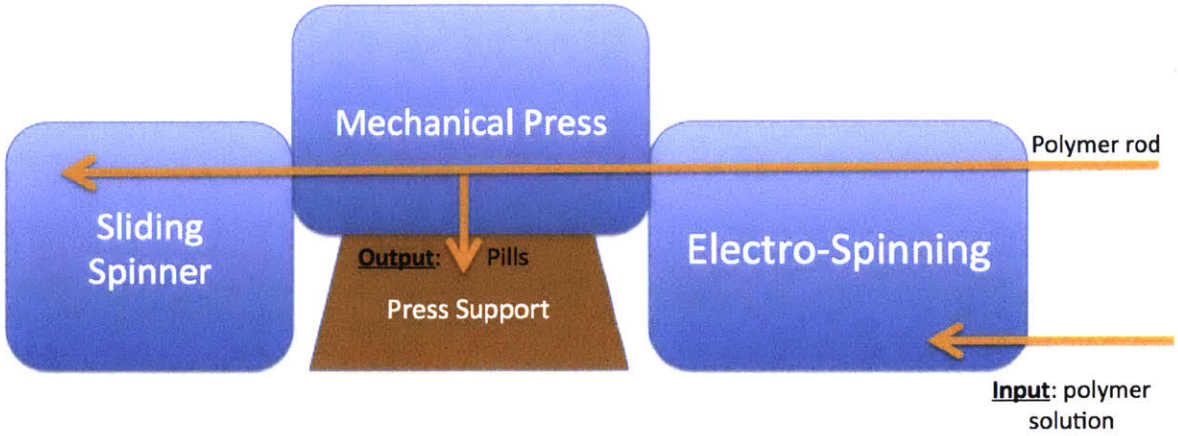

Figure 20: the three main mechanisms of the machine

Throughout this process, the pill's materials are spun, stripped, and stomped. The first step, **spinning**, is where the fibers are drawn vertically upwards from the polymer bath to the spinning rod collector using the high electrical potential difference as their driving force. The second step, **stripping**, is where the fibers are stripped from the rod collector into the press's die cavity. The third step, **stomping**, is where the material inside the die cavity is pressed into the pill shape, creating our final product.

The starting point of the machine was the existing electrospinning setup in Rutledge lab [40], and the early prototyping of manually extracting and pressing the polymer into a pill [9]. This initial analysis was the thesis project of a former colleague Nicholas Sondej, who was a Masters student in the Precision Engineering Research Group at MIT. This thesis combines both to make an automated mechanism. The early prototype gave us the following conclusions:

1- It is not possible to spin the fibers directly inside the die cavity, but the second quickest way is to spin it on a body that goes into this cavity.
2- It is possible to spin the polymer to a collecting rod rather than the traditional flat plate collector.
3- The collecting rod needs to spin to spread the polymer all around it, or else bulk fibers will form on one side.

All of these conclusions were used as building blocks for the functional requirements of the machine, and the challenges faced in the earlier design were taken into consideration during the whole design process. The bigger picture of the machine components was then re-imagined. Afterwards each part was further analyzed to design those 3 main machine components and put them all together.

3.2 Electrospinning Design

3.2.1 From flat plate collector to spinning rod collector

The electrospinning chamber in this machine was an updated version of the Rutledge Group setup shown in Figure 21 [8] and Figure 22. In this setup, the fibers were drawn from the polymer bath at the bottom using the rotating wire electrode. These fibers were then collected as a mat on the flat collector plate at the top.

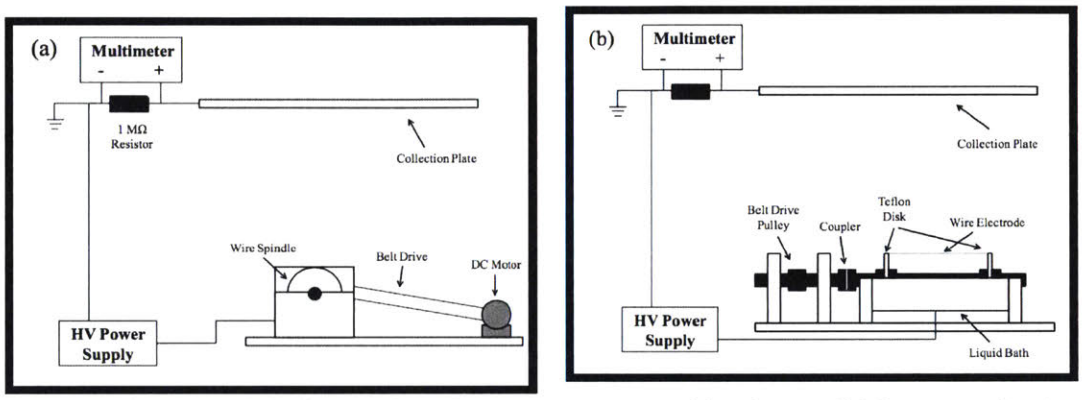

Figure 21: schematic of the free-surface electrospinning setup (a) side view (b) front view [8, Figure 3]

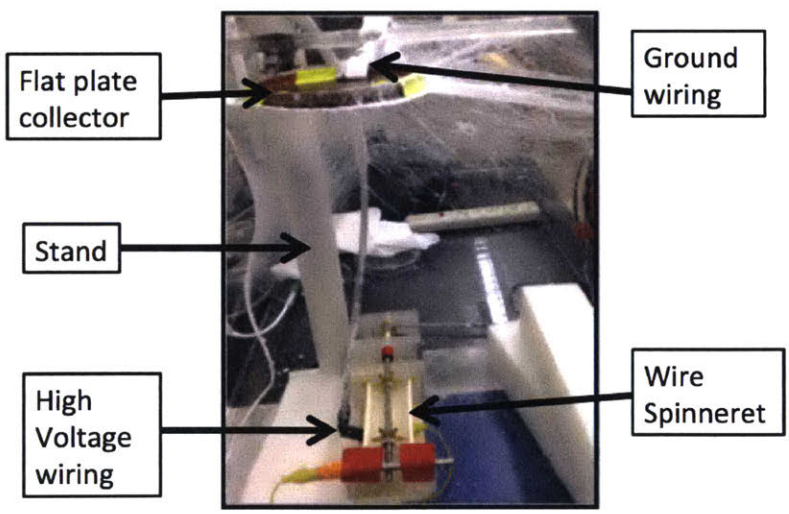

Figure 22: electrospinning to a flat plate collector

The main change in our setup was replacing this flat plate collector with a spinning rod collector, spinning and collecting fibers around it like a cotton candy stick, as shown in Figure 23.

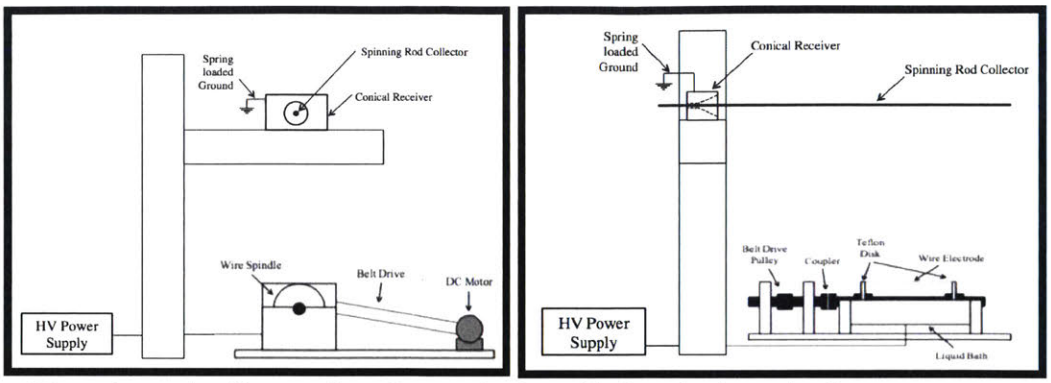

Figure 23: a schematic of free-surface electrospinning with the spinning rod collector

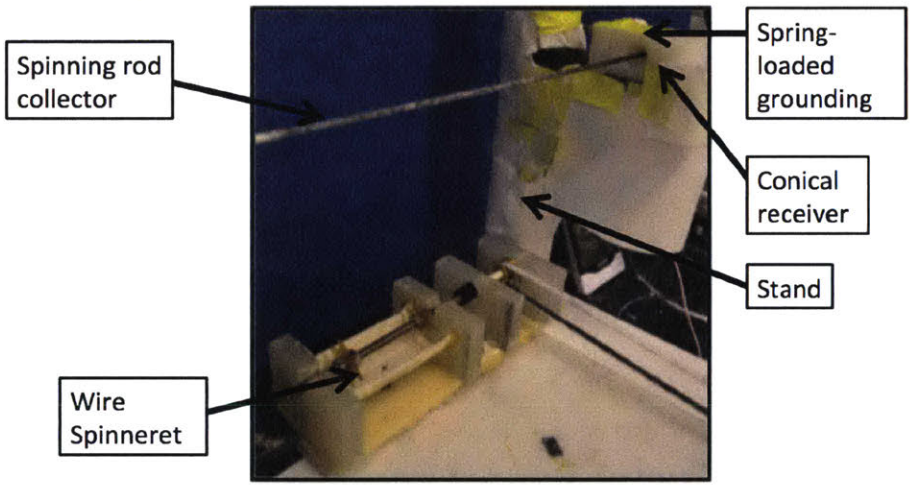

Figure 24: free-surface electrospinning with the spinning rod collector

In order to accommodate this change from a flat plate collector to a spinning rod collector, we had new ***functional requirements*** of:

1- Supporting the rod at its required height.
2- Grounding the spinning rod collector.
3- Allowing the slippage of the spinning rod in its stationary housing.
4- Choosing insulating materials and avoiding sharp edges that may attract fibers onto it, to create an electrically neutral stand.

3.2.2 Stand Design

To fulfill functional requirement (1), a vertical stand made of a set of T- slotted aluminum frames was designed, as seen in Figure 26.

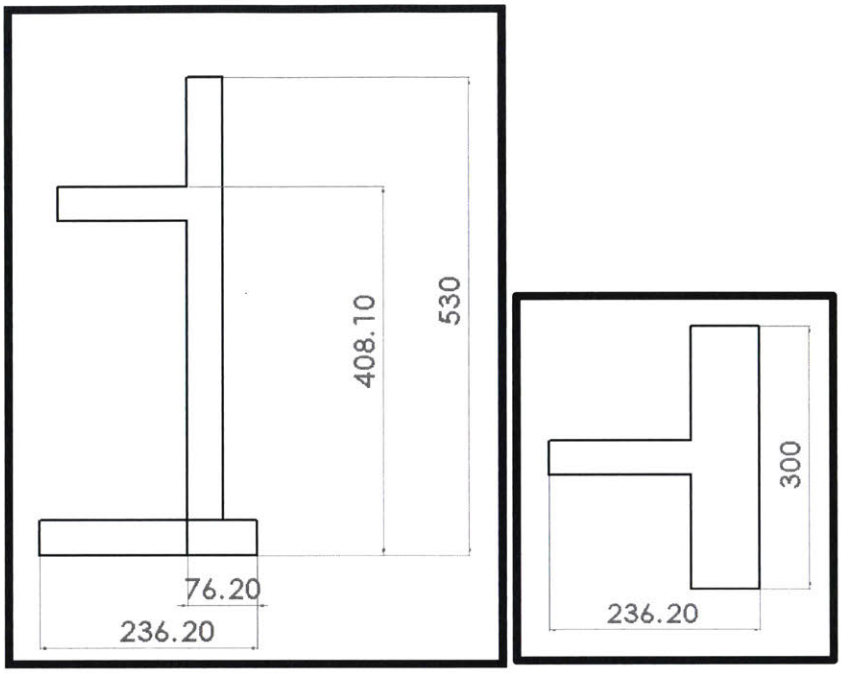

Figure 25: side and top views of the stand's engineering drawing

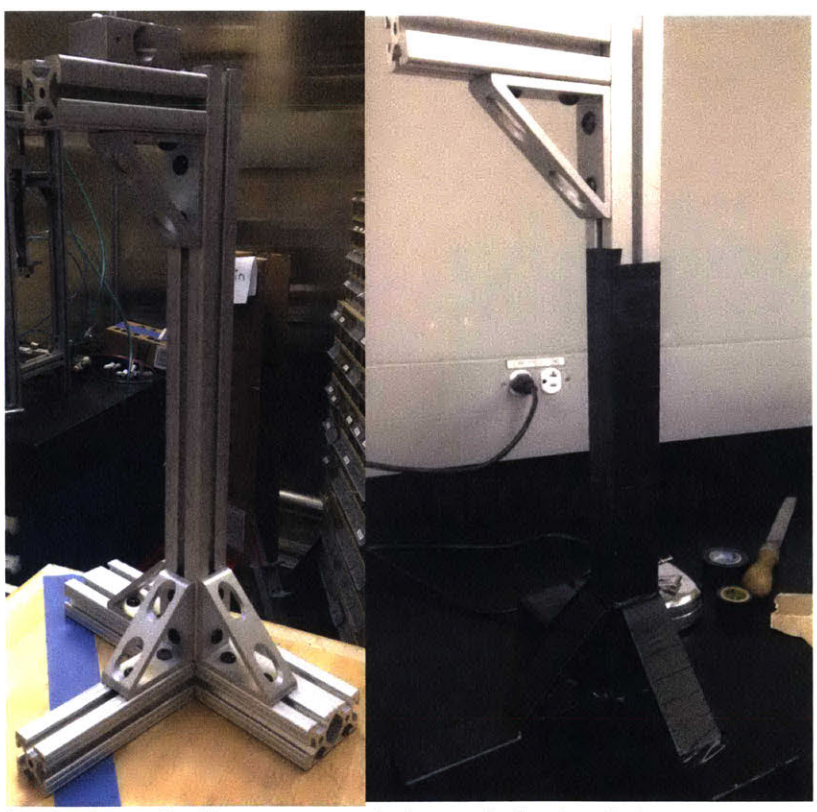
Figure 26: spinning rod collector support before and after insulation

The stand was initially made out of T-slotted aluminum because of its flexibility in geometrical changes. For example, if we decided to move the collector's position up or down, we could

easily slide the structures against each other and securely fasten them at this position. The only drawback of the T-slotted aluminum was that it was electrically conductive. This problem was resolved by covering the whole structure with insulating tape, and adding further insulating layers with high curvature to cover the aluminum's sharp edges. As seen in Figure 26 above, the vertical stand was originally of a rectangular cross-section, but it is wrapped with an insulating layer. After some experimental trials, many fibers were attracted to the sharp edges, so another layer of insulation was added. This additional insulation makes it look more like a cylindrical stand with curved edges in all directions, getting rid of all the sharp edges.

This stand has three bottom legs to enhance its stability if it is subjected to any forces from the spinning rod collector. There are no forces in the fourth direction, so no additional leg was needed. Also the stand needs to be close to one of the walls, to be out of the way during fibers' electrospinning. So the wall side subjected to no forces was chosen as the no leg side, with the three legs spreading in the three other directions.

The force and moment that the stand needs to resist were as follows:

Force calculations:

$$F_{sl} = \frac{T_{sl}}{R_{py}}$$

Equation 2

Where F_{sl} is the sliding force that the rod collector slides in with, T_{sl} is the torque of the sliding motor at its driving speed, R_{py} is the radius of the belt's pulley that the motor rotates in order to slide the rod collector back and forth. The sliding torque was calculated in the sliding mechanisms section 3.3, and the radius of the pulley was obtained from its manufacturing company, BrecoFlex.

Plugging our numbers of:
R_{py} = 20 mm = 0.02 m
T_{sl} = 273 Nmm = 0.273 Nm

Gave a sliding force of:
F_{sl} = 13.65 N
which is equivalent to the horizontal force that the stand needs to resist.

Moment Calculations:
The stand needs to resist the rotational moment around the tipping point of the stand on the ground. This is governed by the following equation:

$$M_{tipping} = F_{sliding} * H_{rod}$$

The tipping moment $M_{tipping}$ is equivalent to the rod's sliding force $F_{sliding}$ multiplied by the height of this rod above the ground H_{rod}.

Plugging our numbers of:
$F_{sliding}$ = 13.65 N

H_{rod} = 370 mm = 0.37 m

Gave a tipping moment of:
$M_{tipping}$ = 5.05 Nm
which is equivalent to the moment that the stand needs to resist.

3.2.3 Conical Support design

To fulfill functional requirement (3), a conical shaped support was designed to guide the rod into its cavity in the support. This conical support has a through cavity slightly bigger than 3.25 mm (1/8 inch) to fit our 3.25 mm (1/8 inch) collector, in addition to a cone shaped entrance for the rod that goes from a diameter of 20.32 mm (0.8 inches) to the diameter of the 3.25 mm through hole. This shape was made to accommodate any bending of up to 10 mm in the rod in all directions and guide it into its designated position.

Earlier Design:

The first conical support was made out of aluminum, and it had two main design features:

1- The conical entrance narrowing down from 4/5 inch to the 1/8 inch hole.
2- Two 5/16 inch holes for the bolts that attach this conical support to the stand.

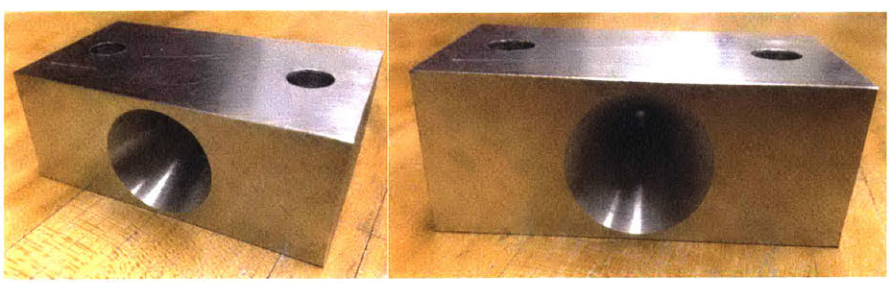

Figure 27: earlier conical support design

The conical support's design problems were:

1- It was **not electrically insulating** even after surface insulation, **because it was made out of aluminum**. It still conducts electricity from the rod collector and electrifies the whole stand.
2- **The pills were contaminated with metal**. This happens when the rod collector spins inside the **aluminum hole**. It wears some of the aluminum surface off, which then gets stripped with the polymer and stays with it.
3- There was **no hole to insert the crocodile clip** of the ground wiring. So the wire was attached to the edge of the conical surface as shown in Figure 28 below. This made the wire very close to the rod collector, so a lot of fibers were always attracted to the wire.
4- The two bolts had **sharp edges**, so they attracted some fibers.

Figure 28: grounding wire clipping onto the conical support

Modified Design:

As discussed above, the three main problems of the first design were that:

1- It is made out of aluminum
2- There is no hole for the grounding wire to be properly attached and out of the fibers way.
3- The bolts' sharp edges would attract fibers.

So the three changes in the new design were:

1- It is made out of polytetrafluoroethane (PTFE)
2- It has a special grounding setup out of the fibers way
3- It has no exterior edges, because the bolts sink in their holes.

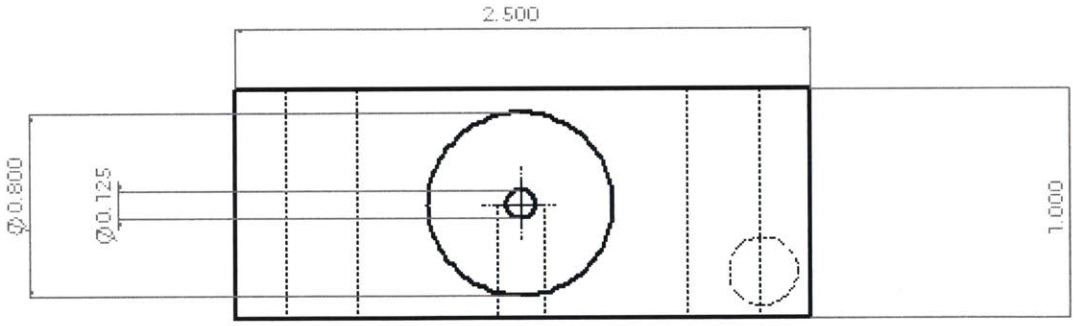

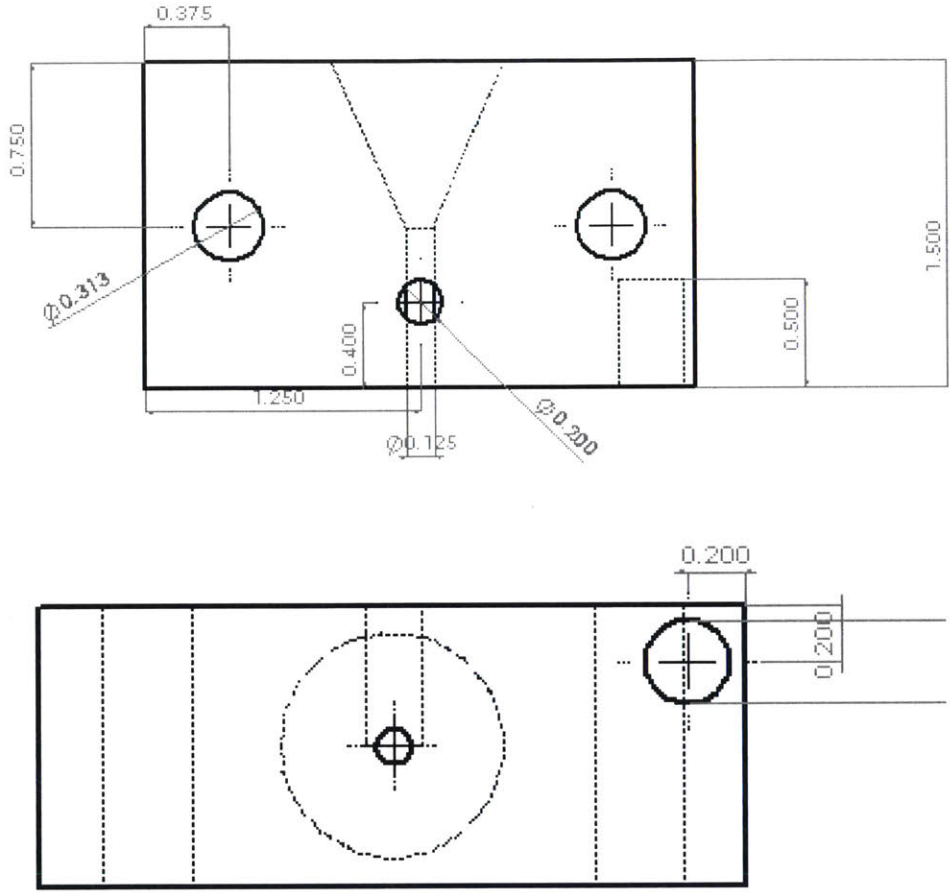

Figure 29: engineering drawing views of the modified conical shaped support (dimensions are in inches)

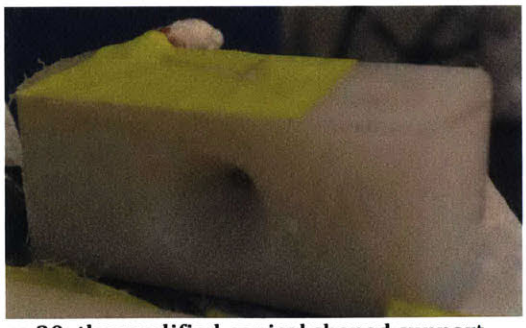

Figure 30: the modified conical shaped support

As seen in Figure 30 above, the new support was made out of PTFE. It had the special spring loaded brass grounding, which connected the spinning rod with the ground crocodile clip. The ground crocodile clip was attached to the back of the support, so it was totally out of the fibers' way. The two holes for the bolts were sinking rather than having their heads out of the structure.

3.2.4 The Spring loaded Brass Grounding

To fulfill functional requirement (2), a dynamic grounding system made of a spring-loaded brass ball, as shown in Figure 31, was designed. Fibers will only attach to the collector if it was correctly grounded and if all of its surroundings were insulated and uncharged. By adding this component vertically into the conical support, its top end connected to the ground wiring and its bottom end was the ball pressing against the rod. Therefore, the rod collector kept spinning while touching this brass ball that was connected to the spring and the ground wiring to ground all the components.

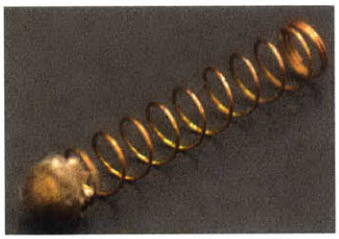

Figure 31: the spring-loaded brass ball grounding

The material of this part was chosen to be brass because of its:

1- **High electrical conductivity**: connecting the ground wiring to the spinning rod collector.
2- **High wear resistance**: solving the problem of metal contamination by the earlier aluminum design

3.2.5 The scissor lift setup

Since the nature of the experiment might require changing the distance between the spinneret at the bottom and the collector at the top, the bottom spinneret was placed on a scissor lift, and the top part with more components was kept stationary. The top part also had to stay stationary because it had to be in parallel with other machine components; such as the press's die cavity and the sliding spinner.

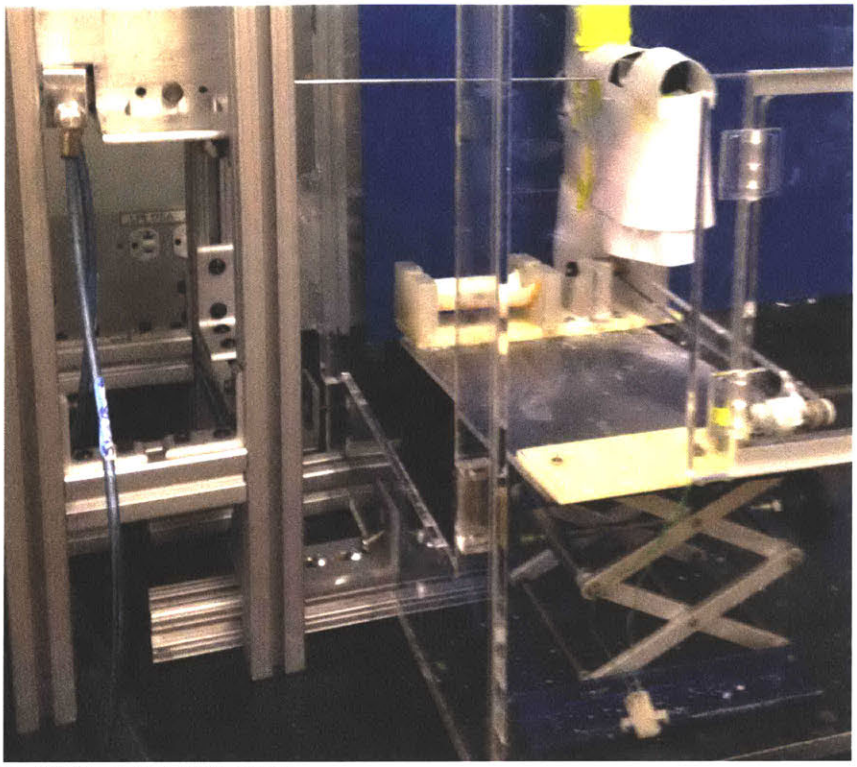

Figure 32: the scissor lift setup

3.3 The Sliding Spinner Design

This mechanism has two main functions, as its name elaborates. The first function is spinning the collector rod inside the chamber to collect the fiber all around it like a cotton candy machine. The second function is sliding this rod into the press's die cavity to strip the polymer off the rod, then the rod slides out and the drug material stays inside the cavity. These two main functional requirements in addition to others are shown in

Table 2 below.

No.	Functional Requirements	Design Parameters	Analysis	References	Risk	Counter- measures
1	Retract the Rod	1- Belt Drive 2- Screw Drive	Calculate and compare sizes, geometry, forces and power requirement of both	Lecture slides, available motors on Mcmaster, Machine design book	Backlash, Inaccuracy, Bending	Create error budget and correct sizing for target bending and allowable error
2	Spin the Rod	1- Motor on Carriage 2- Motor by E-spin 3- Motor on rod guide 4- Transmitted rotation	Choose motor location, calculate motor power, size and analyze mount/mesh mechanism	Lectures, course book	1- Wearing of loose wires 2- Dynamic motor mesh collision/breaking	1- Avoid having loose wires 2- Stationary Motor preferable 3-Guiders and covers for meshing mechanism
3	Accuracy of rod inside hole	1- Add rod guide at the end of slider 2- Add rollers/guiders by hole entrance	Analyze correct rollers location, size, friction, taper size, and its tolerance	Lectures and book	1- Over constraining the mechanism 2- Collision due to different rollers misalignments	Have minimal number of rollers, lined up, same material, same tolerance
4	Electrical Safety	1- Have all motors static 2- Have minimal number of motors 3- Cover all motors/preferably on 1 side	Compare number of parts, complexity, and accuracy of different motor spots	Mcmaster motors and book	Motor contact with polymer or meshing mechanism, loose wiring, motor vibrations wiggling rod	Keep motor far away from moving rod to minimize noise, place away from polymer zone to avoid contact
5	All polymer goes on hole	1- Have a tapered hole 2- Have hole of different diameters 3- Have a very large	Polymer physics and micro fluids course for polymer behavior analysis at different shapes	Polymer fluids course notes, PVA handbook	Polymer stripped off hole, sticking to walls, or ruining polymer Nano sizing	Have a bigger hole, avoid applying any forces on polymer

Table 2: functional requirements of the sliding spinner

3.3.1 Linear Actuator Design

3.3.1.1 Review of current linear actuators:

1- Air slider: it uses pneumatic power.

2- Hydraulic/Electro-hydraulic pistons: Because liquids are incompressible, a hydraulic cylinder can control precise uni- directional displacement of a piston. **Advantages**: rapid acceleration, large masses durability. **Limitations**: proper sealing required, oil change, maintenance, and polymer contamination issues. Its motion is less accurate motion than electro-mechanical. **Applications**: oil and gas, cranes, agriculture, concrete, snow control, mining, military, and almost all industries.

3- Mechanical actuators:

a) Screws:

i- Acme screw: it has large frictional losses, it is not used for high power, but for intermittent use (not for this application) . **Applications**: machine tool, vise, machine press, jack.

ii- Roller screw: it is a low friction precision screw, expensive complex mechanism for high precision, high speed, heavy load, long life, and heavy use applications (not for this application). **Applications**: motion and positioning in aerospace.

b) Wheel and axle:

i- Hoist: it lifts or lowers loads by drum/wheel lift. It could be operated manually, electrically, pneumatically. **Limitation:** only pull. **Applications**: construction and mining

ii- Winch: it works by winding rope in and out to control its tension. **Applications:** theatres' back-stage equipment, water and snow sports.

iii- Rack and pinion: it has a pinion attached to the driving motor and the rack that moves back and forth. It has reduction gears to reduce its high driving torque. **Applications**: stair lifts, steering, rack railways, and pipeline transport.

iv- Chain drive: it transmits mechanical power from one place to the other (like chain sprocket and roller chains). **Limitation:** only pull. **Applications**: bicycles and automotive.

v- Mechanical belt: it links 2 or more shafts mechanically from the source of motion to the required output. **Limitation**: only pull. **Applications**: linking gearboxes to machine driving shafts.

vi- Rigid chain actuator: it is the same idea of the rack and pinion, but with articulated racks. **Limitation**: only pull. **Applications**: windows, lifts, push-pull handling.

vii- Rigid belt actuator: it is a rack and pinion attached to a moving belt. **Limitation**: only pull. **Applications**: push-pull and lift applications

c) Cams: it is a rotating/sliding piece that transforms rotary to linear motion depending on the cam's geometry. **Limitation**: only push. **Applications**: repetitive motion that needs special

speed, motion patterns.

4- Piezo-electric actuators:

It depends on the special material properties that expand when voltage is applied to it. Very high voltage gives very small expansion. **Advantage**: extreme fine positioning. **Limitations**: short range of motion and hysteresis problems in repeatability.

5- Electro-mechanical Actuators:

Controlling one of the mechanical systems discussed above to a motor controlling their motion, this could be: a) Stepper motor, b) DC brush, c) DC brushless, d) Induction motor, e) Linear motor.

3.3.1.2 Initial sketching of the overall machine:

Figure 33 below shows the thought process of connecting the three machine components: the sliding spinner, the press, and the electrospinning chamber.

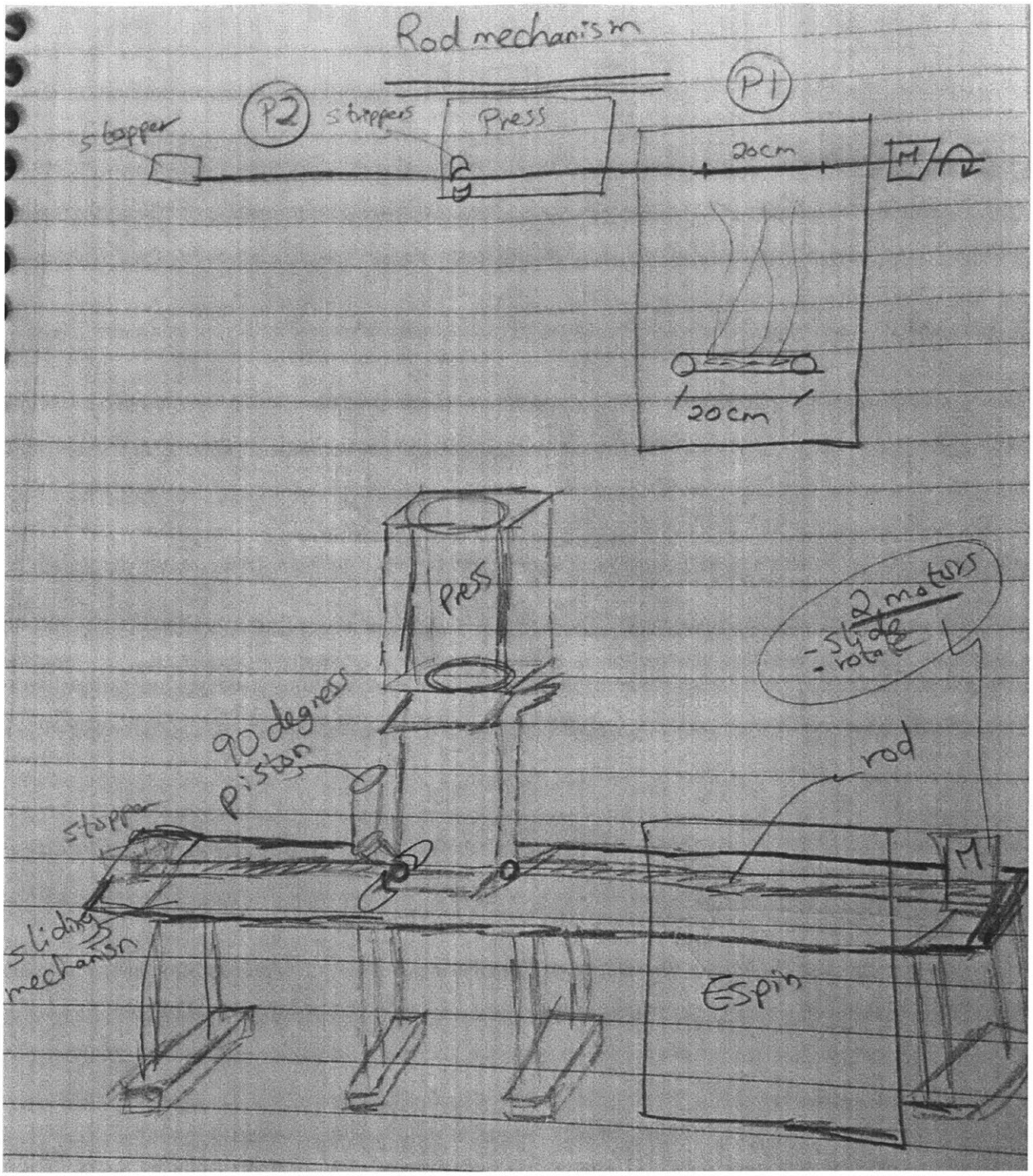

Figure 33: connecting the three mechanism components

Figure 34 and Figure 35 below show the sketches and the SolidWorks of the spinning slider's movement between its two positions.

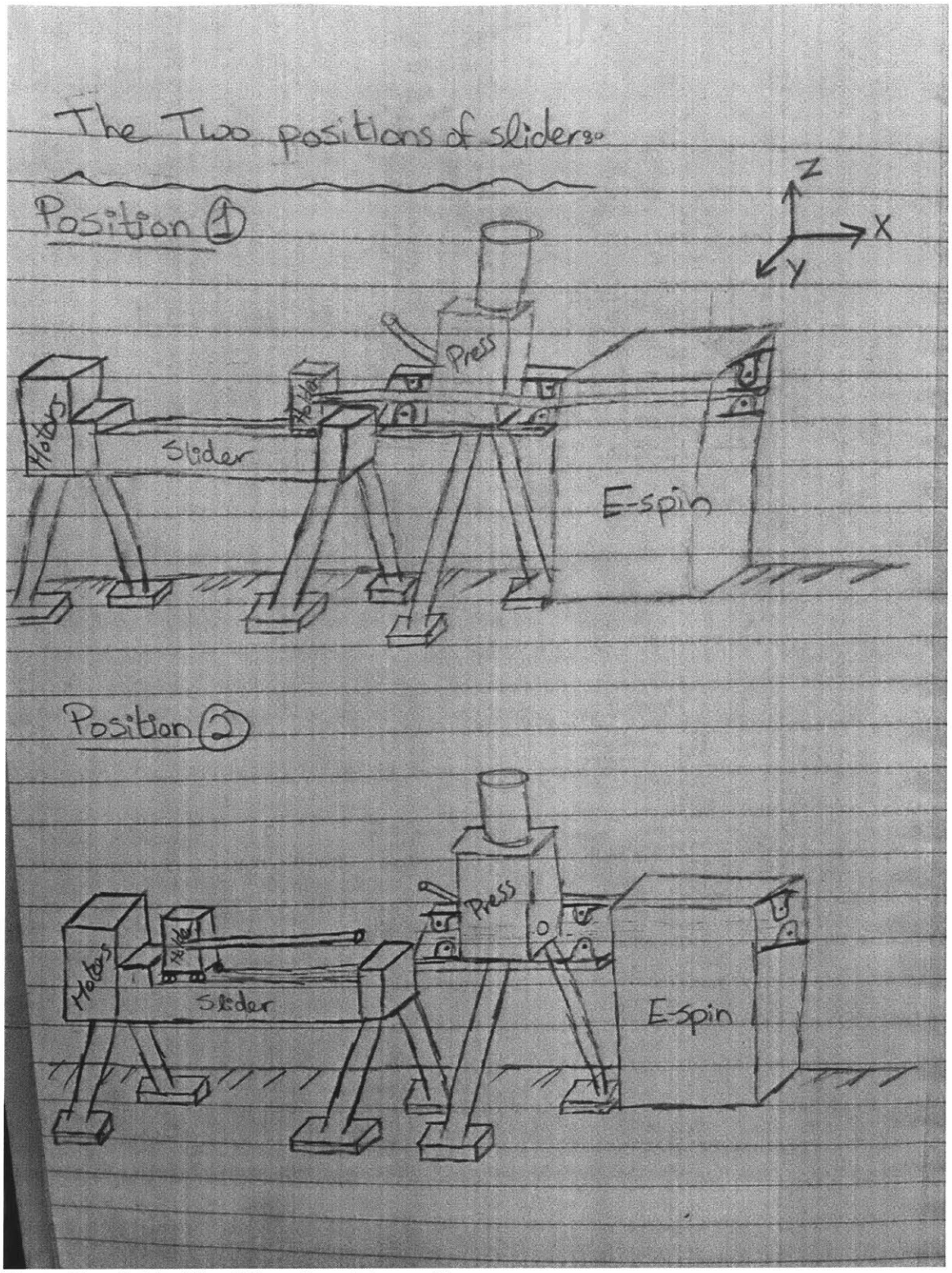

Figure 34: a sketch of the sliding spinner's two positions

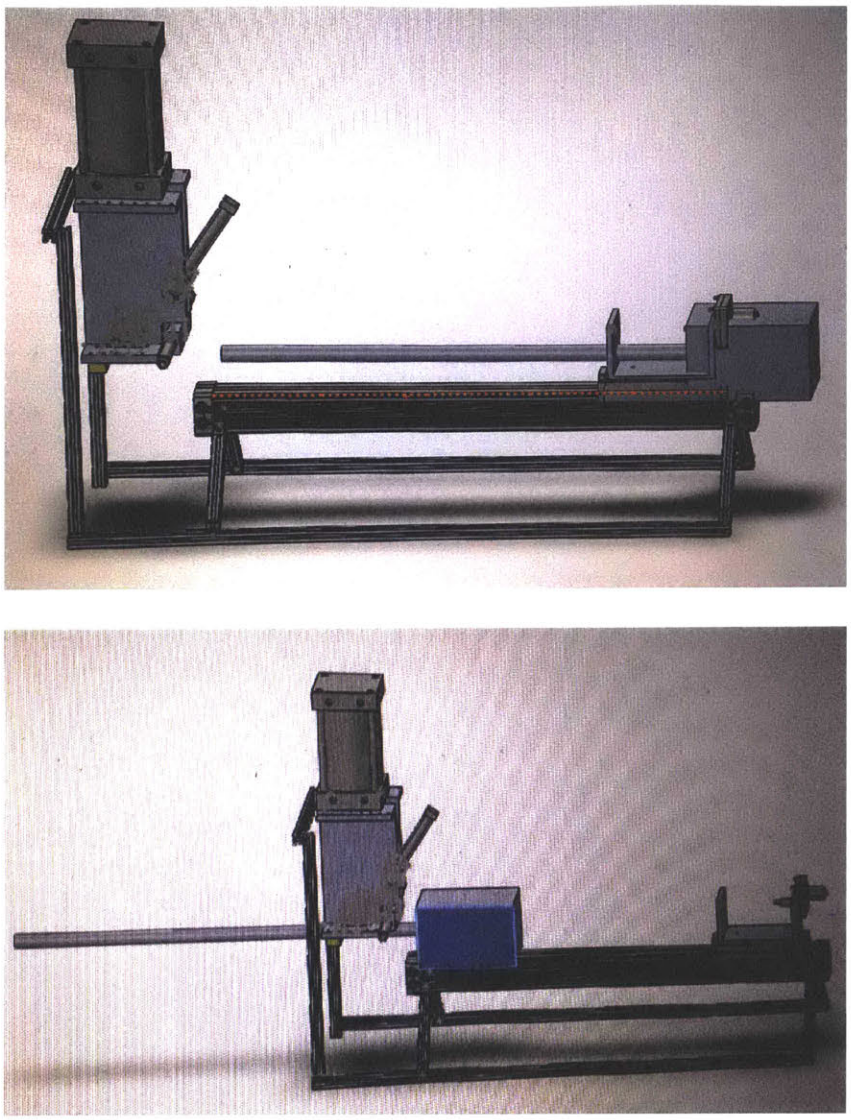

Figure 35: SolidWorks motion of the sliding spinner's two positions

3.3.1.3 Linear actuator initial design requirements:

Narrowing down the functional requirements of the machine, and adding some quantitative requirements, more specific functional requirements would be:

1) Move a 0.125 inch rod horizontally in both directions
2) Fit into the press hole open/closed positions
3) Self rotation of the rod (while electrospinning)
4) Move between the two positions (electrospin and out of the press)
5) Have rigid supports and casing for safety
6) Avoid having reactive parts in the electrospinning high voltage area
7) Choose a rod material that does not react with the polymer

8) Make sure the polymer will not rip off while entering the die cavity
9) Fit in a 0.25 inch hole
10) Have a total length that is slightly more than the total length of electrospinning and press assemblies.
11) Have a motor fixturing/mounting space.
12) Have supports (bearings or rollers) on both sides and in between mechanisms.
13) Have high linear speed and low rotational speed.

<u>Forces applied on the mechanism</u>**:**

There are three kinds of forces applied on this mechanism: (1) the weights of its components, (2) torsional moment, and (3) horizontal forces.

(1) The weights of the components include:

1. 1/8 inch rod
2. The rod's mounting
3. The attached polymer (about10mg, could be neglected)
4. Two motors and their motor mounts
5. The vertical force from the press's pressure
6. The press assembly (it should be attached directly to supports, but there might be partial load)

(2) The torsional moment comes from the positions of the two motors' with respect to the center.

(3) The horizontal forces are:

1. The rotary piston's 90 degrees motion
2. The slider's horizontal motion and braking force

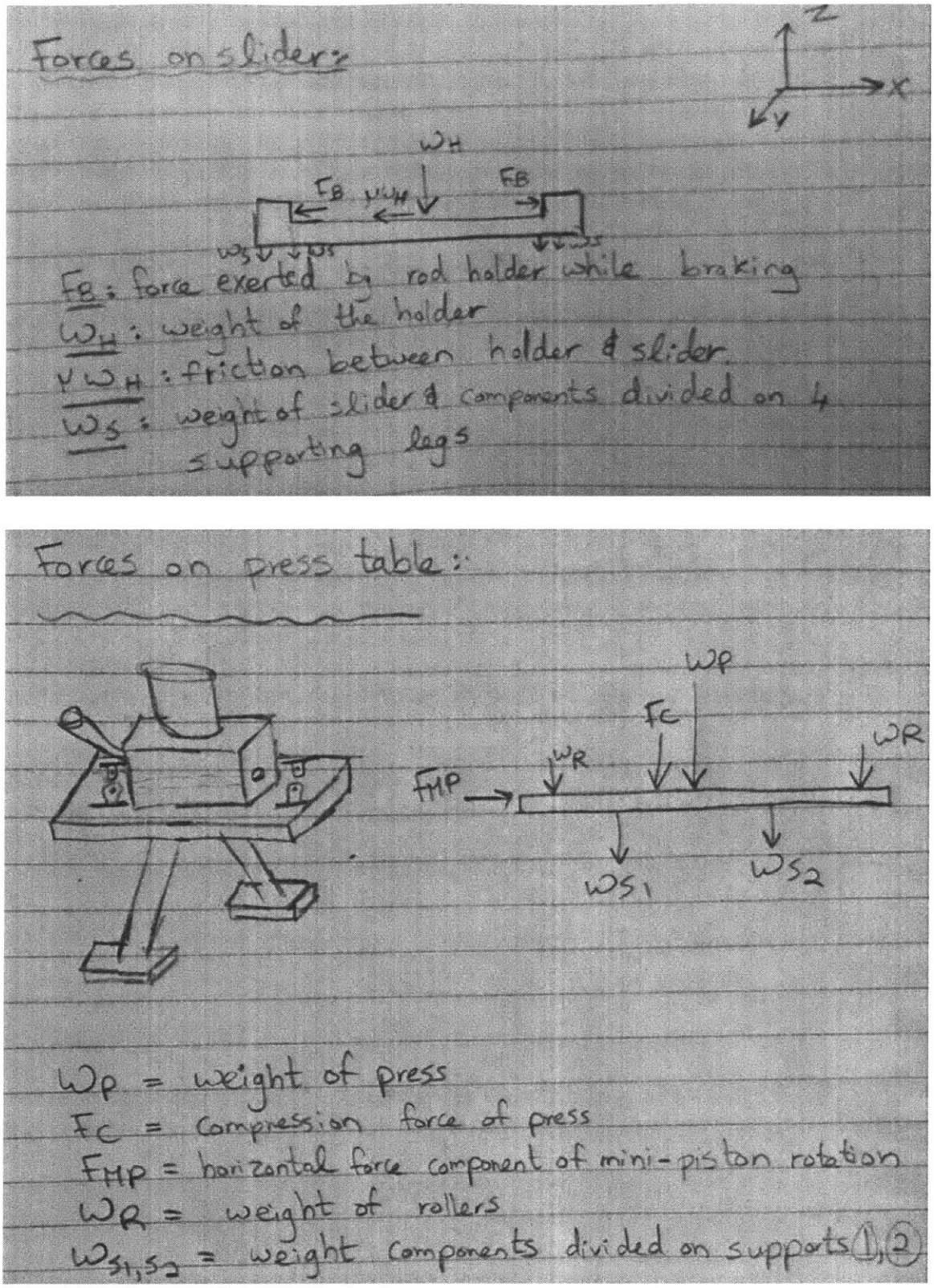

Figure 36: sketches of forces applied on the mechanism

Desired accuracy and stiffness:

The function of this mechanism is to hold the rod in both positions. The accuracy should result in:

1- Sliding the rod back to the exact electrospinning spot each time, to get consistent amount of polymer and produce reliable pills.
2- Sliding the rod beyond the two strippers so that they won't slam and close over it. This should be accompanied by extra safety distance travelled.

Solution (1): Since the rod is about 20 cm, 99% reliability means ±0.2 cm or ± 2mm deflection, and 95% reliability means ±1 cm or ± 10 mm deflection.

Solution (2): Since the rod's diameter is 0.125 inches and the hole is 0.197 inches, the maximum deflection could approximately be 0.072 inches.

Required stiffness:

The maximum deflection of a cantilever beam is governed by the equation:

$$Deflection = \frac{FL^3}{3EI}$$

Equation 3

Where (F) is the applied force, (E) is the modulus of elasticity, (I) is the moment of inertia, and (L) is the length of the beam.

Using and approximate number of (k = 0.072 in = 0.1825 cm), these parameters (E, I, and L) need to be chosen to give the allowable maximum deflection.

Structural loop:

The estimated dimensions of the mechanism are:

Rod length:	cm
E-spin Length=	40
Press Length=	11.5
safety Length=	5
Roller lengths=	15
Total Length=	71.5
App. Length=	75

Rod travel distance:	
Rod length=	75
Rod holder box length=	10
Total length=	85

Slider Mechanism Length:	
Travel Distance=	75
Side stoppers=	5
Motor mount =	20
Total Length=	100

Table 3: the mechanism's estimated dimensions

The structural loop is three times the sum of distances each axis might travel. This machine has one axis, and the distance travelled is the total length of the electrospinning and press assemblies. This gives a total length is 120 cm, so the structural loop is 360 cm.

To size the moving carriage, initial calculations were carried out for two possible geometries, a rectangular rube cross-section, or a C-shaped tube cross section.

For the rectangular and C- shaped tube cross-section, the outer dimension calculation was:

$$Outer\ Dimension = \frac{1}{5} * total\ length$$

Equation 4

Plugging the numbers in gives:

$$Outer\ Dimension = \frac{1}{5} * 120\ cm = 24\ cm$$

The wall thickness calculation was:

$$Wall\ thickness = \frac{1}{20} * Outer\ dimension$$

Equation 5

Plugging the numbers in gives:

$$Wall\ thickness = \frac{1}{20} * 24\ cm = 1.2\ cm$$

The assumptions on proportions were that the height would be 10 cm, to match the 24 cm outer dimension calculated using Equation 4 above.

Using the initial sizing above, and assuming the mechanism will be machined out of aluminum. The volume and density calculations would give a beam mass of 12.75 kg. The natural frequency of the beam structure, assuming it is fixed on both ends, would look as seen below (column 4 in Table 4):

Length L (m, mm)	1.2	1200
Height, h (m, mm)	0.1	100
Width, w (m, mm)	0.24	240
density rho (kg/m^3)	2700	
Modulus E (M/m^2)	6.90E+10	
Calculated cross section area (m^2)	2.40E-02	
Calculated moment of inertia (m^4)	2.00E-05	

	Cantilevered	Simply Supported	Fixed-simple	fixed-fixed
Buckling load (N)	2367083	9458750	19358333	37854167
First critical frequency (Hz)	57	159	249	361
2nd critical frequency (Hz)	355	637	806	995
3rd critical frequency (Hz)	995	1433	1681	1950
4th critical frequency (Hz)	1950	2547	2875	3223

Table 4: natural frequency calculation of the beam

3.3.1.3.4 Geometric error budget:

An estimation of the mechanism's geometric error budget looks as follows:

Number of axes, N	1							
Total allowable error, dtot (microns)	1000	what the customer wants from their machine						
				Apportion of error within each axis (amount allocated to each of X, Y, Z directions) to be determined by sensitive directions				
				Bearings (fb)	Structure (fs)	Actuator (fa)	Sensor (fs)	Cables (fc)
Source of error	Factor (f)	Apportion of error (dtot/f)	Apportion of error per axis	1	0.5	0.2	0.2	0
			Based on linear sum of errors					
Geometric, fg	0.40	333	333	175	88	35	35	0
Thermal, ft	0.50	417	417	219	110	44	44	0
Load-induced (deflection), fl	0.10	83	83	44	22	9	9	0
Process, fp	0.20	167	167	88	44	18	18	0
			Based on root square sum of errors					
Geometric, fg	0.40	590	590	511	256	102	102	0
Thermal, ft	0.50	737	737	639	320	128	128	0
Load-induced (deflection), fl	0.10	147	147	128	64	26	26	0
Process, fp	0.20	295	295	256	128	51	51	0
			Average (expected case) of linear and RSS					
Geometric, fg	0.40	462	462	343	172	69	69	0
Thermal, ft	0.50	577	577	429	215	86	86	0
Load-induced (deflection), fl	0.10	115	115	86	43	17	17	0
Process, fp	0.20	231	231	172	86	34	34	0

Table 5: geometric error budget

As seen in Table 5 above, the most influential factors on the mechanism's error are the geometric errors and the thermal errors. This is because the mechanism is supposed to have high speed, which might drive the temperature higher. On the other hand, the deflection and process errors have minimal effects because the mechanism is relatively light and small. The sliding rod is 1/8 inches in diameter and the transported mass of polymer is 10 milligrams, so minimal deflections are expected.

3.3.2 Sliding mechanism selection

3.3.2.1 Comparison of five design strategies

These are some sketches for the different design strategies considered:

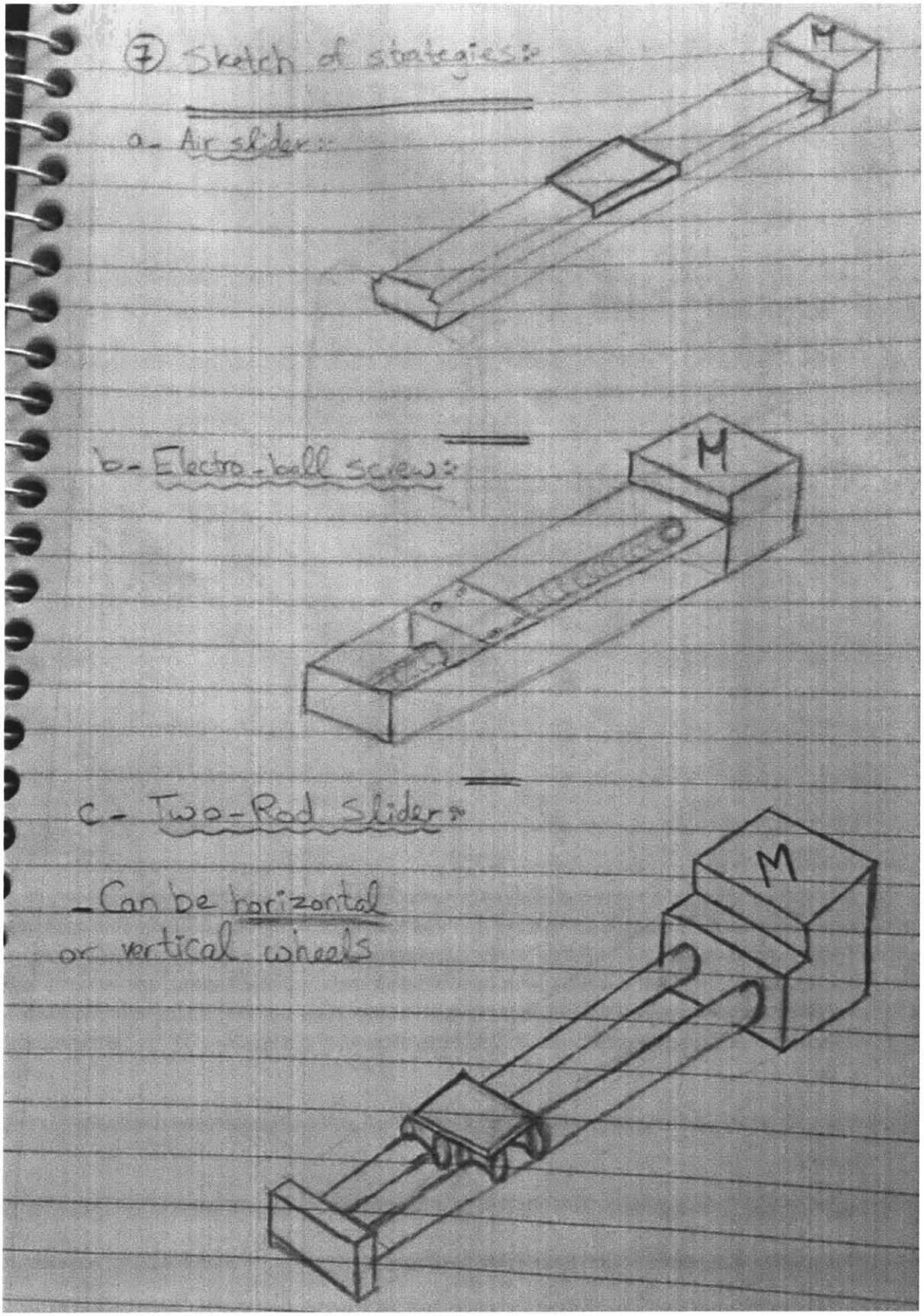
7 Sketch of strategies:
a- Air slider:
M
b- Electro-ball screw:
M
c- Two-Rod Slider:
- Can be horizontal or vertical wheels
M

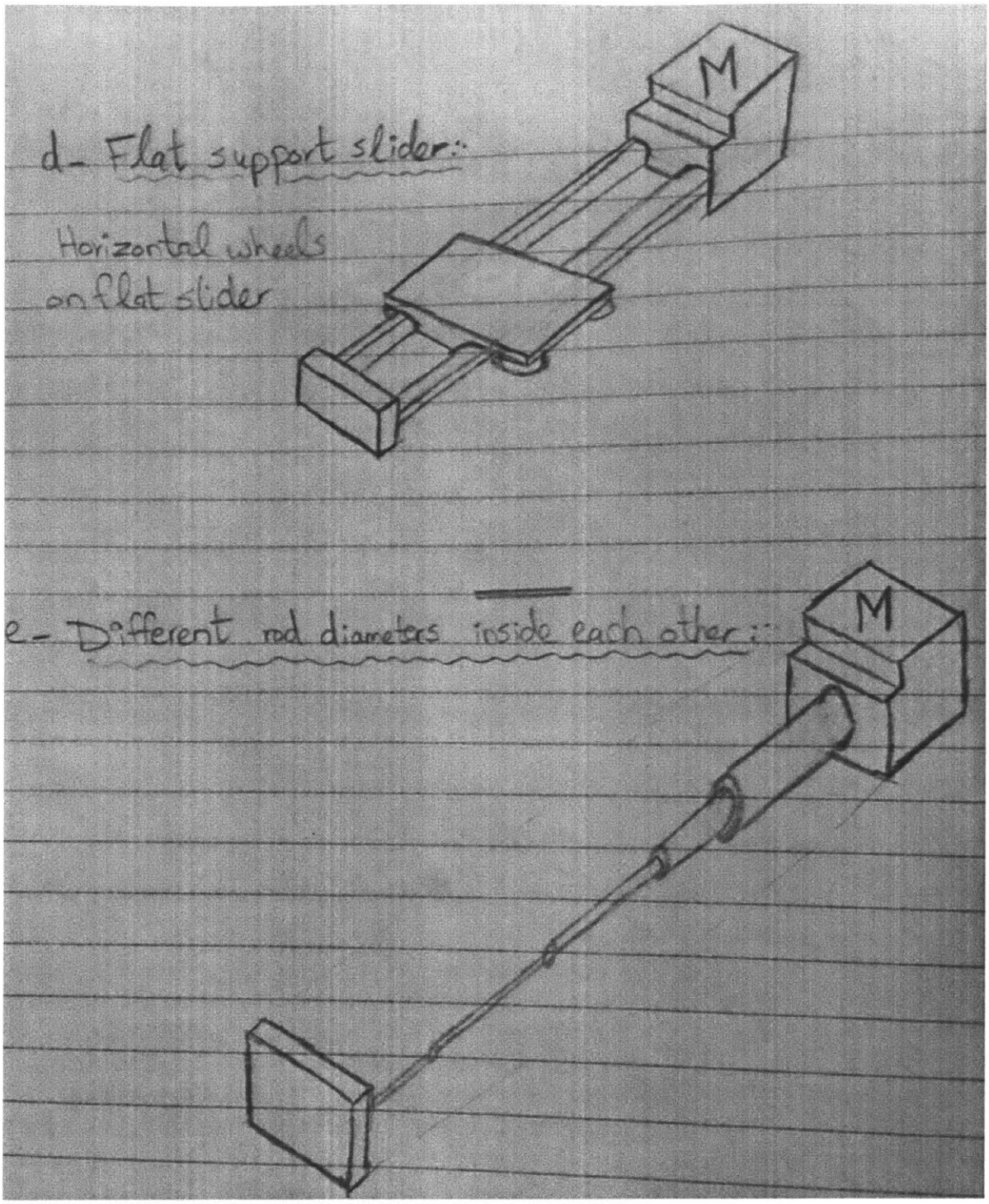

Figure 37: sketches of different sliding design strategies

A comparison between these designs is in this table:

No.	Strategy	Thoughts	Error
1	Air slider	Should be very accurate and rigid, but it has geometrical limitations of inserting the rod solely in the hole needs consideration.	Highest on X-axis (due to air pressure variation), and minimal on Y and Z-axis.
2	Ball screw	Guarantees high accuracy of the horizontal position, it should be very rigid, has low stiffness and geometrical error.	Minimal error but expensive
3	Two rod slider	May have less Y-axis accuracy than the other strategies according to the wheels motion and tolerance	Less weight, less stable
4	Flat support slider	Might have more deflection that the other cross-sectional geometries (because the low height [which is raised to the power of 3] will give lower Inertia and higher deflection)	Average good accuracy
5	Extending meshed rods	The challenges of polymer material getting stuck in	Not very accurate but great advantage of reducing the length

Table 6: comparison of the slider's five design strategies

The comparison between the errors of these five mechanisms in the 3-axis looks as follow:

No.	Strategy\Axis	X	Y	Z	Total
1	Air slider	--	+	-	-
2	Ball screw	++	+	-	++
3	Two-rod slider	+	++	-	++
4	Flat support slider	+	+	-	+
5	Different rod diameters	-	-	-	---

Table 7: comparison between the errors of the five design strategies

From the comparison above, the two top choices were the ball screw or the two-rod slider.

3.3.2.2 Narrowing down to two design strategies

On the power source side, the electrically controlled actuator was chosen over the pneumatic one because of its motion accuracy and variable speed control. This means that design (1) in Table 6 was excluded. The electric actuator could be used to trigger the

velocity of the slider at different stages, especially in the initial testing phase that needs quick accommodation to design changes.

On the sliding mechanism side, out of the five concepts above, design (5) was excluded because meshed rods will have complications with polymer sticking, and design (4) was excluded because it will produce more errors because of its low height and low moment of inertia. The remaining designs are designs (2) and (3), the ball screw and the two-rod slider.

A more detailed functional requirements table for the two-rod slider design looks as follows:

No.	Functional Requirements	Design Parameters	Analysis	References	Risk	Counter- measures
1	Meet the required range of motion	Slider, 2 stopper, and motor box	Calculate the required length and width	previous project work, EP and Design handbooks	insufficient length when adding extra supports	Have an extra safety length, it is fine if not the whole slider range is used thereafter
2	Correctly aligned with press and EP mechanisms	Machine structure	Calculating the required structure sizes using current geometrical and force constraints	Machine Design handbooks	Misalignment of the 3 parts	re-designing either the supports or the machine part, or adding a fitting in between (which could reduce the accuracy, so not a very good option)
3	Minimizing Y&Z wiggle of rod inside the hole	Rod and hole geometry and external supports	error aportionment and allowed range of motion	Machine Design handbooks	rod wiggling	additional rod guidance, re-design rod/hole shape into conical or different cross-sectional areas
4	Minimal geometrical error	Sliding box and slider interface	Analyze various geometries	Course notes, Machin	Yaw, pitch, roll,	Adding additional fittings for desired tolerance

	between sliding box and slider		and choose the most stable	e Design handbooks	and straightness errors	achievement, rollers lubrication
5	Minimzing the force required to move it	sliding interface analysis	frictional force to be overcome with rollers, fittings, or metal metal interface	Machine Design handbooks	Wear of sliding surface due to high friction	Add a replacable piece between the 2 sliders to be changed to reduce big parts maintenance
6	Variable speed control	Deceleration before stopping,fast without polymer and slow with polymer	Experiment speeds where the polymer could drip, fall off and design arduino control accordingly	EP and Machine Design handbooks	Jerk may affect the Abbe' errors	Test the various decelerations, and make sure all transitions are smooth enough, do not use option unless really needed

Table 8: updated functional requirements table for the two-rod slider

The functional requirements table for the ball screw would be the same as Table 8 except for number 4:

4	Minimal geometrical error between sliding box and slider	Sliding box and slider interface	Analyze various ball screw sizes and choose the most stable	Course notes, Machine Design handbooks	Yaw, pitch, roll, and straightness errors	Adding additional fittings for desired tolerance achievement, rollers lubrication

Table 9: updated functional requirements table for the ball screw

After a more detailed risk analysis, we have the following three risks:

1) **Rod/hole misalignment**: it could make the rod hit the die cavity's sides rather than get into the hole.
   Countermeasureà Using extra roller/guiders to keep it on the way and planning minimal error in my error budget
2) **Polymer left behind**: it could happen is the rod and hole are misaligned while the rod slides back from electrospinning
   Countermeasureà Designing a cone shaped hole entrance. This will enhance the polymer flow and have minimal polymer loss.
3) **Polymer left overs**: it will affect the accuracy and repeatability of the mechanism
   Countermeasureà Having a sweeper around the rod before going back to

electrospinning. This should get off any polymer remains and decrease errors .

Some numerical calculations of these risks gave:

Design:

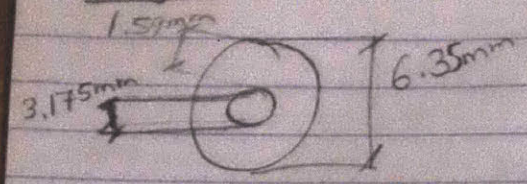

clearance = 3.175mm

All. Height incr/dec = 1.59 mm

Misalignment ① (Z-axis)

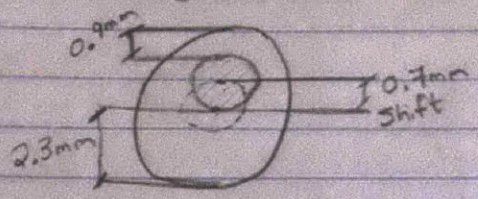

If middle rod shifts up for 0.7mm:

$$\% \frac{\text{error Height}}{\text{Max. All.}} = \frac{0.7}{1.59} \approx 44\%$$

* The problem is not only in the height error, but the attached polymer on the rod could probably not fit into the whole!

⇒ Assuming polymer thickness is 1mm, so through the top part 0.9mm passed from the 1mm thickness, which will look as follows:

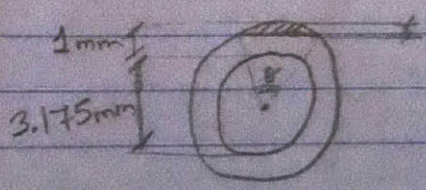

H = 20cm = 200mm

$$\forall \text{ of polymer} = \pi r_B^2 H - \pi r_S^2 H$$
$$= 200\pi\left(4.175^2 - 3.175^2\right)$$
$$= 4618 \text{ mm}^2$$

→ For $\theta = 45° = 0.785$ rad

$$\text{chord } L = C = 2R\sin\frac{\theta}{2} = 2\left(\frac{5.175}{2}\right)\frac{0.785}{2} = 2.03 \text{ mm}$$

$$\text{A circular sector} = \frac{R^2}{2}(\theta - \sin\theta) = \left(\frac{5.175}{2}\right)^2 \cdot \frac{1}{2}\left[0.785 - \sin(0.785)\right]$$
$$= 0.26 \text{ mm}^2$$

$\forall_{sector} = 0.26 \times 200\,mm$
$= 52.4\,mm^3$

$\frac{\forall_{lost}}{\forall_{total}} = \frac{52.4}{4618} = \underline{1.13\%}$ error in pill's weight!

Misalignment ② (Y-axis)

Since polymer is circularly wrapped around the rod, any slight motion in the y-direction will have the same effect

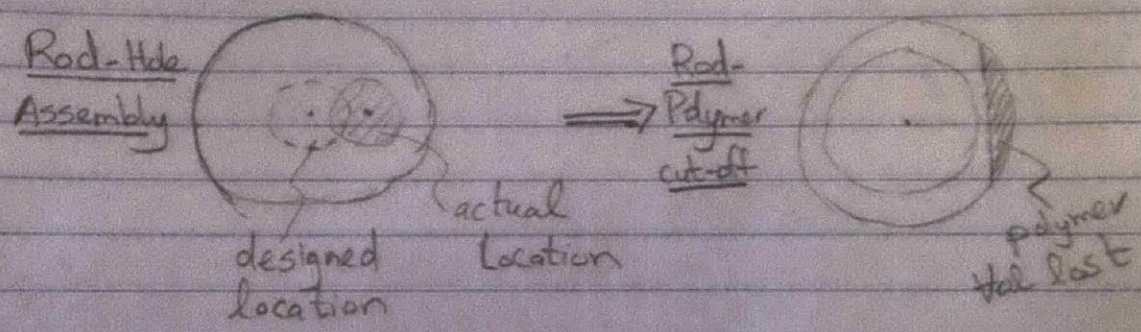

Mis alignment ③ (Y-Z axis mix)

A mix of the 2 errors occuring together

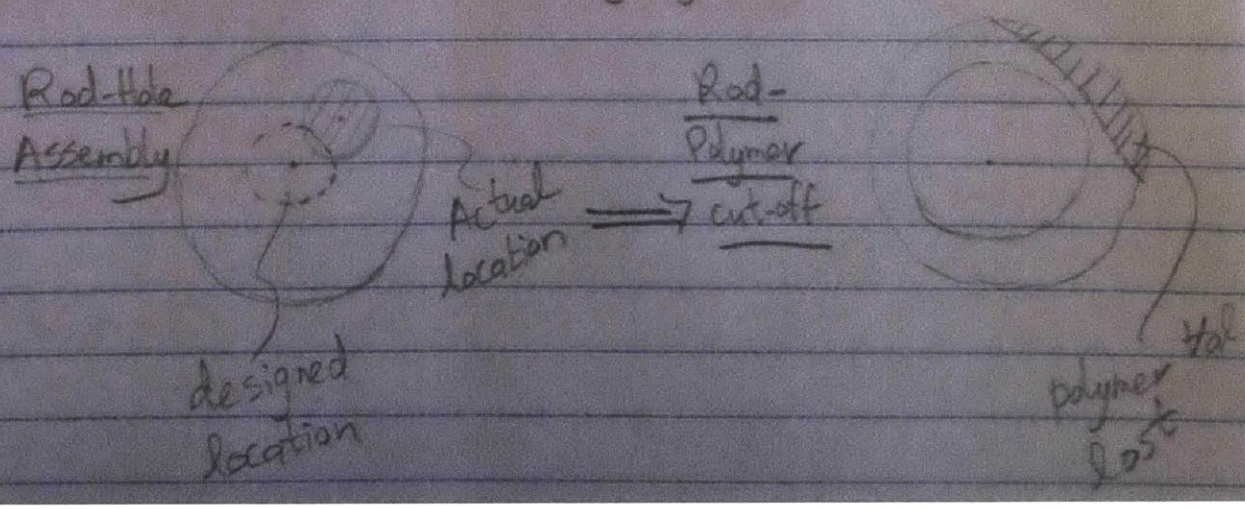

Figure 38: numerical calculations of the polymer/hole accuracy risk

These preliminary calculations showed the effect of the Y or Z-axis errors on the accuracy of the pills' masses. The shape of polymer lost would be more circular but it was linearized to ease of calculations for first order estimates.

Comparing other user centered aspects of the two mechanisms gives:

	Two-rod Slider	**Ball Screw**
Safety	The 2 rods need to be enclosed inside a body to avoid personal contact	Safer-All sliding components inside the bearing
Wiring	Could be in or out	Could be in or out
Weight	Can be set for high/low, could probably be low	Ball screw will probably have higher weight due to
Ergonomics	The two rods make a balanced concentrated weight on both sides	Screw mechanism and housing container needed
Stability	Less stable- Components are externally attached together	More stable-Mechanical components internally attached together
Price	Could be cheap	More Expensive
Stiffness	Lower- could be variable	Higher

Table 10: user centered comparison between the two top designs.

It has been decided to move further with the two-rod slider because it will be home made in MIT's hobby shop, it will be more flexible for future design changes, and more alignment components will be added to increase its precision and accuracy.

3.3.3 Driving Mechanism of the linear actuator

The numerical requirements of the mechanism were as follows:

Factor	Value	Reason
Maximum slider velocity	20 cm/s	For a total travel time of 3 seconds required by Novartis
Slider Travel distance	75 cm	For electrospinning and press lengths
Total slider length	100 cm	For the slider, motor mount, and side supports

Table 11: numerical requirements of the mechanism

The two top choices for the driving mechanism were:

1) A belt drive.
2) A ball screw.

To compare the two systems, their stiffness, rpm, and torque was analyzed. The mechanism with the maximum stiffness, minimal rpm and torque should be the best fit.

The stiffness was calculated using this equation:

Fixed-fixed

$$\frac{1}{k} = \frac{1}{k_s} + \frac{1}{k_N} + \frac{1}{k_{B1} + k_{B2}} + \frac{1}{k_{H1} + k_{H2}}$$

k: Axial rigidity of linear motion system [N/m]
k_s: Axial rigidity of screw shaft [N/m]
k_N: Axial rigidity of nut [N/m]
k_B: Axial rigidity of support bearing [N/m]
k_H: Axial rigidity of support housing [N/m]

Equation 6

For ball screw:

Components	Stiffness	
Supports Housing (2)=	1,130,000	
Bearing (2)=	355,000	
Threaded rod=	566,188	N/m
Threaded nut=	42,000	
Total stiffness=	34,000	N/m

Table 12: stiffness calculation of the ball screw

For belt drive:

Components	Stiffness	
Supported Housing (2)=	113,000	N/m
Bearing (2)=	355,000	N/m
Belt drive=	212	N/m
Belt pulley=	6,600	N/m
Total stiffness=	205	N/m

Table 13: stiffness calculation of the belt drive

The stiffness of the belt drive system appears to be much lower than the ball screw due to the low stiffness of neoprene belt compared to high stiffness of the hardened alloy steel of the screw.

To calculate the torque and rpm requirements, the estimated volumes of the components and their material's density would be used to calculate the total weight of the sliding components. After having the weights, the forces needed to slide these weights using the belt or the screw would be calculated as follows:

Ball Screw Sizing, Torque, and RPM:

Masses:		
Mass of rod box:		
Lo	10	cm
Wo	10	cm
Ho	10	cm
Outer volume	1000	cm3
Li	9.5	cm
Wi	9.5	cm
Hi	9.5	cm
Inner Volume	857.375	cm3
Metal volume	142.625	cm3
Density	7.8	g/cm3
Mass=	**1112.475**	**g**
Mass of carriage:		
Lo	8	cm
Wo	8	cm

Ho	2	cm
Outer volume	128	cm3
Li	6	cm
Wi	6	cm
Hi	1.5	cm
Inner Volume	54	cm3
Metal volume	74	cm3
Density	7.8	g/cm3
Mass=	**577.2**	**g**
Mass of rod:		
Diameter	0.5	cm
Length	75	cm
Volume	14.72621556	cm3
Density	7.8	g/cm3
Mass=	**114.8644814**	**g**
Total Mass=	**1.804539481**	**kg**

Acceleration:		
Vo=	0	cm/s
V1=	20	cm/s
T=	0.1	s
A=	200	cm/s2

Forces:		
MA=	3.609078963	N
Rolling Frictional coeff=	0.003	
Weight=	17.70253231	
Frictional force=	0.053107597	N
Fnet=	3.555971366	

Deflection:		
F (weight) =	17.70253231	N
Length=	0.375	m
E (modulus of Elasticity)=	78000000000	Pa
I (Inertia)=	3.97608E-08	kgm2
Radius =	0.015	m
Deflection=	6.27102E-06	m
Stiffness=	567047.9881	N/m
Deflection/micrometers=	6.271023689	micrometers
Bearing's Max Clearance=	10	
Safe Bearings=	1	
Bearings FOS=	1.594635979	

Ball Screw Torque and RPM:

Ball screw Dimensions:		
Radius	19	mm
Lead	12.7	mm
RPS	15.7480315	
RPM	944.8818898	

Torque:		
For carriage rotation:	(F=ma)	
F=	3.55	N
R=	0.015	m
T=	**0.05325**	**Nm**
For rod rotation:		
R=	0.015	m
M=	4.13512133	kg
I=	0.000465201	
RPM=	944.8818898	
Rad/s=	98.94780011	
time=	0.01	s
Ang/ Acc.=	9894.780011	rad/s2
Tstart=	**4.603063037**	**Nm**
Ttotal=	4.656313037	Nm

Table 14: ball screw sizing

Belt Dimensioning, Torque and RPM:

Dimensions:		
Total Belt Length=	177.8	cm
Width=	3.81	cm
#Teeth=	18	
Pitch=	1.27	cm
Material=	Neoprene	
Pulley Outer Diameter=	7.9	cm
Pulley Inner Diameter=	4.75	cm
Perimeter=	24.81858196	cm
RPS=	0.805847813	
RPM=	48.35086879	

Mass of pulley:		
Do=	0.079	m
Di=	0.0475	m
W=	0.0381	m
V=	0.000119238	m3
Density=	7800	kg/m3
Mass=	0.930059084	kg

Torque:		
For carriage motion:	(F=ma)	
F=	3.55	N
R=	0.0395	m
T=	**0.140225**	**Nm**
For pulley rotation:		
R=	0.02375	m
M=	0.930059084	kg
I=	0.000262306	
RPM=	48.35086879	
Rad/s=	5.063291139	
time=	0.01	s
Ang/ Acc.=	506.3291139	rad/s2
Tstart=	**0.132813026**	**Nm**
Ttotal=	0.273038026	Nm

Table 15: belt sizing

From the results in Table 14 and Table 15 above, the rpm and torque comparisons would be:

RPM: for travelling at 20 cm/s, the ball screw needs to operate at **950 rpm** while the belt only needs **50 rpm** (Almost 20 times less)

Torque: for the given rpms above, the Torque required by the ball screw is **4.66 Nm** and the belt needs only **0.27 Nm** (Almost 17 times less)

The conclusion from this analysis would be proceeding with a belt driven system rather than a ball screw because:

1- The belt needed less rpm and less torque (almost 20 times less).
2- Due to reason (1), the belt mechanism would need a smaller motor and less power to drive the system
3- The high accuracy of the ball screw was not a hard requirement for this slider.

4- The ball screw would have higher accumulated error in the error budget because the system would be heavier, having more deflection in the long travel distance.
5- The ball screw would be an over-design for this application, in terms of motor sizing and required accuracy.

Further risks analysis

After choosing the belt driven mechanism, further risks specific to this design were analyzed in Table 16 below:

No	Risks	Counter Measures
1	Belt slack and tension change	1- Preload the belt before operation starts 2- Have an accessible access in structure for belt adjustment 3- Have a self- adjusting belt/movable pulley 4- Have an outside handle connected to belt tension to be rotated if needed
2	Carriage motion errors (Pitch, yaw, and roll)	1- Have 2 separate carriages to cancel each other's deflection errors. 2- Have 1 carriage of the correct length to avoid these errors. 3- Have the correct preload on kinematic bearings moving it. 4- Choose the correct kind of rails (flat, 2 tubes, maybe 2 belts if needed?)
3	Polymer leftovers getting into the mechanism	1- Adding an iris to strip off any left polymer. 2- Have a closed structure of casing around all mechanical and electrical components
4	Having moving motor with the carriage for the spinning	1- Building a gear mechanism to the rod guide support that meshes and rotates the rod at it s final position (check figure). 2- Having the motor attached on the outside with a complementing rod on the other side of motion (with the complication of adding more parts then) 3- Having a motor that meshes with the rod on the other side of the mechanism (better to keep my mechanism all together though!)

Table 16: risks of the belt drive design

For risk (1), counter measures 1,2, and 3 would be used. For risk (2), counter risk (3) would be used. For risk (3), counter risks 1 and 2 would be used. For risk (4), counter risk 1,2, and 3 would be further studied below to choose the most appropriate option. These three options are:

1- The meshing gears/coupling
2- The motor attachment to complementing rod.
3- The separate spin motor assembly on the electrospinning chamber's side.

The meshing gears/coupling design would look as follows:

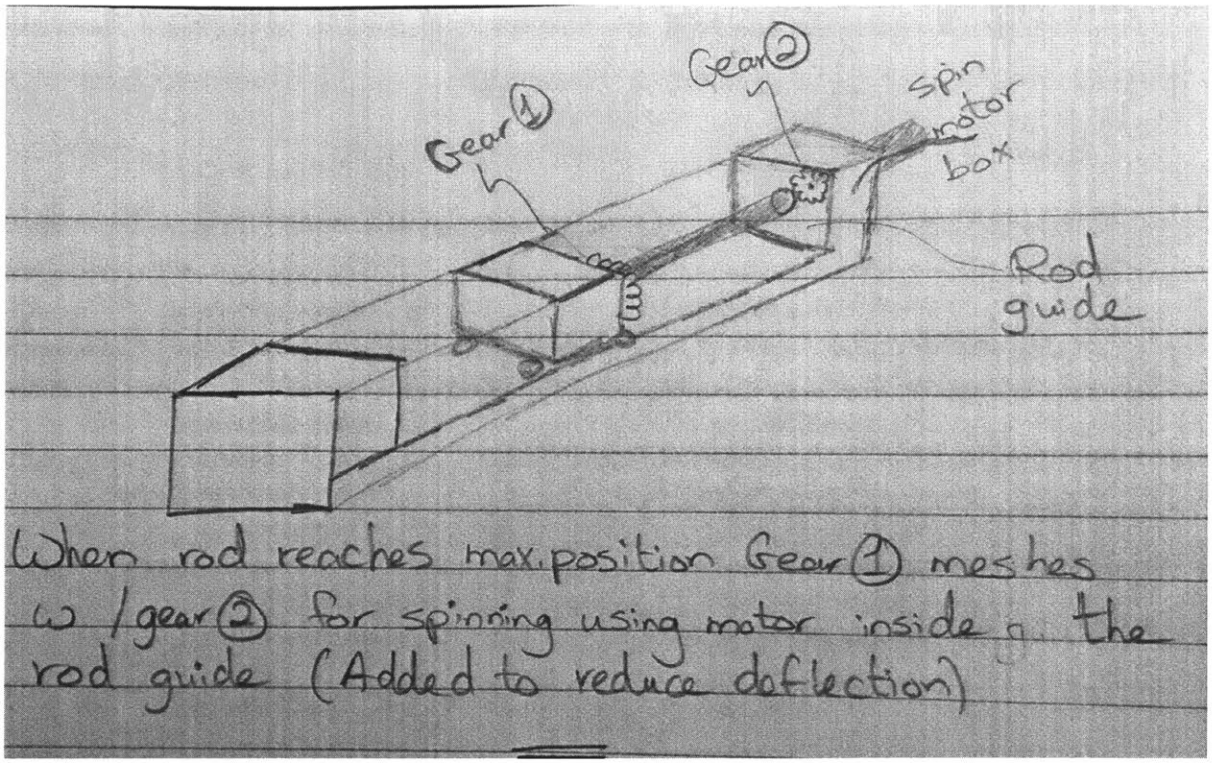

Figure 39: the meshing gears/coupling design

Attaching a motor to complementing rod would look as follows:

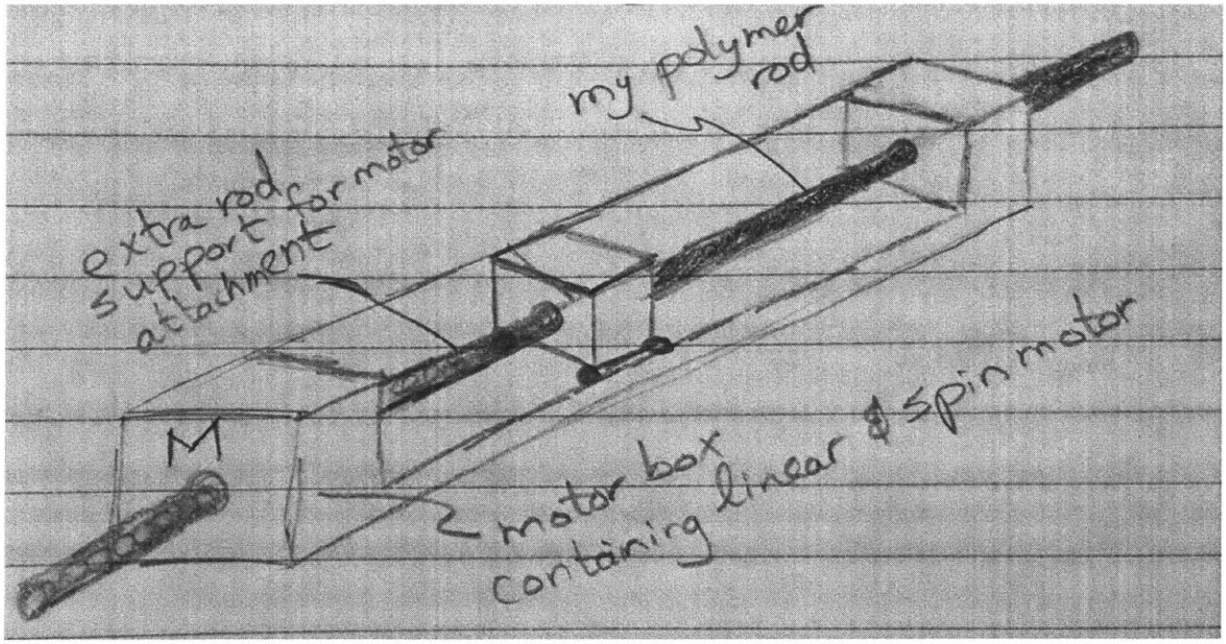

Figure 40: motor attachment to a complementing rod

The separate spin motor assembly on the electrospinning side would look as follows:

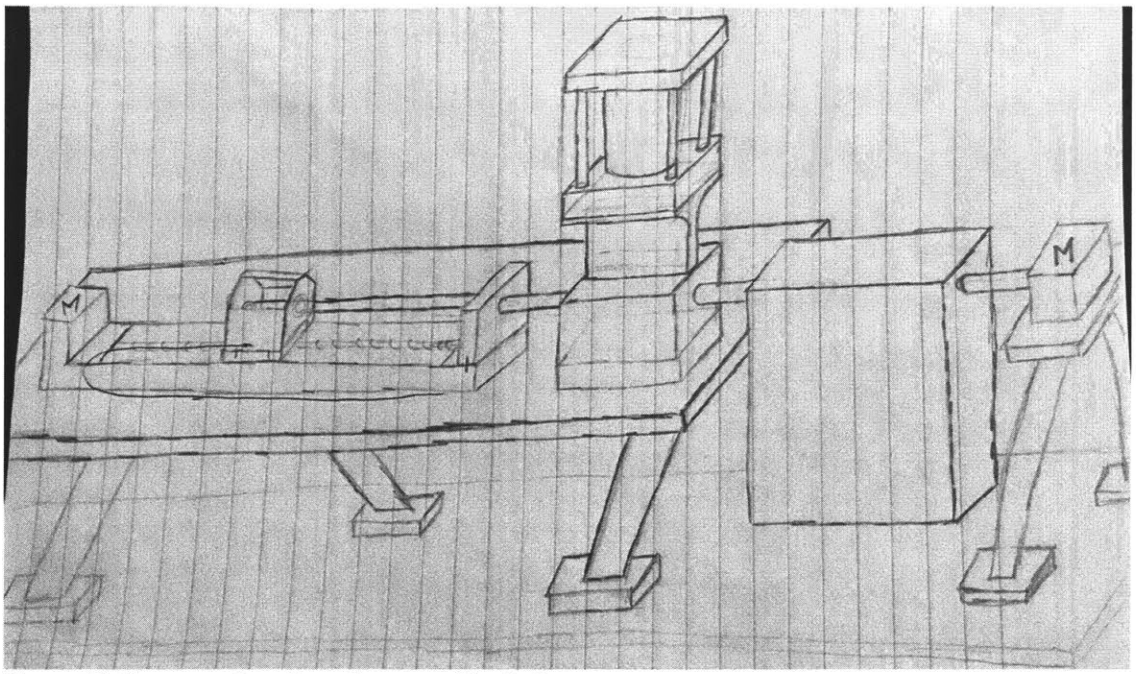

Figure 41: the separate spin motor assembly design

As seen in Figure 41, the separate spin motor assembly is the box with the letter M at the rightmost side of the assembly and the sliding motor is the box with the letter M on the leftmost side of the sketch. After comparing the three spinning ideas, shown in Figure 39, Figure 40, and Figure 41 above, the meshing gears/coupling design was chosen, because it has the least components and it keeps all the electrical controls in one side for ease of assembly, control, and safety.

3.3.3.3 Belt design calculations

After sizing the belt components, we will use their power and torque requirements to pick the most appropriate sliding motor.

The power and torque requirements look as follows:

Output/Requirements:	
Max speed (m/s)=	**0.10**
Travel length (m) =	**0.75**
Esmitated Belt Length (m)=	**1.65**

Belt and Pulley Dimensions:	
Total Belt Length (cm)=	**177.80**
Belt Width (cm)=	**3.81**
No. of Teeth=	**18.00**
Pitch (cm) =	**1.27**
Average Thickness (cm)=	**0.30**
Material=	**Neoprene**
Pulley Outer Diameter (cm)=	**7.90**
Pulley Inner Diameter (cm)=	**4.75**
Pulley's width (cm)=	**4.60**
Pulley's Perimeter (m)=	**0.25**
RPS=	**0.40**
RPM=	**24.18**
rad/s=	**2.53**

Torque:	
For slider acceleration:	
Slider Weight (kg)=	**0.36**
Tension Force (N)=	3.55
Radius (m)=	0.04
Slider Torque (Nm)=	0.14
For belt acceleration:	
Belt Volume (m3)=	0.00
Density of neoprene (kg/m3)=	**1600.00**
Belt Mass (kg)=	0.33
Tension Force (N)=	3.19
Radius (m)=	0.04
Belt Acc.Torque (Nm)=	0.13
Friction of linear bearings:	
Bearing's coeff of friction=	**0.002**
Weights of slider, belt, and pulley (N)=	15.86
Bearings Intrinsic Resistance Force =	**0.00**
Radius (m) =	0.04
Bearing's Frictional Torque (Nm)=	0.63
For the pulley's rotational acceleration:	
Radius (m)=	0.04
Mass (kg)=	0.93
Inertia (kg.m2)=	0.0007
Rot. Speed (RPM)=	24.18
Rot. Speed (Rad/s)=	2.53
Required Acc. time (s)=	**0.01**
Angdular Acc. (rad/s2)=	253.16
Starting Torque (Nm)=	0.18
Total Torque Needed (Nm)=	1.08
Motor Power Needed (W)=	2.73

Table 17: torque and power requirements for the sliding motor

The analysis in Table 17 showed that a motor with a minimum torque and power of **0.18 Nm** and **2.73 W** is needed. A Nema17 motor with the following characteristics looks like a good fit:

Manufacturer Part Number	17HS16-2004S1
Motor Type	Bipolar Stepper
Step Angle	1.8°
Holding Torque	45Ncm(63.7oz.in)

Rated Current/phase	2A
Phase Resistance	1.1ohms
Recommended Voltage	12-24V
Inductance	2.6mH±20%(1KHz)
Weight (kg)=	0.31
Rotor Inertia (g/cm3)=	54

Table 18: Nema 17 motor characteristics

This motor has a holding torque of 0.45 Nm and the torque requirement is 0.18 Nm, so it should be a good match.

This motor's frequency was then compared to the natural frequency of the mechanism to make sure they will not resonate. The natural frequency was calculated using the equation below:

$$\omega_n = \sqrt{\frac{k}{m}}$$

Equation 7

Natural Frequency:	
Modulus of Elasticity (E) =	200000000000
I (linear direction) =	0.00000000002593
Length (m) =	0.0042
Stiffness (N/m)=	210000000
Mass(kg)=	0.31
Natural Frequency (rad/s)=	26027

Table 19: the mechanism's natural frequency

The calculation in Table 19 showed that the natural frequency of the mechanism is much higher than the planned speed, so the motor should be stiff and stable enough.

<u>Clamp Design:</u>

The belt was purchased from BrecoFlex, so the following options from BrecoFlex' s catalogue were reviewed to choose the most appropriate clamp:

Aluminum Plate Dimensions - XL, L, H

PITCH	F inches	D inches	B inches	A inches	S inches	Belt Width C (inches)								
						025	037	050	075	100	150	200	300	400
XL	0.24	0.22	0.14	1.67	0.31	1.00	1.12	1.26	1.50	1.77	-	-	-	-
L	0.31	0.35	0.20	3.02	0.59	-	1.41	1.54	1.77	2.03	2.52	3.03	-	-
H	0.39	0.43	0.35	4.21	0.87	-	-	1.77	2.00	2.26	2.75	3.26	4.25	5.27

Table 20: BrecoFlex clamps dimensions

The clamp's dimensions P, F, D, B, A, S, and C are shown in Figure 42 below:

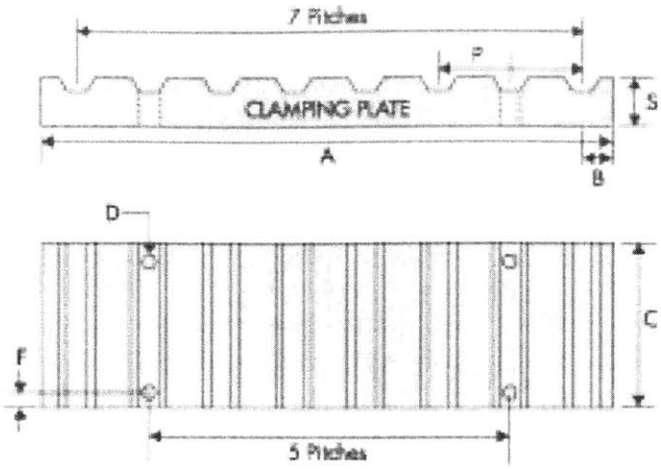

Figure 42: BrecoFlex clamp geometry

Belt clamp (L) was chosen because it fitted into belts of widths between 1.41 and 1.54 inches, and our required width was 1.5 inches. Its total length (A) was 3.01 inches and its height (S) was 0.59 inches. Using these dimensions to calculate the volume, and comparing this volume to the density of aluminum gave a clamp mass of 0.046 kg.

<u>Bearings Design:</u>

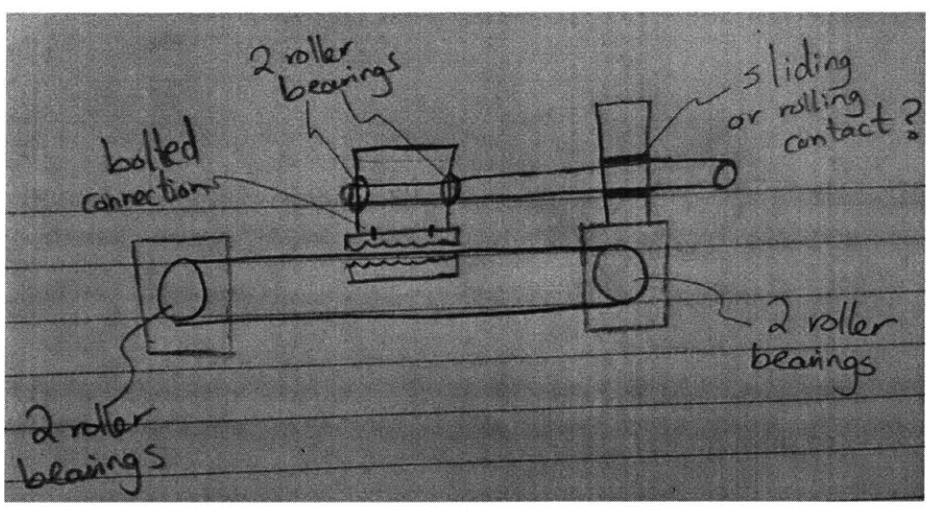

Figure 43: sketching the required bearings

To size the four roller bearings on the pulley's shafts, the following calculations were carried out:

Bearing loading:	
Torque (Nm) =	0.45
Fr (N) =	9.47
Fa (N) =	2.567
Rot. Speed (/min) =	24.18

Bearings geometry:	
Bearing ID =	SKF Deep groove ball bearing ID 9
D in (mm) =	5
D out (mm)=	16
Width (mm) =	5

Table 21: sizing of the shaft's roller bearings

For the current loading, choosing the smallest bearing of inner diameter 3 mm would have a factor of safety of 18, but a bigger bearing was chosen to match the motor's shaft diameter of 5 mm and be easier to assembly. This bigger bearing has a safety factor of 40.

For the two roller bearings between the polymer rod and the sliding box, an analysis using the MiTCalc software gave the following output:

Bearing loading:	
Torque (Nm)=	0.603315
Fr (N)=	0.40221
Fa (N)=	0.40221
Rot. Speed (/min) =	60

Bearings geometry:	
Bearing ID =	SKF Deep groove ball bearing ID 1
D in (mm) =	3
D out (mm)=	10
Width (mm) =	4

Table 22: sizing of the rod and sliding box's roller bearings

The only load on these bearings was the mass of the rod, which was very low. Using the smallest SKF bearing, of inner diameter 3 mm, would have a factor of safety of 450.

The rotational speed of 60 rpm was used above was a higher estimate of the expected speed of 10 rpm. The accurate number would be found out through further electrospinning experimentation, but it should be between those two values.

The spinning mechanism's design:

This mechanism needs to allow the rod to slide and rotate inside the system, an initial sketch of the components looked as follows:

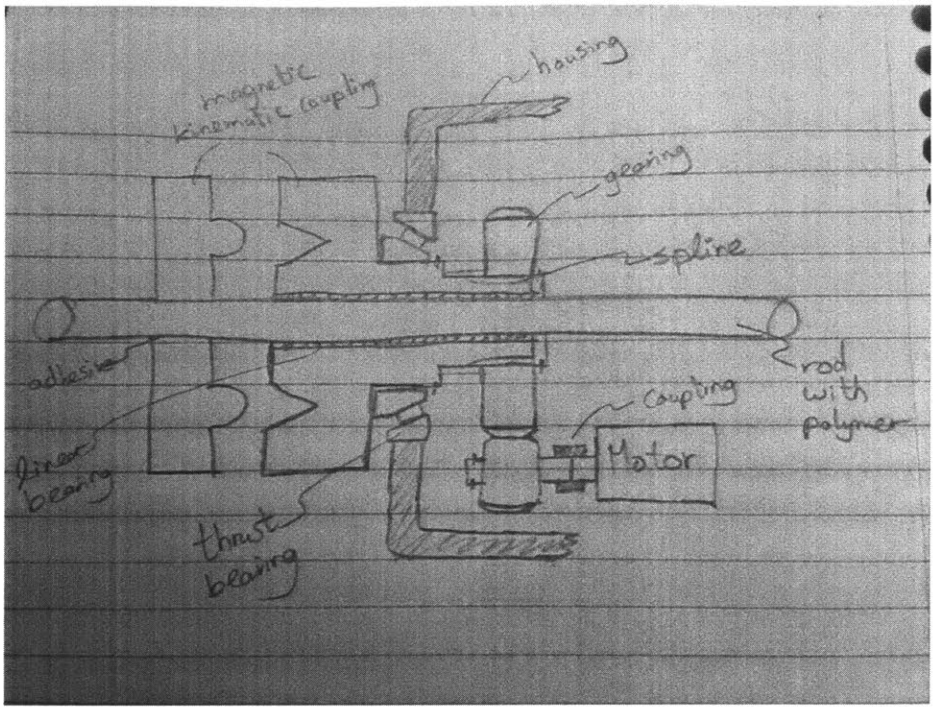

Figure 44: sketching the spinning mechanism

The loading on those thrust bearings was used to size them as shown below:

Bearing loading:	
Torque (Nm)=	0.45
Fr (N)=	60
Fa(N)=	0.299
Rot. Speed (/min) =	40

Bearings geometry:	
Bearing ID =	SKF taper roller bearing ID 1
D in (mm) =	15
D out (mm)=	42
Width (mm) =	13

Table 23: sizing the thrust bearings

The bearings' capacity was compared to their loading to calculate the expected bearing life

as seen below:

Bearing Location	Load capacity	Applied Load	Bearing life (hours)
Belt pulley/Motor shaft	1140	11	5.2E+06
Rod/Rod box	540	0.4	2.7E+10
KC and housing	22400	300	3.7E+08

Table 24: bearing life calculation

This bearing life table shows that the chosen bearings have a very long expected life of more than 5,000,000 hours each, and that the bearing with the shortest life is the pulley's shaft one.

Structure design:

The required dimensions of the belt's structure are:

Dimensions:	
Structure Length (mm) =	1300
Belt Travel Length (mm) =	800

Table 25: dimensions of the belt's structure

The forces applied on these structures looked as follows:

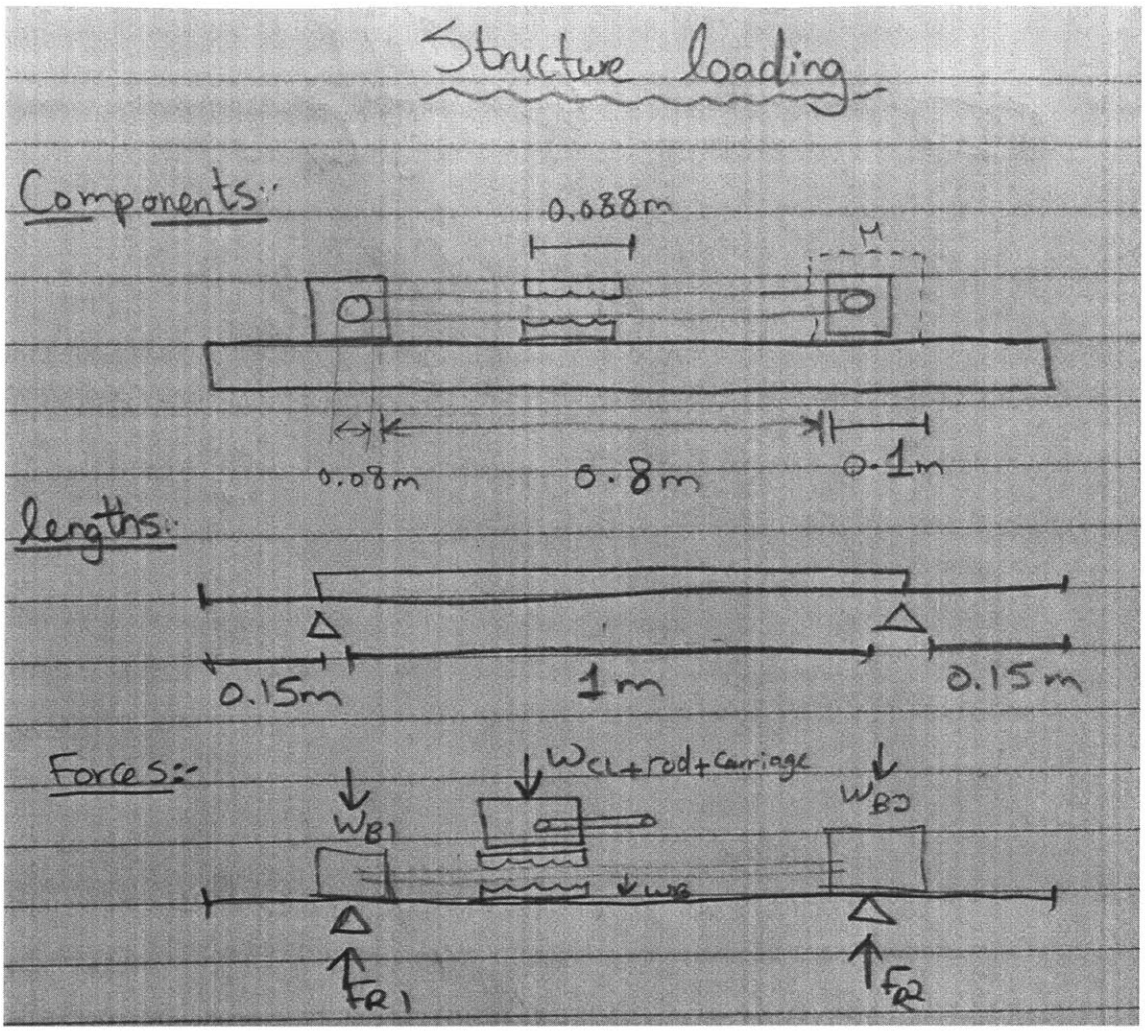

Figure 45: sketch of the forces applied on the structure

The estimated values of these forces would be:

Forces:	
Belt Weight (N)=	3.53
Clamp weight (N)=	0.45
Rod box weight (N) =	10.91
Rod weight (N) =	1.13
Pulley weight (N) =	9.12
Pulley box weight (N) =	15.40
Motor weight (N)=	3.04
Distributed Forces:	
Belt Weight (N/mm) =	0.0044
Torque:	
Moment by Motor (Nm)=	0.45

Table 26: values of forces applied on the structure

The deflection of wood versus steel structures were calculated using MitCalc software, and this was the software's output:

	EC3 steel deflection (mm)	Oak Deflection (mm)
With supports outside of edges:		
Central loading	0.02	0.06
Loading at 2/3 travel distance (motor side)	0.023	0.058
End loading (motor side)	0.022	0.051
With supports 100mm inside of edges:		
Central loading	0.003	0.014
Loading at 2/3 travel distance (motor side)	0.003	0.014
End loading (motor side)	0.004	0.021
With supports 50mm inside of edges:		
Central loading	0.003	0.004
Loading at 2/3 travel distance (motor side)	0.003	0.014
End loading (motor side)	0.003	0.008

Table 27: deflections of various structural loading using steel versus wood

The results in Table 27 have shown that the best location for the supports is 50 mm on the inside of the actuator's edges. This gives only 0.003 mm deflection when the belt clamp is in the middle, halfway, or even close to the edges. The other observation is that steel always had less deflection than wood, so it is a better candidate material for the structure.

Putting these design details together gave an updated CAD drawing for the mechanism that looked as follows:

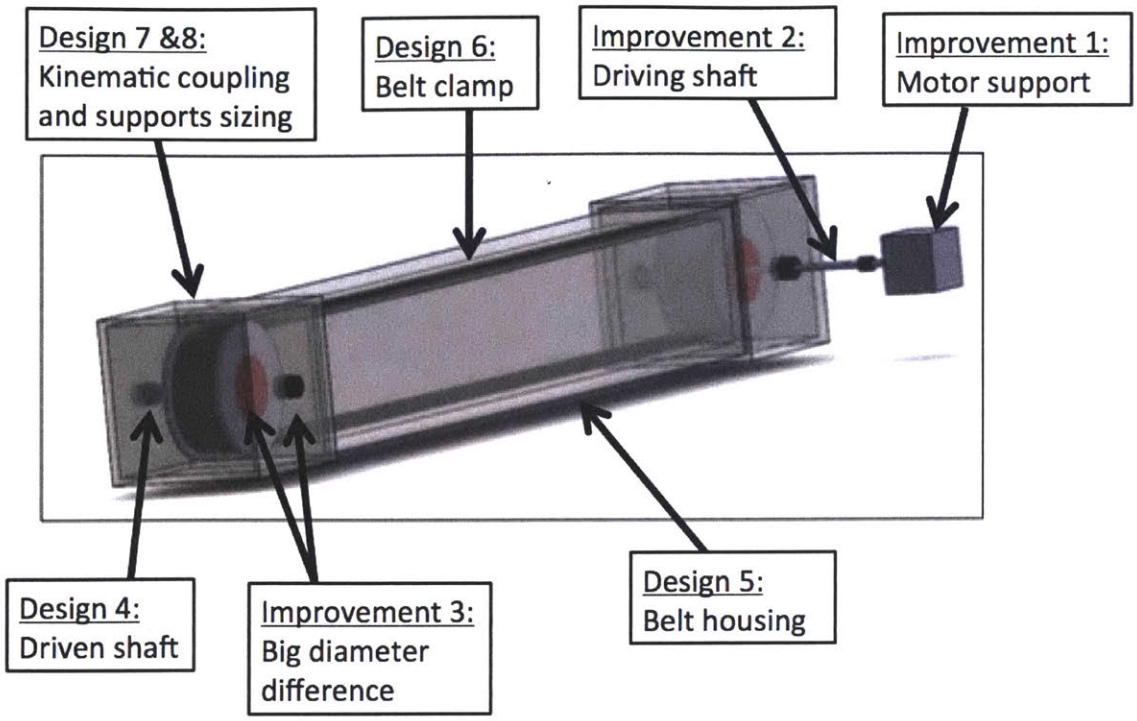

Figure 46: proposed SolidWorks CAD for the linear actuator design

This solid works model gave us a lot of insights about additional parts and calculations to be carried out. Some of the improvements are:

1- Motor support box needs to be at the same height as the pulley box.
2- Detailed design of the driving shaft that connects the motor to the pulley needs to be re-assessed.
3- The inside diameter of the pulley of 50 mm and the motor shaft diameter of5 mm needed a coupling with a huge variation in the radius.

Some of the additional parts to be designed were:

4- Designing the shaft on the other side, which connects the pulley center and the side bearings.
5- Sizing of the belt housing (long rectangular box) relevant to the belt's pulley boxes (2 side boxes) to account for load distribution on both and leave spaces on the sides for the linear axis end of travel braking.
6- Analyzing different geometries for the belt clamp to slide on this housing so that it

is in contact with the belt, but at the same time the belt is sealed inside to protect it from dust.

7- Designing the kinematic coupling as an additional box on top of one of the side boxes. It would have higher electrical safety if it is at the same side of the sliding motor, or it will have less vibrational effects if it is on the other side of the sliding motor.

8- Redesigning the side boxes to accommodate any limitations of the kinematic coupling design.

3.3.4 CAD modeling

As discussed in the early analysis stage, it has been decided to choose:

- An *electromechanically driven system* over pneumatic and hydraulic because it is cleaner, simpler, and easily controlled at this early prototyping stage.
- A *belt driven system* over a lead screw because it needs less power, less rpm, and is more suitable for my high-speed application.
- S *double rod slider system* because it is cheap and flexible in changing sizing and designs.
- A *spur gear spinning* mechanism because it needs fewer parts than kinematic coupling and would work with misalignments better than bevel gears.

Moving to the CAD modeling stage, the belt components (from BrecoFlex) were placed with the auxiliary components (from McMaster)and the rest of the machined components. This CAD model will keep evolving until the final sizing and design is reached.

Design 1:

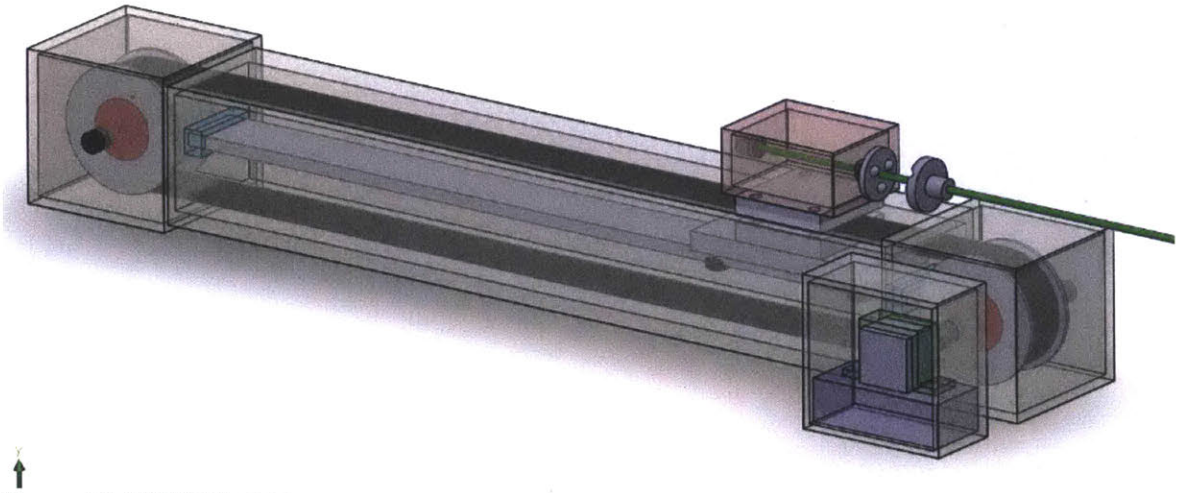

Figure 47: 1st CAD Design

This first design, shown in Figure 47, was made to show the whole system. It had a flat middle slider and a carriage rolling on four wheels. The spinning engagement method was a kinematic coupling. It still does not have specific parts like its shaft and its spur gears. It has been decided to remove the kinematic coupling and spin the rod directly with spur gears because it is simpler and more flexible. The rolling wheels have also been switched to linear bearings on two sliding rods because they have better sliding engagement and less error.

Design 2:

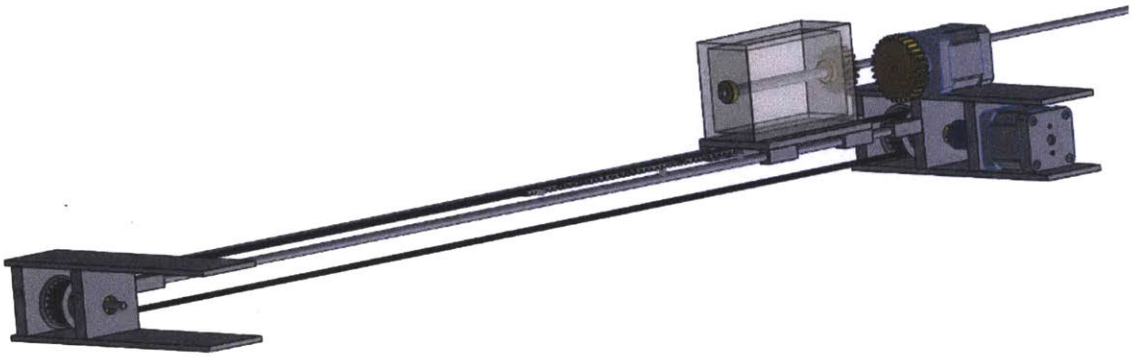

Figure 48: 2nd CAD design

After changing the spinning mechanism to a direct gear mesh and the sliding mechanism to the two-rods mechanism, as seen in Figure 48. We began thinking about a carriage design that provides the required stiffness and weight. This could be a box, a C-section, or two flat plates. After evolving the design to this stage, we decided that we did not need this whole box sliding back and forth, but we could design a smaller and flatter carriage. We also started getting concerned with the alignment to make sure the rails would be straight enough.

Design 3:

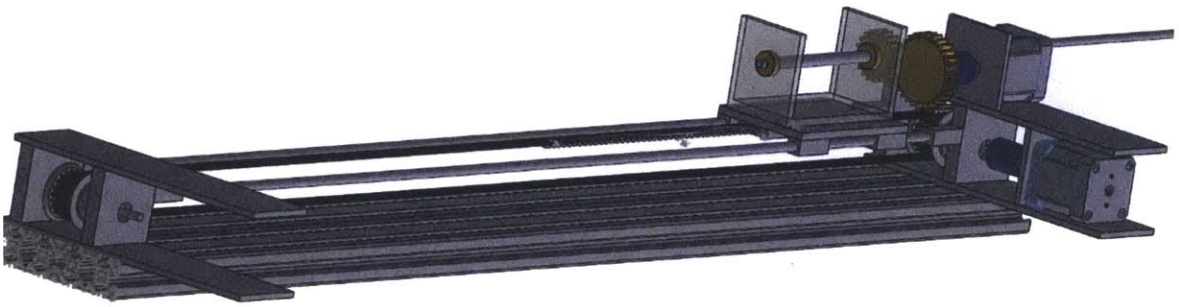

Figure 49: 3rd CAD Design

In the 3rd design, shown in Figure 49, we decided to use t-slotted aluminum structures as a base to give us the required straightness. We were not sure how wide it should be, and how it should be mounted to the structure. We were also not sure how it would interfere with the guiding rails and the belt's motion. We changed the carriage to a C-section and added the spinning motor mounts.

Design 4:

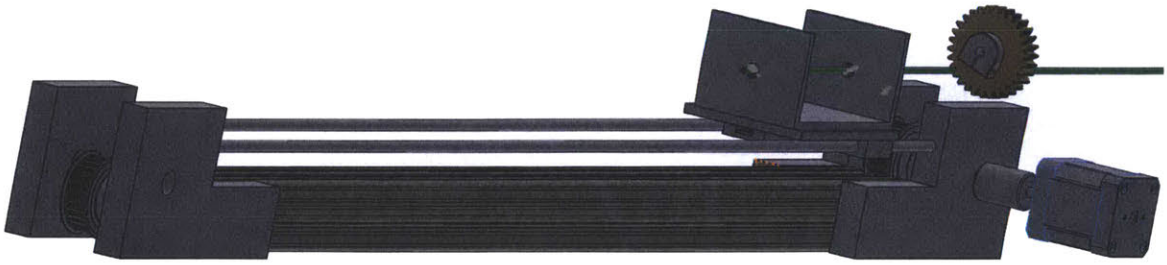

Figure 50: 4th CAD Design

In the 4th design, we managed to wrap the belt mechanism around the 1.5 inch t-slotted aluminum structure, as shown in Figure 50. Thus, the bottom half of the belt was in the aluminum's bottom slot. But we still had to calculate the most efficient spacing between the sliding rods and the belt system and find the optimum shape of the carriage having minimum number of parts and maximum stiffness.

Design 5:

Figure 51: 5th CAD design

The carriage design was updated, as seen in Figure 51. It was re-designed so that the carriage and the linear bearings' housing were merged to be one part. The pulley was also changed for a bigger one of 40 mm hub diameter rather than 30 mm. This bigger pulley helped move the carriage upwards, and move the sliding rails downwards. Then the belt and the rails were all in line, to avoid any motion errors. We have also enhanced the motor's housing from two parallel sheets to a U-section giving it more stiffness and less weight.

Design 6:

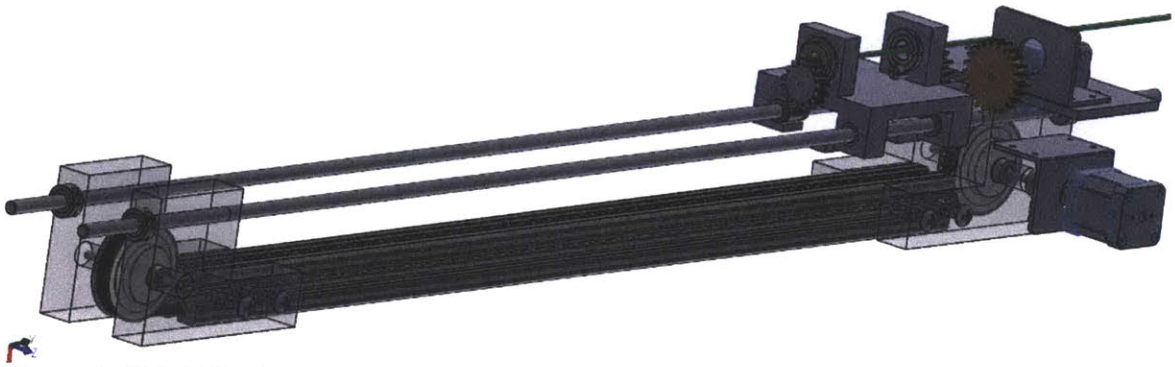

Figure 52: 6th CAD Design

In the 6th design, the carriage was compacted to be a smaller piece and reduce the machining time. The sides of the square shaped carriage were also removed because it was too much weight to be pulled back and forth. The heights of motor mounts were also adjusted accordingly, to fit the required gear mesh with the new carriage design.

Design 7:

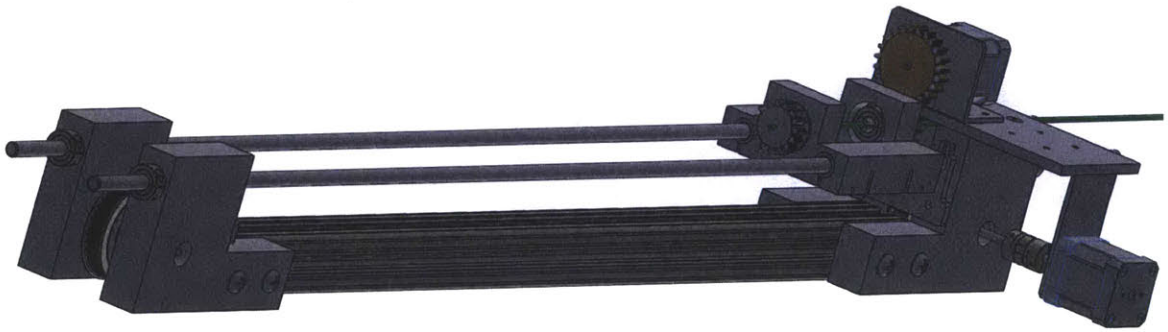

Figure 53: 7th CAD Design

In this semi-final design, Slocum's concept of reciprocity (flip the part if you are not so happy with it!) was used:

$$\frac{1}{☹} = ☺$$

Equation 8

The gear and the linear bearings were flipped to be almost in line. The output rod was also flipped to be under the top support rather than above it, which brought it closer to the linear bearings. In the final design, the motor support was changed to a rectangular tube, the spinning motor's mount was meshed into the top support, and the linear bearing support was moved below the top support for ease of assembly.

3.3.5 Final design components

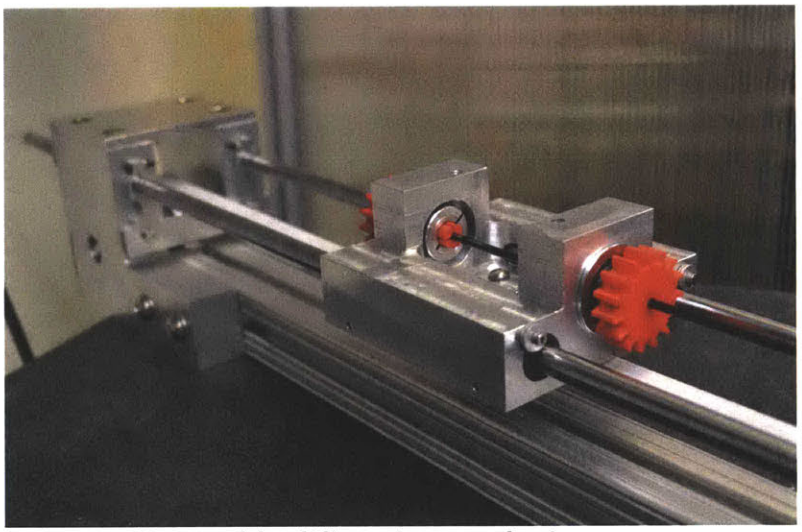

Figure 54: a real image of the sliding spinner mechanism

An **electro-mechanical mechanism** was chosen over a pneumatic one due to its higher positional accuracy and variable speed control, as discussed in earlier sections. For the driving mechanism, a **belt driven mechanism,** was found to be the most appropriate because it would require the minimal motor requirements. The sliding Motor (Part 9) was attached to the pulley's shaft (part 12) using a coupling. This shaft rotates the pulleys (part 14), moving the belt (part 11) accordingly. These components are visible in Figure 55 below.

Sliding Mechanism:

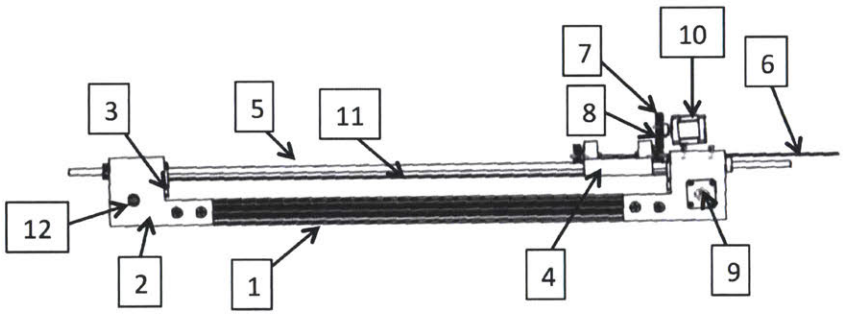

No.	Part
1	T slotted Aluminum
2	Side supports
3	Flexure bearing
4	Carriage
5	Rails
6	Polymer rod
7	Driving gear
8	Driven gear
9	Sliding Motor
10	Spinning Motor
11	Belt
12	Pulley's shafts
13	Pulley
14	Belt Clamp
15	Spinning Motor Mount

Figure 55: The sliding spinner's parts

For the sliding mechanism, we have chosen the **double sliding rails** (part 5) because the CNC machine could monitor its precision and straightness, and because it was easy to manufacture in the MIT machine shop. Those sliding rails were mounted on the side supports (part 2) and machined on the CNC mill with a precision of 0.001 inches. To ensure straightness of the rails, the mechanism was mounted on T-slot aluminum structure (part 1) because of its precise straightness is 0.0125" per foot of length and its commercial availability. Additional flexure bearings (part 3) were mounted on the side supports (part 2) for more precise straightness. On these sliding rails (part 5), the carriage (part 4) slides on self-aligning linear bearings with a misalignment capability of 0.5°. This carriage is moving the polymer rod (part 6) back and forth into and out of the electrospinning chamber.

3.3.6 Design equations

The sliding motor's design was governed by the equation:

$$T_{sl} = F_{sl} * R_{py}$$

Equation 9

where T_{sl} is the sliding motor's torque requirement, F_{sl} is the sliding force, and R_{py} is the radius of the belt's pulley. F_{sl} can be calculated by:

$$F_{sl} = (\mu_{slb} * W_{sl}) + F_{str}$$

Equation 10

where F_{sl} is the sliding force; W_{sl} is total weight of the sliding components including the carriage, its attached gears, and couplings; F_{str} is the force with which the strippers press on the rod.

Substituting these numerical values in Equation 10:

Sliding mass [kg]	1.8
Rolling frictional coefficient	0.003
Sliding Force [N]	**0.053**
Pressure by the strippers [KPa]	103
Diameter [m]	0.003
Thickness [m]	0.01
Area of contact [m2]	7.8125E-06
Strippers' Force [N]	**0.805**
Sum of strippers and sliding forces [N]	**0.858**

Table 28: sliding forces calculations

$$F_{sl} = (0.003 * 17.66) + 0.858 = 0.91\ N$$

Multiplying this force by the pulley's radius of 40 mm, gave the following torque:

$$T_{sl} = 0.91 * 0.04 = 0.036\ Nm$$

This torque is much less than the Nema 17 motor's capacity of 0.45 Nm, so this calculation verified that the Nema 17 motor was a good fit for the design.

Spinning Mechanism:

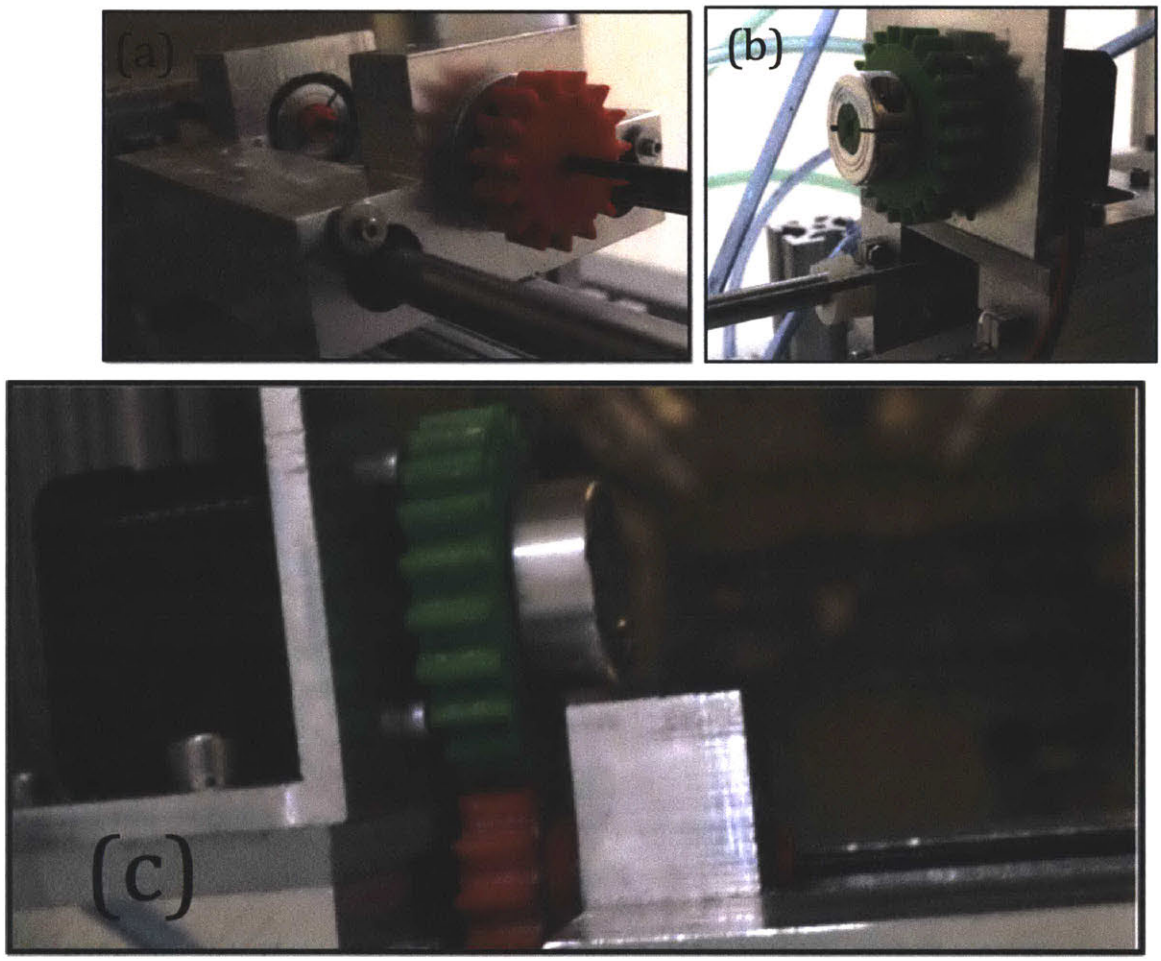

Figure 56: The filleted gears coupling (a) driving gear (b) driven gear (c) driving and driven gear meshed

The polymer rod needs to spin only when it is at the rightmost position of the slider, when the rod is fully contained in the electrospinning_chamber. The most traditional way of spinning the polymer rod would have been to install a spinning motor in the carriage (part 4) that moves back and forth with the mechanism. However, we did not go with this design because firstly the electrical wiring would be dangling and unsafe, and secondly the wires' movement back and forth would shorten their lifespan and need higher maintenance. Thus, the spinning motor (part 10) was fixed on the top of the rightmost side support (part 2) to connect to the carriage (part 4) that carries the polymer rod (part 6) using a kinematic coupling. We have excluded bevel gears because they need high

positional accuracy, and we did not want to increase the design complexity using a special kinematic coupling design. We made a unique design by adding rounded teeth to a spur gear, as shown in Figure 57. The design was re-iterated, 3D printed, and tested four times to come up with the most appropriate shape of fillets to assist the meshing between the two gears in case of a slight misalignment.

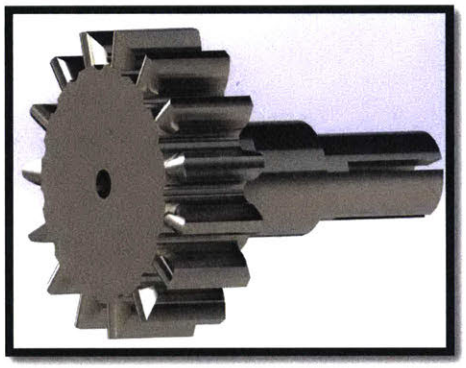

Figure 57: Spur Gear with rounded teeth and extended hub

Making these gears out of ABS plastic had the advantage of isolating the polymer rod from the rest of the metallic components to ensure the polymer rod is properly grounded in the electrospinning chamber. This isolation was done by extending the gear's hub and attaching the bearings to the outside of the squeeze collars on the hub, such that the metal bearings would not touch the polymer rod at all. The spinning motor sizing is governed by this relationship:

$$T_{sp} = F_{sp} * R_{driven}$$

Equation 11

where T_{sp} is the spinning torque required, R_{driven} is the radius of the driven gear, and F_{sp} is the force required to spin the polymer rod inside the electrospinning chamber.

$$F_{sp} = W_{gr} + W_{rod} + W_{cp} + W_{poly}$$

Equation 12

where W_{gr} is the weight of the driven gears, W_{rod} is the weight of the polymer rod, W_{cp} is the weight of the coupling attaching the gear on the polymer rod, and W_{poly} is the weight of the polymer collected. This equation assumes that the fit between the rod and its grounding support is a clearance fit, so it is frictionless.

Plugging in the values gave:

Polymer rod:	
Diameter [m]	0.0032
Length [m]	0.91
Volume [m3]	7.20E-06
Density [kg/m3]	2700
Mass [kg]	0.0195

Two Gears:	
Diameter [m]	0.03
Thickness	0.02
Volume [m3]	1.41E-05
Density [kg/m3]	1052
Mass [kg]	1.49E-02
Two shaft collars:	
Outer diameter [m]	0.02
Inner diameter [m]	0.01
Thickness [m]	0.01
Volume [m3]	2.36E-06
Density [kg/m3]	2700
Mass [kg]	6.4E-03
Total mass [kg]	**4.07E-02**

Table 29: spinning motor calculations

The mass of 0.04 kg translates to a force of 0.39 N, multiplying this force by the 1.5 cm radius of the driven pulley, as mentioned in Equation 11 gave:

$$T_{sp} = 0.39 * 0.015 = 0.006\ Nm$$

Equation 13

The resulting value from Equation 13 was used to pick a motor with a higher torque capability that the torque needed. The Nema 17 motor's capacity was 0.45 Nm, so this calculation verified that this motor was a good design fit.

3.4 Mechanical Press Design

3.4.1 The press's main functional requirements

The main functional requirements of the press were as follows:

No.	Functional Requirement	Design Parameters
1	Receive the polymer coming from the electrospinning process	Make a body that surrounds the polymer rod collector to receive it when it is back
2	Strip this polymer of the rod and keep it inside a body	Design a stripping mechanism that slides the collector rod out and keeps the polymer inside the body
3	Press the polymer into a pill shape	Design a punch that goes into this body to press the pill
4	Eject the pill from the body	Design an ejection mechanism using the existing components, or design a separate one

Table 30: the press's functional requirements

As shown in Table 30 above, the press had four main functions: receiving the polymer, stripping it off the rod, pressing it, and ejecting it. The main goal of this design was to use the least number of steps changing the polymer from a fibrous form to a pill form. In the upcoming section, we would discuss how to receive, strip, press, and eject the pill with almost the same mechanism. This would help increase the production rate of the nanofibrous pills and make it closer to the current pill pressing techniques.

<u>3.4.2.3 Stripper's design:</u>

<u>3Stripper's functional requirements:</u>

The stripping mechanism was designed to:

1) Accommodate the rod collector's rotation during electrospinning
2) Surround the rod collector tightly, to help slide it out and keep the polymer in.
3) Act as the bottom of the die cavity during the pressing process.

<u>Strippers' design process:</u>

The stripper assembly was designed as an independent module by Slocum and Rojas that could independently tested and additional features for versatility of incorporating with the rest of the machine. At the time of designing and manufacturing the unit, we were evaluating an array of designs for the other elements to simplify the existing design. As shown in Figure 58, the stripping mechanism consisted of four elements: compression

block, sliders, slider mount, and actuation system (air cylinders). The compression block served to collect the spun material of a rod (not shown).

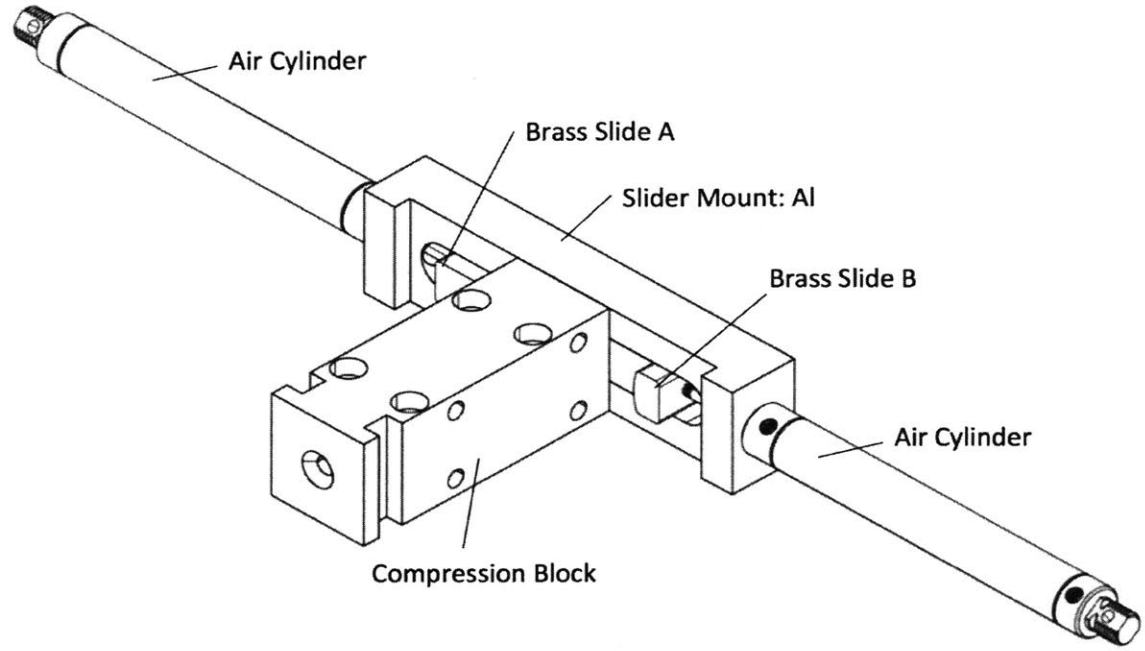

Figure 58: strippers' assembly view one

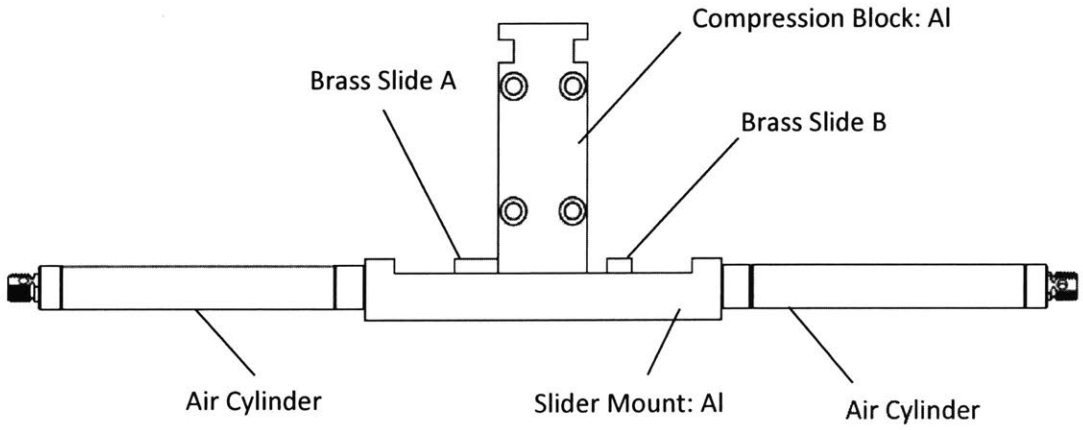

Figure 59: strippers' assembly view two

Stripper's final design:

Figure 60: the strippers' mount

This mount consisted of three main parts: the outside mount, stripper one, and stripper two. The outside mount was made of stainless steel, and the strippers were made of brass to apply pressure on the rod and strip the polymer off without wearing out. The inner geometry of the strippers formed a 1/8 inch hole to contain the polymer rod, and the outer lips constrained its linear motion to stop at the required position. During the first step, to strip the polymer off the rod, the lip of stripper one is at its maximum position around the die cavity. During the second step, stripper one contracted back and stripper two went all the way in until its lip touched the die cavity. In this case, the bottom of the cavity was fully blocked to press the pill into its required shape. The third step was when stripper two retracted back, so the press went down again to eject the pill out of the machine.

	Stripper (1)	**Stripper (2)**	**Position**	**Use**
Position (1)	OFF	OFF	Hole fully open	Spinning the rod, and sliding it in and out
Position (2)	ON	ON	Hole partially closed	Stripping the polymer off when the rod slides back
Position (3)	OFF	ON	Hole fully closed	Pressing the material into pill shape with this stripper acting as a flat bottom

Table 31: the three different positions of the strippers

3.4.2 Die cavity design

3.4.3.1 Die cavity's functional requirements

The die cavity had two main functional requirements:

1) Collecting and containing the stripped polymer when in the horizontal position (1)

2) Receiving the punch in its cavity to press the pill when in vertical position (2)

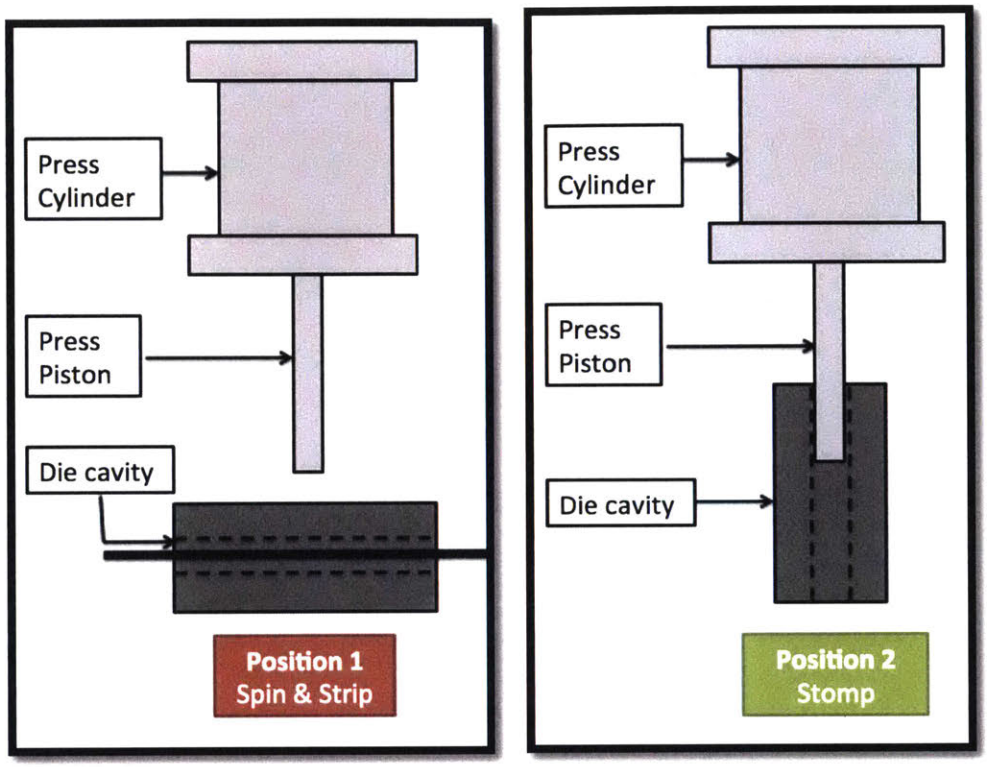

Figure 61: the two positions of the die cavity

Figure 61 above shows these two positions. In position (1), the cavity is horizontal and the rod spins inside to collect the polymer during the electrospinning process. It also stays horizontal during the stripping step, where the 2 strippers close on the rod so the rod slides out leaving the polymer inside the cavity. In position (2), the cavity is vertically aligned to allow the piston to slide in and press the pill into its shape and then it slides in again to eject it when the strippers are open.

3.4.3.2 Die cavity's design process

The die cavity rotates relative to the side supports through shafts on either side which are fixed to the side supports. These shafts interface with the die cavity through oil-embedded bronze bushings, which were selected because they would be able to support the maximum load of the compression piston, which could not be supported by standard plastic bushings.

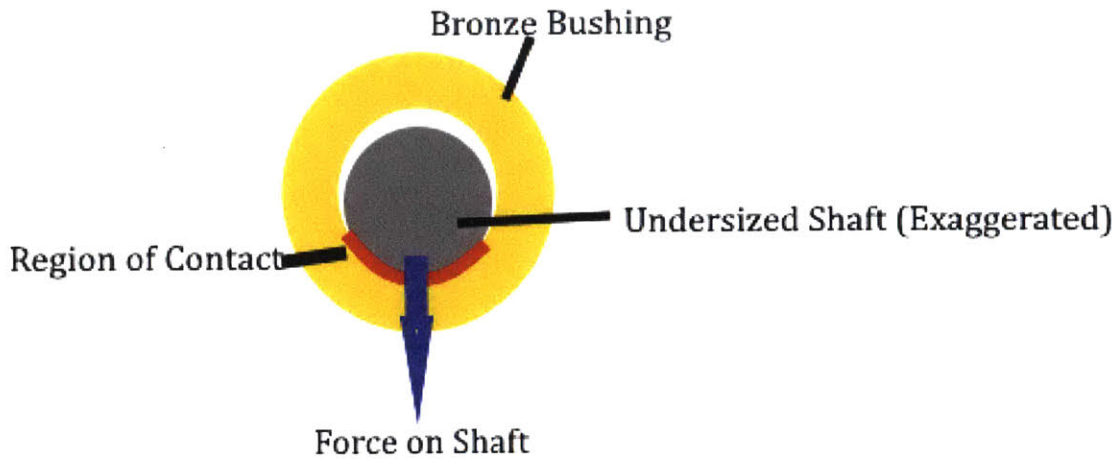

Figure 62: forces applied on the bronze bushings

$$\sigma = \frac{F}{A}$$

Equation 14

$$\sigma = \frac{F}{\frac{1}{4} * \frac{\pi D^2}{4}}$$

Equation 15

The value ¼ used in Equation 15 was the assumed fraction of the area of the bushing that is the contact region. Running this equation for the applied force showed that nylon bushings would fail.

The oil embedded into the bushing lubricates the shafts connected to the die-cavity, decreasing the friction between the two components when the die cavity rotates. The holes inside of the bushings were expanded 0.005" to account for potential misalignment of the two shafts caused by misalignment of the two side supports.

3.4.3.3 Die cavity's final design

Figure 63: the die cavity

This die cavity was made out of anodized aluminum to avoid metal contamination of the pill's material. It has two journal bearings fitting in its two side holes. Their function is mounting this die cavity on the side supports (part 7 in Figure 66) to restrict its movement to pure rotation. The hole on top serves as the polymer rod inlet when the cavity is horizontal, and it serves as the die cavity where the pill material is pressed when it is vertical. It also has four threaded holes at the bottom to attach the strippers' mount to this die cavity piece.

3.4.3 Punch Assembly design

In designing the punch assembly; punch, bearings, and pneumatic piston, the following functional requirements were first taken into consideration:

3.4.4.1 Punch's functional requirements:

The main requirements for the punch assembly were to:

1) Press the polymer into a pill shape
2) Eject the pill out of the assembly
3) Accommodate the rotating die cavity's design by designing a special housing for it, as shown in Figure 64.

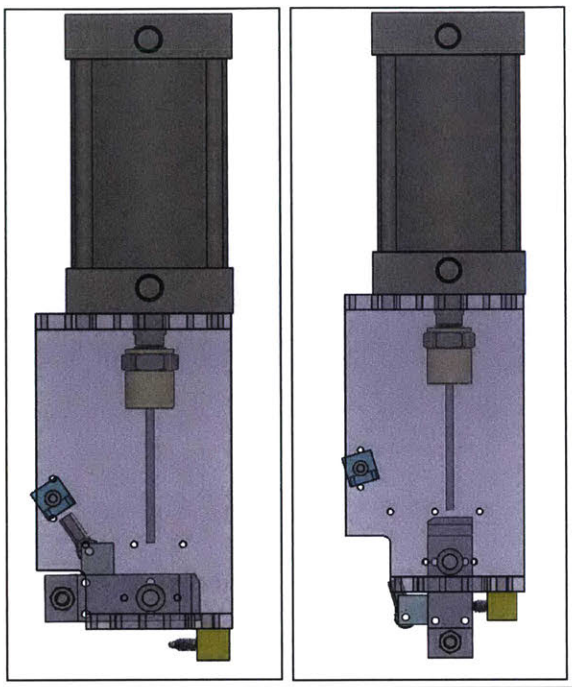

Figure 64: designing punch length for die cavity rotation

3.4.4.2 Punch's design process:

The piston used for the punch was chosen based on the 2,000 pounds force used to make commercially available tablets compressed from powder. The maximum air pressure output from the source used to originally test the compression system was 100 psi, which translated to a force of 1590 lbs. from the piston. While this is less than the **2,000 pounds** used commercially earlier, this is still significantly less than the predicted force required to compress electrospun material into a tablet. The cylinder is also still small enough to be able to test the effect of different compression forces on the tablet shape with good resolution for differences in input pressure of 5. The stroke length of the piston was 15" to provide ample travel length for the punch even if the length of the die cavity were changed.

The rotary shafts which allow both the die cavity and rotary piston to rotate are fixed to the side support through commercially available machinable shaft collars which are bolted to the side supports. These were chosen for their simplicity, low cost, flexibility in case the shaft diameter was increased, machinability, and commercial availability.

Since the side supports could not both be machined at the same time, all holes were designed with proper tolerancing based off of the milling machines that were used to make sure that none of the rotary shafts would bear load. This would be especially important for the shafts connecting the die cavity to the supports.

3.4.4.2 Punch's final design:

The punch's length was designed such that when it retracts, the cavity can freely rotate 90 degrees, and when it goes into the cavity, it goes all the way through to eject the pill. In other words, the distance between the piston and the die cavity was slightly more than the length of the die cavity to perform these two functions, as observed in Figure 61.

The die punch (part 2 in Figure 66) was made of stainless steel. It had an outer diameter of ¼ inches as it goes into a ¼ inches die cavity with a clearance tolerance. It was attached to the pneumatic piston using a threaded coupling, which goes through its ¼-20 threading.

3.4.4 CAD modeling

A machine design group was hired early to design an integrated unit. Dr. Rojas was hired to evaluate the existing design, consider the manufacturability, and evaluate the modularity of the unit. Figure 65 shows the design where a slider carriage moved via a belt drive along a mounted rod. The slider carriage interacted with an anchoring mechanism to hold the device where the fibers were compressed.

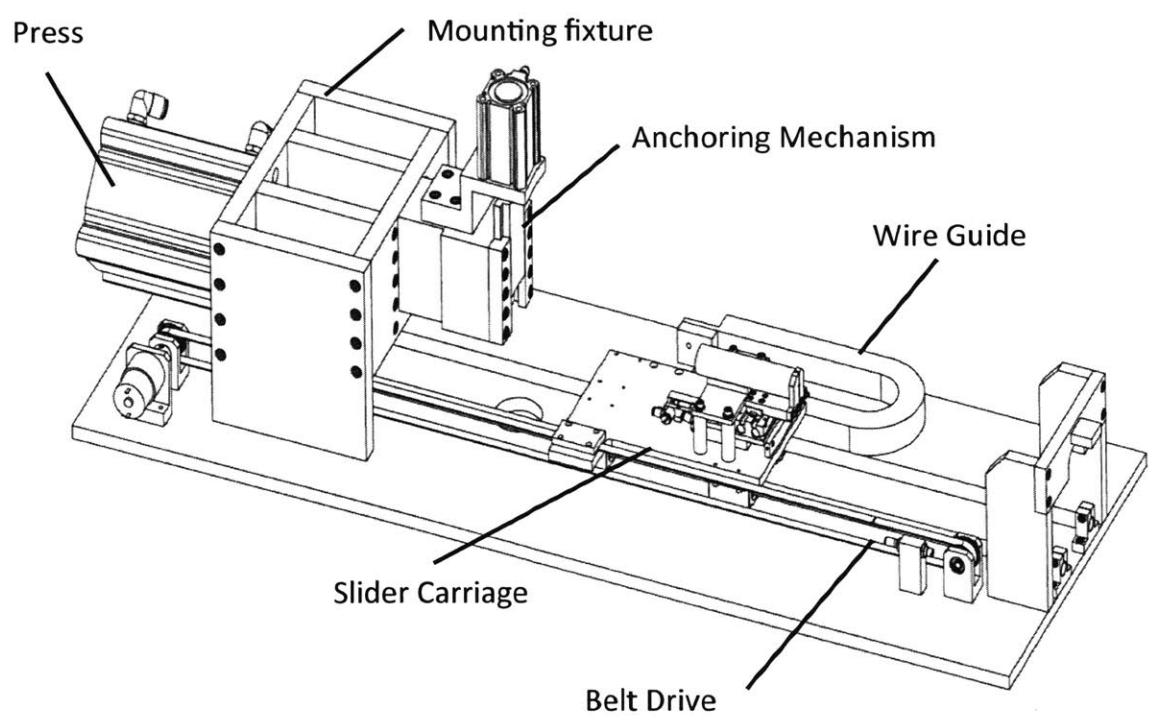

Figure 65: Prior design

The design was considered to be too complex and with too many parts. A modular design was adopted where each module can be independently tested. The mechanism for the press mechanism also needed the versatility to be integrated with the design in Figure 65.

3.4.5 Final design components

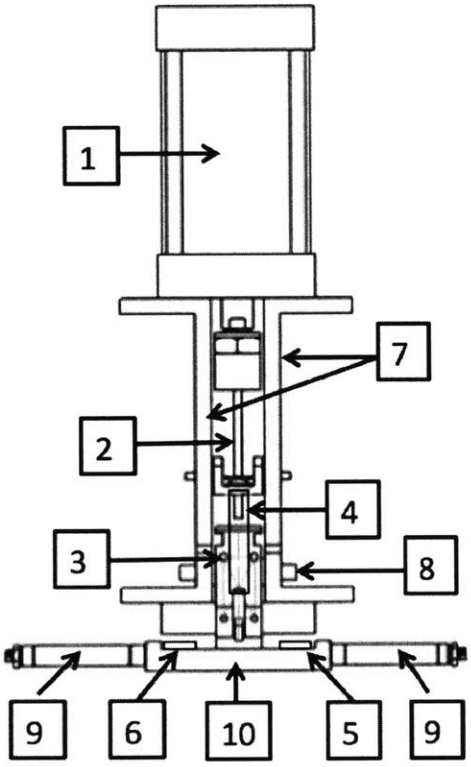

No.	Part
1	Press piston
2	Punch
3	Die Cavity
4	Rotary piston
5	Stripper 1
6	Stripper 2
7	Side supports
8	Rotary bearing
9	Strippers pneumatic pistons
10	Strippers' housing

Figure 66: the mechanical press components labeled

The press design consists three main assembles; the punch, the die cavity, and the strippers. The three functional requirements of this piece are: (1) Stripping the polymer off the rod, (2) Rotating the die cavity 90 degrees, and (3) Pressing the polymer into a pill shape and ejecting it.

3.4.6 Design equations

Press Sizing:

This press is designed to process the polymer coming from the electrospinning chamber. It takes the polymer collected on the rod, and strips it into the die cavity. So the die cavity was sized according to the following equation:

$$L_{cavity} = 0.25 * L_{pr}$$

Equation 16

where L_{pr} is the length of the polymer collected on the rod. After the polymer is stripped, it shrinks according to: (1) the speed of stripping, (2) the stripping force, and (3) the material being stripped. The length of the stripped polymer during our experimentation was about 5% to 10% of the polymer length, so the cavity was designed to be approximately 25% of the polymer length to be in the safe side if any other material or stripping conditions were used.

After the cavity's size was determined, the length of the punch going into this cavity was calculated by:

$$L_{punch} = L_{cavity} + L_{eject}$$

Equation 17

where L_{punch} is the length of the punch, L_{cavity} is the length of the die cavity, and L_{eject} is the additional distance that the punch travels beyond the cavity to eject the pill.

Then the distance between the piston and the die cavity was determined by the equation:

$$L_{piston.cavity} = L_{punch} + L_{gap}$$

Equation 18

where $L_{piston.cavity}$ is the distance between the piston and the cavity, L_{punch} is the length of the punch, and L_{gap} is the distance between the end of the punch and the die cavity when the punch is fully retracted. This distance was used to determine the size of the side supports (part 7) shown in the press components Figure 66 earlier. Then the total length of the press mechanism is then determined by:

$$L_{press\ total} = L_{piston} + L_{side\ suports} + L_{strippers}$$

Equation 19

where $L_{press\ total}$ is the total vertical length of the press assembly, L_{piston} is the length of the press's piston (part 1 in Figure 66), $L_{side\ supports}$ is the length of the side supports (part 7 in Figure 66), and $L_{strippers}$ is the length of the strippers' assembly.

However, this whole press assembly could not be placed on a surface, it has to be placed on a structure to lift it up and align the polymer rod between the three mechanisms; electrospinning, the sliding spinner, and the press. The critical alignment point was having the polymer rod slide in between the three mechanisms precisely. This was done by aligning the polymer rod (part 6 in the sliding spinner assembly), the die cavity (part 3 in the press assembly), and the end support (in the electrospinning chamber) in one line.

Structure:

The structure of the machine was made out of 1.5 inches t-slotted aluminum framing. The main functional requirements of this structure are providing the required alignment and stiffness to the mechanism. The critical alignment point was having the sliding spinner, the die cavity (part 3 in the press assembly), and the electrospinning's end support in one line. This would make the polymer rod slide in between mechanisms precisely. The stiffness had to provide enough stability to accommodate the movements of the pressing and sliding parts. The height of the structure was determined from the height of the polymer rod above the electrospinning spinneret, so the die cavity and the spinning slider mechanism held the polymer rod at this height of 42 cm.

As seen in Figure 67 below, the total width of the structure was 192.1 cm, the total height was 82 cm, and the width was 50 cm. The box on the right was the electrospinning chamber, the middle structure was for the press, and the rightmost structure was for the sliding spinner.

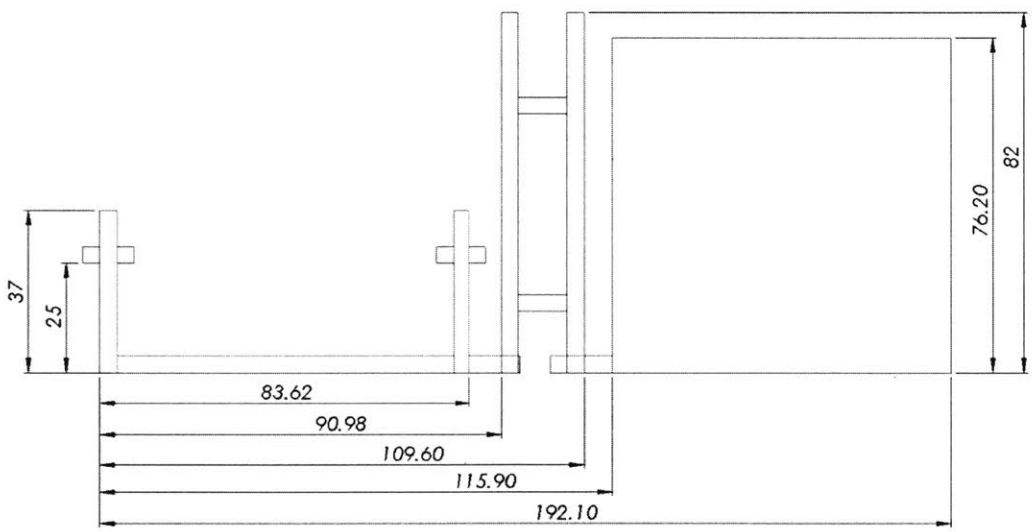

Figure 67: Engineering drawing of the machine's structure

Chapter Four: Building The Machine

"Knowing is not enough, we must apply. Willing is not enough, we must do."
Bruce Lee

4.1 Electrical Controls

4.1.1 Stepper Motors for the sliding spinner

There were two stepper motors in the sliding spinner setup, the sliding motor and the spinning motor.

The Spinning Motor:
The spinning motor (part 10 in the sliding spinner assembly) used was Nema 17 (17HS13-0404S) purchased from Stepper online Motors & Electronics. Nema 17 has a holding torque of 0.26 Nm, a step angle of 1.8°, drawing a current of 0.4 A at 12 V.
The function of this spinning motor was to spin the polymer rod collector inside the electrospinning chamber. It required a very low torque because it just spins the mass of the polymer rod, the gear, the coupling, and the attached polymer, which did not exceed 40 grams.

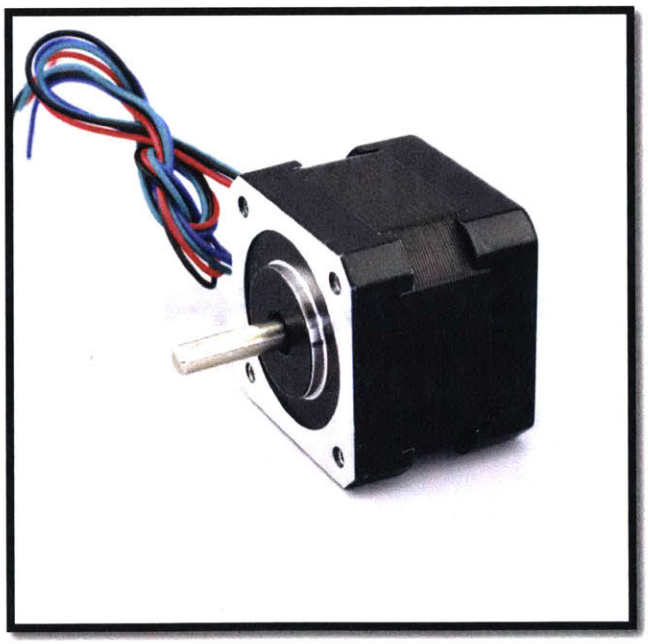

Figure 68: Nema 17 stepper motor

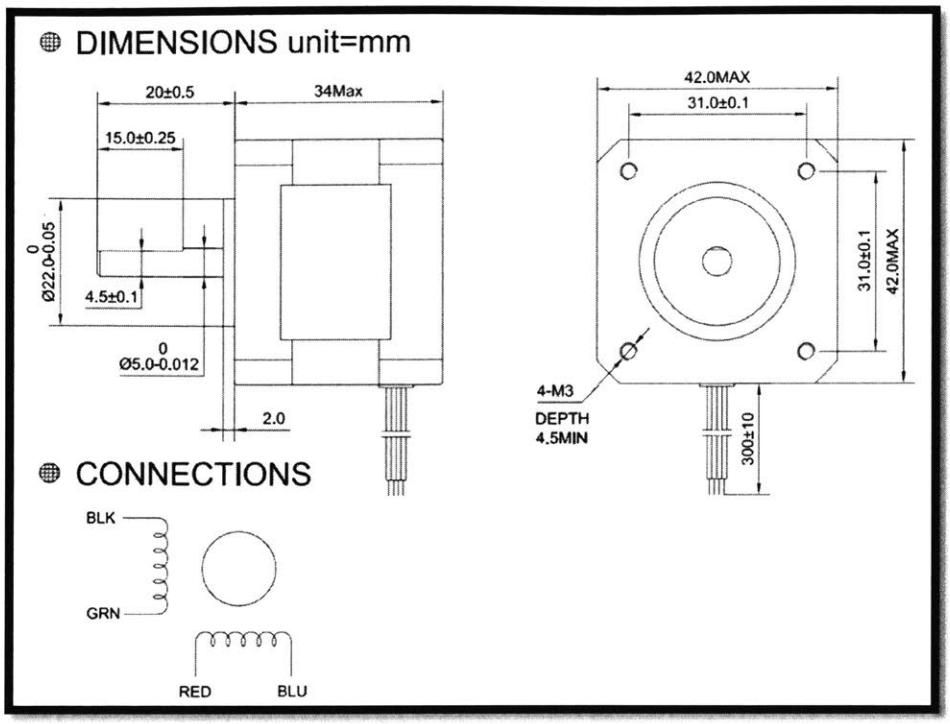

Figure 69: Nema 17 stepper motor's dimensions

The Sliding Motor:

The sliding motor (part 9 in the sliding spinner assembly) was a High Torque/Speed Nema 34 (34HS59-5004S). It was also purchased form the same manufacturer. It has the same phase angle, but a holding torque of 13 Nm, drawing a current of 5A from a 60V power supply.

The function of this sliding motor was to retract the rod back from the electrospinning chamber. It had to resist the strippers' high pressure (around 15 Psi) and the frictional force of the sticky polymer on the rod, so the required torque was of a much bigger value.

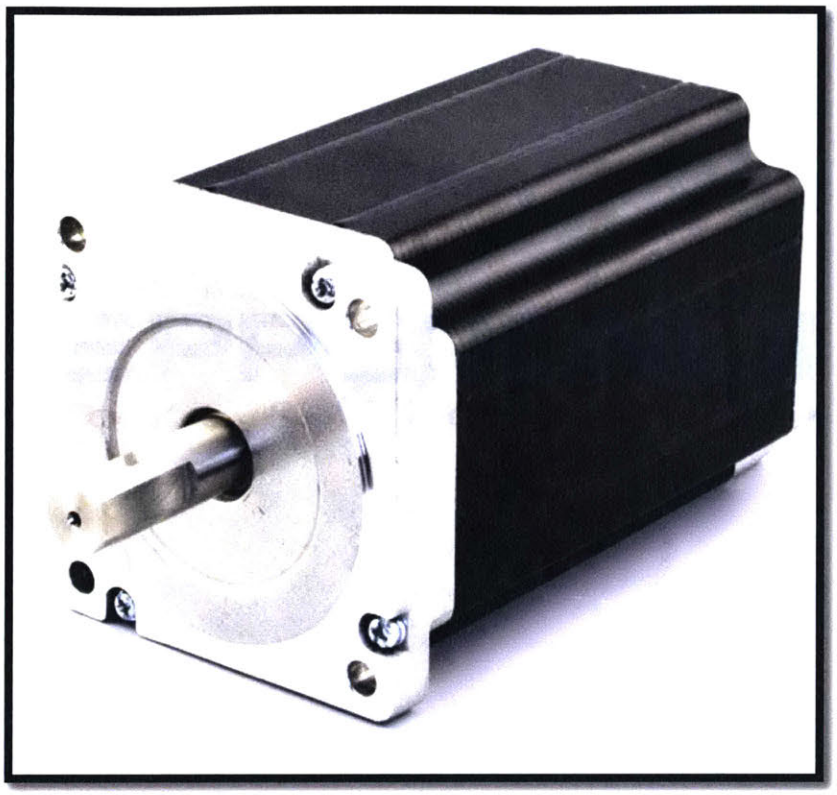

Figure 70: Nema 34 Stepper Motor

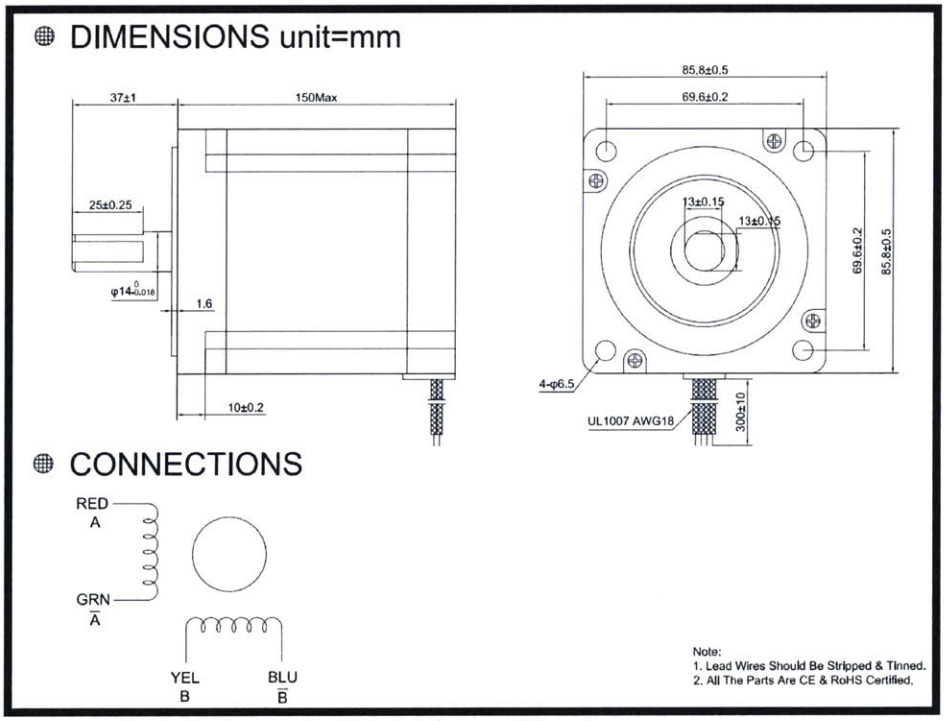

Figure 71: Nema 34 Stepper Motor's dimensions

4.1.2 Stepper Motors' Additional Hardware

The spinning motor, Nema 17, was controlled by a Big Easy driver (ROB 12859) connected to our main Arduino Mega, both purchased from Sparkfun.

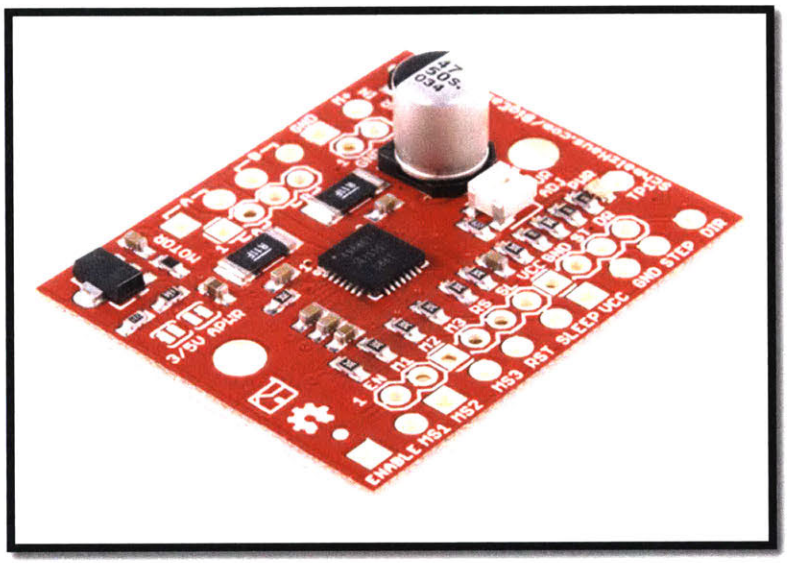

Figure 72: Big Easy Driver (ROB 12859)

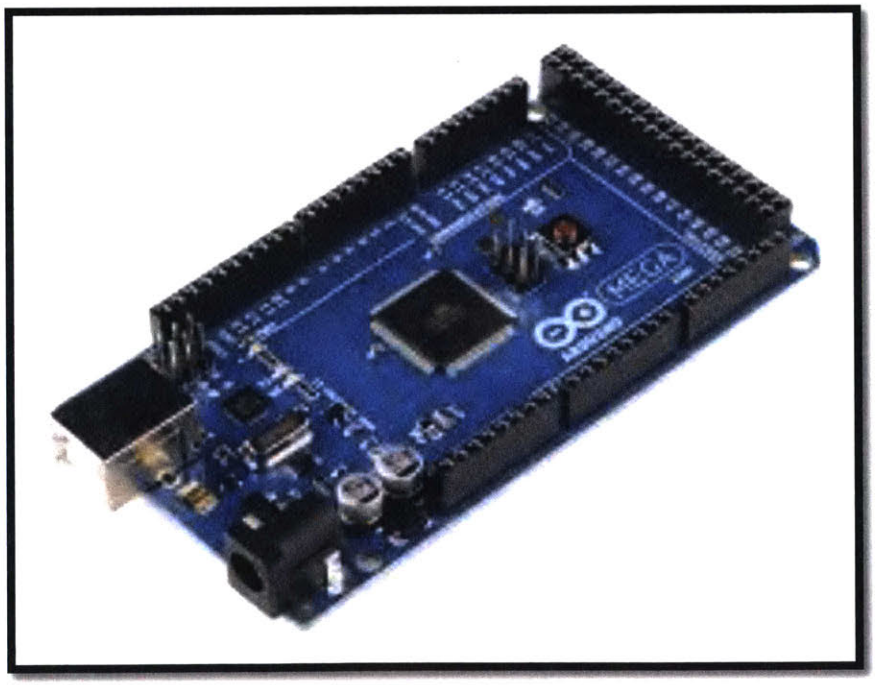

Figure 73: Arduino Mega

The sliding motor, Nema 34, was controlled by a MA860H stepper motor driver and S 350-60 60V switching power supply purchased from Stepper Online Motors and electronics.

Figure 74: MA860H Microstep Driver

Figure 75: S 350-60 60V Switching Power Supply

4.1.3 Electrospinning Spinneret Motor

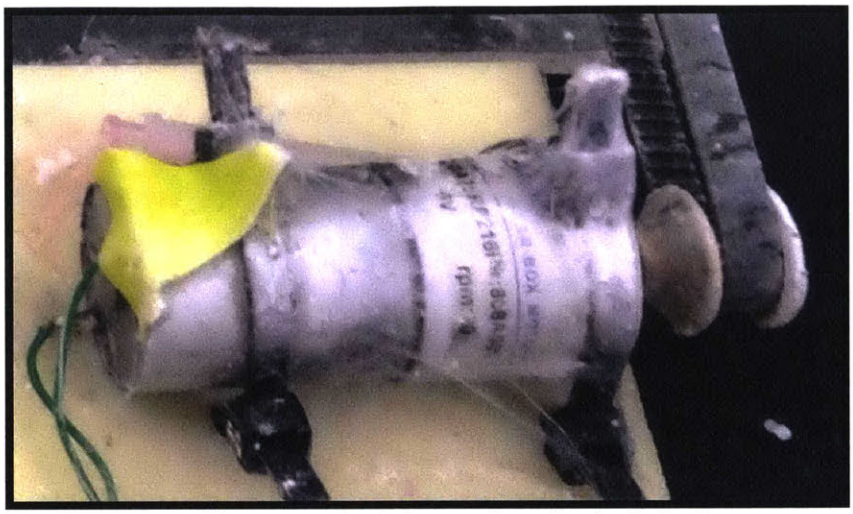

Figure 76: Small DC Motor for Spinneret Rotation in the bath

In the electrospinning chamber, the wire electrode spins at a very low speed and torque. The function of this spinning mechanism is to continuously dip the wire in the polymer solution to get more solution and form droplets that are easy to spin into nanofibers. A small 6V 20 rpm DC gearbox motor purchased from Zheng was used. Its specifications are shown below:

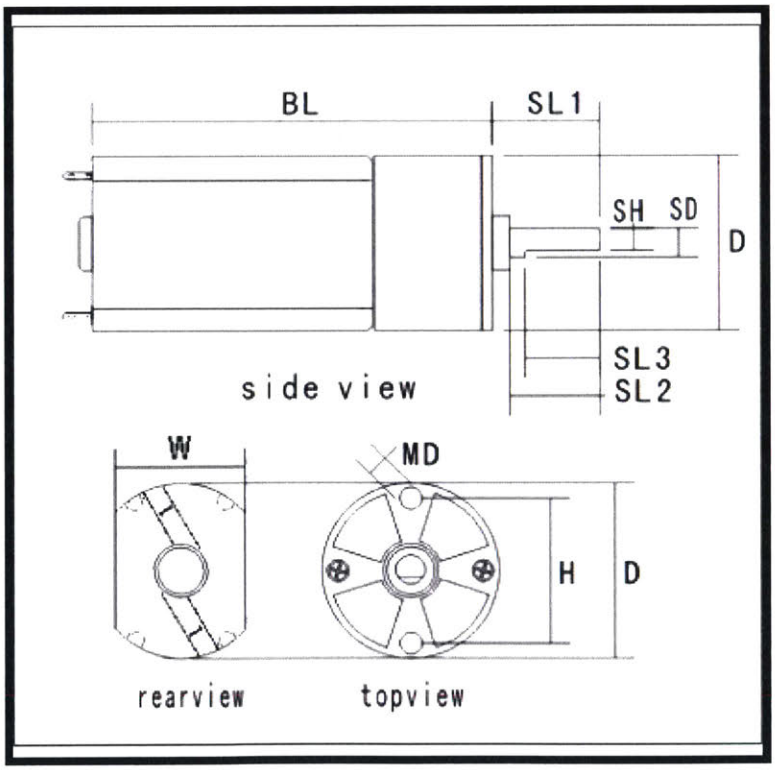

Figure 77: sketch of DC motor's specifications

Horse Power Cont.	0.1 W	**Length of Motor Body(excluding spindle) (BL)**	41.0mm
Gear ration	1:191	**Full Length of Spindle (SL1)**	9.5mm
Voltage & Current	6 V DC	**Length of Spindle (SL2)**	8.0mm
RPM	20	**Length of Spindle Flat(SL3)**	7.5mm
Reversibility	Reversible	**Diameter of Spindle (SD)**	2.96mm
Length of Motor (including spindle)	51.5 mm	**Height of Spindle (no a flat) (SH)**	2.45mm
Diameter of Motor (D)	20.0 mm	**Center Distance of Mount Hole(H)**	11.0mm
Stall Torque	4.5 Kg.cm	**Diameter of Mount Hole(MD)**	1.6mm(M2)

Figure 78: DC Motor's specifications

The equation for the voltage input versus the rpm output was:

$y = 3.0944x - .5549$

where (y) was the rpm and (x) was the voltage input. Thus, 1V gave 2.5rpm.

4.1.4 Electrospinning High Voltage Power Supply

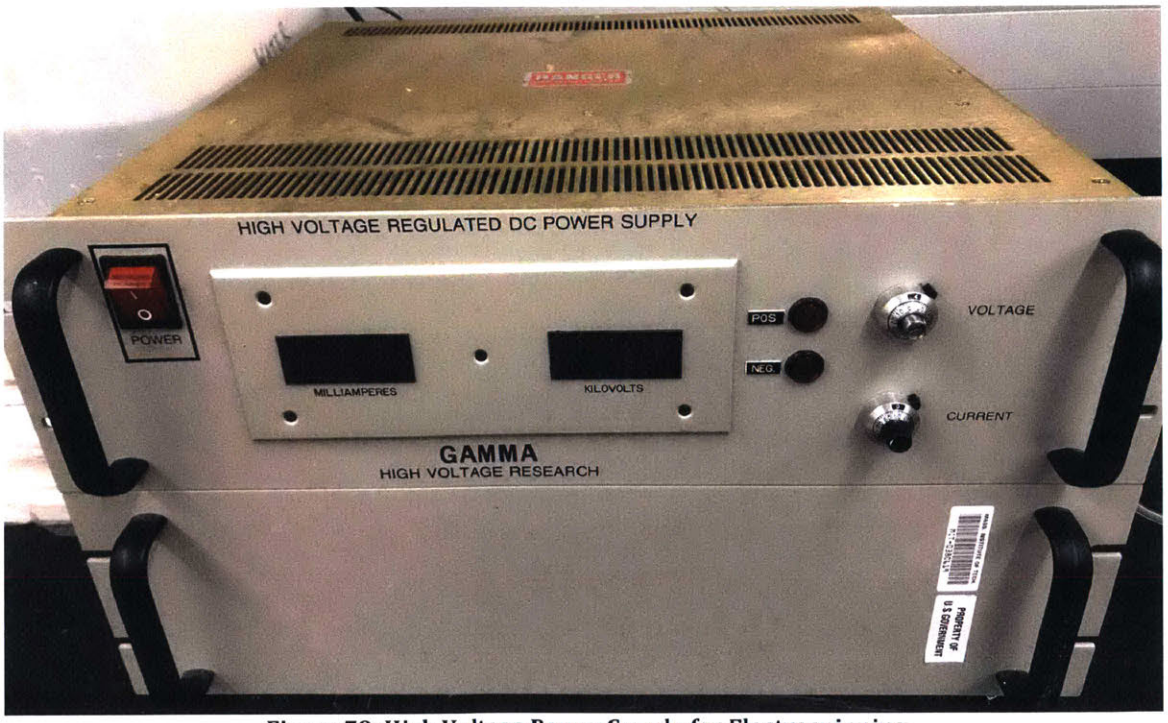

Figure 79: High Voltage Power Supply for Electrospinning

The applied voltage for the electrospinning process was controlled by the Gamma High voltage power supply shown in Figure 79. Its model number was (model RR40-1.5) and the applied voltage ranged from 34 to 42 kV.

4.1.5 Pneumatics Power Supply

The power supply used for the pneumatics' controls was a DC regulated power supply from TENMA, shown in Figure 80. Its model number was 72-6626. Its function was operating the switches of the pneumatic controls. It provided a voltage of 15 Volts, and a current of less than 1 Ampere at all times.

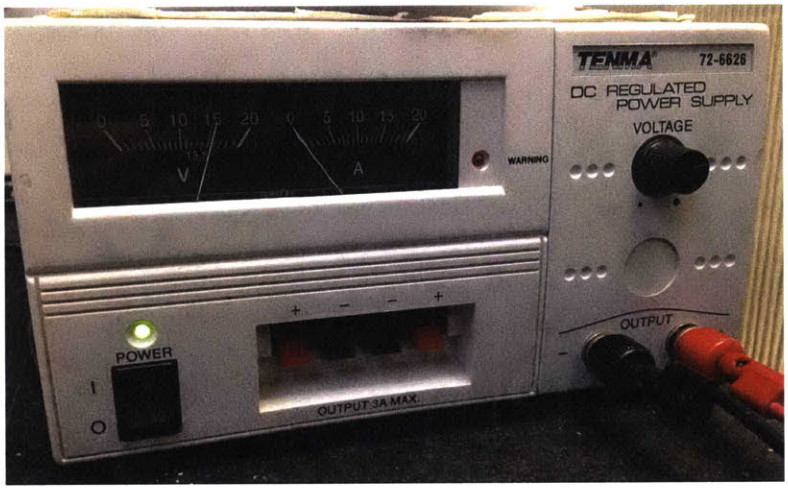

Figure 80: pneumatic control's power supply

4.2 Pneumatic Controls

There were four pneumatic pistons in this mechanism: the press's piston, the rotary piston, and the two strippers' pistons.

Main Pressure source:

The main pressure was supplied by a Porter Cable C2002 compressor. It had a capacity of 150 Psi, flow rate of 2.6 SCFM, and a volume of 6 gallons.

Figure 81: Porter Cable C2002 Compressor

The values shown in Table 32 below were the pressure distribution from the main source into its three uses: the pressing piston, the rotary piston, and the strippers' pistons. These values were found to be the most appropriate after multiple experimentations and trials.

Part Name	Pressure [psi]
Main Pressure	100
Pressing Piston	50
Rotary Piston	20
Strippers' Piston	15

Table 32:table of pressure distribution

Press's Piston:

The press's piston (part (1) in the press assembly) had a model number of D160SENC SL5 RA1. It was purchased from Motion Controls LLC. It had a bore of 4.5 inches, a rod diameter of 1 inch and a maximum pressure rating of 250 Psi.

Rotary Piston:

The rotary piston (part (4) in the assembly) of model number UM ¾ x 4-M was purchased from Phd Inc, and its model number is 11417362-01. Its function was to rotate the die cavity 90 degrees, from its horizontal position to its vertical position.

Strippers' Pistons:

The function of these two pistons was to push the two strippers back and forth.
Their cylinders were purchased from Bimba Manufacturing. When these two strippers moved back and forth, they formed three different positions, and gave three functions mentioned in Table 33 below.

	Stripper (1)	**Stripper (2)**	**Position**	**Use**
Position (1)	OFF	OFF	Hole fully open	Spinning the rod, and sliding it in and out
Position (2)	ON	ON	Hole partially open	Stripping the polymer off when the rod slides back
Position (3)	OFF	ON	Hole fully closed	Pressing the material into pill shape with this stripper acting as a flat bottom

Table 33: The 3 different positions of the strippers

The visual representation of the strippers' three positions looks as follows:

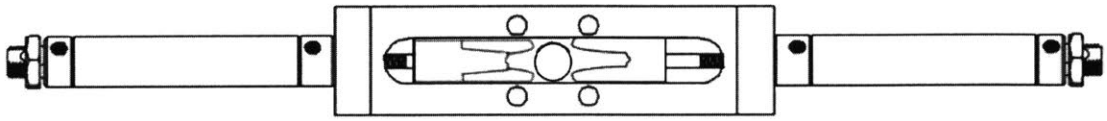

Figure 82: stripper's position one

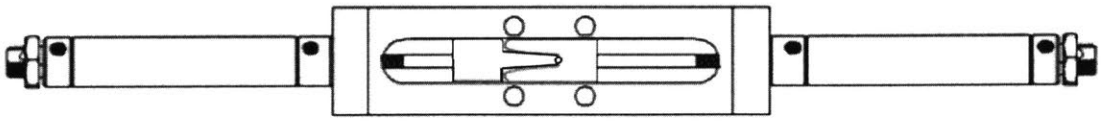

Figure 83: stripper's position two

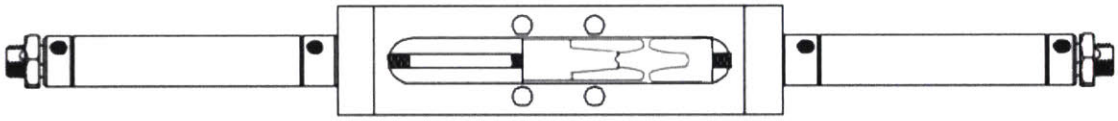

Figure 84: stripper's position three

4.3.1 Re-building the electrospinning chamber:

As discussed in the electrospinning design chapter three, the chamber was an adaptation of an existing chamber design in the Rutledge group [40]. The main change was replacing the flat plate collector with a spinning rod collector. This rod added three extra parts to the system: 1) the conical support, 2) the stand, and 3) the spring-loaded grounding. The stand was made out of t-slotted aluminum framing, and the spring-loaded grounding was made by sticking the brass ball to the spring using Loctite. All of these components were readily purchased from McMaster. The only machined part was the conical support.

The two iterations of the machined conical support, shown in Figure 85 and Figure 86, were made using a CNC lathe purchased from South Western Industries, model TRAK DPMSX2. The main cubical body was trimmed into the required sizing using an end mill. The holes were drilled by regular drill bits, and the cone shape was drilled using a countersink tool.

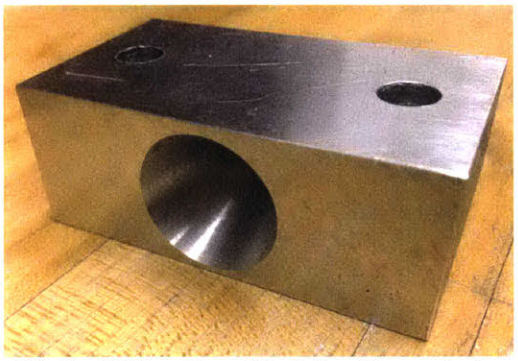

Figure 85: the 1st iteration of building the conical support

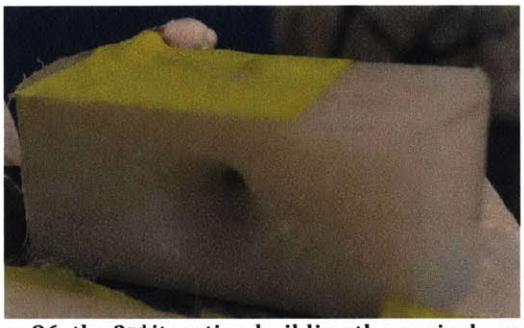

Figure 86: the 2nd iteration building the conical support

The engineering drawing used for building the 2nd iteration of building the conical support was as follows:

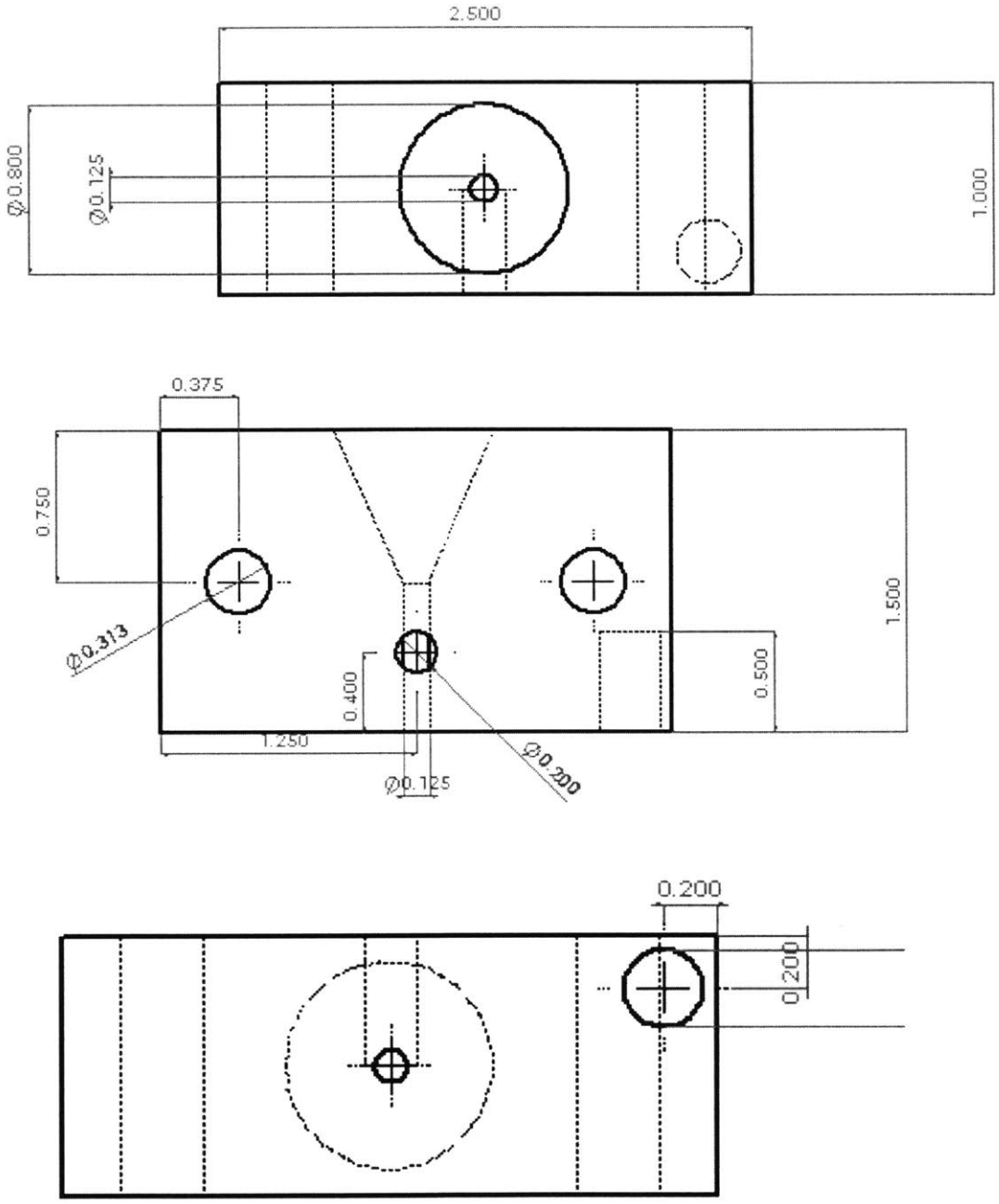

Figure 87: engineering drawing views of the modified conical shaped support (dimensions are in inches)

4.3 The sliding spinner building process

4.3.1 Gears' 3D Printing

The gears for the spinning mechanism were 3D printed as shown below:

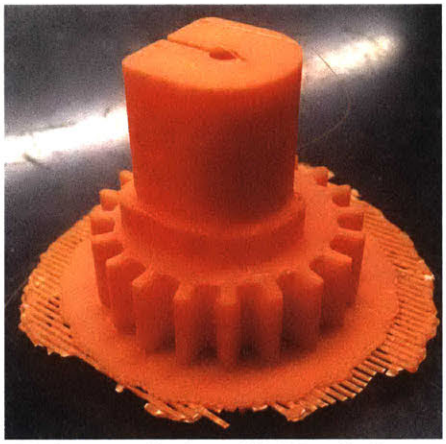

Figure 88: 1st gear design with 3D printing supports

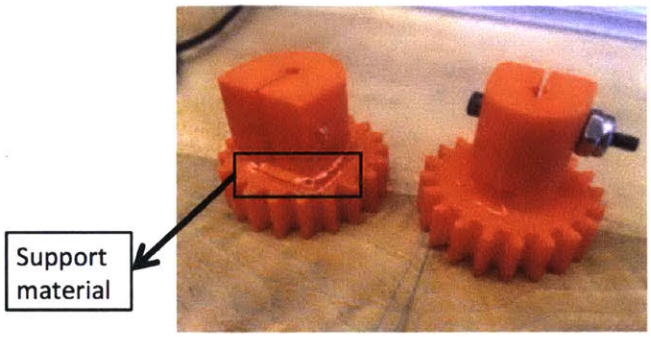

Figure 89: 1st gear design after removing 3D printing supports

The first design, shown in Figure 88 and Figure 89, had a major problem in the amount of support material needed for 3D printing. Removing this support material damaged the piece most of the time. The gear's hub was oversized compared to the gear itself, this was because it had to fit a bolt and have some skin around it. Also fitting a bolt and a nut in the gear's hub left the gear's rotation unbalanced because the bolt was relatively heaver than the gear itself. Thus, we had to re-iterate the design process to solve these challenges.

In the second iteration, the gear's hub design was changed from a U-shaped clamp to a squeeze collar. Then a shaft collar could be attached to it, having smaller size and higher rotational stability.

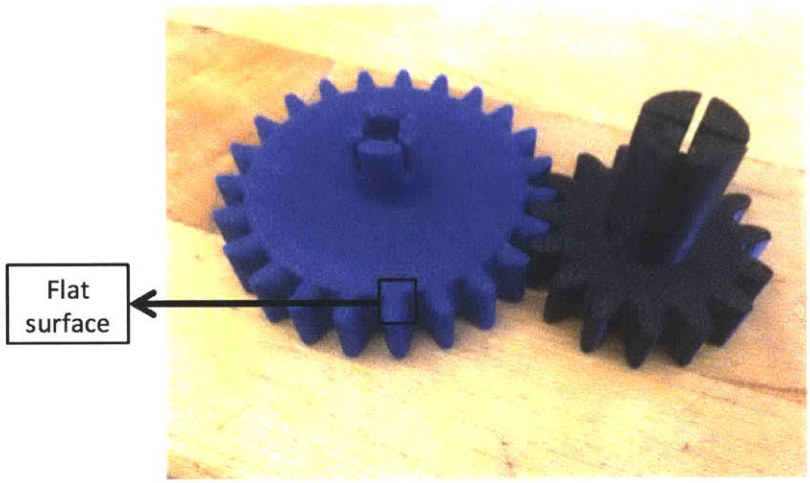

Figure 90: 2nd gear design

The squeeze collar hub design worked well, but the fillet geometry was still not at the right angle. As seen in the bigger gear in Figure 90, there was still a small flat surface at the end of the gear's fillet. This flat surface made the gears bump and break if they slid into each other.

In the 3rd gear design, shown in Figure 91, the gear's teeth were fully rounded with no flat surface. Now the smaller gear could easily mesh in and out without any problems.

Figure 91: 3rd gear design

4.3.2 Most critical module for carriage & spinning design

Before building the designed belt for the sliding spinner, an initial carriage was designed and tested using an air slider. This helped analyze the performance of the sliding and the spinning mechanisms. For this prototype, some parts were purchased and others were made.

Parts purchased:

1- Carbon fiber rod

2- 1/8 inches bearings
3- U-section carriage

Parts made:

1- **Gears**: they were both 3D printed
2- **Carriage:** it was made by drilling holes for bearings and mounting bolts on the milling machine in the hobby shop. The engineering drawing of the part can be seen in Figure 92 below.

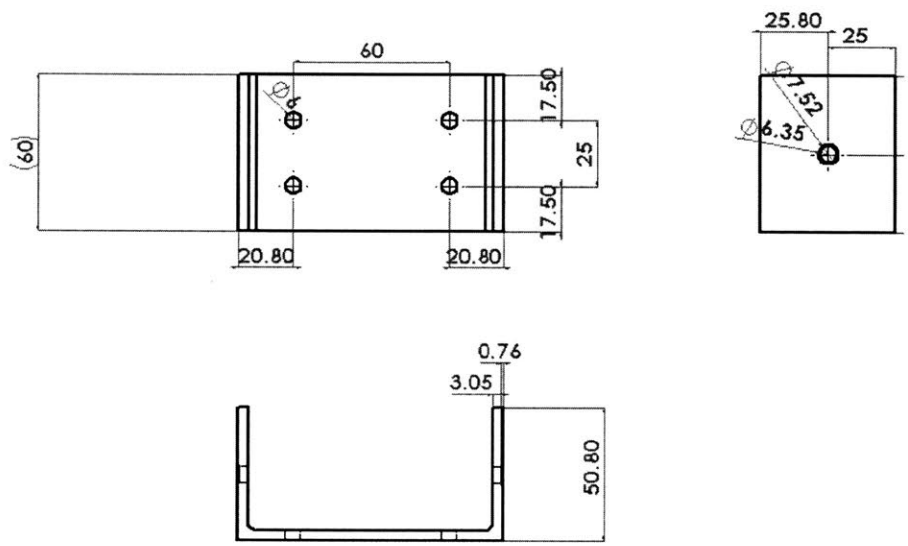

Figure 92: carriage engineering drawing

3- **Motor mount**: it was used to connect the spinning motor to the end of the pneumatic slider. Figure 93 shows the engineering drawing used for its machining.

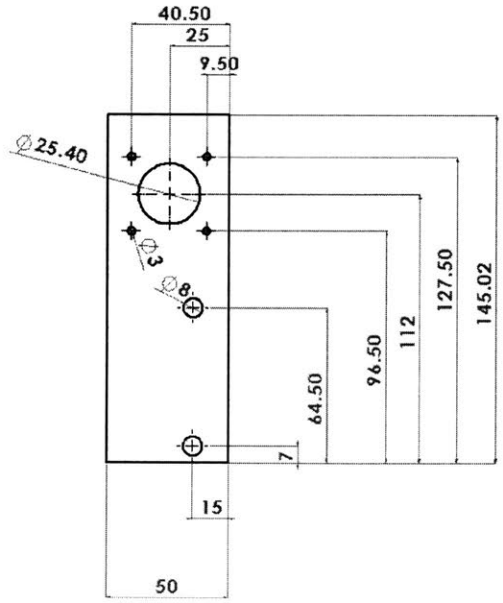

Figure 93: motor mount engineering drawing

Testing Challenges:

1- The first problem was that the rod was too flimsy, swinging up and down too much. The deflection was a lot more than the calculated one. This might have happened because the carbon fiber purchased from McMaster was not as stiff as the numbers used for calculations.

> ***Solution**: Looking into more materials, thicker rods, thicker bearings holding the rod, and more guiders for the rod.*

2- The second problem was the gears' meshing force. Whenever the gears turned, their radial force pushed the other gear away, separating from each other and stopping the spin.

> ***Solution**: Also adding the guiders at the end of the slider and straightening the rod would help in keeping the rod in place.*

3- The third problem was the positioning of the gear relevant to the carriage. In the earlier design, the gear was slightly far from the carriage, so it had a lot of bending, as seen in Figure 94 below, due to Saint Venant's principle.

> ***Solution:** keeping the gear at a minimal distance from the carriage or even touching it, to avoid any bending.*

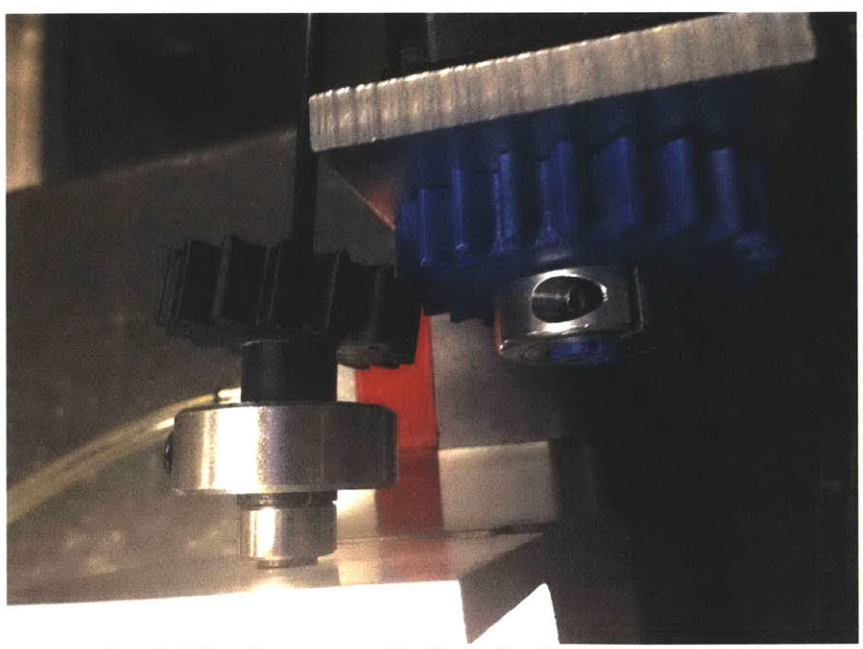

Figure 94: Gear's is bending as a result of no adhering to Saint Venant's principle.

As seen in Figure 94, the meshing was not successful as a result of not adhering to Saint Venant's principle. The solution is reciprocity, using Slocum's design equation of:

$$\frac{1}{☹} = ☺$$

Equation 20

When the gear was turned around, the hub moved to the outside and the gear moved closer to the support bearing. This minimized the bending effect and solved gear misalignment problems.

4.3.3 Machining the sliding spinner components

Most of the components were machined on the CNC TRAK DPMSX2. Some of the flat components were water jetted like the flexural bearings and the top supports.

Figure 95: machining the side supports (Part 1C)

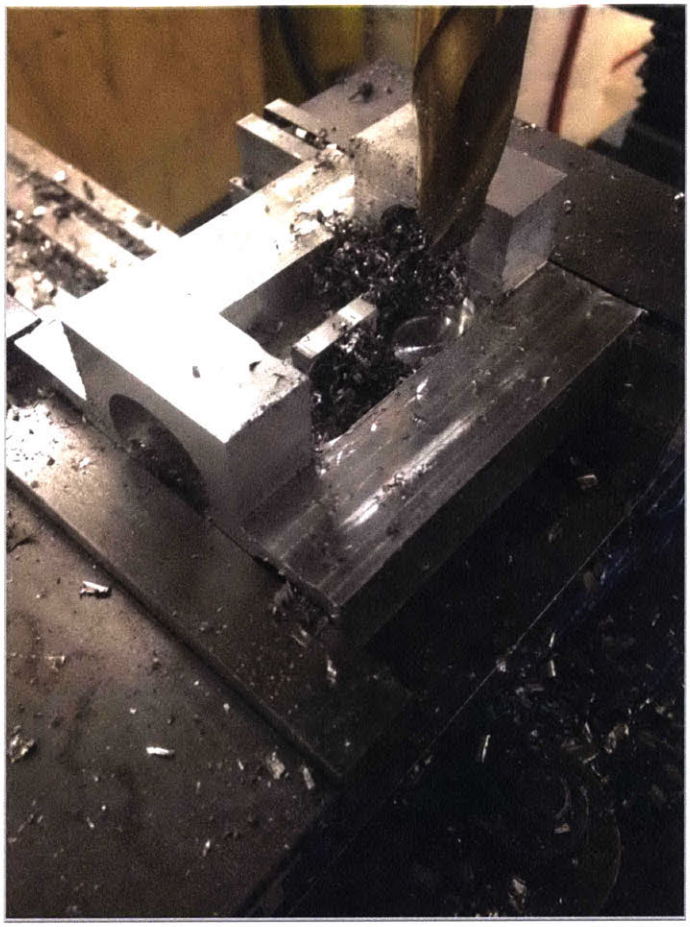

Figure 96: machining the carriage (Part 4H)

The engineering drawings of some of the parts look as follows:

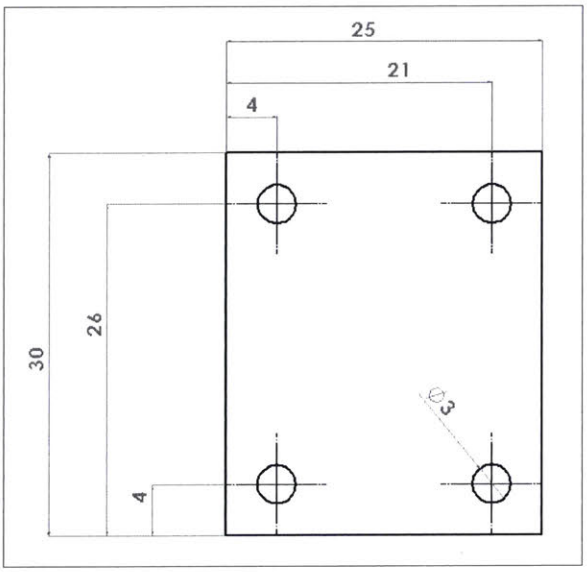

Figure 97: engineering drawing

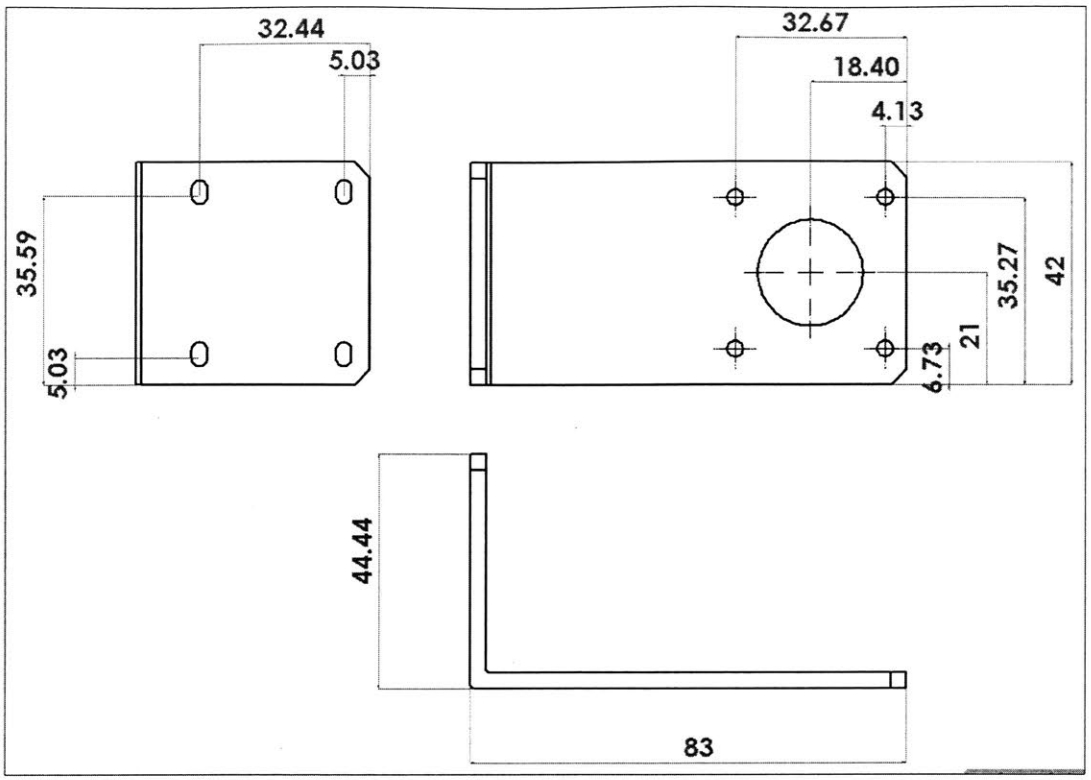

Figure 98: Motor L- sectional mount engineering drawing (Part 5G)

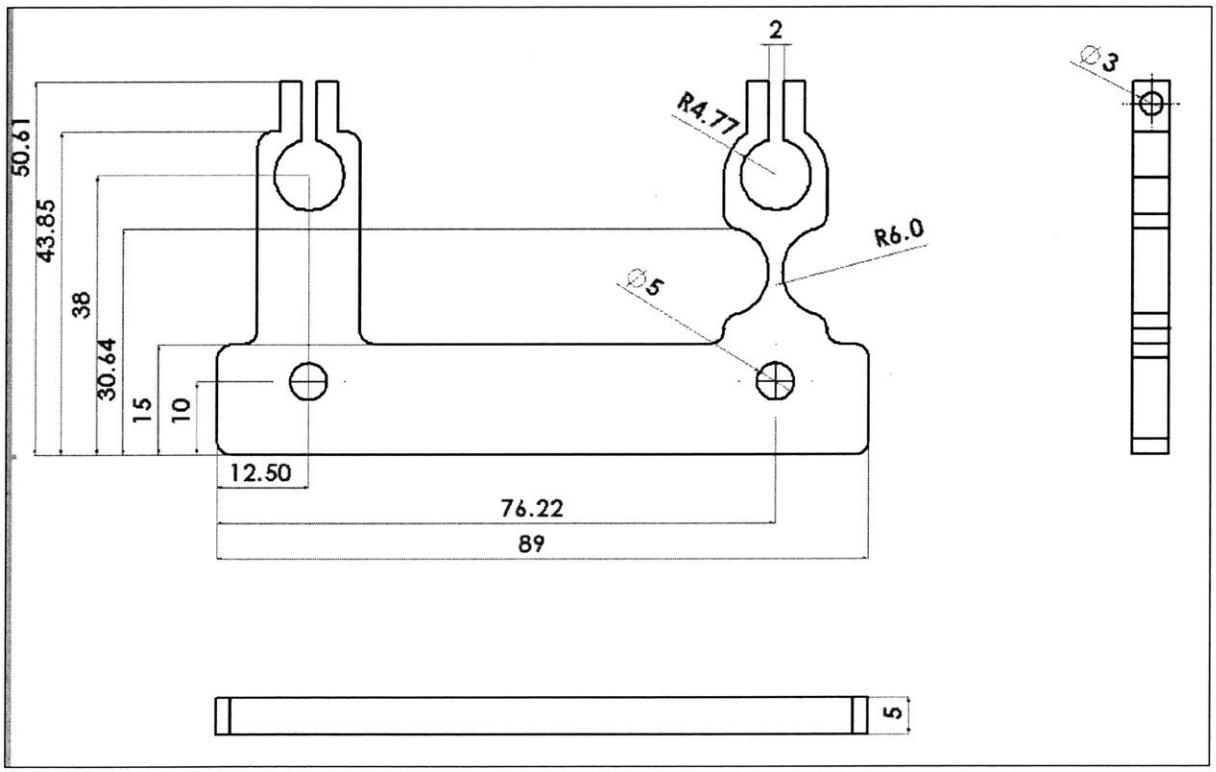

Figure 99: Flexure supports engineering drawing (Part 4E)

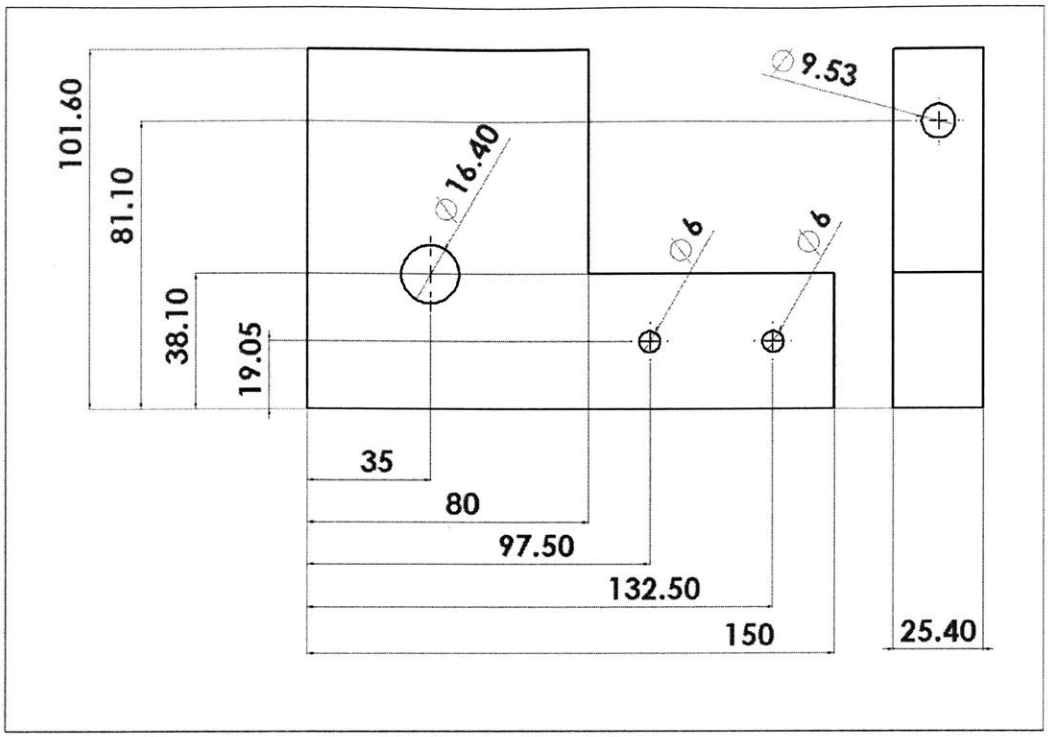

Figure 100: Side supports engineering drawing (Part 1C)

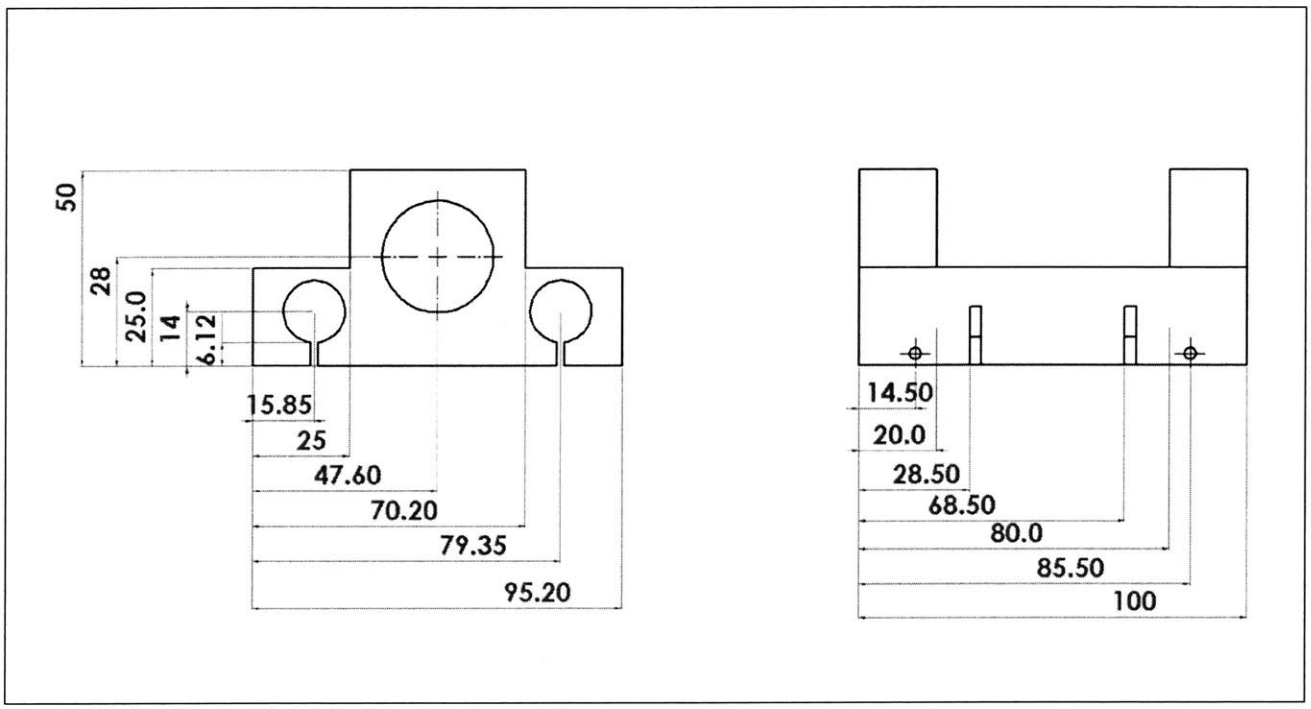

Figure 101: Carriage engineering drawing (Part 4H)

4.3.4 Final Bill of Materials

The final bill of materials for the sliding spinner is:

Sub-Assembly	Part Number	Part name	Quantity
Pulley base 1	1A	Pulley	1
	1B	0.25 inch ball bearings	2
	1C	Side Supports	2
	1D	Pulley screws - M3-25 mm L	2
	1E	0.25 inch ID spring	1
	1F	Driving shaft	1
Motor Drive	2A	Stepper motor	1
	2B	Flex coupling	1
	2C	Motor screws- M3- 8 mm L	4
	2D	Motor housing	1
	2E	Housing screws- 1/4-20	8
Pulley base 2	3A	Pulley	1
	3B	0.25 inch ball bearings	2
	3C	Side Supports	2
	3D	Pulley screws - M3-25 mm L	2
	3E	0.25 inch ID spring	1
	3F	Driven shaft	1
	3E	Top support	1
	3F	Top support flat bolts	4
Sliding mechanism	4A	Sliding rods	2
	4B	Linear bearings	4
	4C	Linear bearings' mount bolts- 3-48	4
	4D	Linear bearings' mount washers3-48	8
	4E	Flexure supports	2
	4F	Flexure shaft bolts and nuts- M3	4
	4G	Flexure mount bolts-M4	4
	4H	Combo box	1
	4I	Belt	1
	4J	Clamp	1
	4K	Clamp bolts-10-32	4
	4L	Clamp 10-32 nuts	4
	4M	Sliding rods clamps-3/8"	4
	4N	Al 80-20 structure	1
	4O	Bolts' slot (side supports+8020)	8
	4P	Bolts (sides+80-20)	8
	4Q	Teflon stoppers	4
Spinning mechanism	5A	Carbon Fiber rod	1
	5B	Small gear	2
	5C	3/8" shaft collars-small gear	2
	5D	Big gear	1
	5E	Big gear shaft clamp- 12 mm ID	1
	5F	2nd Stepper motor	1
	5G	Motor L section mount	1

	5H	Motor screws- M3- 8 mm L	4
	5I	Motor side top support	1
	5J	Top support	1
	5K	Top support hex bolts- 1/4-20	4
	5L	Small gear bearings	2
Guiding Linear bearing	6A	Teflon linear bearing	1
	6B	Bearing housing	1
	6C	Bearing's bolts-M4	2
	6D	Bearing's nuts-M4	2

Table 34: The sliding spinner's bill of materials

4.3.5 Manufacturing processes for the mechanism

Most of the parts above were bought from McMaster and BrecoFlex, with exception of these parts machined in the MIT hobby shop:

Sub-Assembly	Part Number	Part name	Machines
Pulley Base 1	1C	Side Supports	lathe, Band saw
	1F	Driving shaft	Rotary lathe, Band saw
Sliding Motor mount	2D	Motor housing	Lathe, Band saw
Pulley Base 2	3C	Side Supports	Lathe, Band saw
	3F	Driven shaft	Rotary lathe, Band saw
Sliding Mechanism	4E	Flexure supports	Water jet
	4H	Combo box	Lathe, Band saw
	4J	Clamp	Lathe, Band saw
Spinning Mechanism	5B	Small gear	3D print
	5D	Big gear	3D print
	5G	Motor L section mount	Lathe, Band saw
	5I	Top support	Water jet
Linear bearing	6B	Bearing housing	Water jet

Table 35: the manufacturing processes for the sliding spinner's parts

4.3.6 Building the press mechanism

Building the strippers assembly:

The die cavity was made from aluminum 6061 stock material. The minimum length of the cavity was designed with Saint-Venant's principle of characteristics dimensions in mind, thus it had to be at least 10 pill diameters in length. The additional length was to allow for additional features like threaded holes, clearance holes, and a pair of horizontal slits on the die cavity that could serve as a known gripping region for integrating the module with the rest of the machine. The maximum length of the die cavity was dictated by the length of a standard ¼" drill bit. The

operation for the die cavity reservoir had to be drilled and reamed without removing the part from the mill. The reaming operation should be done with an over/under reamer set thus allowing for at least 0.002" clearance for the compression process. The threaded mounting holes on the square face of the die cavity were used to join the strippers' assembly to it via four 8-32 screws.

The strippers' assembly was also made from aluminum 6061 extrusions, selected for readability. One material consideration was that the strippers and strippers' mount could not both be made from aluminum, as it would have lead to galling between the rubbing surfaces. The static frictional coefficient between two dry aluminum surfaces was between 1.05 and 1.35. A pocket on the strippers' assembly held the pair of strippers in place. The width of the pocket was dictated by the size of the rod diameter that collects the fibers as shown in Figure 102. The raised regions on the strippers' assembly were to provide enough material for the threaded connection for the actuators.

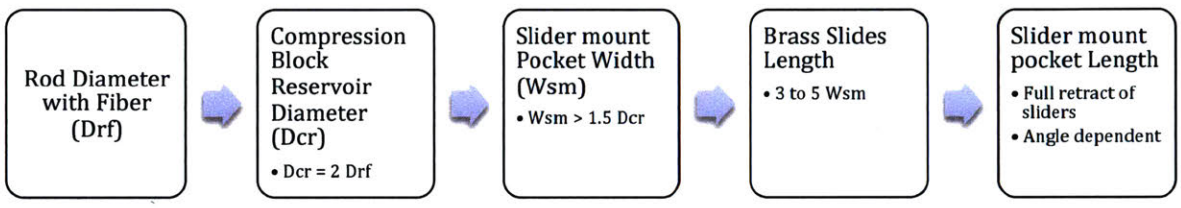

Figure 102 Process for specifying geometry of components

The die cavity and strippers' assembly (Figure 103) allowed for interchanging the components as the design evolves with minimal impact on the rest of the structure. If for some reason we needed to modify the internal hole of the die cavity we had the versatility to change components in the module.

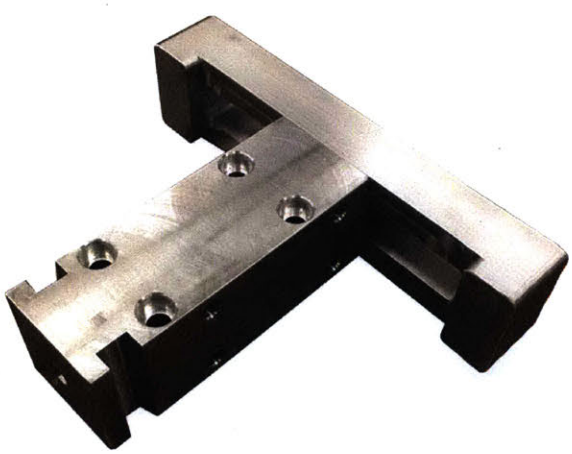

Figure 103: Die cavity and strippers' assembly

The strippers' assembly and the die cavity were machined at the same time to maintain the same alignment and thickness of the parts. The center hole that strips the fiber material was pre drilled and reamed prior to machining off the excess material; this process guaranteed a vertical

smooth hole (especially with a low feed rate and pecking). Cutting the same geometry with a small end mill had the potential to create a tapered geometry where fibers could collect.

Figure 104: Fabrication of the matching sliders

The brass strippers had three configurations: 1) completely open for spinning, 2) partially closed for material stripping, and 3) fully closed for compaction. When the strippers were in the fully opened configuration (Figure 105) their blades were fully retracted and the rod with the fiber material could be easily introduced into the mechanism with minimal alignment. Upon actuating both cylinders, the strippers closed to the material-stripping configuration (Figure 106). After the fiber material was stripped off the rod, the rod was removed from the mechanism in the process of pulling the rod to strip off the fiber material. With the rod out of the way, the strippers were actuated to configuration three fully closed for compaction.

The height of level two had to be at least two to three rod diameters for alignment.

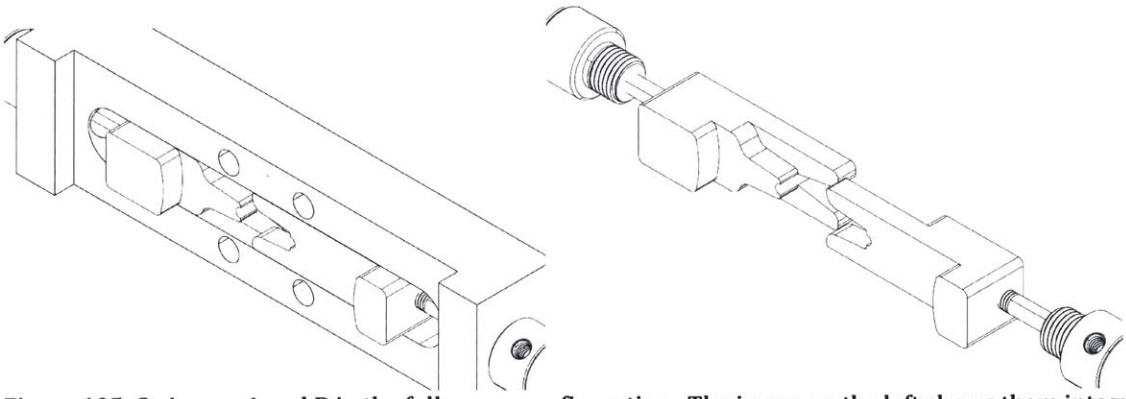

Figure 105: Strippers A and B in the fully open configuration. The image on the left shows them integrating with the strippers' assembly. The image on the right shows the three-layer slider geometry

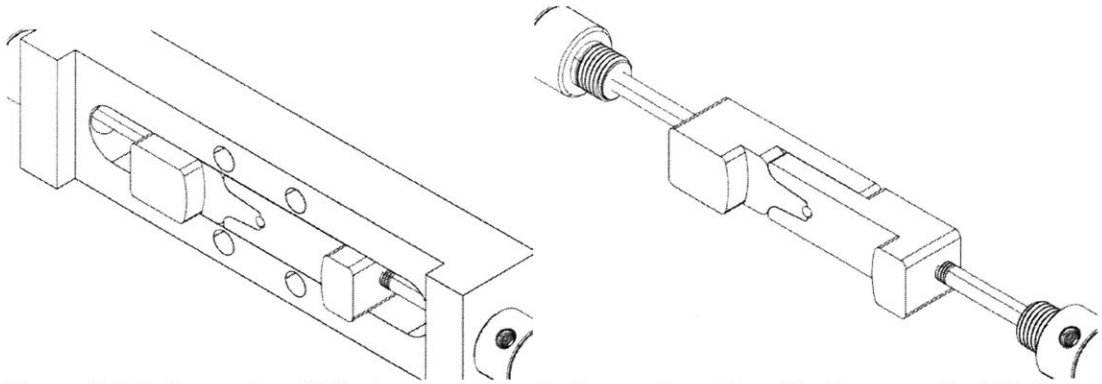

Figure 106: Strippers A and B in the material stripping configuration. The image on the left shows the strippers compressed concentric with the die cavity. The image on the right shows the strippers joined without the stripper's assembly.

The strippers had three levels of geometry each with its own purpose, Figure 107. The first level consists of an over lapping region that keep the strippers aligned along the z-axis. When the strippers are in their fully retracted position level 1 of stripper A is always in contact with the bottom surface of stripper B level 2. The rod with the spun fiber enters the die cavity and passes between the strippers' blades. As the strippers start to close before the start of the fibrous region of the rod, the "V" shape of stipper A level one starts to pre-align the rod concentric with the bore of the die cavity. With increasing closure the level 2 of strippers A and B continue aligning the rod and create a concentric seal around the rod.

In the second configuration, level 3 of stripper A makes contact with the side of the die cavity acting as a hard stop. To achieve configuration 2, the pneumatic cylinder A is pressurized higher than the pneumatic cylinder B. Once the rod is completely out of the mechanism, cylinder B is pressurized higher than cylinder A; thus reaching the fully closed compaction configuration. To achieve configuration 3, stripper B level 3 contacts the side of the die cavity. Both of the interior surfaces of level 3 strippers A and B are curved to create a Hertizian contact between the surfaces.

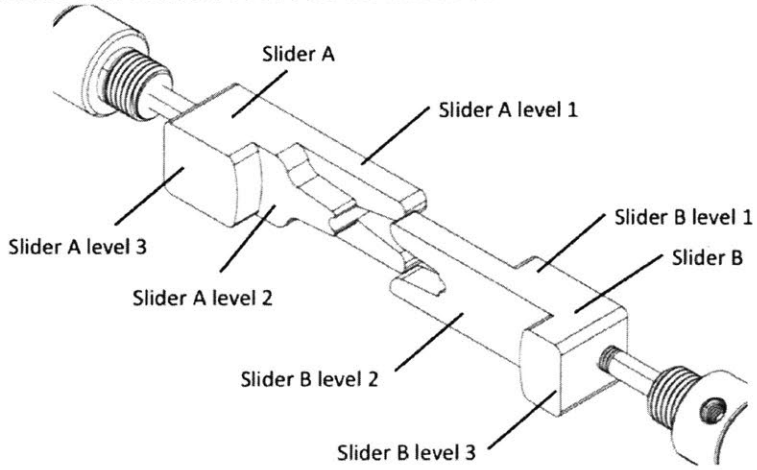

Figure 107 Stripper (Slider) levels

The actuation of the strippers is done with double acting pressure cylinders, which can be quickly actuated.

Machining the side supports:

Once the side supports were cut to the required specifications, standard drilling and reaming operations were done to both to meet the required tolerances and locations of holes. The side supports were each made from solid C-channel. Since the C-channel had tapered inner faces on the legs, these were machined down so that mounting bolts could properly interface with the legs.

The machinable shaft collars for the rotary shafts connecting to the rotary piston were not machined, they were just purhased with the correct shaft diameter. The shaft collars for the rotary shafts connecting to the die cavity were machined so that there was a sliding fit between the shaft and collar when the collar was completely loose. This guaranteed that a tight fit could be created when the **shaft collar** was tightened.

Machining the rotary piston's auxiliary parts:

Most of the auxiliary parts for the rotary piston were machined directly from stock so that they would interface properly with the rotary piston. The stopper was positioned properly by first putting the punch in its tablet compression orientation into the die cavity, so that the die cavity was held vertically. The stopper was then placed so that it was in full compression mode. This process guaranteed the die chamber would repeatedly settle into the correct location.

The Press's bill of materials:

The bill of materials of the purchased parts looked as follows:

Part Name	**Part No.**	**Quantity**
Oil-Embedded Flanged Sleeve Bearing for 1/2" Shaft Diameter, 5/8" OD, 1/2" Length	6338K418	2
Oil-Embedded Flanged Sleeve Bearing for 1/4" Shaft Diameter, 1/2" Length	6338K413	2
Machinable-Bore Clamping Shaft Collar for 1/8" to 3/4" Diameter	9964K10	2
Machinable-Bore Clamping Shaft Collar for 1/2" to 1" Diameter	9964K120	2
Steel Ball Joint Rod End, 1/4"-28 RH Female Shank, 1/4" Ball ID, 11/16" Long Thread	60645K321	1
Slotted Long-Nose Spring Plunger with Steel Nose, Black-Oxide Steel, 3/8"-16 Thread, 2.8-7.2 lb. Nose Force	3126A44	1
Tie Rod Air Cylinder, Double Acting, 4-1/2" Bore Size, 5-1/8" Wide, 5" Stroke Length	6491K237	1
Tie Rod Air Cylinder, Double Acting, Sensor Ready, 3/4" Bore, 4" Stroke Length	6453K118	1
Round Body Air Cylinder, Double-Acting, Universal Mount, 5/8" Bore Size, 2" Stroke	6498K432	2

The final bill of materials of the press assembly looked as follows:

Sub-Assembly	Part Number	Part name	Quantity
Press System	1A	4.5" Bore Pneumatic Piston	1
	1B	Piston-Punch coupler	1
	1C	Punch	1
	1D	Side Supports	2
	1E	Piston-Side Support Bolts	4
Die Cavity System	2A	Die Cavity	1
	2B	Die Cavity Rotary Shafts	2
	2C	Die Cavity Rotary Bushings	2
	2D	Collars for Die Cavity Rotary Shaft Constraint	2
	2E	Bolts for Die Cavity Collar-Side Support Connections	4
	2F	Stripper Housing	1
	2G	Stripper Housing-Die Cavity Bolts	4
	2H	Strippers	2
	2I	5/8"Bore Pneumatic Pistons (Stripping Piston)	2
	2J	¾" Bore Pneumatic Piston (Rotary Piston)	1
	2K	Rotary Piston Mount	1
	2L	Rotary Piston Mount – Die Cavity Bolts	4
	2M	Rotary Piston Rotary Shafts	2
	2N	Rotary Piston Rotary Shaft Bushings	2
	2O	Collars for Rotary Piston Rotary Shaft Constraint	2
	2P	Bolts for Rotary Shaft's Collar-Side Support Connections	4
	2Q	Steel Ball Joint Rod End Rotary Piston Connection	1
	2R	Die Cavity – Rotary Piston Mount	1
	2S	Mount Bolts	4
	2T	Rod End – Mount Shaft Connector	1
Stopper System	3A	Stopper Bar	1
	3B	Stopper Bar – Side Support Bolts	2
	3C	Spring Plunger Stopper	1

Sub-Assembly	Part Number	Part name	Machines
Press System	1B	Press-Punch Coupler	Lathe,Mill
	1C	Punch	Lathe
	1D	Side Supports	Mill

Die Cavity System	2A	Die Cavity	Mill
	2B	Die Cavity Rotary Shafts	Lathe
	2C	Die Cavity Rotary Bushings	Lathe
	2D	Collars for Die Cavity Shaft Rotation	Lathe, Mill
	2F	Stripper Housing	Mill
	2H	Strippers	Water jet, Mill
	2K	Rotary Piston Mounts	Mill
	2M	Rotary Piston Rotary Shafts	Lathe
	2N	Rotary Piston Rotary Shaft Bushings	Lathe
	2O	Collars for Rotary Piston-Rotary Shaft Constraint	Lathe, Mill
	2R	Die Cavity – Rotary Piston Mount	Mill
	2T	Rod End-Mount Shaft Connector	Lathe
Stopper System	3A	Stopper Bar	Mill

Table 36: bill of materials for the press assembly

4.3.7 Machine Assembly

Assembly challenges:

One of the challenges while assembling the sliding spinner was aligning the shaft's shoulders in between the supports. The shaft's shoulder should have been 1.5 inches wide, but it was off by around 0.125 inches. Adding a spring on one side, as shown in Figure 108, solved this problem. The spring acted as a shoulder for one of the bearings and stopped it from wobbling right and left.

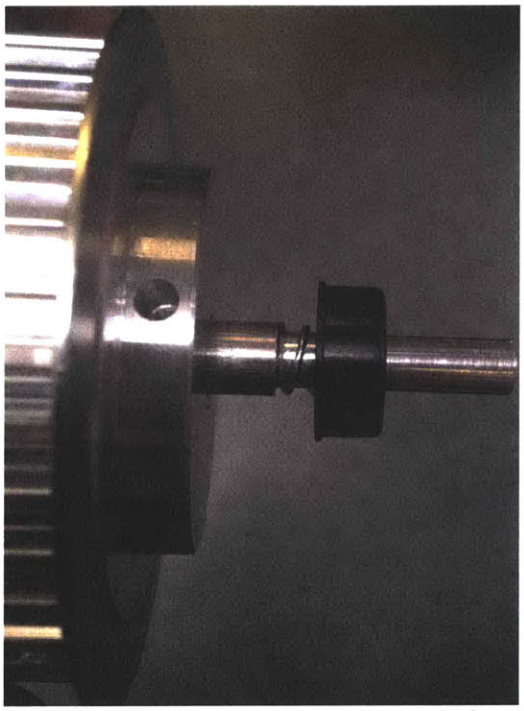

Figure 108: spring loading the driving shaft

The sliding spinner assembly process:

The assembly steps for the three sub-assemblies and the final assembly are shown below:

The motor-side supports sub-assembly:

1- Mount the sliding motor (2A) to its square tube housing (2D) using 4 M3 bolts (2C), using a 2.5 mm hex screw.
2- Mount the belt pulley (1A) on its driving shaft (1F) using the 2 M3- 25 mm pulley screws (1D). Make sure each bolts rests on a flat side of the shaft.
3- Insert 0.25" spring (1E) on one of the shoulders around this pulley.
4- Add the two 0.25"bearings (1B) on both ends of the pulley's shoulders.
5- Rest the pulley-shaft assembly between the two side supports (1C) without further tightening.

6- Place the motor L-section mount (5G) on the motor-side top support (5I) all on top of the 2 side supports (1C) and the pulley shaft assembly loose in between. Then squeeze the 2 side supports closer to each other and mount the four ¼-20 bolts, using a 3/16 Hex key, through the all pieces to live in the threaded hole inside the side supports.
7- Place the flex coupling (2B) on the sliding motor's shaft inside the motor's housing. Then mount the motor's housing (2D) to the side supports (1C) using the four ¼-20 screws (2E) by a 3/16 Hex Key.
8- Press fit the Teflon 1/8" linear bearing (6A) into its housing (6B).
9- Mount the bearing's housing (6B) to the motor-side top support (5I) and spin motor L-section (5G) using the M4 bolts (6C) and nuts (6D) by a 3 mm hex key.

<u>The driven shaft supports sub-assembly:</u>

10- Mount the second belt pulley (3A) on its driving shaft (3F) using the 2 M3- 25 mm pulley screws (3D). Make sure each bolts rests on a flat side of the shaft.
11- Insert 0.25" spring (3E) on one of the shoulders around this pulley.
12- Add the two 0.25"bearings (3B) on both ends of the pulley's shoulders.
13- Rest the pulley-shaft assembly between the two side supports (3C) without further tightening.
14- Place the top support (3E) over the 2 side supports (3C), squeeze them together and mount four ¼-20 flat top bolts (3F) using a big flat key.
15- Place one of the flexure supports (4E) on each of the 2 side supports (1C) and (3C) assemblies using M4 bolts (4G) by a 3 mm hex key. Do not tighten the bolts so much yet.

<u>The sliding carriage sub-assembly:</u>

16- Place the 4 linear bearings (4B) in their holes in the carriage (4H), then place one 3-48 bolt (4C) with 2 washers (4D) and screw them with a 2 mm Hex Key.
17- Place the small gear 0.5" bearings (5L) on the small gears' hubs (5B) and then add the 3/8" collar (5C) on the rest of the hub. Repeat for the 2 small gears.
18- Slide the 1/8" carbon fiber rod (5A) into both gears. Make sure you orient the gears in the directions shown in the assembly picture.
19- Tighten the 3/8" collars (5C) onto the carbon fiber rod (5A) using a 2.5 mm Hex Key.
20- Place the 2 sliding rods (4A) into their designated holes in the side supports (1C), then through the carriage's linear bearings (4B), and then through the other side supports (3C).
21- Place the 8 drops in 80-20 fasteners (4O) in their designated spots in the 80-20 Aluminum structure (4N).
22- Slide the 80-20 structure (4N) in between the 2 side supports' sub-assemblies.
23- Wrap the belt (4I) around the pulleys into the bottom slot of the 80-20 and its slot in the carriage.
24- Align the clamp (4J) with the belt and the carriage holes, then tighten the four 10-32 bolts (4K) and nuts (4L) using a cross key.

Final alignment and spinning mechanism:

25-Place the 80-20 fastening bolts (4P) in their holes and start aligning them with their drop-in fasteners in there. Make sure the side supports are horizontal and straight on the ground, and that the 2 side supports on each are aligned well together, then pull the 2 side supports apart to the desired belt tension and tighten the 80-20 bolts (4P) using a cross key.
26-Slide the carriage back and forth to feel the tightness or smoothness of the mechanism and tighten the shafts accordingly.
27-After you reach the desired vertical alignment location of the sliding rods, tighten the flexure supports (4E) top M3 bolts and nuts (4F) using a 2 mm hex key.
28-Tighten the bottom M4 bolts (4G) using a 3mm hex drive accordingly.
29-Place the four 3/8" clamps (5C) on the outside of the sliding rods (4A) using a 7/64 Hex Key.
30-Slide the carriage towards the spinning motor direction to observe the correct required height of the big driving gear (5D).
31-Mount the spinning motor (5F) to its L-section (5G) according to this desired gear height. You will need to screw four M3 (5H) bolts using a 2mm hex key.
32-Place the big driving gear (5D) on the spinning motor (5F) shaft.
33-Place the 12 mm ID shaft collar (5E) on the big gear (5D)'s hub and tighten it using a 3 mm Hex key.
34-Test your sliding and spinning mechanism and make sure to re-tighten the relevant bolts if any misalignments are observed.

The Bolts types and keys required were:

Part Number	Part Name	Bolt Type	Key Required
1D	Pulley screws	M3-25mm	2.5 mm Hex Key
2B	Flex coupling	M3	2.5 mm Hex Key
2C	Motor screws	M3-8mm	2.5 mm Hex Key
2E	Motor housing screws	1/4-20	3/16 Hex Key
3D	Pulley screws	M3-25mm	2.5 mm Hex Key
3F	Top support flat bolts	1/4-20	Flat key
4C	Linear bearings' mount bolts	3-48	2 mm Hex Key
4F	Flexure shaft bolts	M3	2.5 mm Hex Key
4G	Flexure mount bolts	M4	3 mm Hex key
4K	Clamp bolts	10-32	Cross key
4M	Sliding rods clamps-3/8"		7/64 Hex Key

4P	80-20 Bolts		Cross key
5C	Small gear collars	M3	2.5 mm Hex Key
5E	Big gear shaft clamp- 12 mm ID	M4	3 mm Hex key
5H	Motor screws	M3-8mm	2.5 mm Hex Key
5K	Top support bolts	1/4-20	3/16 Hex Key
6C	Linear Bearing's bolts	M4	3 mm Hex key

Table 37: Bolts and nuts needed for sliding spinner's assembly

The press assembly process:

1- Attach the piston-punch coupler (part 1B) to the pneumatic piston (Part 1A) by threading it in.
2- Attach the punch (part 1C) to the piston-punch coupler (1B) by threading it in.
3- Attach the rotary piston (part 2J) to the rotary piston mount (part 2K) using the steel ball joint (part 2Q).
4- Attached the rotary piston mount (part 2K) to the die cavity (part 2A) using the piston mount-die cavity bolts (part 2L).
5- Place the rotary piston shafts (2M) and bushings (2N) into their holes in the rotary piston (2J).
6- Place the rotary piston mount (2K), shafts (2M), and bushings (2N) in their hole in the side supports (1D).
7- Place the die cavity rotary shafts (2B) and bushings (2C) into their holes in the die cavity (2A).
8- Place the die cavity (2A), the die cavity rotary shafts (2B), and bushings (2C) in their hole in the side supports (1D).
9- Attach the side supports (1E) to the pneumatic piston (1A) by screwing the Piston-Side Support bolts (1E) through the side supports and into the pneumatic piston's threaded holes.
10- Add the die cavity's collars (2D) around the die cavity's rotary shafts (part 2D) and lock them in using the collars' bolts (2E).
11-Add the rotary piston's collars (2O) around the rotary piston's shafts (part 2M) and lock them in using the collars' bolts (2P).
12-Place the strippers (part 2H) into their housing (part 2F) with the stripping pneumatic pistons (2I).
13-Attach the stripper's assembly (2H, 2F, and 2I) to the die cavity (2A) with the stripper- die cavity bolts (2G).
14- Attach the stopper bar (3A) to the side supports (1D) using their bolts (3B).
15-Add the spring plunger (3C) into the stopper bar (3A) using its threading, and fix its position to align with the die cavity's perfectly vertical position.

Full machine assembly process:

The sliding spinner is then attached and bolted to its structure, and the press assembly is also bolted to its structure. The main constraint afterwards was to align the rod in the sliding spinner in the same horizontal level as the die cavity in the press structure. This is when the t-slotted aluminum frames were very useful in sliding the structures up/down and side to side very easily until the perfect position was achieved.

4.3.8 Machine Re-design

After some pills were made, as seen in Figure 109, their two main problems were:

1) Uneven and Bulging shape
2) Metal contamination

Figure 109: first batch of pills

To solve problem one, the pill's bulging shape, the following actions were taken:

1- Testing different pressing pressures to find the one that gave the best pill shape.
Conclusions: less than 10 Psi does not give flat surfaces and more than 25 Psi make the edges curl up.

2- Machining the die cavity's bottom chamfer, because it was one of the reasons the pill's bottom bulged out.

Figure 110: the die cavity 's chamfers

As seen in Figure 110 above, there is a bottom chamfer opposite to the top visible chamfer. This chamfer was machined off to have a completely flat bottom surface.
Conclusion: the bulging effect became less, but it was still there at a minimal level due to the small gap between the moving strippers and the die cavity.

3- After machining the chamfer off, the pills still had minimal bulging. This was due to the clearance tolerance between the strippers and the die cavity at the spot shown in Figure 111. This tolerance had to be of a clearance fit to allow the movement of

the strippers back and forth, but the effect of pressing forces on them was not estimated correctly in the design of the original strippers.

Conclusion: Initial designs for spring-loading the strippers upwards were analyzed, but they were not carried forward due to the time limitations of the project.

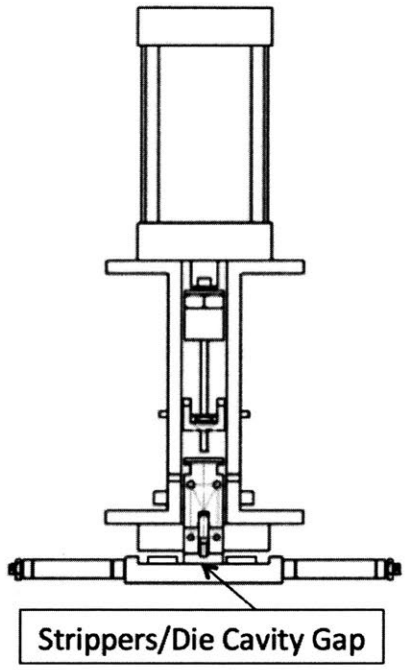

Figure 111: strippers/die cavity gap

To solve problem 2, the metal contamination, the components touching the polymers were analyzed one by one:

1) The spinning rod collector:
   The two important characteristics in choosing the material for the rod collector were high electrical conductivity and high wear resistance. First, an **aluminum** rod was used, but it stripped off a lot of metal with the polymer. Secondly, a **carbon fiber** rod was used, and its pills had no metal contamination, but the productivity was very low due to its low electrical conductivity. Thirdly, **17-4 PH hardened steel** was used, but it still stripped off a lot of steel with the polymer, and had lower productivity due to the steel's low electrical conductivity. Finally, **anodized aluminum** was used. It had much better electrical conductivity and it did not strip off any of metal with the polymer.
2) The conical support:
   As discussed earlier in the electrospinning chamber design section, there were two conical support designs. The first design was made out of aluminum, but some aluminum wears off while the rod spins in its hole. The second design was made out of Polytetrafluroethane (PTFE), so the metal wear and pill contamination problem by this piece was resolved.
3) The die cavity:

While running the machine's first trials, there were many misalignments between the punch and the cavity. This made the punch scratch the cavity's sides and strip some metal off. Anodizing this aluminum die cavity enhanced its wear resistance and resolved this problem.

4) The punch:
   It was made out of stainless steel. After running many experiments, it was observed that it did not add any metal contamination to the pills. Thus, the material did not need any changes, because it was not subjected to any wear or high forces.
5) The strippers:
   Brass was chosen over steel and aluminum for this model, because it has higher wear resistance and it is easy to manufacture. But some of the brass chipped off and appeared in some pills. The industrial prototype is intended to have ceramic strippers, because ceramic has a much higher wear resistance. Ceramic was not used in this prototype because it is hard to manufacture and it is not flexible if any design changes were needed.

A third problem was observed while running the machine. This problem was that the sliding motor was too small for the torque required. Thus, a bigger motor with more torque had to replace the Nema 17 motor used. The first calculations of the spinning motor were carried out using the equations:

$$T_{sl} = F_{sl} * R_{py}$$

Equation 21

where T_{sl} is the sliding motor's torque requirement, F_{sl} is the sliding force, and R_{py} is the radius of the belt's pulley. F_{sl} can be calculated by:

$$F_{sl} = (\mu_{slb} * W_{sl}) + F_{str}$$

Equation 22

where F_{sl} is the sliding force; W_{sl} is total weight of the sliding components including the carriage, its attached gears, and couplings; F_{str} is the force with which the strippers press on the rod .

Plugging in the numbers gave a sliding torque of 0.036 Nm, which was much less than the motor's capacity of 0.45 Nm. But after starting the experimental work, it was observed that the force with which the polymer sticks to the rod was the most dominant force, and it was not included in the earlier analysis, so Equation 22 had to be updated to Equation 23 by adding the polymer's force as follows:

$$F_{sl} = (\mu_{slb} * W_{sl}) + F_{str} + F_{poly}$$

Equation 23

where F_{poly} is the frictional force with which the polymer sticks to the rod.

$$F_{sl} = 0.858 + F_{poly}$$

Studying the exact force exerted by the polymer needed further analysis and experimentation. In the interest of time, the motor was oversized to ensure the system would function.

A sudden rotation of the die cavity was observed every time a pill was pressed. This was the fourth main problem encountered. This bent the punch so many times, as seen in Figure 112 below:

Figure 112: the bent punch challenge

After carrying out the test multiple while changing different parameters, it was concluded that it phenomenon was due to the high pressure difference between the pressing piston (50 Psi) and the rotary piston (20 Psi). Every time the press's punch goes down, it sucks 50 Psi out of the compressor. To recover those 50 Psi, it quickly sucks the 20 Psi holding the rotary piston in place. Thus, the rotary piston rotates and bends the punch.

Part Name	Pressure [psi]
Main Pressure	100
Pressing Piston	50
Rotary Piston	20
Strippers' Piston	15

Table 38:table of pressure distribution

This challenge was resolved by connecting the high pressure tubing (of the pressing piston) to one of the compressor's outputs, and the low pressure tubing (of the rotary and strippers pistons) to the other compressor's output. This separated the high pressure from the low pressure and avoided any interference between them.

4.4 Chemical preparations

4.4.1 Polymer solution preparation

In the previous work by Indrani Bhattacharyya [40], two kinds of solutions were tested: poly(vinyl alcohol) (PVA) dissolved in water, and poly (vinyl pyrrolidone) (PVP) dissolved in ethanol. This work proceeded with PVA in water because water is safer than ethanol, especially in environments where the chamber is open from some sides with parts moving in and out. The chemicals were purchased from Sigma Aldrich.

The chemicals and their percentage added by weight were as follows:

1- 20wt% PVA (Mowiol 4-88) (Mw ~ 31,000)
2- 1.5wt% High desnity PVA (146-186kDa)
3- Deionized (DI) water

The materials looked as seen in Figure 113 below:

Figure 113: polymer materials used

High density PVA was added to the Mowiol 4-88 because it is directly correlated to higher productivities and better fiber quality[27,30]. The tools used to prepare the samples were: a college B1302 scale, a thermoscientific magnetic heater and stirrer, and sealed glass laboratory bottles. All the laboratory materials were purchased from VWR. The samples were prepared in batches of 300 mL. This quantity makes 10 experiments, as the polymer bath is fills up using 30 mL. The mix was composed of:

Chemical	Percentage Weight	Weight [grams]
PVA	20	60
High density PVA	1.5	4.5
De-ionized (DI) water	100	300

Table 39: Quantities used for mixing PVA in water

The steps for preparing this sample were as follows:

1- Fill the bottle with 300 grams of DI water.
2- Place the bottle over the heater and stirrer, with the magnetic stirrer placed inside the bottle.
3- Turn the stirring on to 500 rpm and heat to 90 degrees Celsius.
4- Start adding the measured weights of PVA and high density PVA gradually
5- Keep the mixture on the heater and stirrer overnight until the solution is completely clear.

4.4.2 Polymer and API mix preparation

The Active pharmaceutical ingredient (API) used in this experimentation was Fenofibrate. Fenofibrate is a drug used to treat high levels of cholesterol for diabetes patients. Eletrospinning nanofibers has the great advantage of quick drug release, which is highly needed in lowering the levels of cholesterol for diabetes patients. In the previous work of Indrani Bhattacharyya, 2.3% and 12.% weights of Fenofibrate were dissolved in the PVA solution [40]. In this work, the same percentages were used to have comparable results.

The 2.5% weight Fenofibrate mix was composed of:

Chemical	Percentage Weight	Weight [grams]
PVA	20	20
High density PVA	1.5	1.5
De-ionized water	100	100
Fenofibrate	2.5	0.55

Table 40: Quantities used for mixing 2.5% Fenofibrate and PVA

The 12.5% weight Fenofibrate mix was composed of:

Chemical	Percentage Weight	Weight [grams]
PVA	20	20
High density PVA	1.5	1.5
De-ionized water	100	100
Fenofibrate	12.5	3.07

Table 41: Quantities used for mixing 12.5% Fenofibrate and PVA

The steps for preparing this sample were as follows:

1- Place the specified quantity of the PVA solution on the magnetic heater and stirrer.
2- Turn the stirring on 500 rpm and heat to 40 degrees Celsius (to avoid reaching Fenofibrate degradation temperature.
3- Start adding the measured weights of Fenofibrate and to the mixture gradually.
4- Keep the mixture on the heater and stirrer overnight until the solution is of a cloudy white color with no particulate suspension.

Immediately before electrospinning, suspensions were mixed with IKA 24 ULTRA-TURRAX using a coarse rotor stator generator to confirm dispersion.

4.5 Pill Pressing Process

The pill pressing process is carried out in the 11 steps mentioned below:

1- Sliding Spinner moves forward

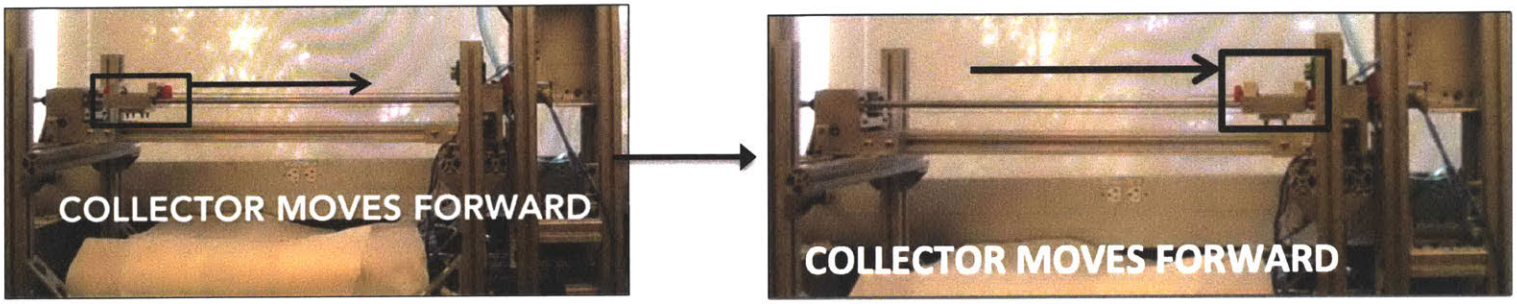

2- The gears engage and start spinning the polymer rod

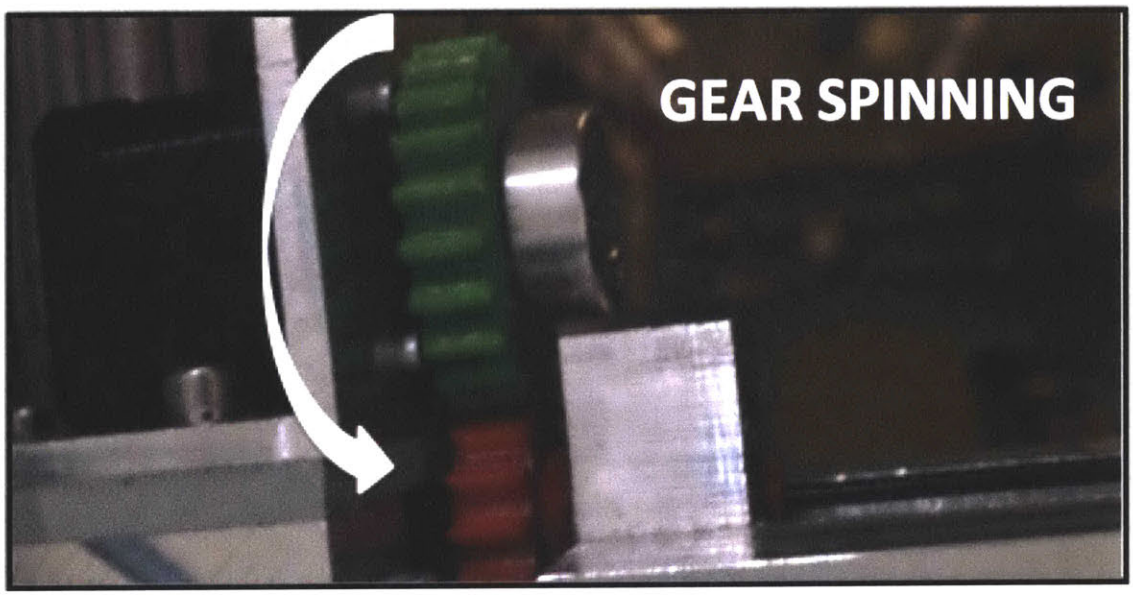

3- Polymer Electrospinning

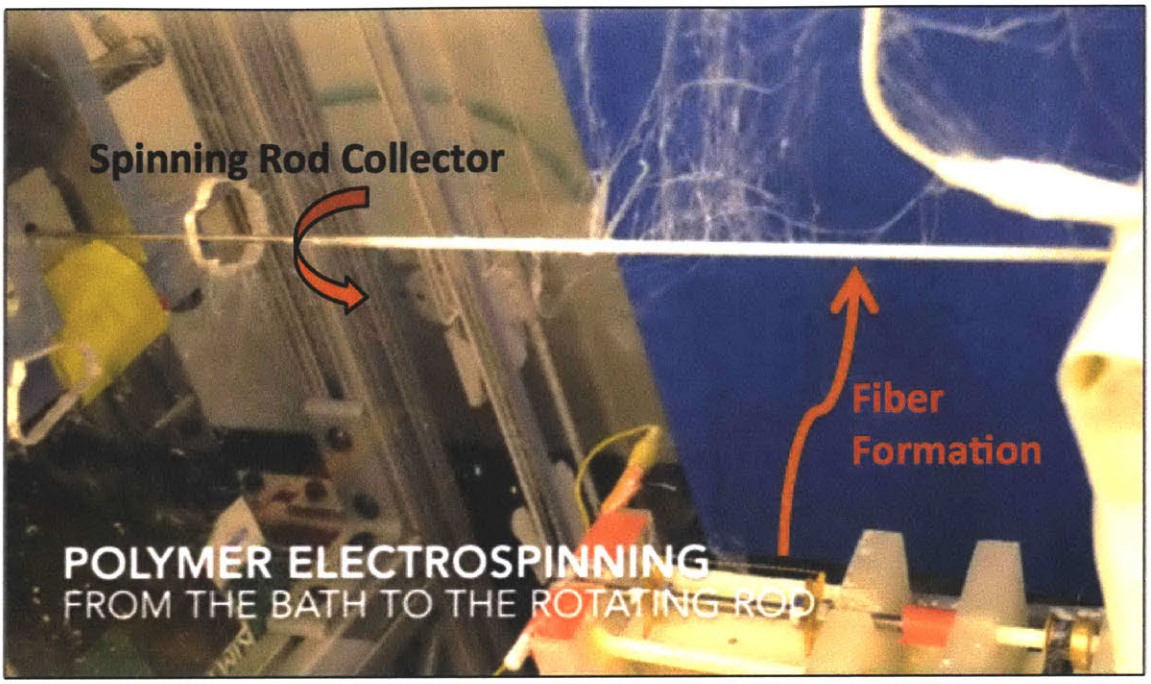

4- Stripper one closes

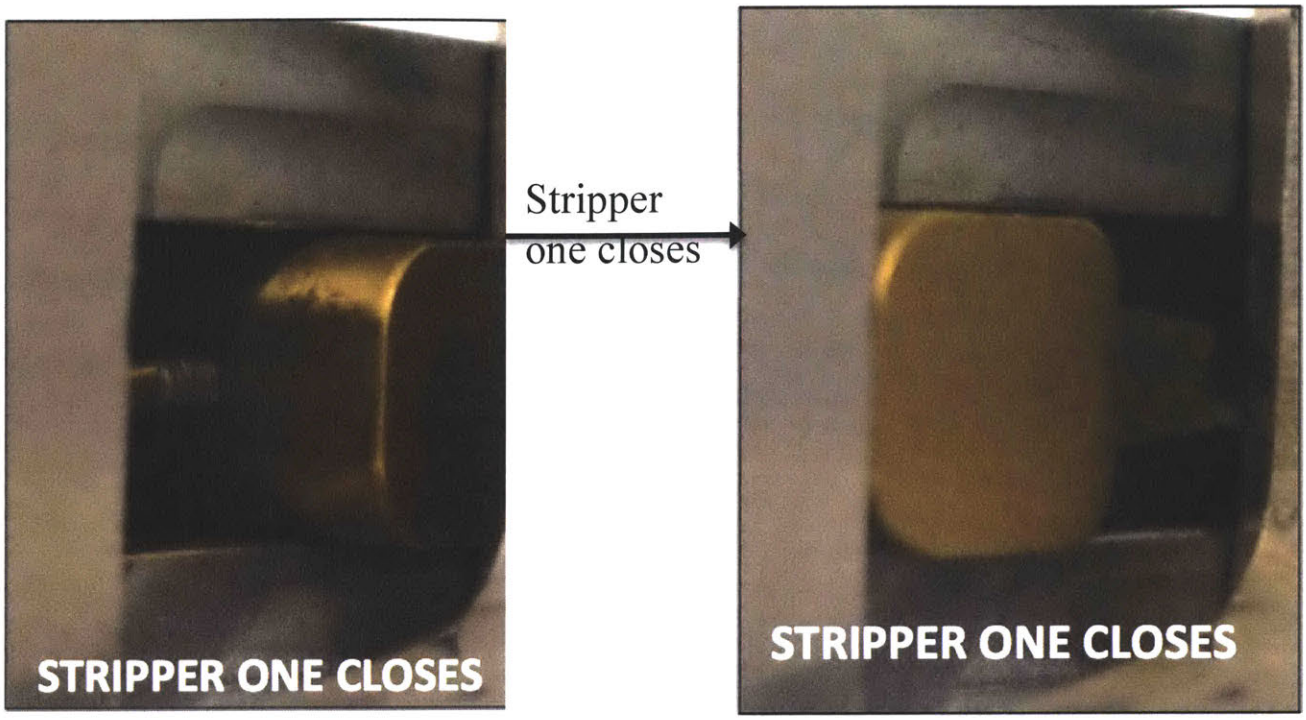

5- Stripper two closes

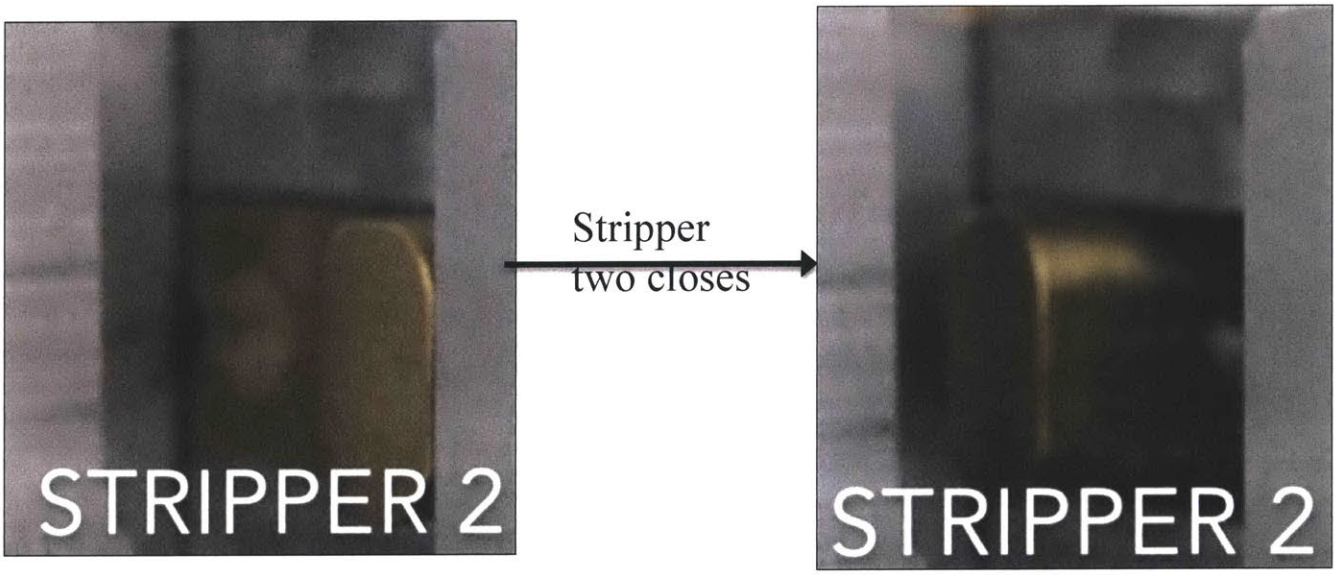

6- Collector Moves backward and the polymer is stripped off the rod, from the outside it looks like:

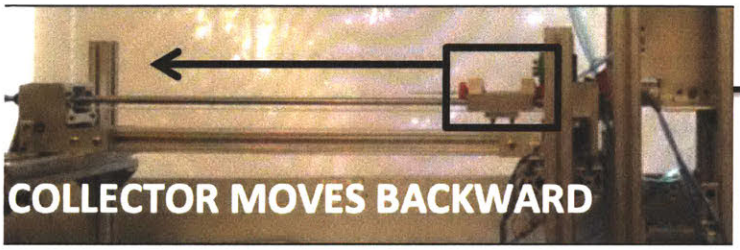

From the inside, this is how the stripping process looks like:

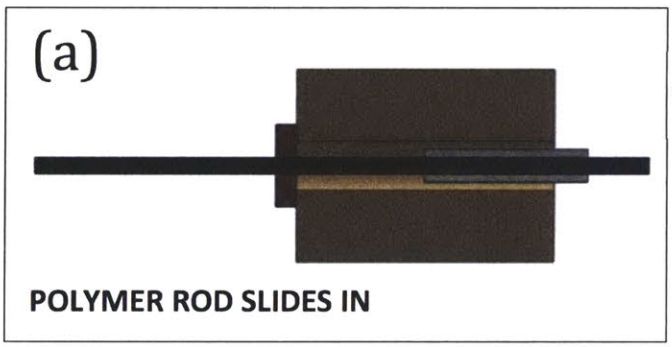

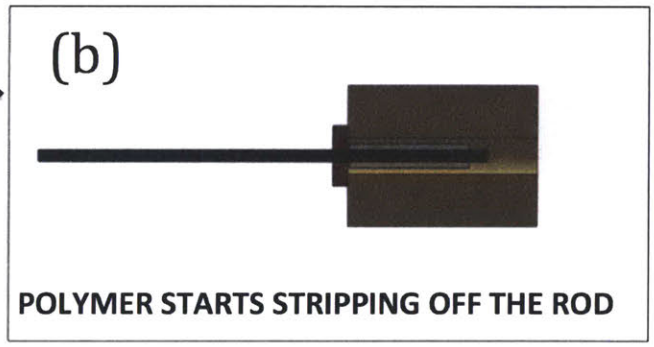

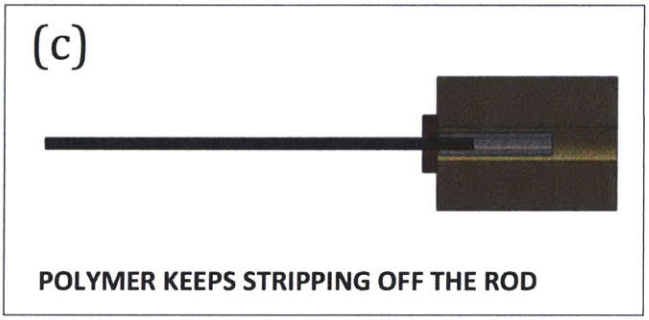

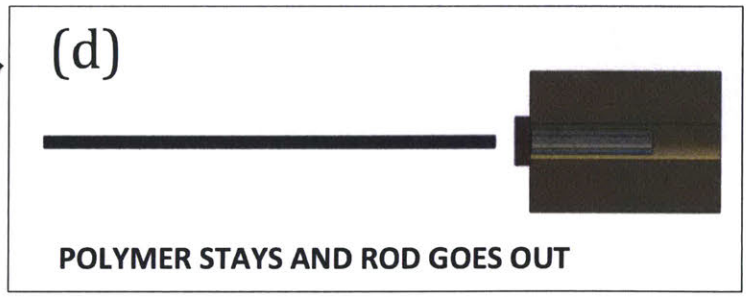

7- Stripper one opens:

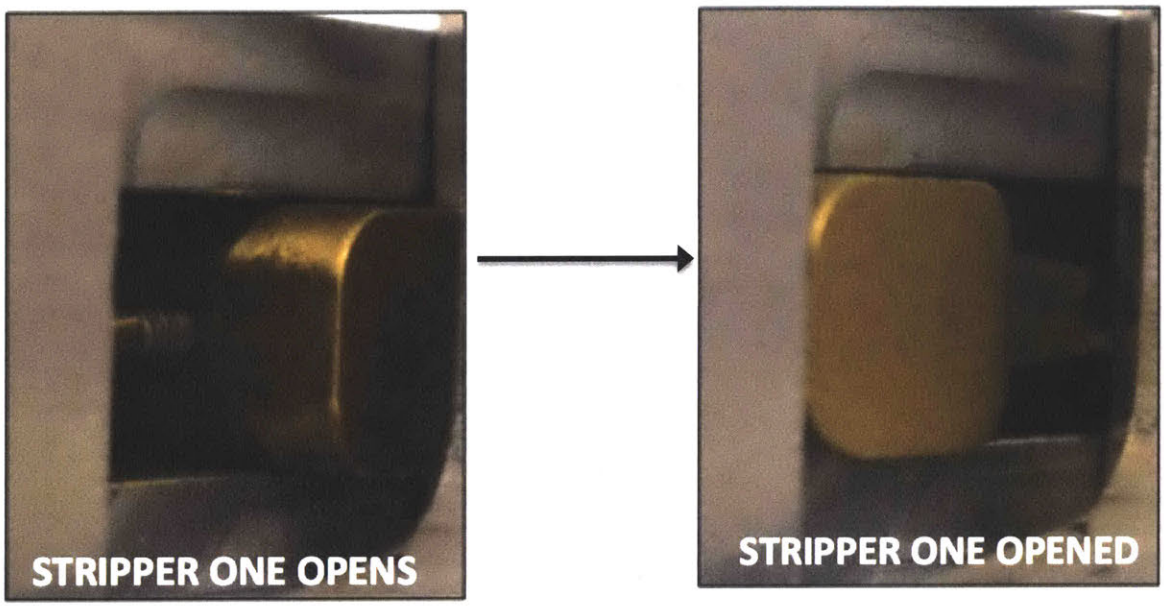

So stripper two is fully closed:

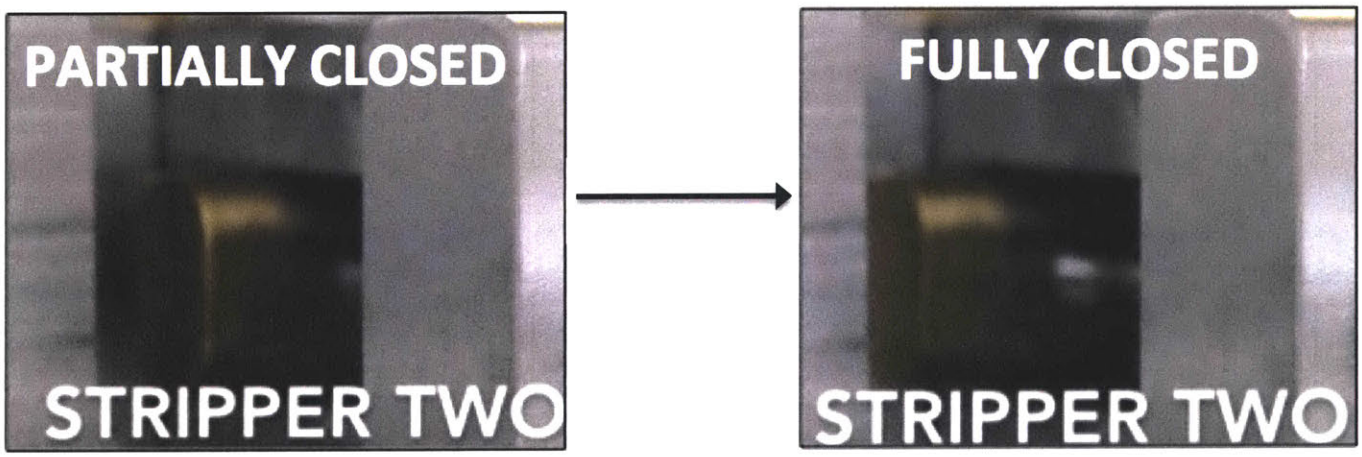

This is the interior view of the polymer locked inside, and the fully closed position of stripper two to become base for the pressing process:

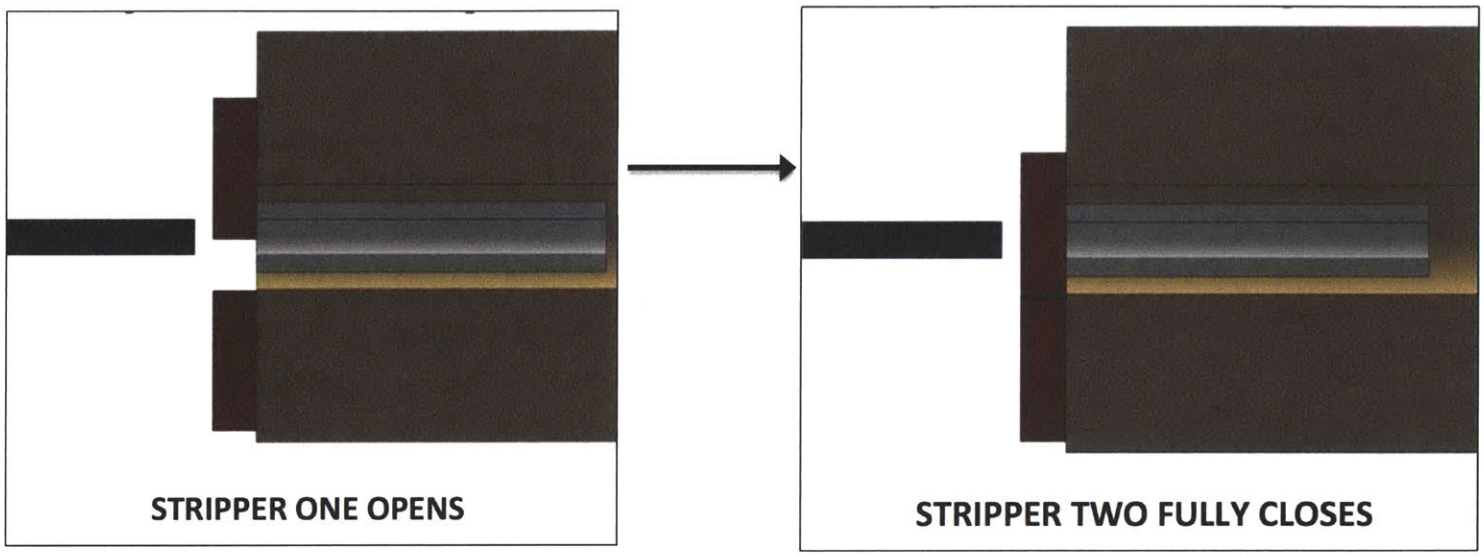

8- Die cavity 90 degrees anti-clockwise rotation

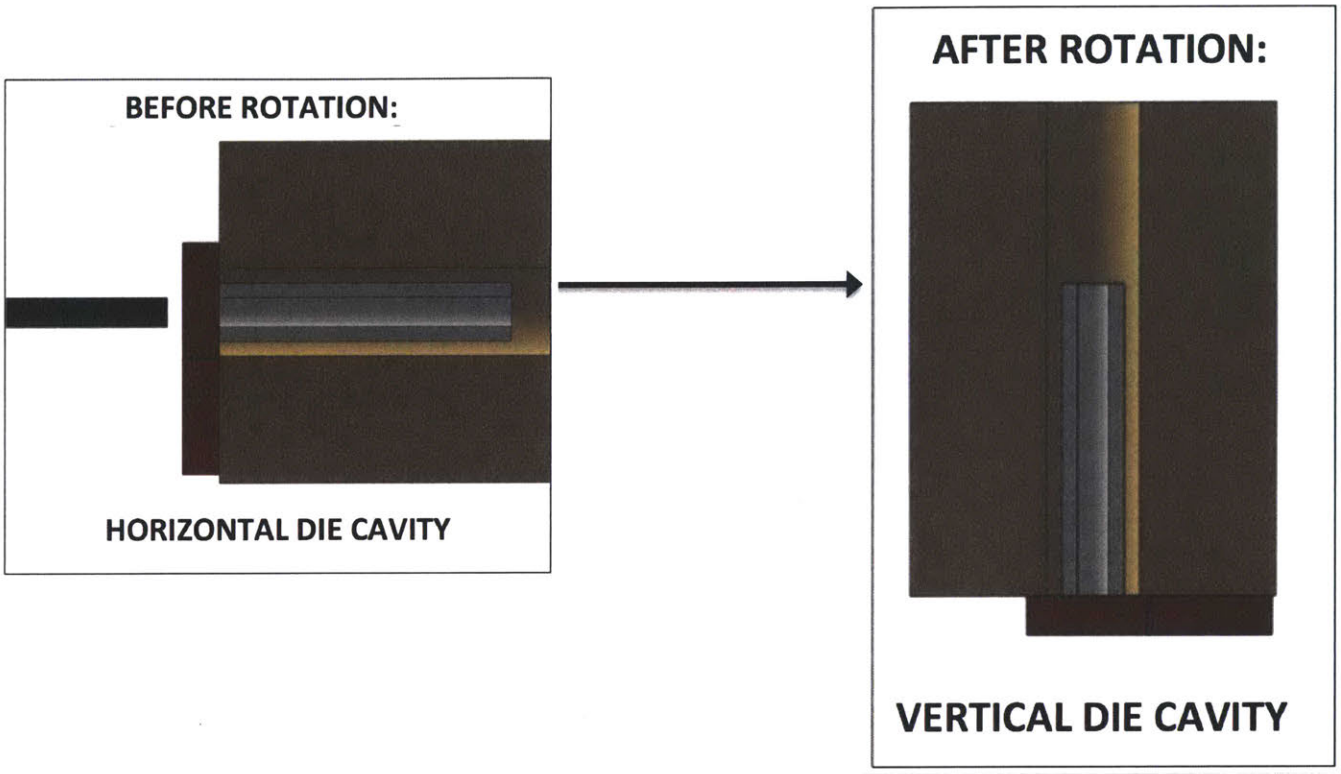

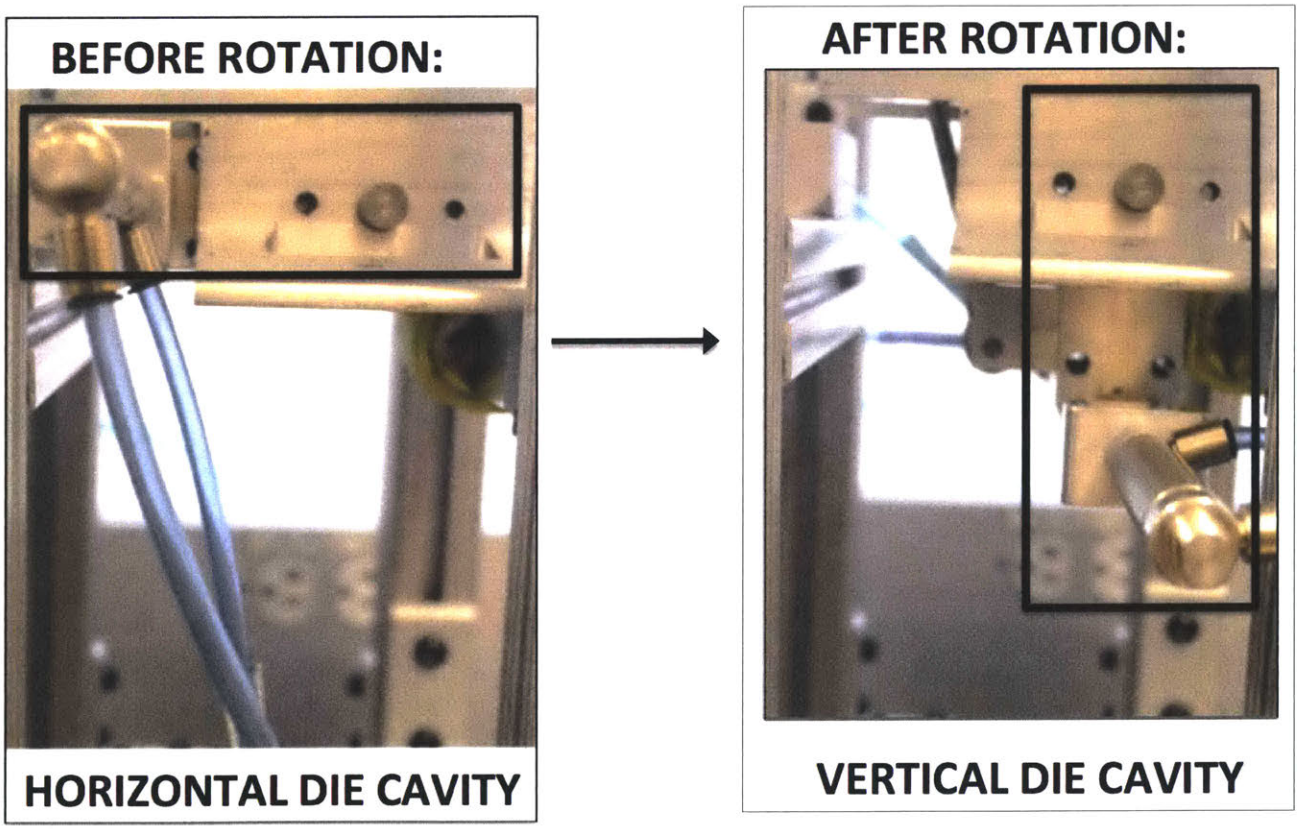

9- Press goes down to press the pill

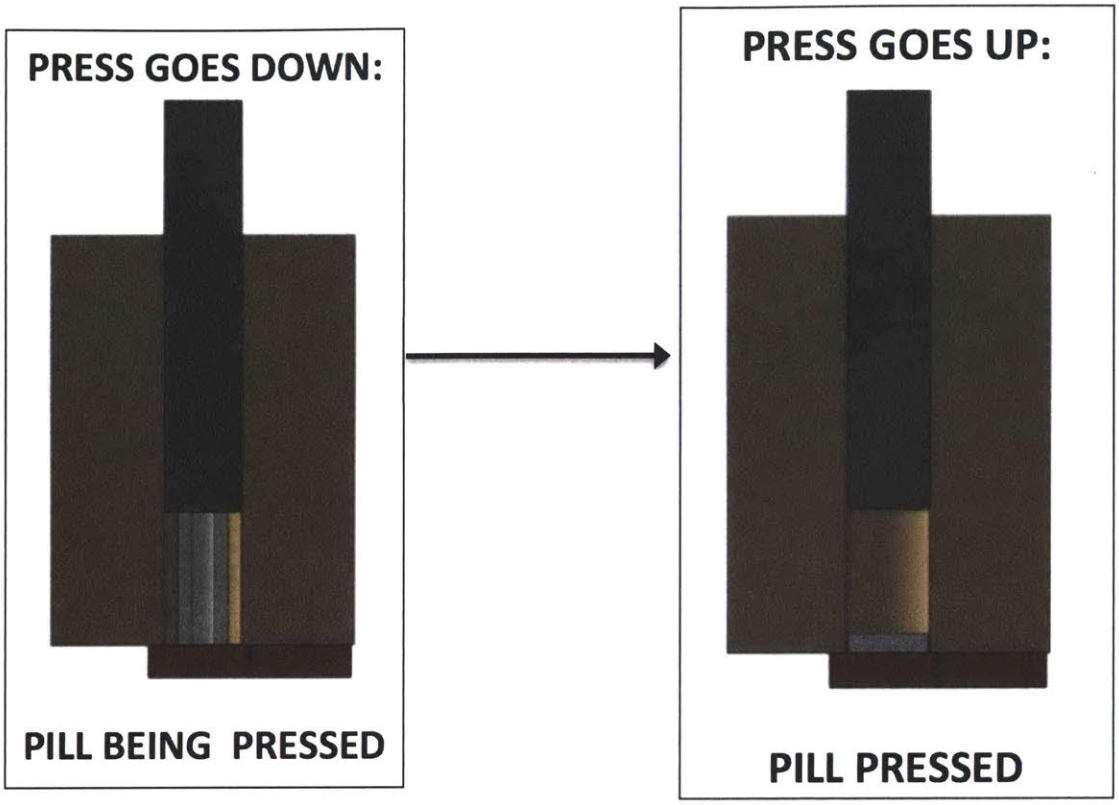

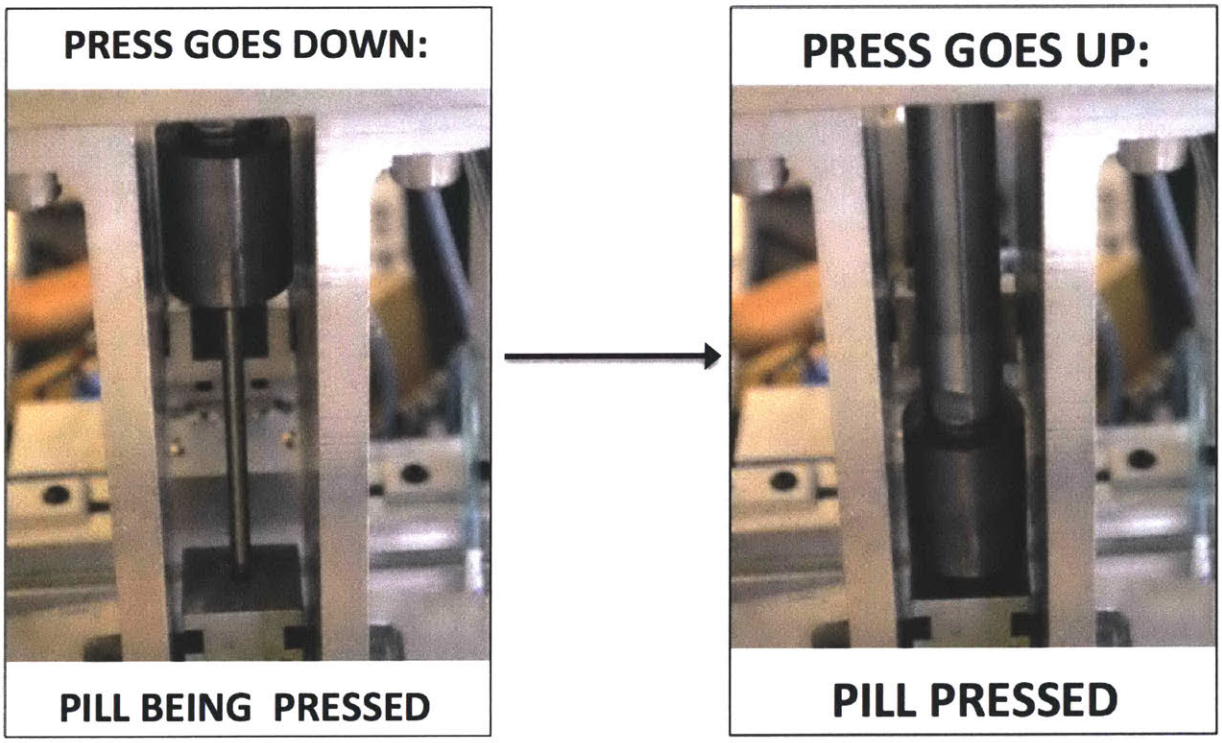

10-Stripper two opens

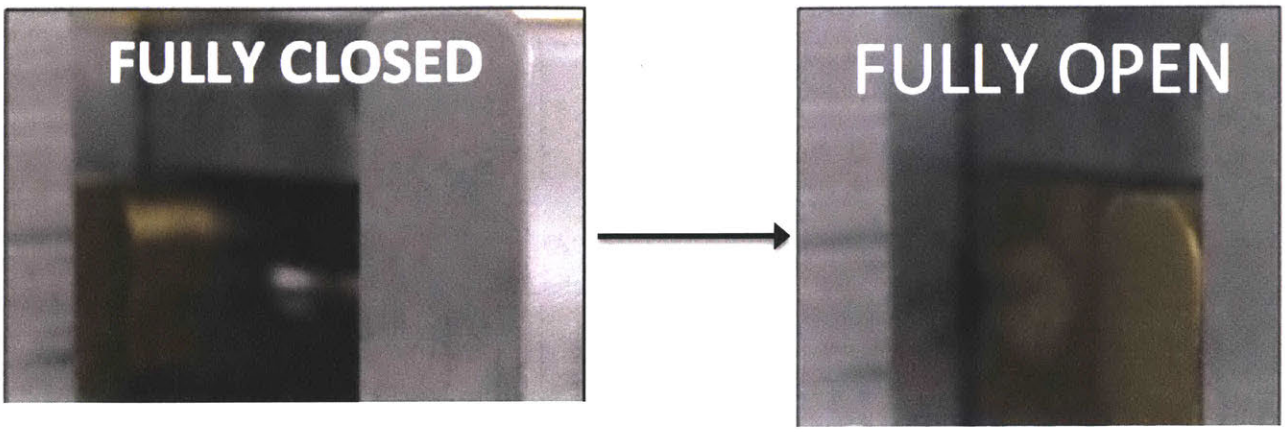

From the inside, opening stripper two would look like this:

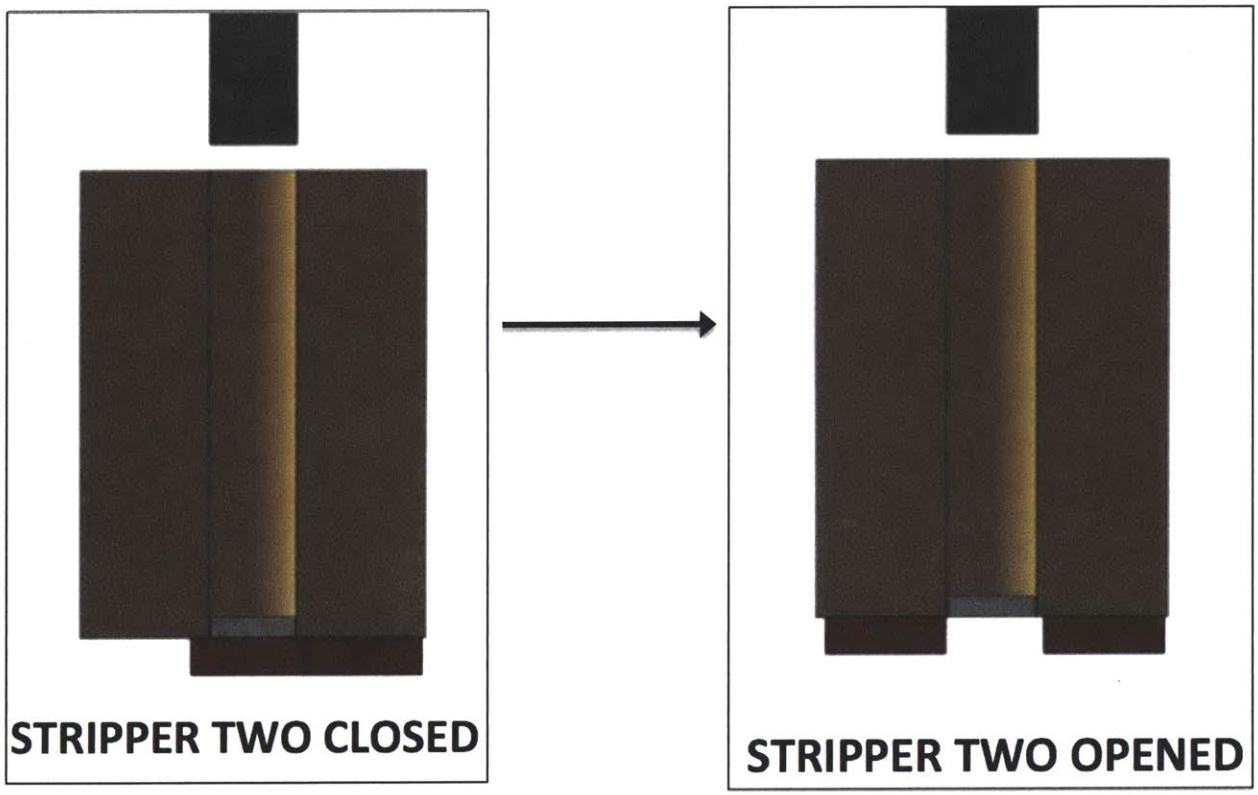

11-Pill Ejection

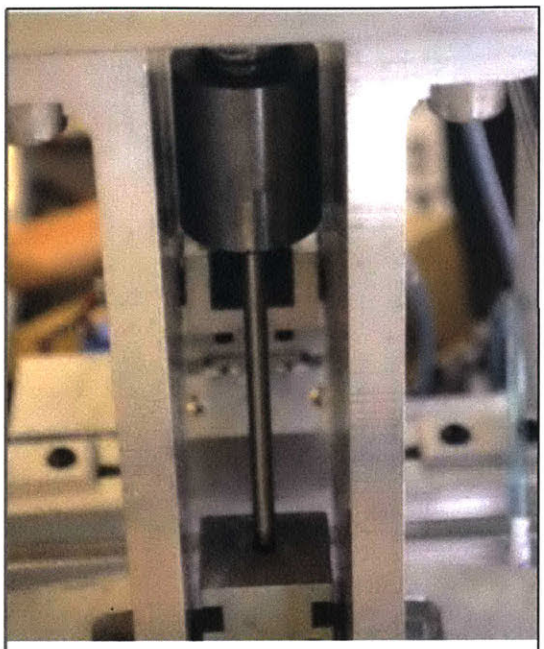

BEFORE PILL EJECTION

AFTER PILL EJECTION

An inside look of the ejection looks like:

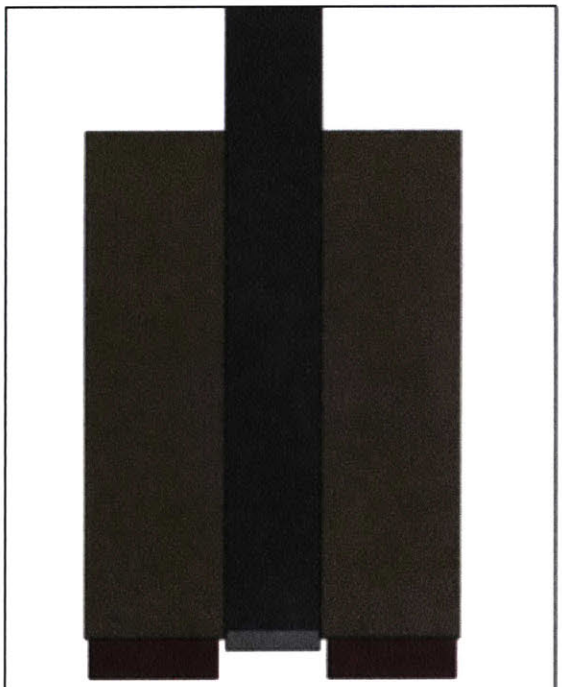

BEFORE PILL EJECTION

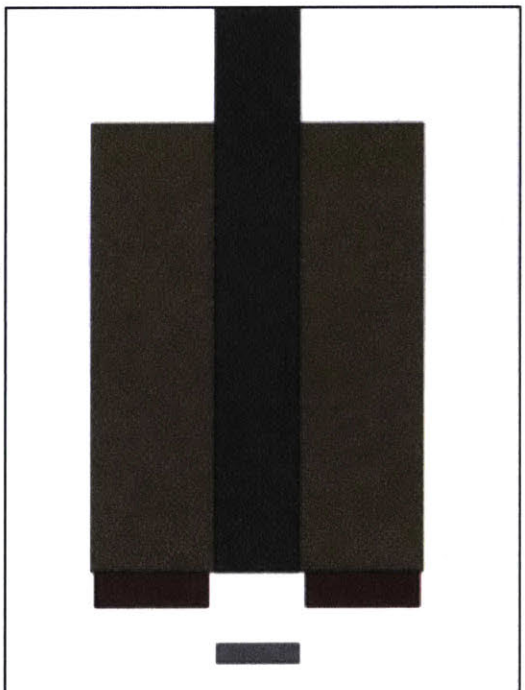

AFTER PILL EJECTION

The pill is ejected in its receiver that looks as follows:

12-Die cavity 90 degrees clockwise rotation: to re-align the mechanism horizontal and restart the process again.

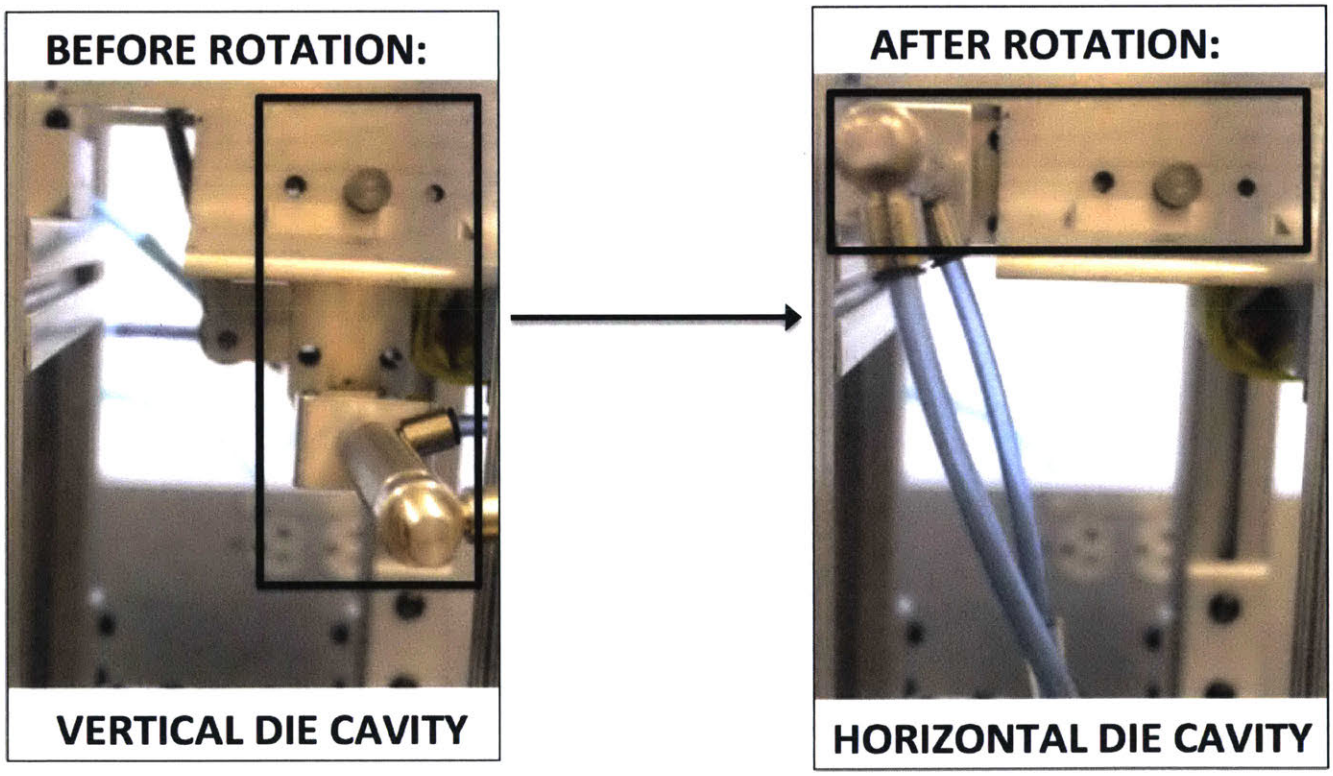

The methods of carrying out each of the previous steps were as follows:

No.	Name	Function	Method
1	Sliding Spinner moves forward	To slide the rod collector into the electrospinning chamber on top of the wire spinneret	Sliding Stepper Motor
2	The spinning gears start spinning the polymer rod	To collect the polymer homogenously around the rod	Spinning Stepper Motor
3	Polymer Electrospinning	To spin nanofibers from the wire spinneret to the rod collector	High Voltage Power Supply, Spinneret Spinning Motor, Rod Collector Spinning Motor
4	Stripper 1 closes	To wrap tightly around the rod collector and strip the polymer off when the collector slides in	Strippers' pneumatic piston 1
5	Stripper 2 closes	To wrap tightly around the rod collector and strip the polymer off when the collector slides in	Strippers' pneumatic piston 2
6	Collector Moves backward	To strip the polymer off the rod	Sliding Stepper Motor
7	Stripper 1 opens	For stripper 2 to fully close, and become the press's flat bottom	Strippers' pneumatic piston 1
8	Die cavity rotation	To align the die cavity vertically & ready for pill pressing	Rotary Piston
9	Pill Pressing	To press the collected polymer into a pill shape	Press's Piston
10	Stripper 2 opens	To open the base of the press and make it ready for ejection	Strippers' pneumatic piston 2
11	Pill Ejection	To push the pill out of the die cavity	Press's Piston
12	Die cavity rotation	To re-align the die cavity horizontally & restart the process	Rotary Piston

Table 42: The methods for the pill pressing steps

Chapter Five: Testing & Results

"The joy of discovery is certainly the liveliest that the mind of man can ever feel."
Claude Bernard

5.1 Electrospinning Parameters experiments

5.1.1 Flat plate collector results

Some of the main parameters affecting the electrospinning output are: voltage, spinneret's rpm, and the spinneret-collector distance. Before designing the updated electrospinning setup, some experiments were carried out in the previous setup. These experiments assisted us in sizing the new chamber and giving a feel of the expected output from the process.

Throughout all the experiments, the temperature was 25 degrees Celsius, the relative humidity was kept constant at 20% and the same amount of polymer solution (30 mL) was spun for 7 minutes.

1st Variable: Spinneret-Collector Distance:

Keeping the voltage constant at 40 kV, and the spinneret's at 2.5 rpm, the collected data looks as follows:

Distance [cm]	Productivity [mg/cm/min]
28	0.481
25	1.424
23	1.455
20	3.127
18	3.613
15	9.011

Table 43: spinneret- collector Distance and productivity

The distance versus productivity relationship looks as follows:

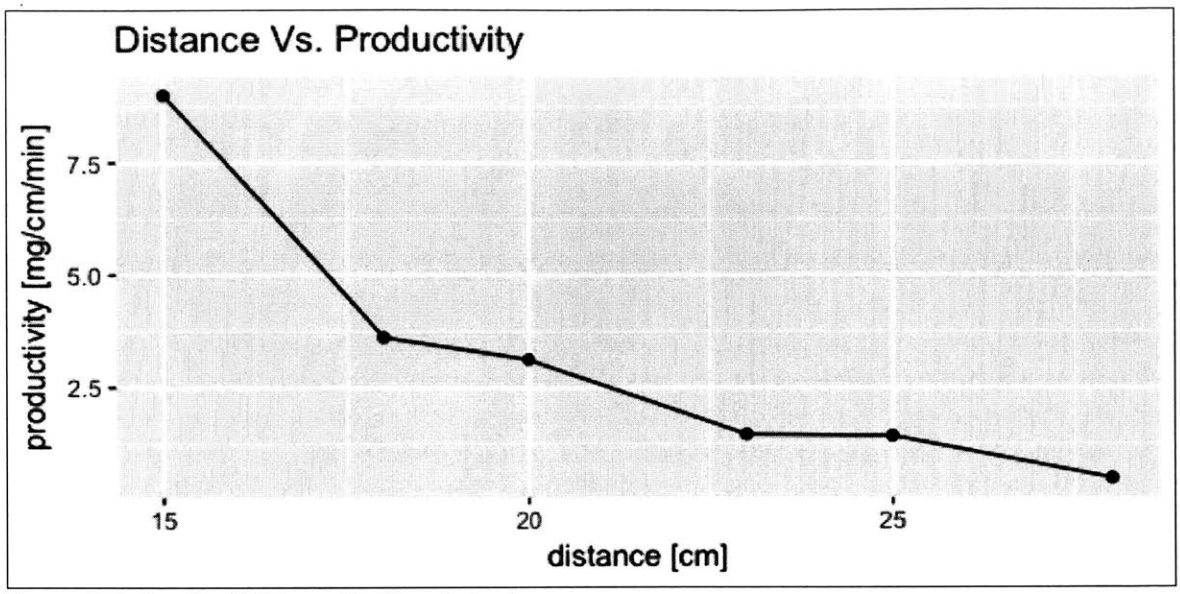

Figure 114: Graph of Distance Vs. Mass Output

As seen in Figure 114, the productivity at a distance of 15 cm is much higher than the trend. This is probably due to immature wetting of fiber.

Excluding this extreme point, the data would be:

Distance [cm]	Productivity [mg/cm/min]
28	0.481
25	1.424
23	1.455
20	3.127
18	3.613

Table 44: corrected spinneret- collector distance and productivity

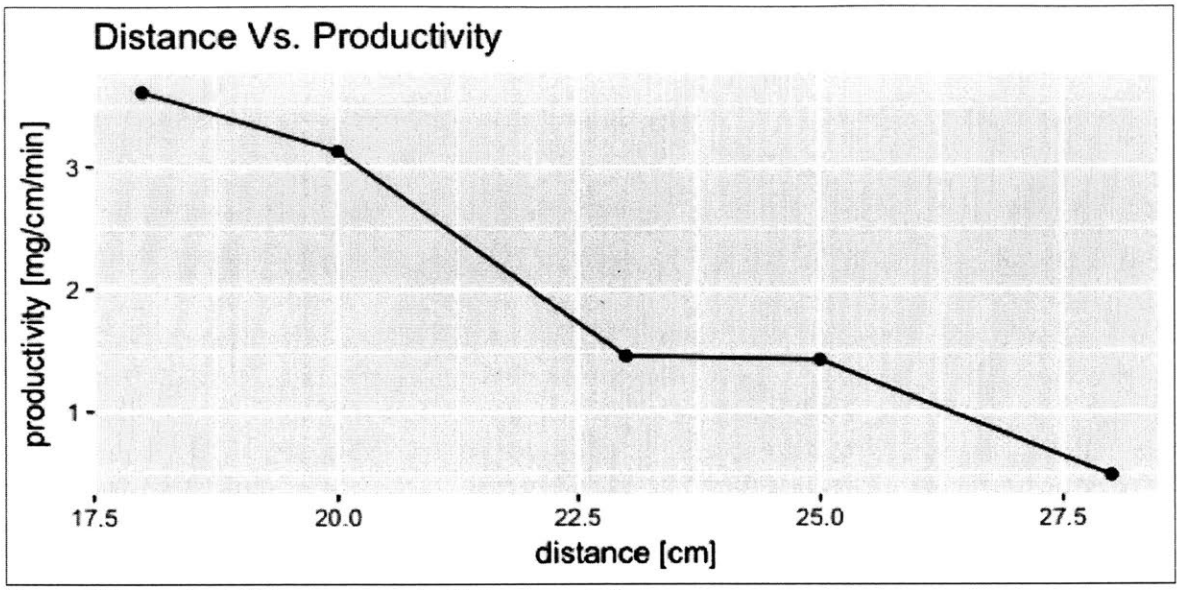

Figure 115: graph of distance vs. productivity corrected

After calculating the electric field using the distances above and the 40kV applied. The data would be:

Electric field [kV/m]	Productivity [mg/cm/min]
143	0.481
160	1.424
174	1.455
200	3.127
222	3.613
267	9.011

Table 45: electric field and productivity due to varying distance

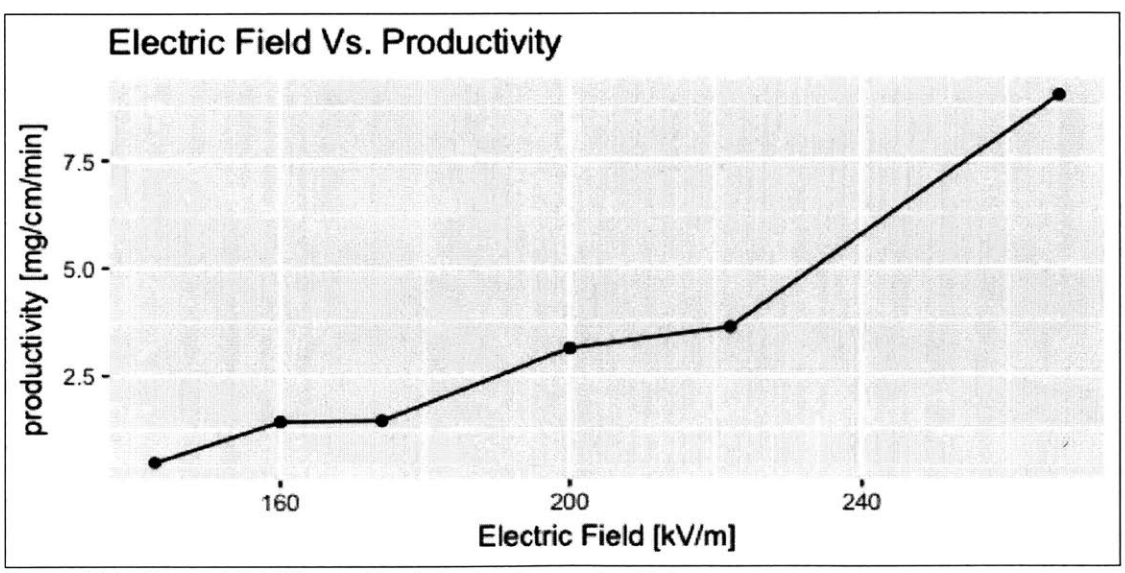

Figure 116: Electric Field Vs. productivity due to varying distance

Figure 116 looks like the reciprocal of Figure 114 because the electric field equation is:

$$Electric\ field\ \left[\frac{kV}{m}\right] = \frac{Applied\ Voltage\ [kV]}{Spinneret\ Collector\ distance\ [m]}$$

Equation 24

2nd Variable: Applied Voltage:

Keeping the distance constant at 20 cm, and the spinneret's at 2.5 rpm, the data collected looks as follows:

Voltage [kV]	E [kV/m]	Productivity [mg/cm/min]
34	170	0.903
36	180	1.345
38	190	2.207
40	200	3.127
42	210	4.044
44	220	4.547

Table 46: applied voltage, electric field, and productivity

The graph of the applied voltage versus productivity looks as follows:

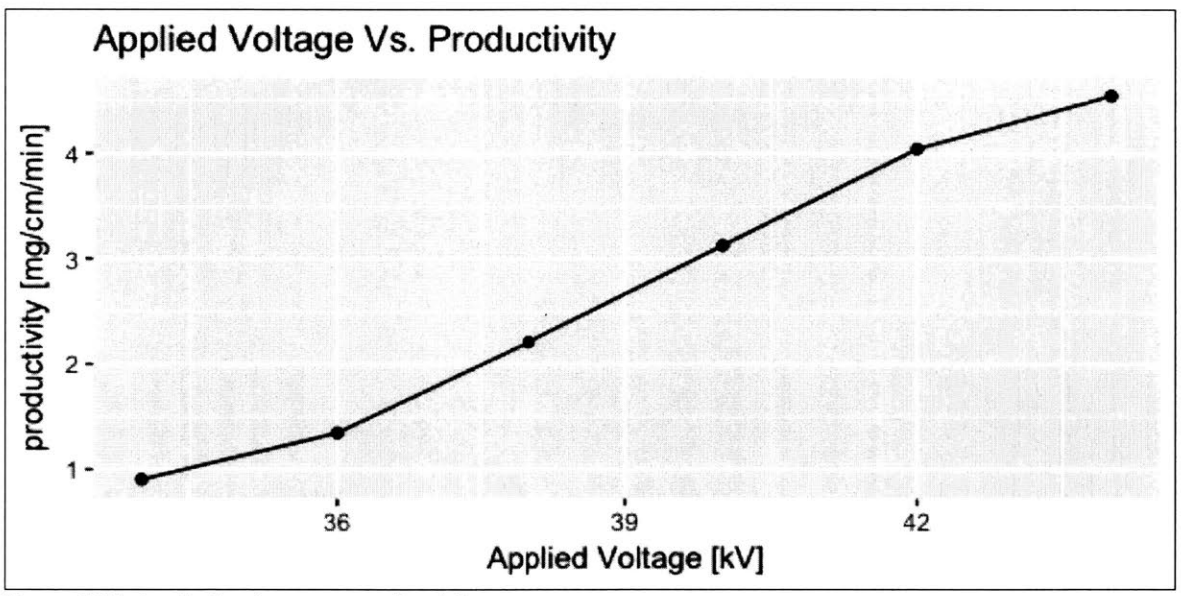

Figure 117: Applied voltage vs. productivity

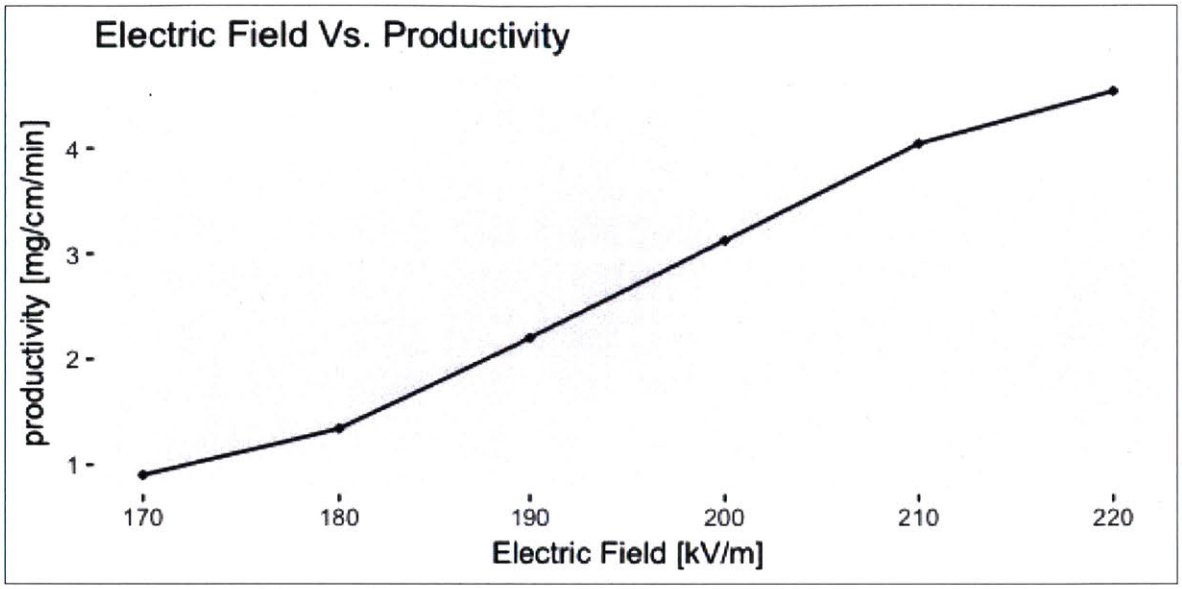

Figure 118: Electric Field vs. productivity due to varying voltage

The relationship between the voltage, electric field, and productivity looks almost linear, as shown in Figure 117 and Figure 118. They are also showing a similar trend because they are directly proportional, as shown in Equation 24.

Comparing the Electric field versus mass output relationship obtained from changing the distance to the one obtained by changing the voltage gives the following graph:

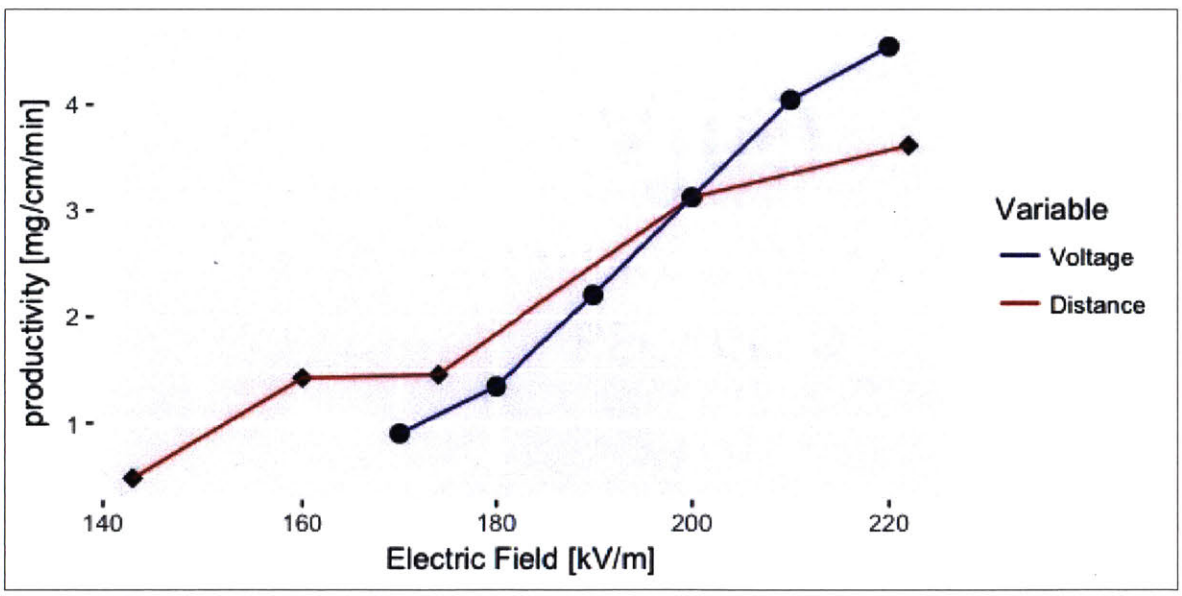

Figure 119: Electric Field vs. productivity due to varying distance & voltage

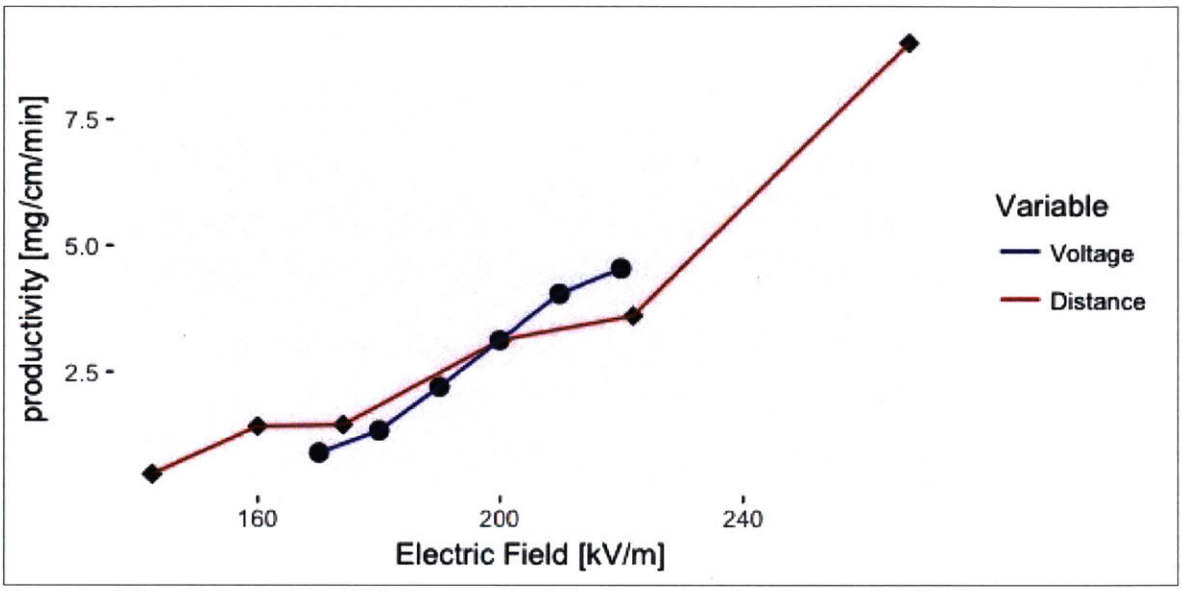

Figure 120: Zoomed out Electric Field vs. productivity due to varying distance & voltage

In concept, both graphs follow the same shape of a third degree polynomial. But the voltage experiment is more reliable and trusted because it is more accurate to change the voltage digital reading than manually changing the distance of the scissors lift and trying to get an accurate vertical measurement. The distance experiments also showed the fact that at lower electric fields, the mass output is almost stabilized at a very low mass, and then it boosts so much at higher values.

3rd Variable: Spinneret's RPM:

The motor used for the spinneret's rotation was inherited from the early setup with the following equation to transform the input voltage to RPM:

$$Y = 3.0944x - 0.5549$$

Equation 25

Where (Y) is the rpm and (x) is the applied voltage, which means that 1 Volt gives 2.5 rpm, and all the voltage values would translate to rpm values as follows:

Voltage	RPM
0.4	0.683
0.6	1.302
0.8	1.921
1.0	2.540
1.1	2.849
1.4	3.778
1.7	4.706

Table 47: Voltage to RPM translation

The temperature, humidity, solution quantity, and time were kept constant at the same values above. While keeping the voltage constant at 40 kV, and the distance at 20 cm, the collected data for different RPM looks as follows:

RPM	Productivity [mg/cm/min]
0.683	0.811
1.302	2.462
2.540	3.020
2.849	3.127
3.778	3.429
4.706	2.785

Table 48: Spinneret's RPM and productivity

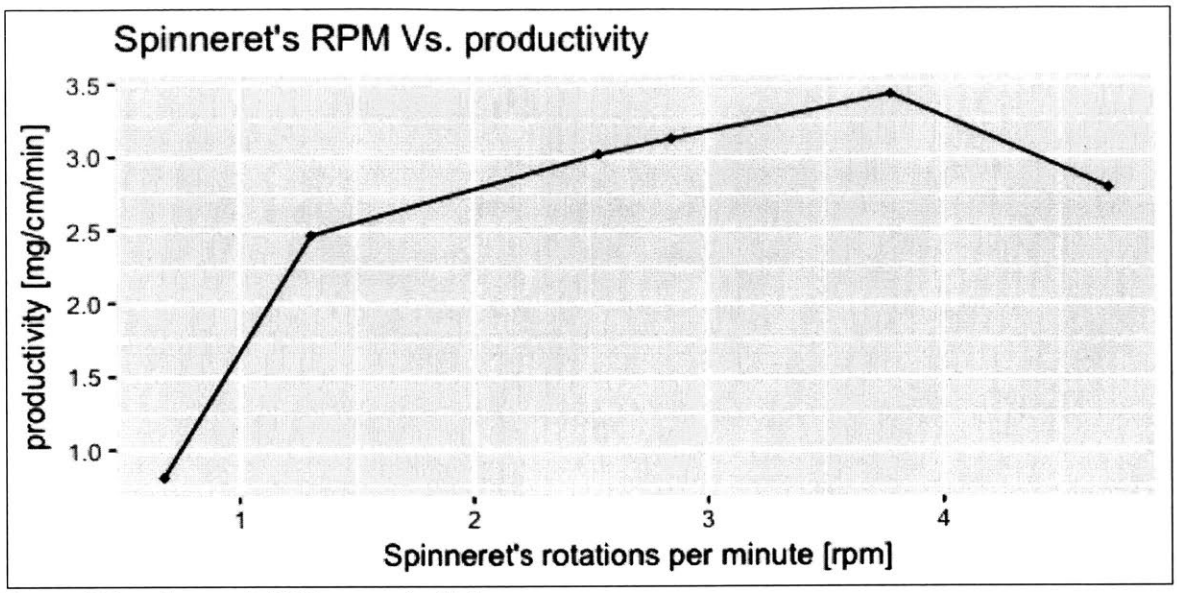

Figure 121: spinneret's RPM vs. productivity

As seen in Figure 121, the mass output keeps increasing with the increase in RPM until around 4 RPM and then it decreases again. Also the values from 2 to 4 RPM are very close, so this window should be the most appropriate for high output.

5.1.2 Spinning rod collector results

The same experiments carried out by the flat plate collector setup were repeated using the spinning rod collector's setup. The parameters tested were: voltage, spinneret's rpm, the spinneret-collector distance, and the collector's rpm.

Throughout all the experiments, the temperature was 25 degrees Celsius, the relative humidity was kept constant at 20% and the same amount of polymer solution (30 mL) was spun for 20 minutes.

1st Variable: Spinneret-Collector Distance:

Keeping the voltage constant at 40 kV, collector's rpm at 60, and the spinneret's rpm at 2.5, the collected data for productivity at different voltages looks as follows:

Electric field [kV/m]	Distance [cm]	Productivity [mg/min/cm]			Average Productivity [mg/min/cm]
286	14	2.91	2.95	2.86	2.90
250	16	1.86	2.77	2.99	2.54
222	18	2.14	2.33	2.59	2.35
200	20	1.55	1.67	1.49	1.57
182	22	0.91	1.36	1.25	1.18
167	24	0.91	0.64		0.77

Table 49: Distance, electric field, and productivity for the spinning rod collector

Each experiment was repeated three times and the average was calculated to graph the data for productivity at different distances.

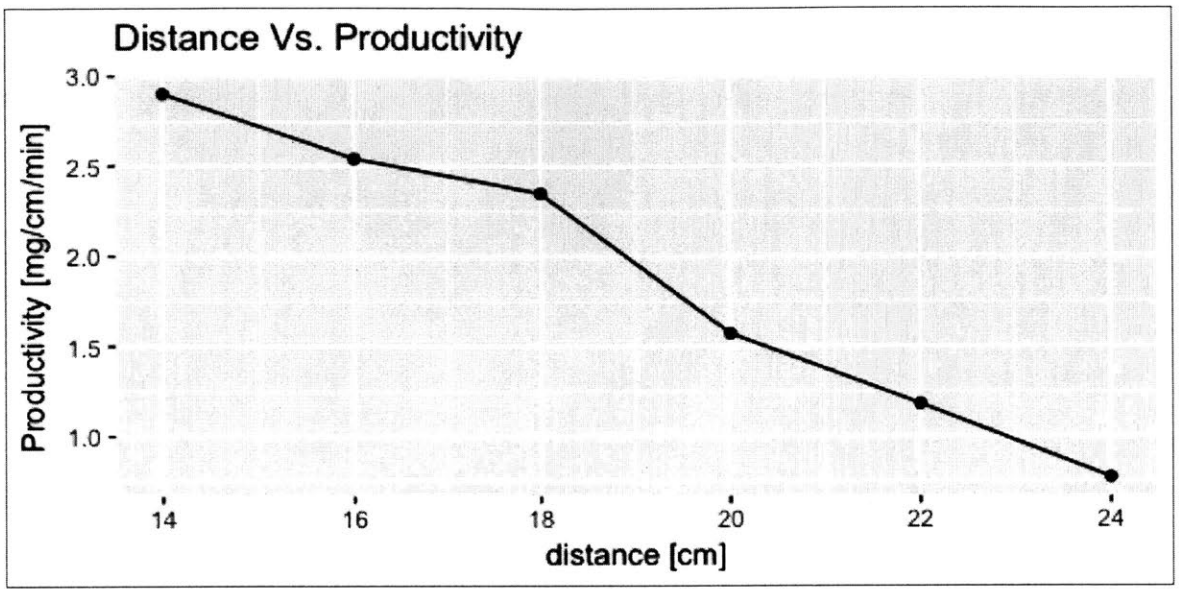

Figure 122: distance vs. productivity for the spinning rod collector

Translating this distance into electric field gives the following:

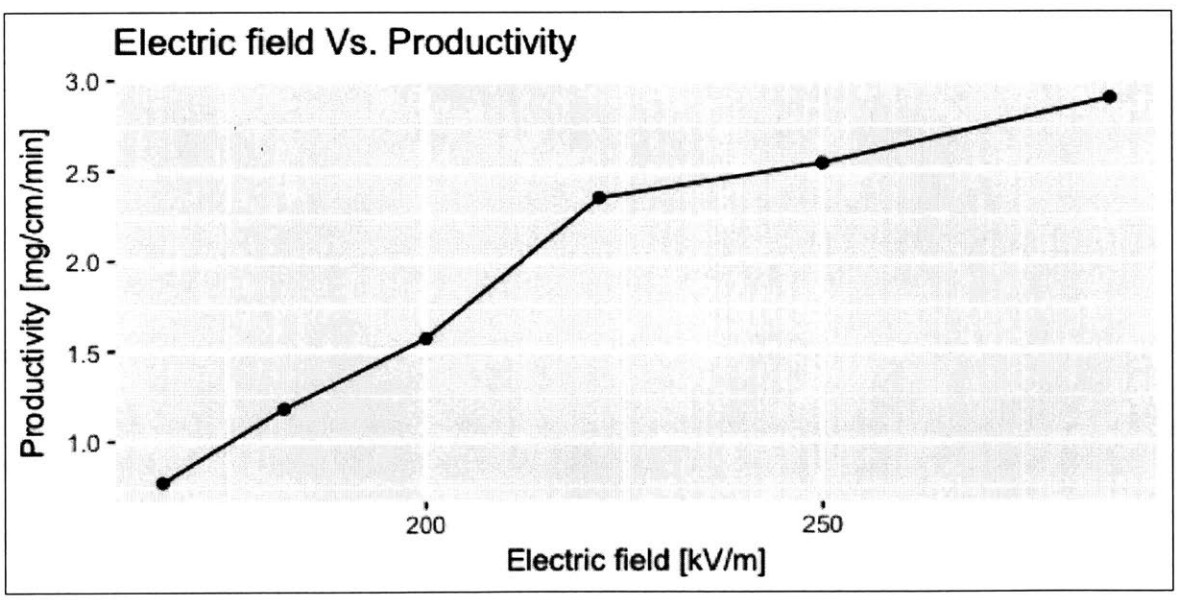

Figure 123: electric field vs. productivity by varying the distance for the spinning rod collector

2nd Variable: Applied Voltage:

Keeping the distance constant at 20 cm, the collector at 60 rpm, and the spinneret at 2.5 rpm, the data collected looks as follows:

E [kV/m]	Voltage	Average Productivity [mg/min/cm]
170	34	0.85
180	35	1.05
185	37	1.16
190	38	1.61
200	40	2.08
210	42	2.74
220	44	3.03

Table 50: Voltage, electric field, and productivity for the spinning rod collector

Each experiment was repeated three times and the average was calculated to graph the data for productivity at different voltages.

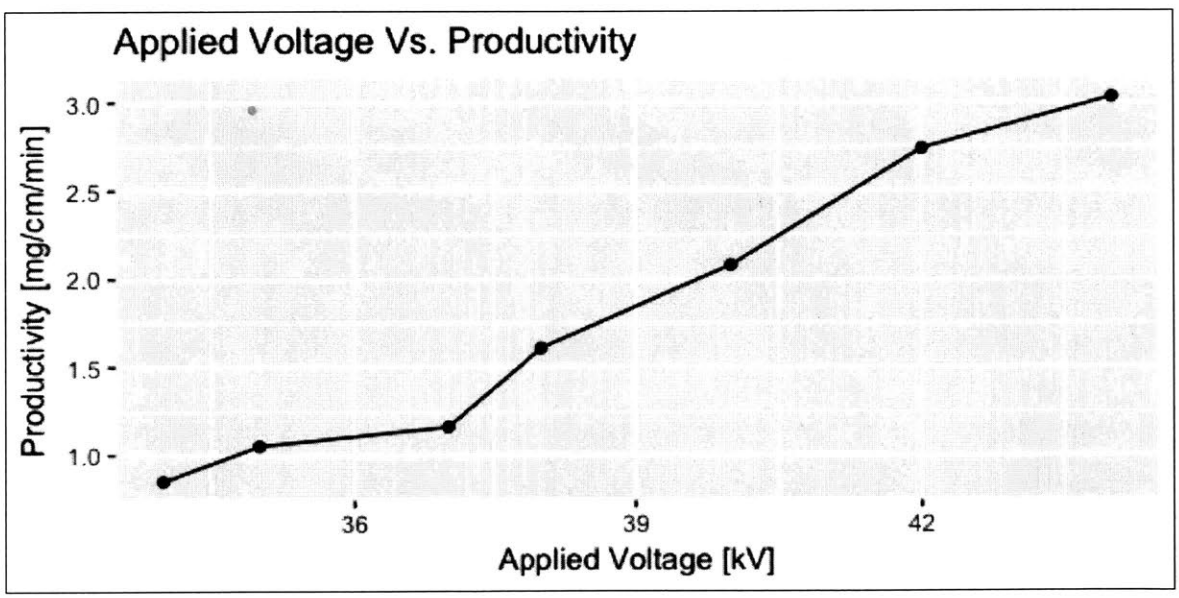

Figure 124: voltage vs. productivity for the spinning rod collector

Translating this distance into electric field gives the following:

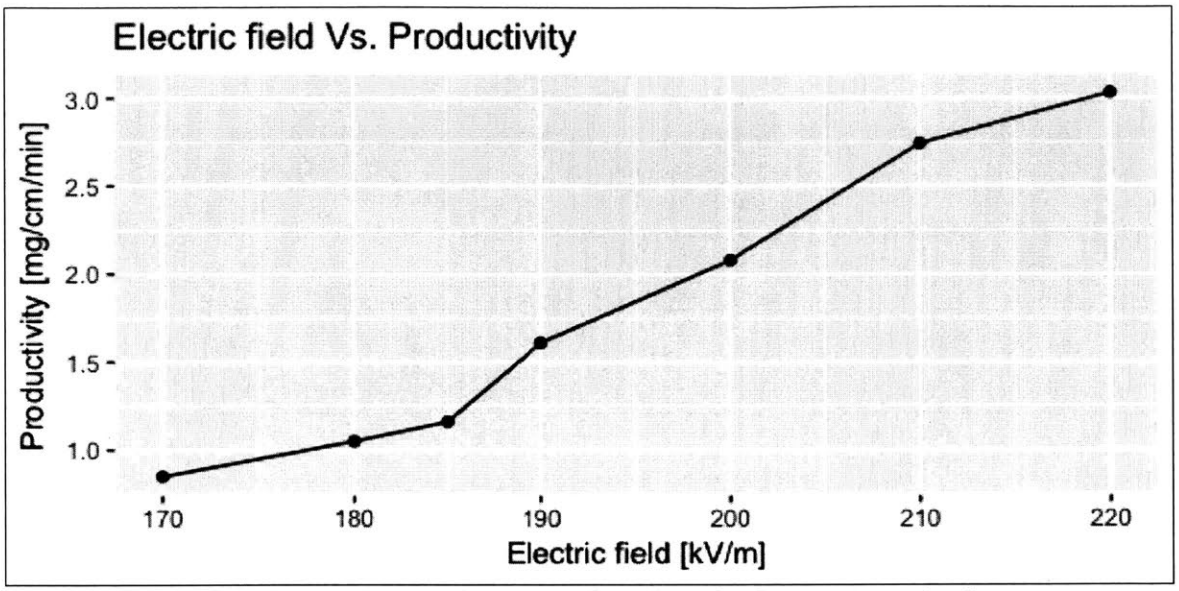

Figure 125: electric field vs. productivity by varying the voltage for the spinning rod collector

3rd Variable: Spinneret's RPM:

Keeping the voltage constant at 40 kV, distance at 20 cm, and collector's rpm at 60, the productivity was collected three times for each spinneret rpm, and the average productivity from these experiments looked as follows:

Spinneret' RPM	Average Productivity [mg/min/cm]
0.68	0.24
0.99	1.03
1.30	1.80
1.61	1.98
2.54	2.24
2.85	2.46
3.78	2.6
4.09	2.2
4.71	1.86

Table 51: spinneret's rpm vs. productivity for the spinning rod collector

Graphing the data for productivity at different spinneret rpm gives:

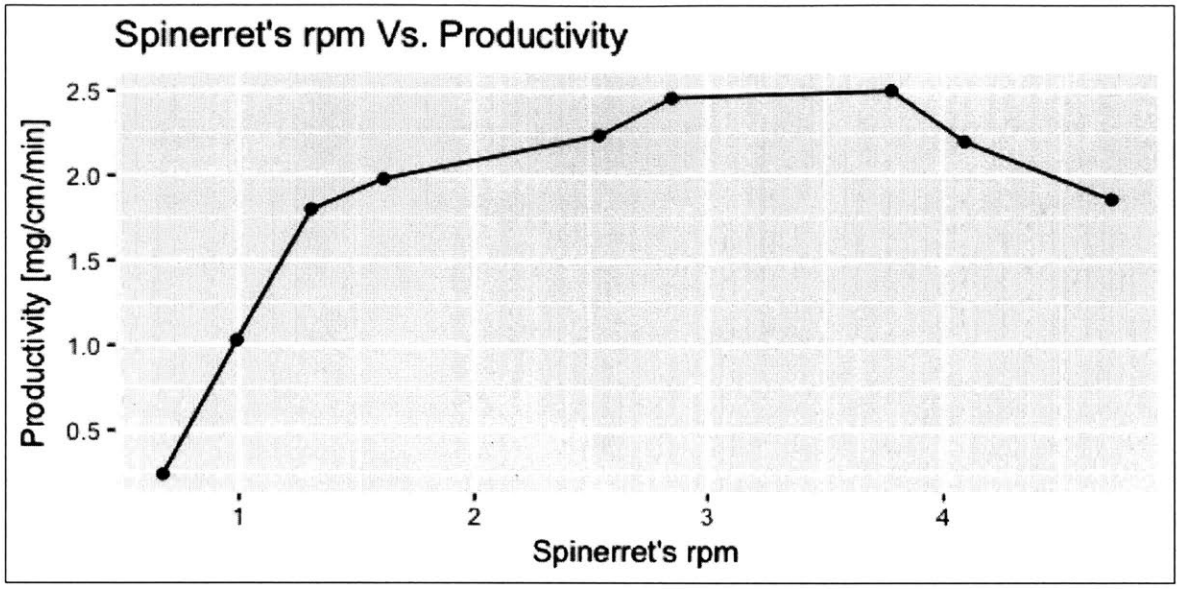

Figure 126: spinneret's rpm vs. productivity for the spinning rod collector

4th Variable: Collector's RPM:

Keeping the voltage constant at 40 kV, distance at 20 cm, and spinneret's rpm at 2.5, the data collected for different collector rpm looks as follows:

Collector's RPM	Productivity [mg/min/cm]
30	2.17
90	1.94
120	1.66
150	1.74
180	2.27
210	2.01
240	2.05
270	1.78
300	2.05
330	2.14

Table 52: collector's rpm vs. productivity for the spinning rod collector

Graphing the data for productivity at different collector rpm gives:

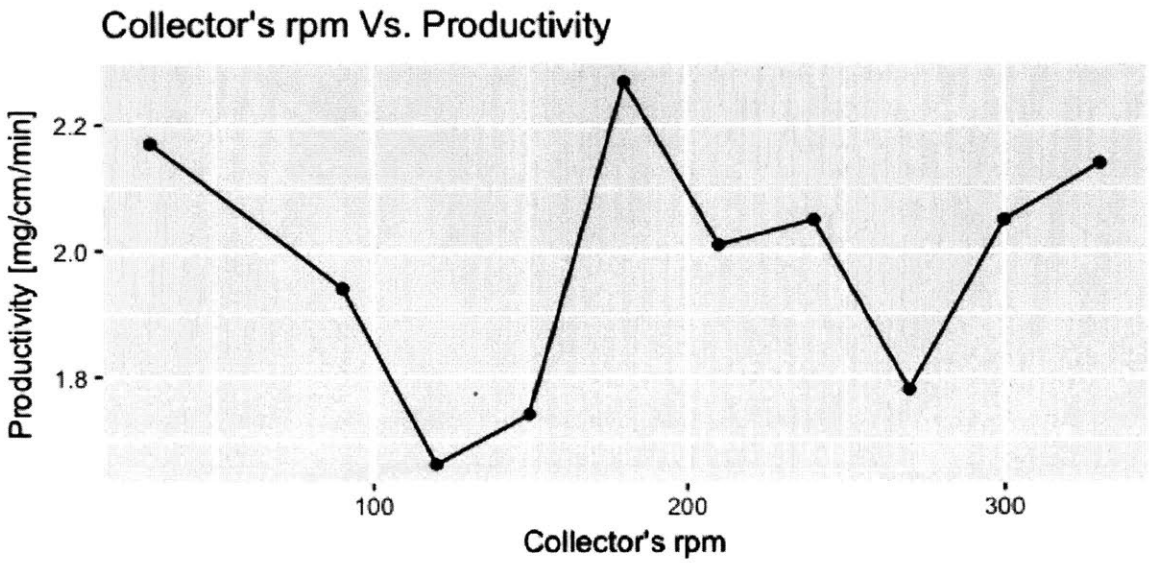

Figure 127: collector's rpm vs. productivity for the spinning rod collector

Zooming out of

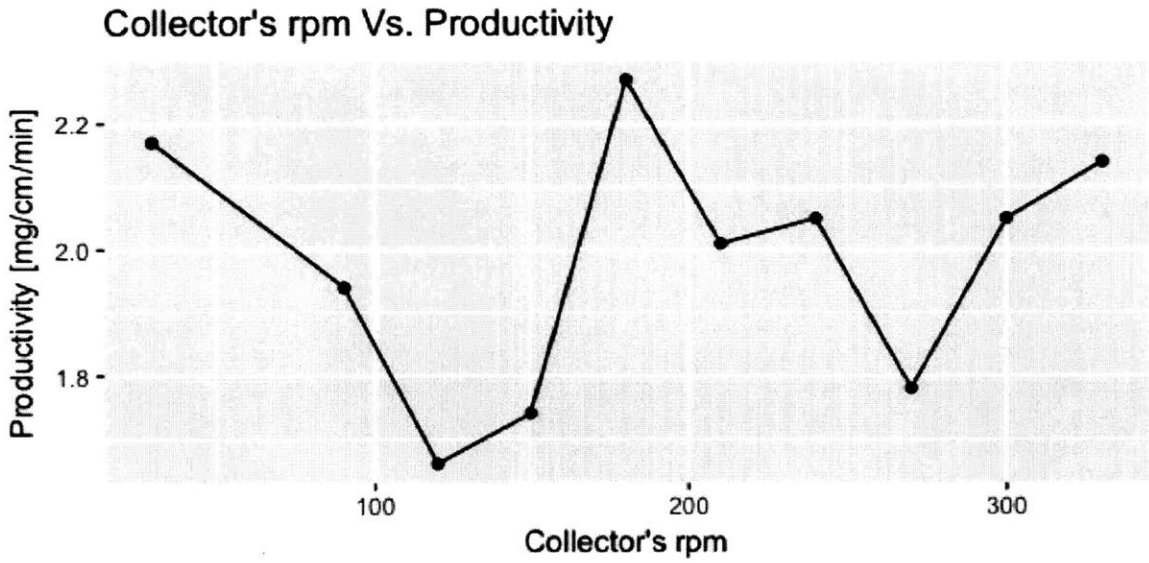

Figure 127 and adding the mean output of 1.98 mg/cm/min, the graph would look like:

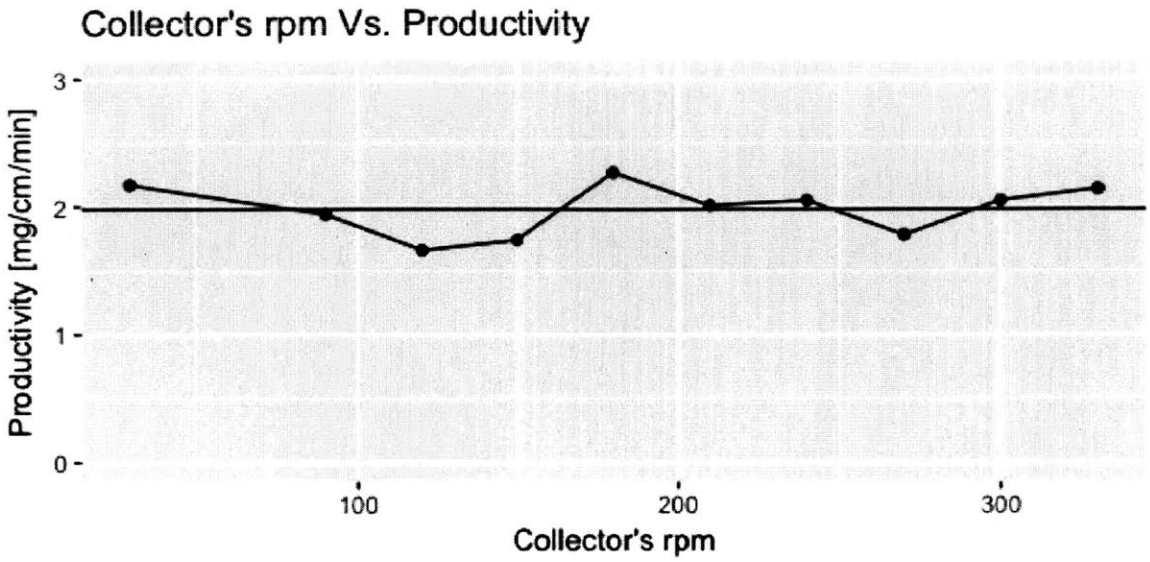

Figure 128: collector's rpm vs. productivity for the spinning rod collector with its mean

Adding the control limits of 3 standard deviations more or less, shows that the output is inside the control limits as seen below:

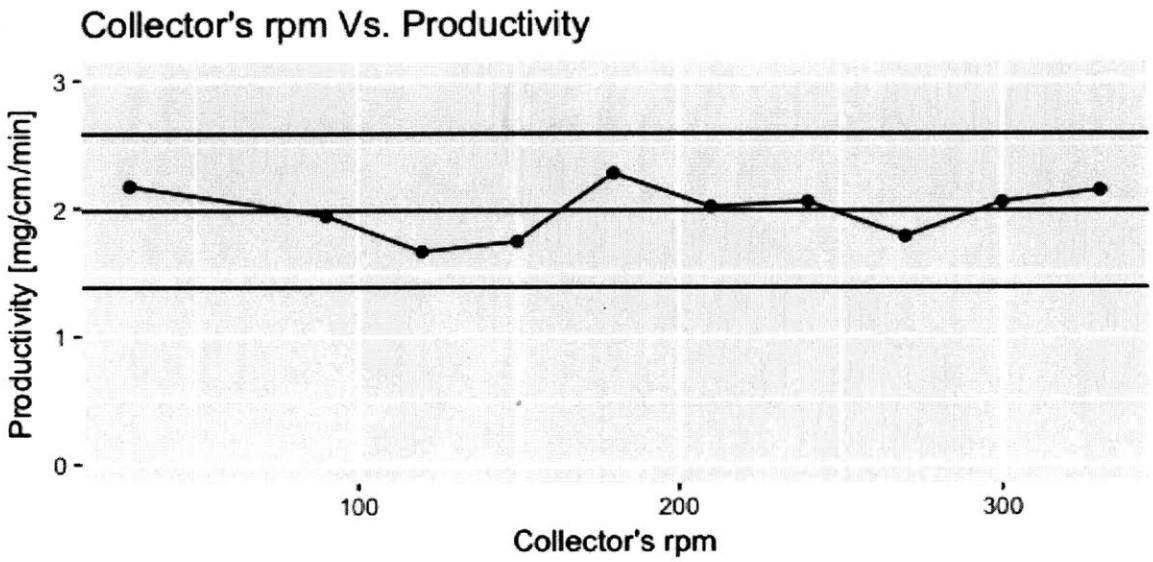

Figure 129: collector's rpm vs. productivity for the spinning rod collector with its control limits

Looking at the graph in Figure 129, it could be observed that changing the collector's rpm does not really affect the productivity. The productivity is randomly distributed around the value of [1.98 mg/cm/min] at different rpms.

When regressing the productivity on the collector's rpm, it was found that there was no significant association (correlation) between the two variables ($r = 0.12$, p-value = 0.7392). The p-value showed that the hypothesis that productivity measures were the same could not be rejected. The correlation coefficient of 0.12 (very close to zero), so there is no significant relationship between the two variables.

```
Call:
lm(formula = prod4 ~ crpm)

Residuals:
     Min       1Q   Median       3Q      Max 
-0.30292 -0.16929  0.03318  0.10750  0.29201 

Coefficients:
             Estimate Std. Error t value Pr(>|t|)    
(Intercept) 1.9327922  0.1547976  12.486 1.58e-06 ***
crpm        0.0002511  0.0007283   0.345    0.739    
---
Signif. codes:  0 '***' 0.001 '**' 0.01 '*' 0.05 '.' 0.1 ' ' 1

Residual standard error: 0.21 on 8 degrees of freedom
Multiple R-squared:  0.01464,	Adjusted R-squared:  -0.1085 
F-statistic: 0.1189 on 1 and 8 DF,  p-value: 0.7392

> cor.test(prod4,crpm)

        Pearson's product-moment correlation

data:  prod4 and crpm
t = 0.34477, df = 8, p-value = 0.7392
alternative hypothesis: true correlation is not equal to 0
95 percent confidence interval:
 -0.5505731  0.6974871
sample estimates:
      cor 
0.1209977 
```

Figure 130: t-test computations for the collector rpm and productivity relationship

5.1.3 Comparison of the flat plate and the spinning rod collectors:

The analysis below was performed for polyvinyl alcohol (PVA) mixtures with no active pharmaceutical ingredient (API), to be comparable to the flat plate collector results.

Comparing the effect of varying electric field (distance dependent) on the productivities of both the flat plate collector and the spinning rod collector gives:

Electric field [kV/m]	**Flat Plate Productivity [mg/cm/min]**	**Electric field [kV/m]**	**Spinning Rod Productivity [mg/min/cm]**
143	0.481	167	0.77
160	1.424	182	1.18

174	1.455	200	1.57
200	3.127	222	2.35
222	3.613	250	2.54
267	9.011	286	2.90

Table 53: electric field (distance dependent) vs. productivity of the flat plate and spinning rod collectors

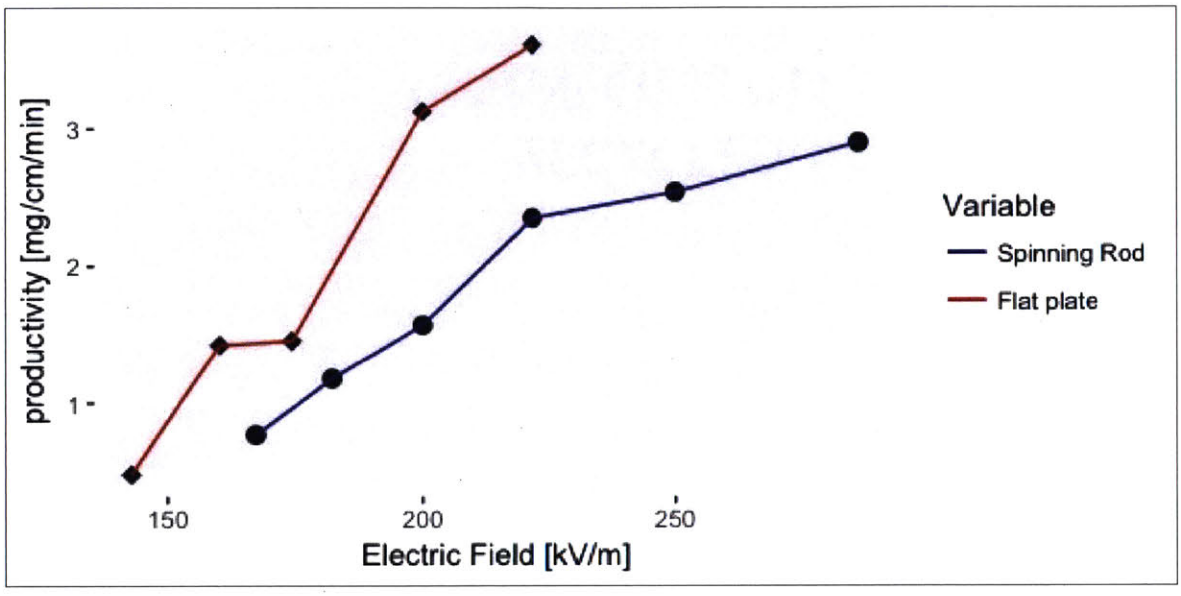

Figure 131: graph of the electric field (distance dependent) vs. productivity of the flat plate and spinning rod collectors

Comparing the effect of varying electric field (voltage dependent) on the productivities of both the flat plate collector and the spinning rod collector gives:

Electric field [kV/m]	Flat Plate Productivity [mg/cm/min]	Spinning Rod Productivity [mg/min/cm]
170	0.90	0.85
180	1.35	1.05
185		1.16
190	2.21	1.61
200	3.13	2.08
210	4.04	2.74
220	4.55	3.03

Table 54: electric field (voltage dependent) vs. productivity of the flat plate and spinning rod collectors

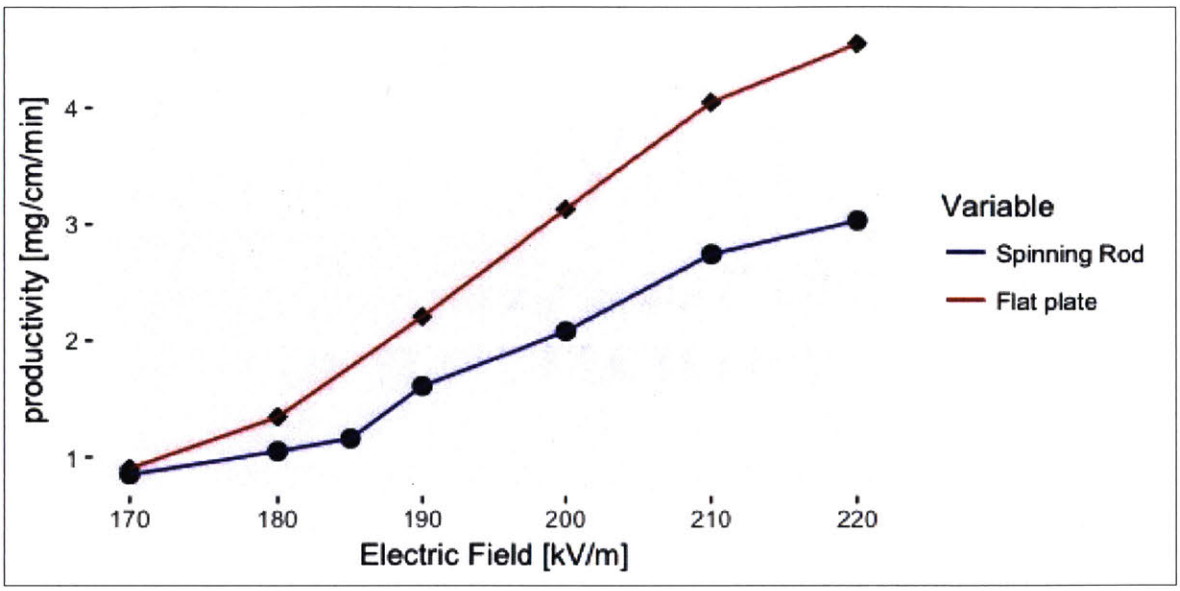

Figure 132: graph of the electric field (voltage dependent) vs. productivity of the flat plate and spinning rod collectors

Comparing the effect of varying the spinneret's rpm on the productivities of both the flat plate collector and the spinning rod collector gives:

Spinneret's RPM	Flat Plate Productivity [mg/cm/min]	Spinning Rod Productivity [mg/min/cm]
0.68	0.81	0.24
0.99		1.03
1.30	2.46	1.80
1.61		1.98
2.54	3.02	2.24
2.85	3.13	2.46
3.78	3.43	2.68
4.09		2.20
4.71	2.79	1.86

Table 55: spinneret's rpm vs. productivity of the flat plate and spinning rod collectors

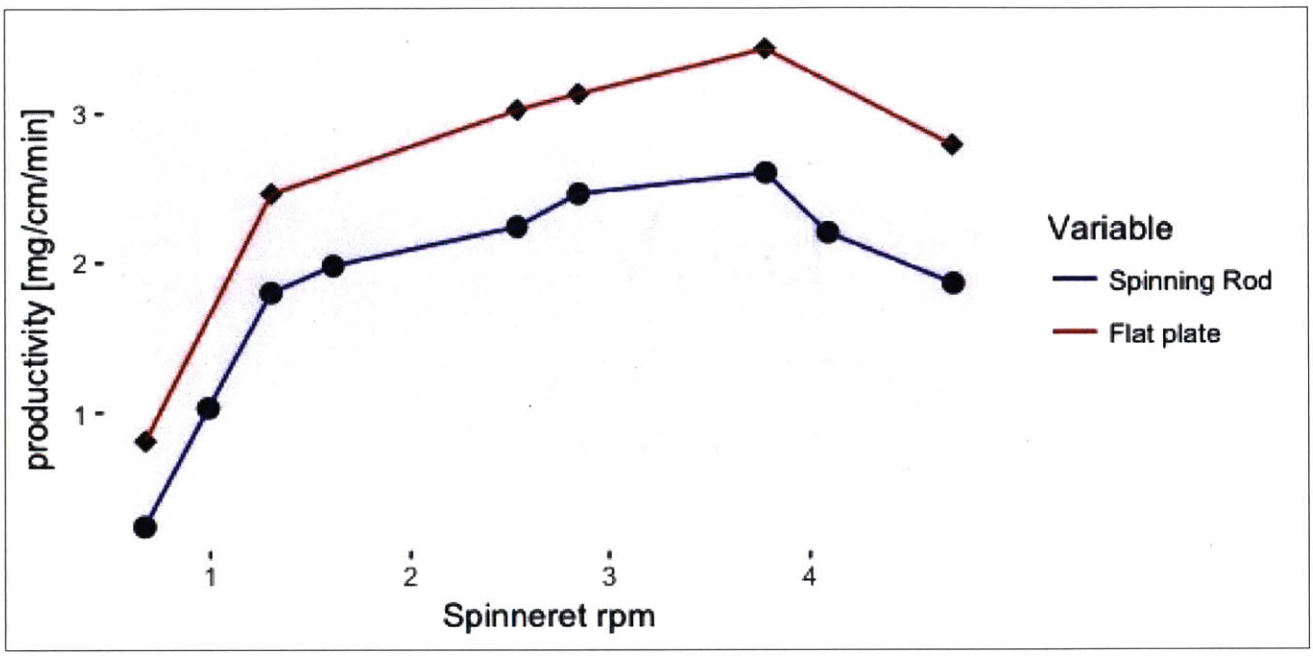

Figure 133: graph of the spinneret's rpm vs. productivity of the flat plate and spinning rod collectors

As seen in Figure 14, Figure 15, and Figure 133, the productivity of the flat plate collector was higher than the productivity of the spinning rod collector at all the experiments done for the three main variables (voltage, distance, and spinneret's rpm). This could be due to the higher grounded surface area of the circular flat plate collector compared to the smaller grounded surface area of the spinning rod. Further comparisons and analysis could be done in this area to quantify the difference in these productivities more accurately.

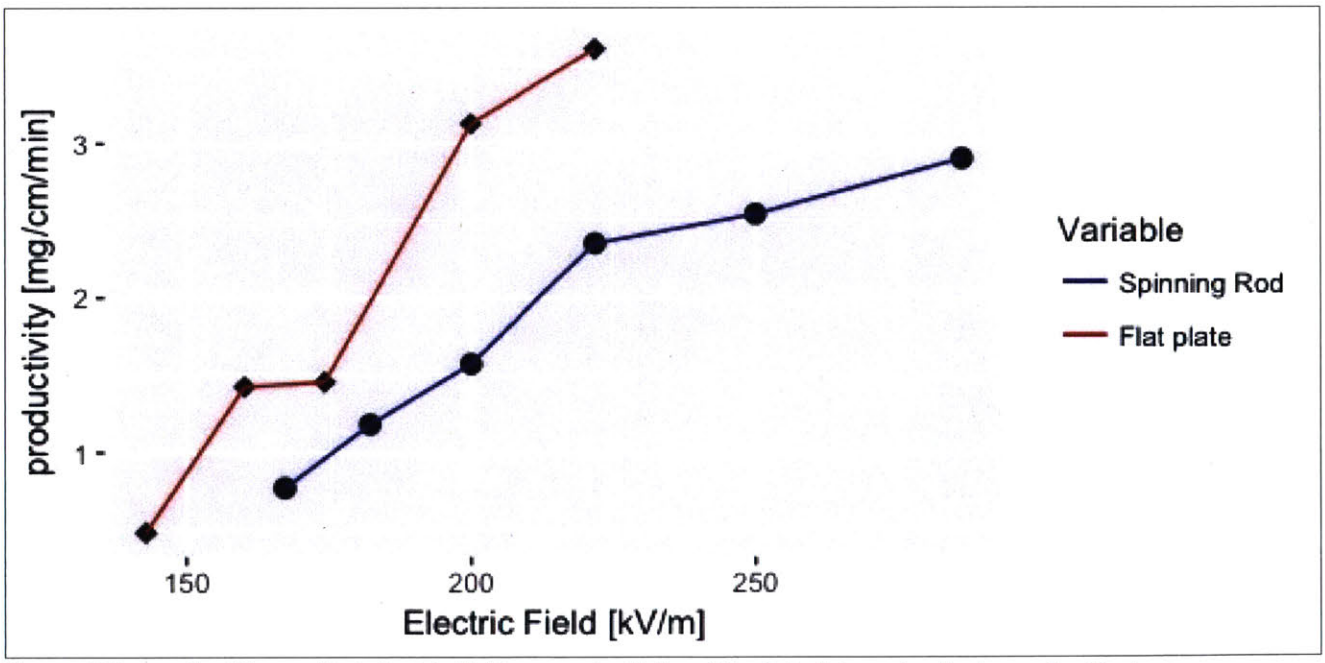

Figure 134: graph of the applied electric field vs. productivity of the flat plate and spinning rod collectors

The spinning rod's surface area was:

Spinning Rod's Surface Area	
Radius [mm]	1.6
Length [mm]	400
Surface area [mm^2]	3927

Table 56: spinning rod's surface area calculation

The flat plate collector's surface area was:

Flat Plate's Surface Area	
Radius [mm]	67.5
Area [mm2]	14,314

Table 57: spinning rod's surface area calculation

The ratio between the surface area of the two collectors would be:

$$Surface\ Area\ Ratio = \frac{Flat\ plate\ collector's\ Surface\ Area\ [mm^2]}{Spinning\ rod\ collector's\ Surface\ Area\ [mm^2]}$$

Equation 26

Plugging the values in Equation 26 gives:

$$Surface\ Area\ Ratio = \frac{14{,}314}{3{,}927} = 3.645$$

The ratio between the productivities of both collector types was calculated using the following equation:

$$Productivity\ Ratio = \frac{Flat\ plate\ collector's\ productivity\ [\frac{\frac{mg}{min}}{cm}]}{Spinning\ rod\ collector's\ productivity\ [\frac{\frac{mg}{min}}{cm}]}$$

Equation 27

Placing these productivity ratios from different experiments in one table gives:

Varying Voltage	Varying spinneret's rpm
1.06	3.39
1.28	1.37
1.37	1.35
1.50	1.19

1.48	1.28
1.50	1.49
Average Productivity Ratio= 1.52	

Table 58: productivity ratios from different experiments

Thus, observing that the surface area ratio is 3.645 and the productivity ratio of 1.52, we could claim that there might be a relationship between the two variables. In other words, when the surface area increases by around 3.645 times, the productivity increases by around 1.52 times.

5.1.4 Comparing the results to the literature

Since the setup was an adaptation of Bhattacharyya's previous setup, it is viable to compare this machine's output to Bhattacharyya's previous output [40].

Compiling various electric fields with different spinneret rpm together gave the following data:

Voltage [kV]	34	37	40
Spinneret's rpm	**Average Productivity [mg/min/cm]**		
0.68	0.55	0.70	0.77
0.99	0.62	0.93	1.45
1.30	0.75	0.97	1.80
1.61	0.82	1.04	1.98
2.23	0.92	1.17	-
2.54	-	1.25	2.24
2.85	1.01	1.45	2.46
3.78	1.26	1.76	2.68
4.09	1.17	1.50	2.20
4.71	0.96	1.36	1.86

Table 59: Productivity at different spinneret rpms and voltages

Graphing the rpm and voltage data in the above table looked as shown:

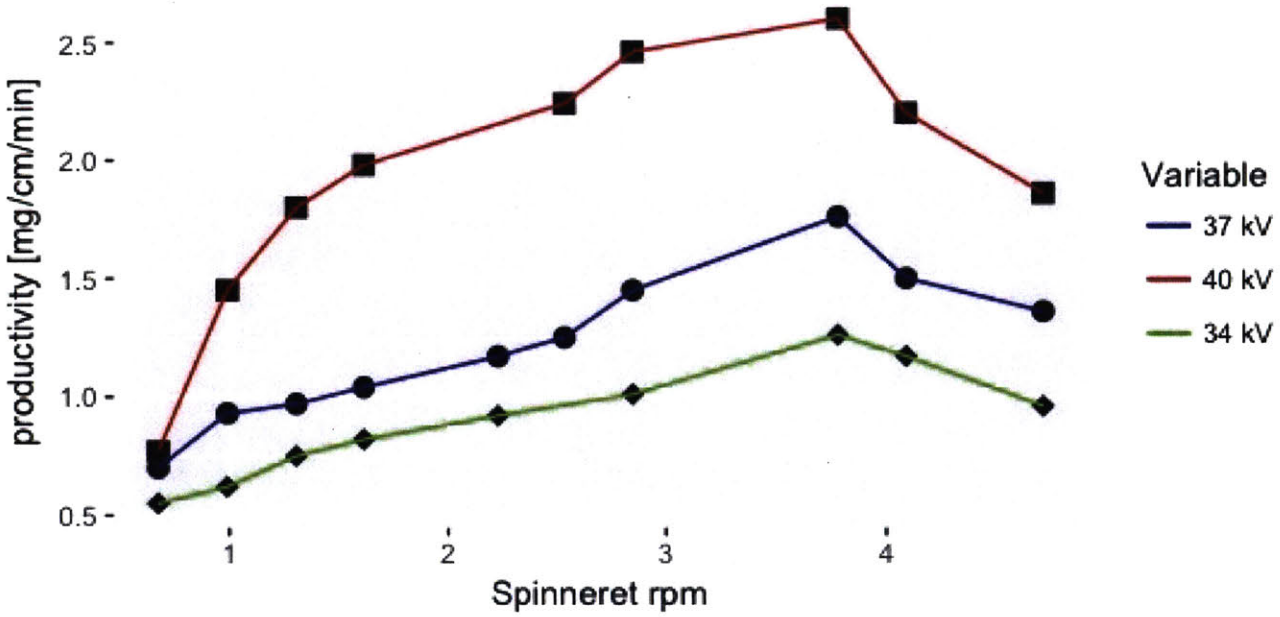

Figure 135: productivity at different spinneret rpms and voltages

Bhattacharyya's graphing of the same parameters looked as follows:

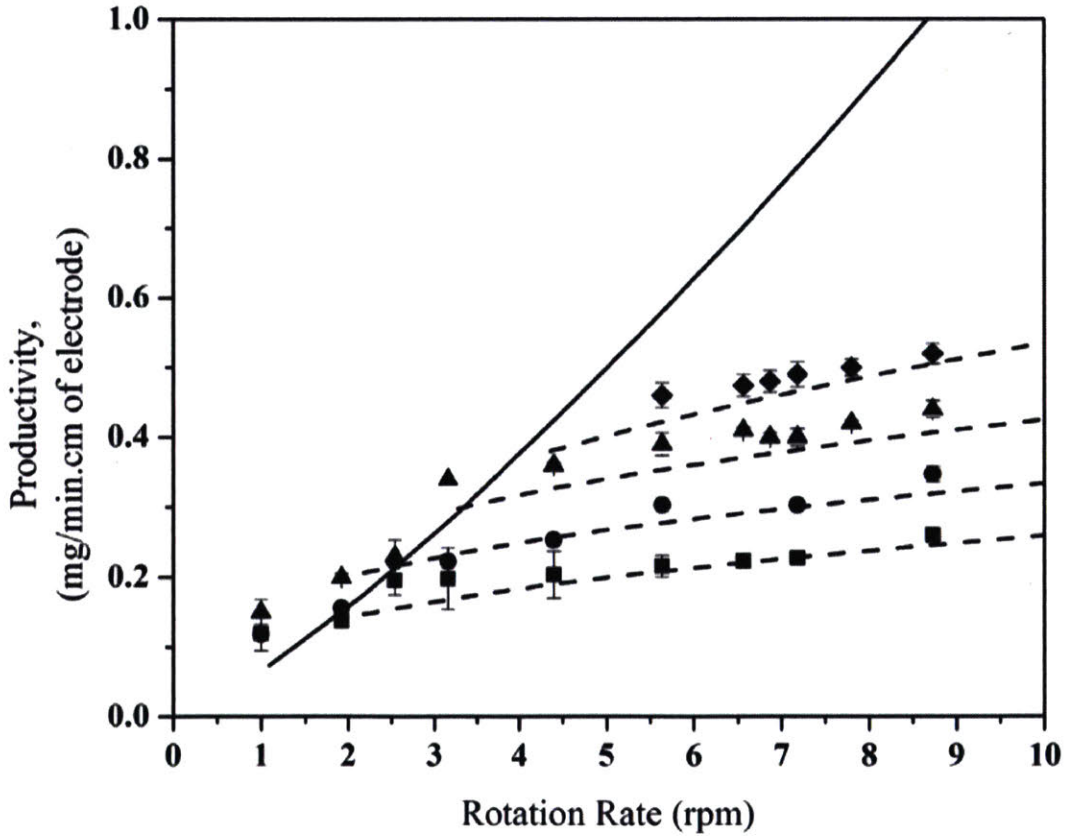

Figure 136: productivity at different spinneret rpms and voltages of 40 kV (square), 42.5 kV (circle), 45 kV (triangle), and 50 kV (diamond) [40, Figure 9]

Since Bhattacharyya's working distance was 25 cm [40], these four voltages translates to electric fields of: 160, 170, 180, and 200 kV/m. Whereas this machine's working distance was 20 cm, which translates to electric fields of 170, 185, and 200 kV/m.

Comparing the productivities of both machines would give:

Conditions	**Current Productivity [mg/min/cm]**	**Previous Productivity [mg/min/cm]**	**Ratio of current and previous productivity**
170 kV/m Electric field & 3 rpm	1.05	0.20	5.25
170 kV/m Electric field & 4 rpm	1.20	0.25	4.80
200 kV/m Electric field & 3 rpm	2.50	0.35	7.14
200 kV/m Electric field & 4 rpm	2.25	0.37	6.08

Table 60: comparison of the current and the previous productivity

According to the data in Table 60, the productivity of the current machine is about 5-6 times the productivity of the previous machine. This could be due to the following reasons:

1- The spinneret collector distance of the current machine was 20 cm, while the distance in the previous machine was 25 cm.
2- Fibers were spun for 7 minutes in the current machine, and for 20 minutes in the previous machine [40]. Even though the productivity is in grams per minute, but the productivity changes with time. The first minute's productivity is not as the last minute's productivity. Thus the average productivity becomes different if it is spun for 7 minutes versus 20 minutes.

5.2 Statistical Analysis of the machine's reliability

5.2.1 General statistical analysis of the data

After making 350 pills using this machine, the repeatability and reliability of the data for the three dosage types: zero, 2.5%, and 12.5% was analyzed, using R Studio software. The aggregated data of the 350 pills looked as follows:

Dosage	Pill number	Mass [grams]	Density [g/cm3]
0	8	0.043	1.006
0	9	0.084	0.941
0	10	0.063	1.023
0	11	0.052	0.917
0	12	0.050	1.018
0	13	0.092	1.006
0	14	0.095	1.056
0	15	0.096	1.000
0	16	0.062	1.191
0	17	0.066	1.121
0	18	0.083	1.110
0	19	0.089	1.092
0	20	0.083	1.056
0	21	0.077	1.077
0	22	0.088	1.058
0	23	0.084	1.044
0	24	0.012	0.000
0	25	0.854	0.000
0	26	0.098	1.068
0	27	0.100	1.096
0	28	0.103	1.145
0	29	0.095	1.104
0	30	0.102	1.105
0	31	0.117	0.000
0	32	0.118	1.132
0	33	0.104	1.127
0	34	0.105	1.102
0	35	0.072	0.678
0	36	0.118	1.761
0	37	0.065	1.104
0	38	0.093	1.085

0	39	0.108	1.051
0	40	0.100	1.018
0	41	0.094	1.009
0	42	0.098	0.930
0	43	0.105	0.976
0	44	0.107	0.974
0	45	0.102	0.986
0	46	0.067	0.984
0	47	0.070	0.931
0	48	0.081	1.108
0	49	0.090	1.112
0	50	0.083	1.053
0	51	0.080	1.073
0	52	0.077	1.097
0	53	0.091	0.000
0	54	0.095	0.000
0	55	0.087	1.131
0	56	0.041	2.106
0	57	0.104	0.903
0	58	0.061	0.744
0	59	0.057	1.955
0	60	0.070	0.969
0	61	0.084	0.704
0	62	0.048	1.411
0	63	0.073	1.206
0	64	0.125	0.415
0	65	0.039	1.835
0	66	0.138	0.963
0	67	0.081	0.492
0	68	0.075	1.979
0	69	0.093	0.916
0	70	0.091	0.930
0	71	0.099	1.000
0	72	0.103	0.994
0	73	0.098	1.078
0	74	0.088	1.319
0	75	0.093	1.125
0	76	0.079	1.124
0	77	0.053	1.014
0	78	0.065	1.077
0	79	0.060	1.027

0	80	0.085	1.062
0	81	0.102	1.128
0	82	0.122	1.094
0	83	0.082	1.068
0	84	0.120	1.107
0	85	0.104	1.067
0	86	0.089	1.037
0	87	0.011	0.679
0	88	0.121	1.109
0	89	0.070	1.075
0	90	0.065	1.085
0	91	0.066	1.090
0	92	0.061	1.057
0	93	0.084	1.102
0	94	0.094	1.014
0	95	0.100	1.125
0	96	0.091	1.101
0	97	0.097	1.094
0	98	0.041	0.918
0	99	0.132	1.036
0	100	0.070	1.038
0	101	0.085	1.070
0	102	0.042	0.904
0	103	0.102	0.811
0	104	0.080	0.572
0	105	0.087	0.371
0	106	0.102	1.033
0	107	0.098	1.171
0	108	0.103	1.133
0	109	0.000	0.000
0	110	0.036	0.914
0	111	0.088	1.109
0	112	0.041	0.860
0	113	0.068	0.947
0	114	0.044	0.839
0	115	0.073	0.965
0	116	0.040	0.940
0	117	0.066	1.026
0	118	0.054	1.027
0	119	0.092	0.941
0	120	0.030	0.845

0	121	0.038	0.848
0	122	0.054	0.968
0	123	0.057	0.987
0	124	0.053	0.894
0	125	0.057	0.945
0	126	0.044	0.842
0	127	0.041	0.967
0	128	0.053	1.034
0	129	0.053	0.979
2.5	130	0.106	1.009
2.5	131	0.131	0.964
2.5	132	0.133	0.982
2.5	133	0.141	1.017
2.5	134	0.137	0.000
2.5	135	0.138	0.000
2.5	136	0.144	1.008
2.5	137	0.141	0.924
2.5	138	0.150	0.000
2.5	139	0.143	0.000
2.5	140	0.137	0.936
2.5	141	0.140	0.000
2.5	142	0.110	0.680
2.5	143	0.120	1.065
2.5	144	0.132	0.783
2.5	145	0.137	0.996
2.5	146	0.139	0.924
2.5	147	0.143	0.754
2.5	148	0.139	0.974
2.5	149	0.138	0.871
2.5	150	0.149	0.478
2.5	151	0.151	1.039
2.5	152	0.151	0.620
2.5	153	0.071	1.064
2.5	154	0.080	0.772
2.5	155	0.095	0.664
2.5	156	0.077	1.019
2.5	157	0.089	0.929
2.5	158	0.072	0.957
2.5	159	0.080	0.792
2.5	160	0.092	1.068
2.5	161	0.080	0.962

2.5	162	0.094	0.557
12.5	163	0.032	0.000
12.5	164	0.064	1.090
12.5	165	0.051	0.591
12.5	166	0.069	0.841
12.5	167	0.082	0.000
12.5	168	0.075	1.062
12.5	169	0.084	0.970
12.5	170	0.097	0.629
12.5	171	0.102	1.116
12.5	172	0.127	0.000
12.5	173	0.130	1.011
12.5	174	0.143	1.003
12.5	175	0.079	0.926
12.5	176	0.099	1.071
12.5	177	0.099	0.000
12.5	178	0.117	0.674
12.5	179	0.127	1.142
12.5	180	0.122	0.981
12.5	181	0.103	1.058
12.5	182	0.127	0.000
12.5	183	0.136	0.878
12.5	184	0.122	1.114
12.5	185	0.122	0.714
12.5	186	0.125	0.945
12.5	187	0.047	0.908
12.5	188	0.051	1.108
12.5	189	0.050	0.338
12.5	190	0.059	1.133
12.5	191	0.064	0.447
12.5	192	0.078	1.161
12.5	193	0.076	0.419
12.5	194	0.103	1.205
12.5	195	0.064	0.286
0	196	0.028	0.726
0	197	0.045	0.883
0	198	0.092	0.960
0	199	0.039	0.925
0	200	0.075	1.027
0	201	0.112	1.012
0	202	0.050	1.001

0	203	0.080	0.998
0	204	0.116	0.957
0	205	0.028	0.848
0	206	0.065	1.001
0	207	0.113	0.922
0	208	0.042	0.891
0	209	0.062	1.036
0	210	0.065	0.995
0	211	0.083	1.004
0	212	0.034	0.707
0	213	0.031	0.845
0	214	0.062	0.965
0	215	0.043	0.882
0	216	0.030	0.747
0	217	0.047	0.869
0	218	0.042	0.949
0	219	0.029	0.685
0	220	0.051	0.990
0	221	0.044	0.769
0	222	0.026	0.728
0	223	0.085	1.043
0	224	0.042	0.826
0	225	0.044	0.992
0	226	0.035	0.841
0	227	0.025	0.830
0	228	0.048	0.913
0	229	0.082	1.021
0	231	0.051	1.010
0	230	0.119	1.004
0	232	0.065	0.955
0	233	0.083	0.919
0	234	0.032	0.889
0	235	0.0.45	0.000
0	236	0.099	1.007
0	237	0.051	0.888
0	238	0.074	0.975
0	239	0.111	0.981
0	240	0.052	0.922
0	241	0.076	0.963
0	242	0.119	0.968
0	243	0.032	0.775

0	244	0.058	0.935
0	245	0.109	0.965
0	246	0.042	0.895
0	247	0.065	0.929
0	248	0.125	0.936
0	249	0.143	0.962
0	250	0.020	0.681
0	251	0.041	0.935
0	252	0.029	0.897
0	253	0.081	0.963
0	254	0.051	0.792
0	255	0.033	0.863
0	256	0.068	0.932
0	257	0.050	0.848
2.5	258	0.077	0.355
2.5	259	0.072	0.264
2.5	260	0.093	0.986
2.5	261	0.079	0.967
2.5	262	0.072	0.730
2.5	263	0.094	0.681
2.5	264	0.055	0.485
2.5	265	0.069	0.396
2.5	266	0.057	0.820
2.5	267	0.068	0.740
2.5	268	0.068	0.660
2.5	269	0.068	0.694
2.5	270	0.074	0.715
2.5	271	0.066	0.709
2.5	272	0.113	0.959
2.5	273	0.101	0.939
2.5	274	0.112	1.115
2.5	275	0.107	1.134
2.5	276	0.143	0.610
2.5	277	0.140	0.707
2.5	278	0.150	0.960
2.5	279	0.147	0.981
2.5	280	0.152	1.073
2.5	281	0.150	1.044
12.5	282	0.078	0.859
12.5	283	0.080	0.825
12.5	284	0.101	0.548

12.5	285	0.086	0.509
12.5	286	0.085	1.002
12.5	287	0.097	1.040
12.5	288	0.096	0.694
12.5	289	0.109	0.749
12.5	290	0.118	0.720
12.5	291	0.090	1.027
12.5	292	0.126	1.044
12.5	293	0.092	0.000
12.5	294	0.071	0.000
12.5	295	0.089	0.792
12.5	296	0.053	0.707
12.5	297	0.048	1.047
12.5	298	0.056	1.138
12.5	299	0.108	0.879
12.5	300	0.116	0.983
0	301	0.095	0.936
0	302	0.069	0.880
0	303	0.117	0.898
0	304	0.094	0.959
0	305	0.11	0.668
0	306	0.106	0.895
0	307	0.099	0.859
0	308	0.071	0.911
0	309	0.12	0.896
0	310	0.125	0.861
0	311	0.113	0.842
0	312	0.075	0.455
0	313	0.139	1.078
0	314	0.106	0.822
0	315	0.072	0.987
0	316	0.065	0.945
0	317	0.116	0.927
0	318	0.138	0.877
0	319	0.117	0.881
0	320	0.062	0.822
0	321	0.084	0.916
0	322	0.049	0.587
0	323	0.101	0.965
0	324	0.088	0.767
0	325	0.058	0.704

0	326	0.142	0.905
0	327	0.115	0.541
0	328	0.045	0.793
0	329	0.096	0.829
0	330	0.067	0.887
0	331	0.156	0.747
0	332	0.056	0.826
0	333	0.152	0.899
0	334	0.029	0.655
0	335	0.077	0.741
0	336	0.101	0.898
0	337	0.071	0.771
0	338	0.039	0.817
0	339	0.134	0.805
0	340	0.038	0.833
0	341	0.126	0.742
0	342	0.057	0.838
0	343	0.106	0.853
0	344	0.076	0.915
0	345	0.136	-
0	346	0.062	0.860
0	347	0.118	0.877
0	348	0.029	0.410
0	349	0.13	-
0	350	0.068	0.895

Table 61: masses and densities of the 350 pills made

The table for the statistical analysis for the first 55 pills made looked as follows:

Factor	Mean	Standard Deviation	Coeff. Of Variation	Minimum	Maximum
Mass [grams]	0.095	0.012	12.766	0.07	0.132
Height [mm]	2.798	0.397	14.189	2.065	4.034
Volume [mm3]	88.61	12.58	14.199	65.4	127.8
Density [grams/cm3]	1.07	0.13	12.15	0.68	1.76

Table 62: mean and variance of the zero dosage pills

These first 55 pills were made at keeping all the variables constant (pressure, voltage, distance, spinneret and collector rpms) to test the repeatability of the mechanism. Comparing these results to the industry needs, their accepted variation is between 0.2% and 0.6%. This is according the "Guidance to the Industry of Power Blends and Finished Dosage Units" [42]. While according to Lahdenpaa, the weight coefficient of variation could be up to 1% [19].

As seen above, the variation in mass, volume, height, and density was around 12-14%, while the pharmaceutical standards allowed only 0.2% to 0.6%. The current variation was much more than the targeted variation because no precision mass measurement mechanism was installed, the polymer was just electrospun for a specific timing. The 12% variation in mass was due to the randomness of the electrospinning process, and fibers diffusion around the chamber and on its walls.

The current precision of mass output was challenging because:

1- The mass of the polymer was around 95 milligrams, so it needed very accurate instrumentation.
2- The collecting rod was continuously rotating, so it was hard to measure the deflection of the rod resulting from mass change.
3- The thickness of the polymer on the collector rod was not uniform along the rod, so it was hard to calculate the polymer mass from its thickness using laser beam technologies.

5.2.2 Comparison of different drug doses

The box plots comparing the masses of the three types of pills looked as follows:

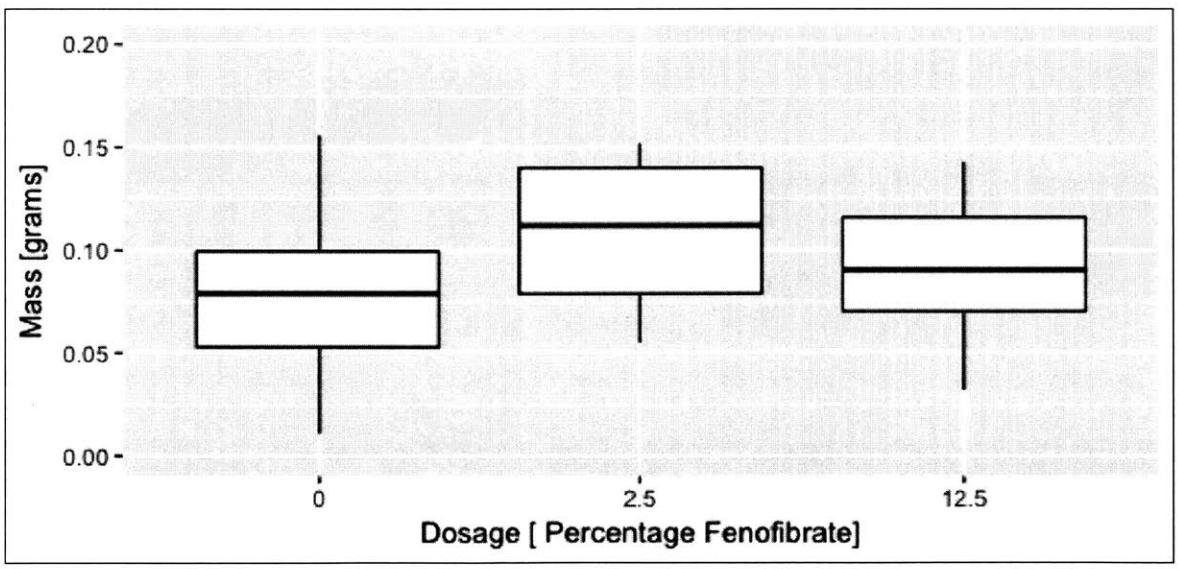

Figure 137: boxplot of the masses vs. pills' dosage

The values of the statistics shown in the boxplot in Figure 137 were as follows:

Pill Type	Mean	Standard Deviation	Coeff. Of Variation	Minimum	Maximum
0	0.081	0.059	73.193	0.011	0.854
2.5	0.111	0.032	28.977	0.055	0.152
12.5	0.091	0.028	30.420	0.032	0.143

Table 63: statistical analysis of the pills' masses

As seen in the boxplot in Figure 137 above, it appears that the 2.5% dosage of fenofibrate had the highest average mass productivity, followed by the 12.5% dosage, and then the zero dosage. This agrees with the previous literature that discussed how the active pharmaceutical ingredient (API) is more electrostatically charged than the polymer [43]. This makes the productivity of fibers with API always higher than the productivity of fibers with no API. The variation of the masses around their mean was expected to be that high (73%, 29%, and 30%) because these pills were made at different voltages, distances, and rpms. Changing these variables gave a wide spectrum of high and low mass outputs. For the 2.5% and 12.5% dosage, the electrospinning parameters were not varied as much, but the variability was in the applied pressure, density, and dissolution.

The boxplot of the densities of the three different types of pills was as follows:

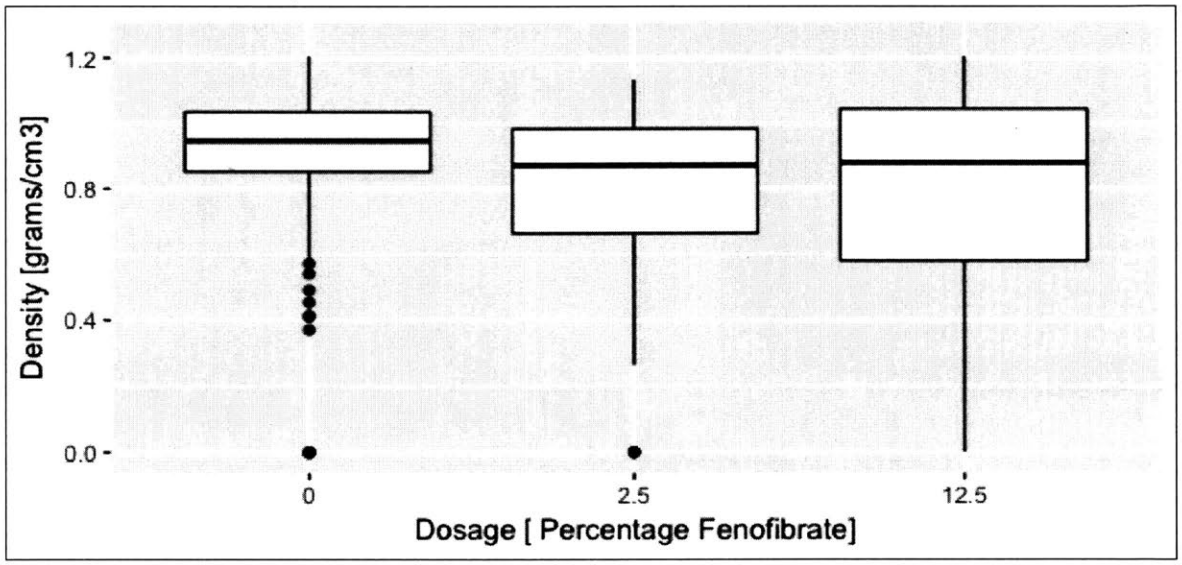

Figure 138: boxplot of the densities vs. pills' dosage

The values of the statistics shown in the boxplot in Figure 138 looked as follows:

Pill Type	Mean	Standard Deviation	Coeff. of Variation	Minimum	Maximum
0	0.936	0.258	27.535	0	2.106
2.5	0.764	0.311	40.770	0	1.134
12.5	0.757	0.374	49.432	0	1.205

Table 64: statistical analysis of the pills' densities

As seen in the boxplot in Figure 138 above, the mean density of the zero dosage was higher than that of the 2.5% and 12.5% dosage. Their means were 0.935 grams/cm^3 for the zero dosage, followed by 0.764 grams/cm^3 for the 2.5 dosage, and 0.757 grams/cm^3 for the 12.5 dosage. This followed the same trend of their theoretical densities, where the density decreased as the dosage increased, due to the lower density of the API. These theoretical densities were 1.269 grams/cm^3 for the PVA, compared to 1.267 grams/cm^3 for the 2.5% API , and 1.258

grams/cm^3 for the 12.5% API. The low and zero values of the density were from the earlier tests where fibers were spun and analyzed without pressing. The variation in density for the 2.5% and the 12.5% dosage was 41% and 49%. Tt was much higher than the 27% variation in zero dosage because most of these tests were made at different pressures to analyze the relationship between their density and dissolution.

5.2.3 Statistical Quality Control Charts

To analyze the repeatability of the mechanism, quality control charts of the mass output were studied, and they looked as follows:

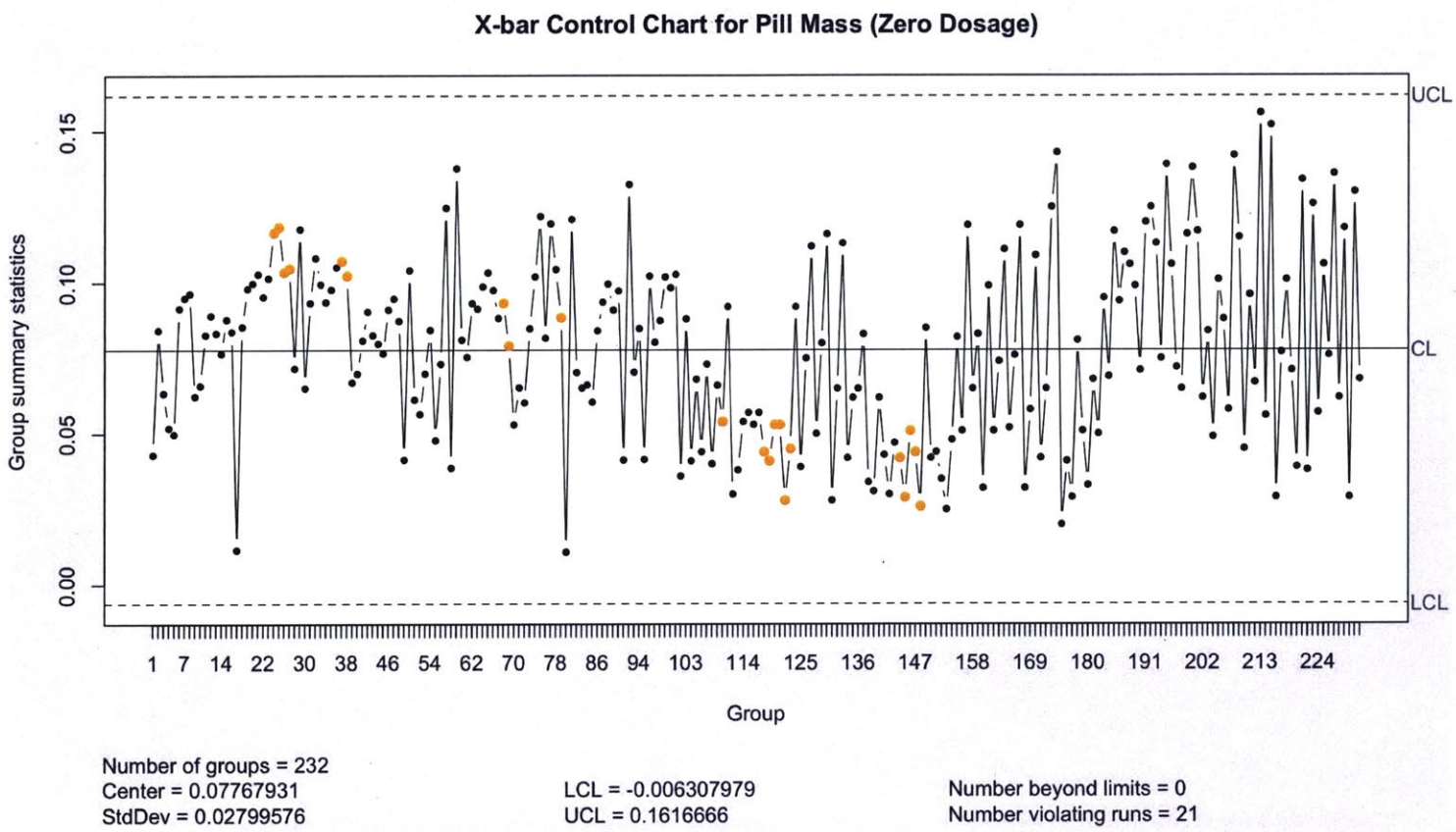

Figure 139: X-bar control chart for pill mass (zero dosage)

As seen in Figure 139 above, the process was under statistical control around its mean value of 0.078 grams, and there were zero points beyond the upper or lower control limits for the 232 zero dosage pills made. It can also be noted from the control chart in Figure 139 above that the first 55 pills are much closer to the mean, this is because they were made at the exact same conditions. The variability in the output increased afterwards because the experimental variables (voltage, rpm, pressure, and distance) were changed and tested.

The control chart for the 2.5% dosage looked as follows:

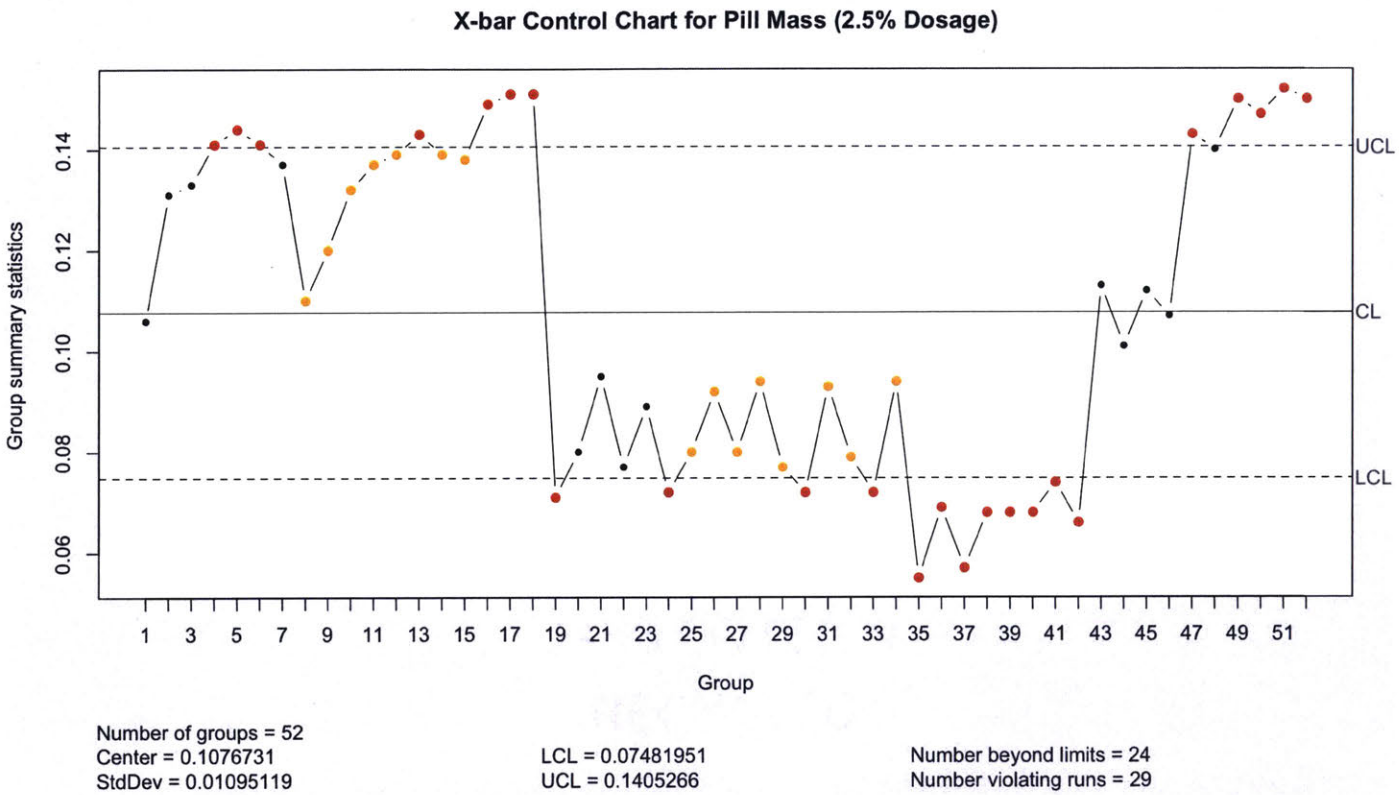

Figure 140: X-bar control chart for pill mass (2.5% dosage)

Figure 140 above showed that the process was not under statistical control, there were 24 out of 52 pills outside the control limit. There are two types trends in the mass, the very high output around 0.14 and the lower output of 0.08 grams. Looking back into the experimental setup details, it was noted that the group of low mass pills (from pill number 19 to 42) were the only pills made in the morning out of the 300 pills. They were also made on a sunny day, so even if the temperature control reading was the regular 25 degrees Celsius, the sun was still shining on the machine, and the higher temperature makes the electrospinning process less efficient. This observation was noted, and all the other pills were then made at nighttime, at the same conditions of earlier batches. The other factor that affected this productivity was the grounding mechanism; the spring-loaded grounding was not properly attaching the rod collector to the ground. This spring-loaded ground was then re-evaluated and attached in the correct position and worked efficiently in the subsequent trials.

Removing the low- productivity points from the control chart above gave the following:

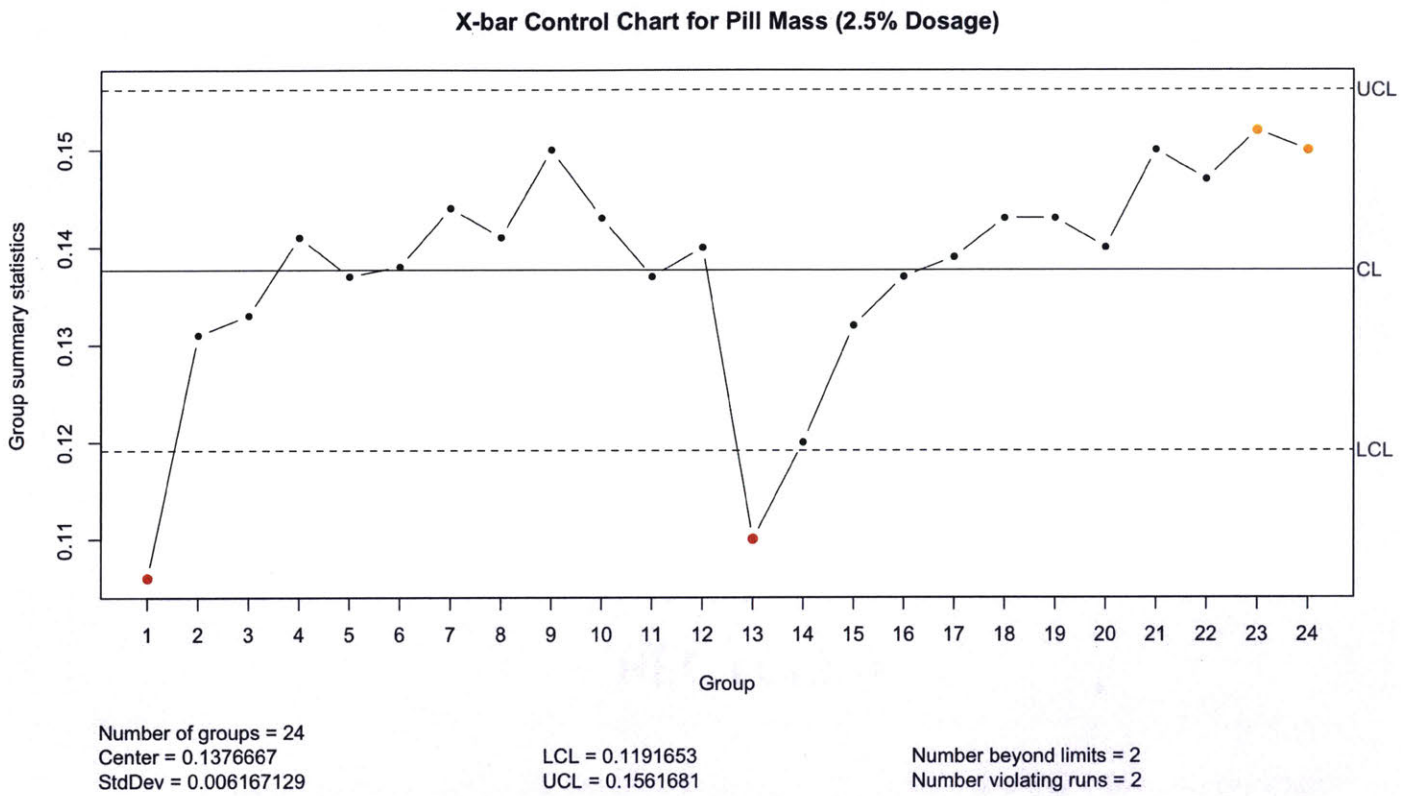

Figure 141: Corrected X-bar control chart for pill mass (2.5% dosage)

Figure 141 showed that the process was under statistical control around its mean value of 0.137 grams, and there were only two points beyond the upper or lower control limits for the 24 pills analyzed. A repetitive trend of increasing mass output could be observed twice; from pill 1 to 9, and 13 to 24. It could be correlated to the fact that the same solution was used to make a batch of 12 pills; pill 1 to 12, and pill 13 to 24. When the same solution was used repetitively. The spinneret accumulated some of the polymer on its wiring and spun more fibers.

The control chart for the 12.5% dosage looked as follows:

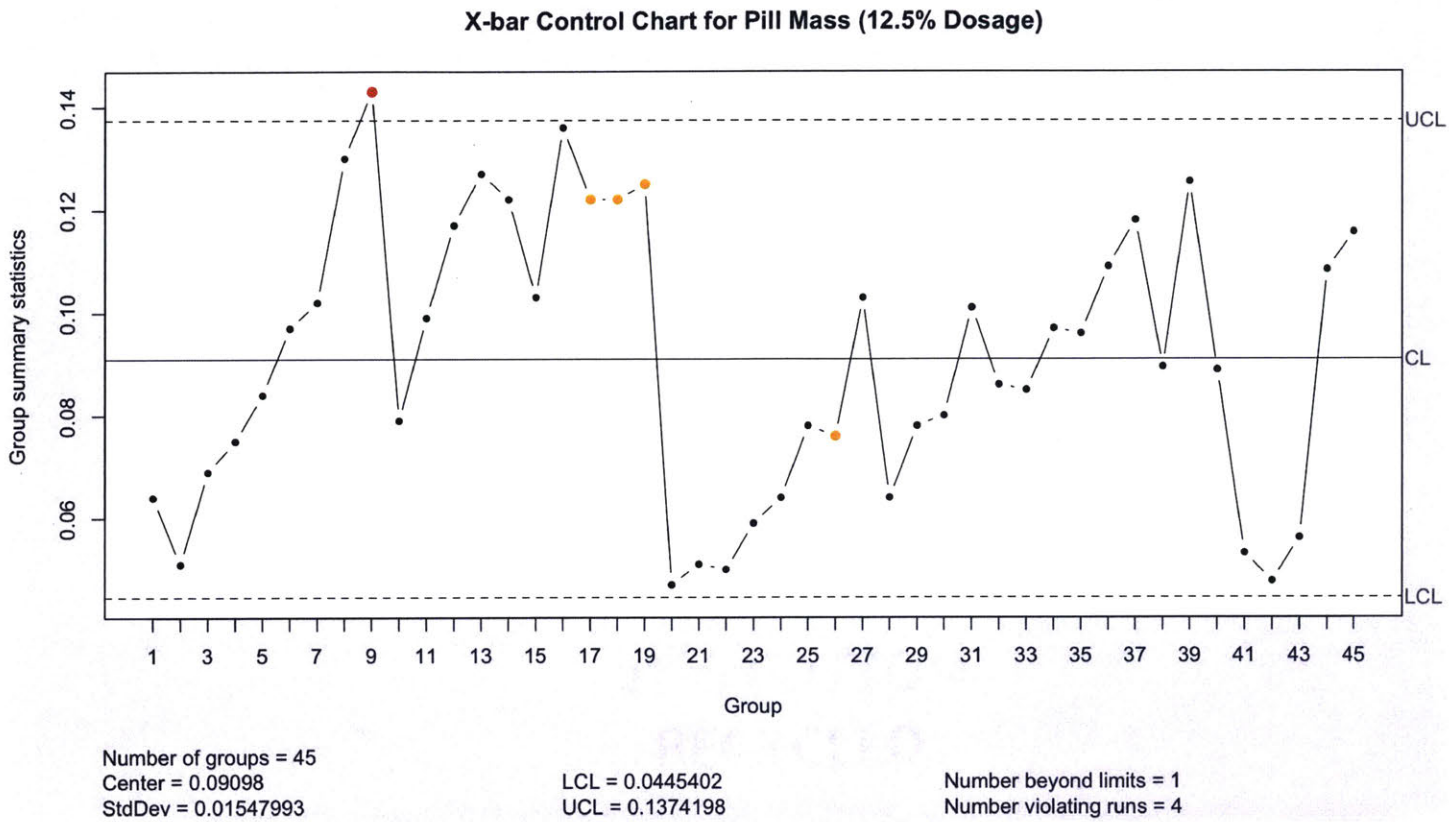

Figure 142: X-bar control chart for pill mass (12.5% dosage)

Figure 142 above showed that the process was under statistical control around its mean value of 0.09 grams, and there was only 1 point beyond the control limits for the 45 pills made with 12.5% dosage. But a repetitive trend of increasing mass outputs could be observed 4 times on this graph; from pill 2 to 9, 10 to 17, 20 to 27, and 28 to 39. Each batch of those 4 trends was done using one solution. It could be correlated to the fact that the same solution was used over and over again, so the spinneret accumulated some of the polymer on its wiring and spun more fibers. This observation did not exist in the zero dosage because its solution was less viscous. Because it was less viscous, it did not stick to the wire spinneret but it would drop into the solution bath. This problem could be solved in the future by either changing the solution or cleaning the wire spinneret before each run.

5.3 Microstructures of fibers and pills

The structure of the electrospun fibers before pressing looked as follows:

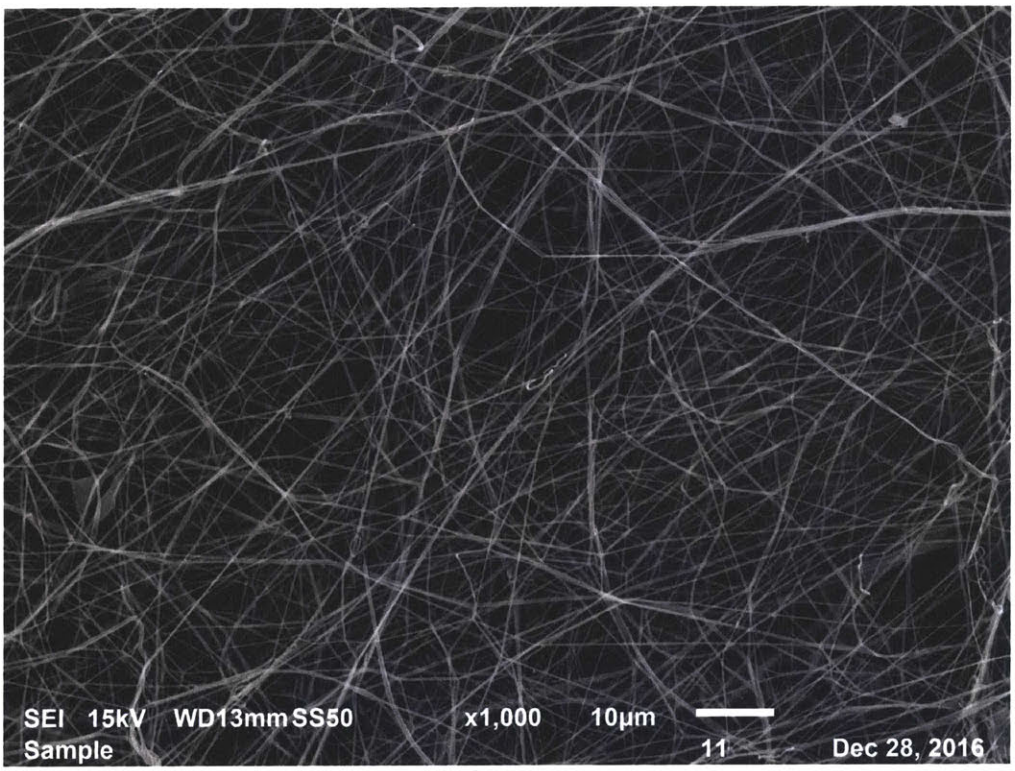

Figure 143: electrospun fiber structure before pressing

After pressing these fibers, the pill's structure looked as follows from the top:

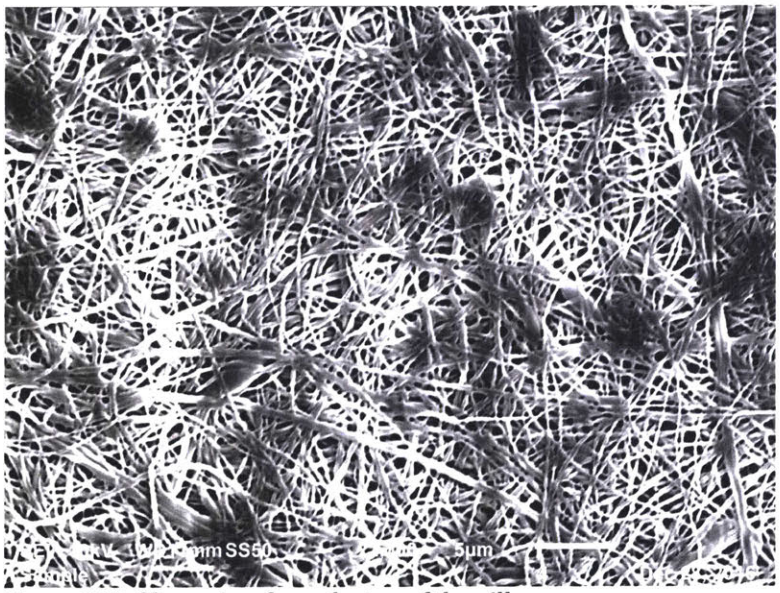

Figure 144: fibers view from the top of the pill

Zooming into the surface of the pill's structure, the structure looked as follows:

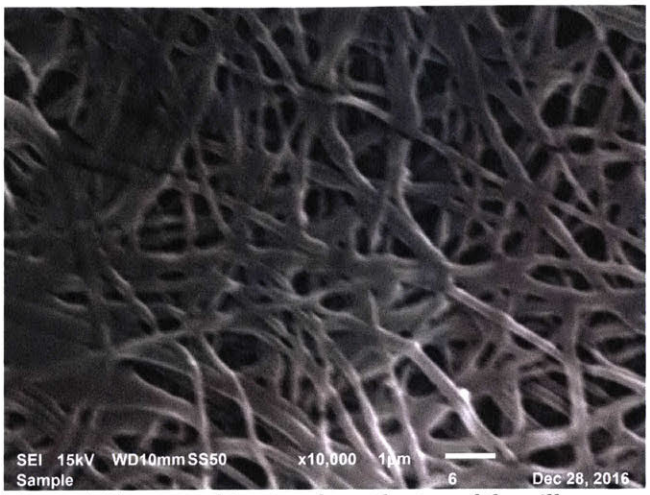

Figure 145: zoomed in view from the top of the pill

Zooming out of the surface of the pill's structure, the structure looked as follows:

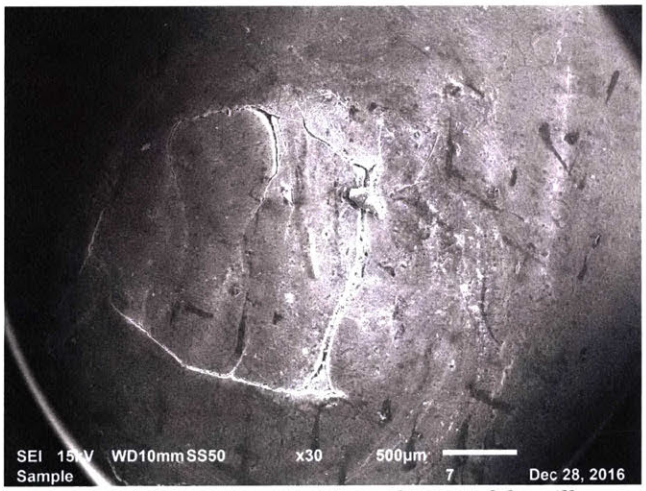

Figure 146: zoomed out view from the top of the pill

This circle in Figure 146 was expected because it was the edges of the stripped polymer (seen in Figure 147) pressed into the flat pill shape.

Figure 147: the stripped polymer before pressing

Structure of the pill's side:

It is important to note that the pill was cut sideways using a razor, so structures might look more stretched than their natural shape. The side view of the fibers' structure looks as follows:

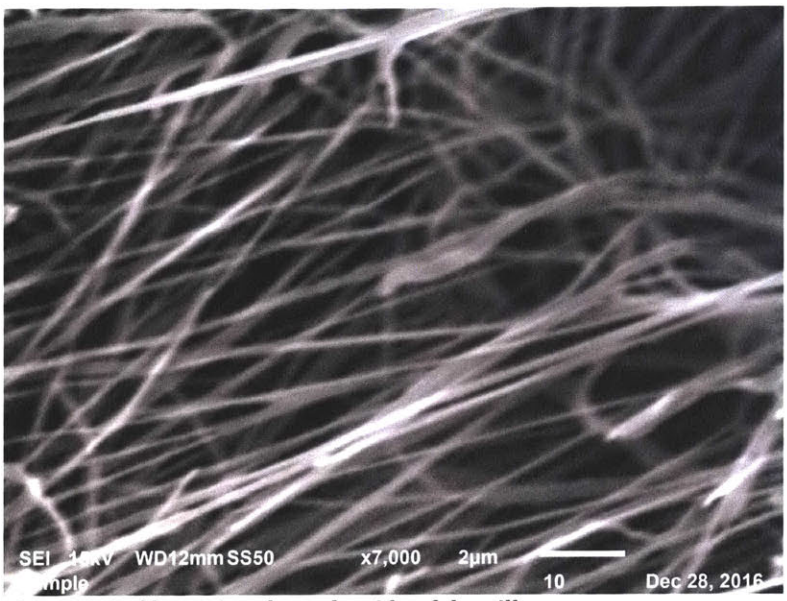

Figure 148: fibers view from the side of the pill

Zooming into the side of the pill, the structure looks as follows:

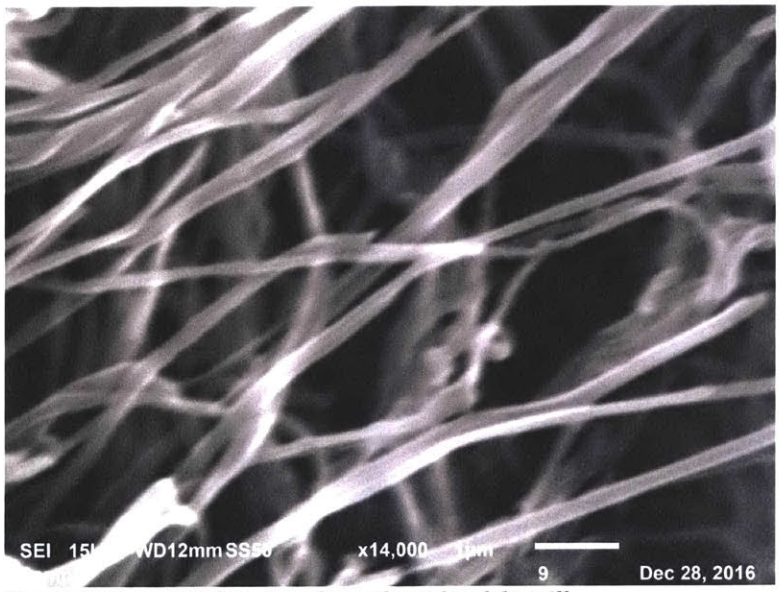

Figure 149: zoomed in view from the side of the pill

The diameter of the fibers before pressing had an average of 0.2 to 0.3 micrometers, as seen below:

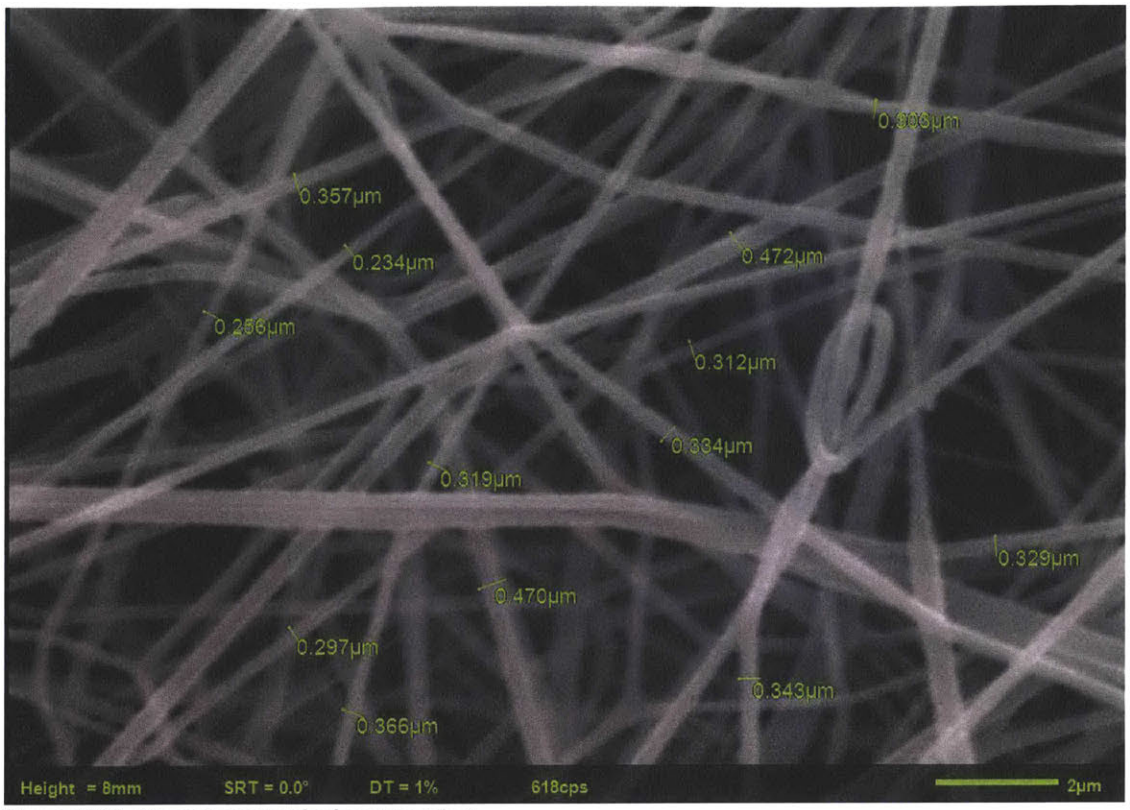

Figure 150: fiber diameter before pressing

The fiber diameter after pressing still had an average of 0.2 to 0.3 micrometers between as shown below:

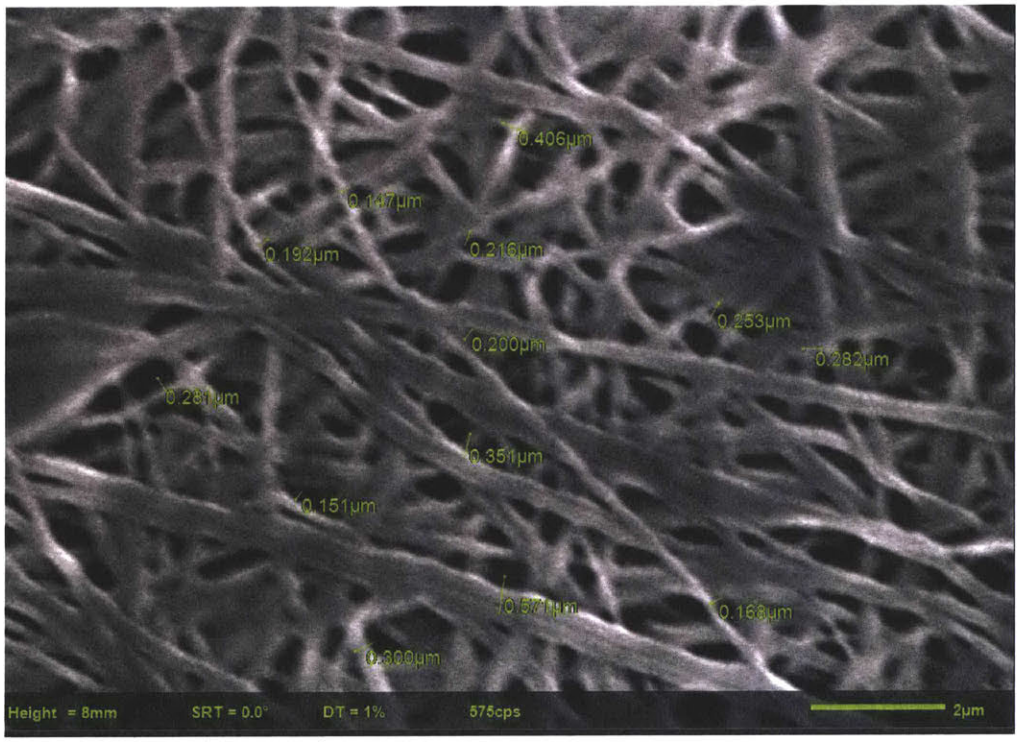

Figure 151: fiber diameter after pressing

Looking at the fiber diameter from the side view gave the same value of 0.2 to 0.3 micrometers on average, as seen here:

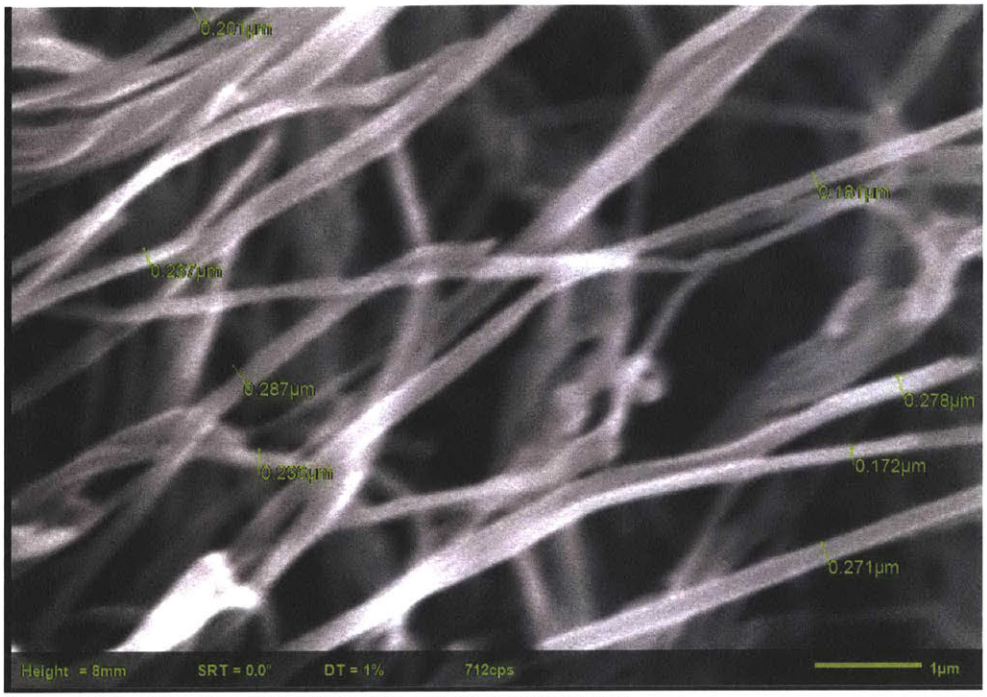

Figure 152: side view of the fiber diameter after pressing

These SEM images show that the fiber diameter stayed between 0.2 and 0.3 micrometers before and after pressing, as seen in Figure 150, Figure 151, and Figure 152. This means that our mechanism did not loose the fibers fine nanostructure in the process. This was one of the main milestones of the project, to have a mechanism that pressed the fibers without changing their fine structure. This fine structure meant that the pill still had their advantages of high dissolution among others. These dissolution profiles would be discussed in more details in the next section.

5.4 Pressure, density, and dissolution profiles of the pills

5.4.1 Theoertical versus Experimental densities

Firstly, the maximum theoretical densities of the pills were calculated using the powder densities from the suppliers' data sheet. Using this density data from the supplier (Sigma Aldrich) and the percentage weight of each component in the mix, the total densities of each mix were calculated as follows:

For the Polyvinyl alcohol (PVA) mix:

Material	**Density (g/cm^3)**	**Percentage**
PVA	1.269	0.93
High Density PVA	1.269	0.07
Total Density (g/cm^3)		**1.269**

Table 65: PVA density calculation

For the 2.5 % fenofibrate and PVA mix:

Material	**Density (g/cm^3)**	**Percentage**
PVA	1.269	0.907
HD PVA	1.269	0.068
Fenofibrate	1.18	0.025
Total Density (g/cm^3)		**1.267**

Table 66: 2.5% fenofibrate and PVA density calculation

For the 12.5% fenofibrate and PVA mix:

Material	**Density (g/cm^3)**	**Percentage**
PVA	1.269	0.814
High Density PVA	1.269	0.061
Fenofibrate	1.18	0.125
Total Density (g/cm^3)		**1.258**

Table 67: 12.5% fenofibrate and PVA density calculation

Secondly, the three types of pills were then pressed with different pressures ranging from zero Psi to 50 Psi, the resulting pills' densities were as follows:

For PVA (polyvinyl alcohol) pills, the results for the 6 pills made were:

Pressure [Psi]	**Density [g/cm3]**	**Solidity**
10	0.81	0.64
5	0.57	0.45

1.8	0.37	0.29
15	1.03	0.81
50	1.17	0.92
30	1.13	0.89

Table 68: data for PVA pills

For 2.5% fenofibrate and PVA pills, the results of the 68 pills pressed were:

Pressure [Psi]	Density [g/cm3]	Solidity
20	1.01	0.80
20	0.96	0.76
20	0.98	0.78
20	1.02	0.80
20	1.01	0.80
20	0.92	0.73
20	0.94	0.74
5	0.68	0.54
25	1.06	0.84
10	0.78	0.62
20	1.00	0.79
15	0.92	0.73
10	0.75	0.59
20	0.97	0.77
15	0.87	0.69
5	0.48	0.38
25	1.04	0.82
5	0.62	0.49
25	1.06	0.84
10	0.77	0.61
5	0.66	0.52
20	1.02	0.80
15	0.93	0.73
20	0.96	0.76
10	0.79	0.63
25	1.07	0.84
15	0.96	0.76
5	0.56	0.44
2	0.36	0.28
2	0.26	0.21
20	0.99	0.78
20	0.97	0.76

7	0.73	0.58
7	0.68	0.54
2	0.49	0.38
2	0.40	0.31
10	0.82	0.65
10	0.74	0.58
5	0.66	0.52
5	0.69	0.55
7	0.72	0.56
7	0.71	0.56
15	0.96	0.76
15	0.94	0.74
50	1.12	0.88
50	1.13	0.90
5	0.61	0.48
5	0.71	0.56
25	0.96	0.76
25	0.98	0.77
50	1.07	0.85
50	1.04	0.82
5	0.68	0.54
25	1.06	0.84
10	0.78	0.62
20	1.00	0.79
15	0.92	0.73
10	0.75	0.59
20	0.97	0.77
15	0.87	0.69
5	0.48	0.38
25	1.04	0.82
5	0.62	0.49
20	0.97	0.77
15	0.87	0.69
5	0.48	0.38
25	1.04	0.82
5	0.62	0.49

Table 69: data for 2.5% fenofibrate and PVA pills

For 12.5% fenofibrate and PVA pills, the results for the 45 pills made were:

Pressure [Psi]	**Density [g/cm3]**	**Solidity**

25	1.09	0.87
5	0.59	0.47
10	0.84	0.67
20	1.06	0.84
15	0.97	0.77
5	0.63	0.50
25	1.12	0.89
15	1.01	0.80
20	1.00	0.80
10	0.93	0.74
20	1.07	0.85
5	0.67	0.54
25	1.14	0.91
15	0.98	0.78
20	1.06	0.84
10	0.88	0.70
25	1.11	0.89
5	0.71	0.57
15	0.94	0.75
20	0.91	0.72
50	1.11	0.88
2	0.34	0.27
50	1.13	0.90
2	0.45	0.36
50	1.16	0.92
2	0.42	0.33
50	1.21	0.96
2	0.29	0.23
10	0.86	0.68
10	0.82	0.66
5	0.55	0.44
5	0.51	0.40
20	1.00	0.80
20	1.04	0.83
7	0.69	0.55
7	0.75	0.60
7	0.72	0.57
20	1.03	0.82
20	1.04	0.83
10	0.79	0.63
10	0.71	0.56

50	1.05	0.83
50	1.14	0.90
15	0.88	0.70
15	0.98	0.78

Table 70: data for 12.5% fenofibrate and PVA pills

5.4.2 Pressure and Density Relationships

The graphs for pressure versus density for each of the pill types looked as follows:

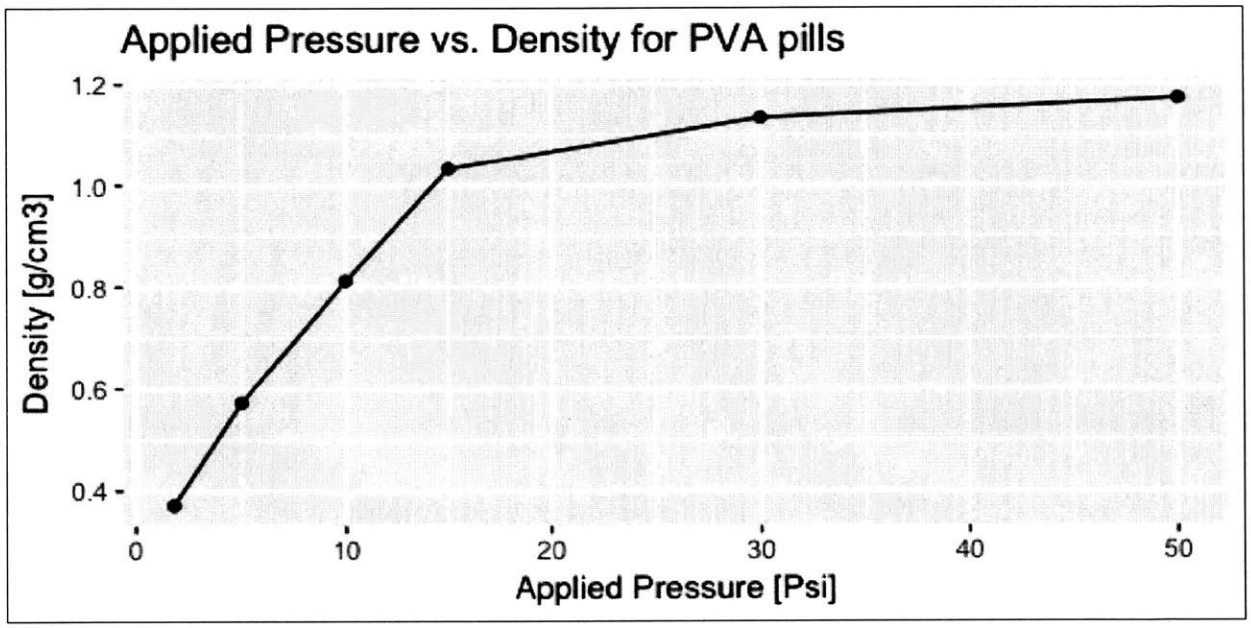

Figure 153: graph of applied pressure vs. density for PVA

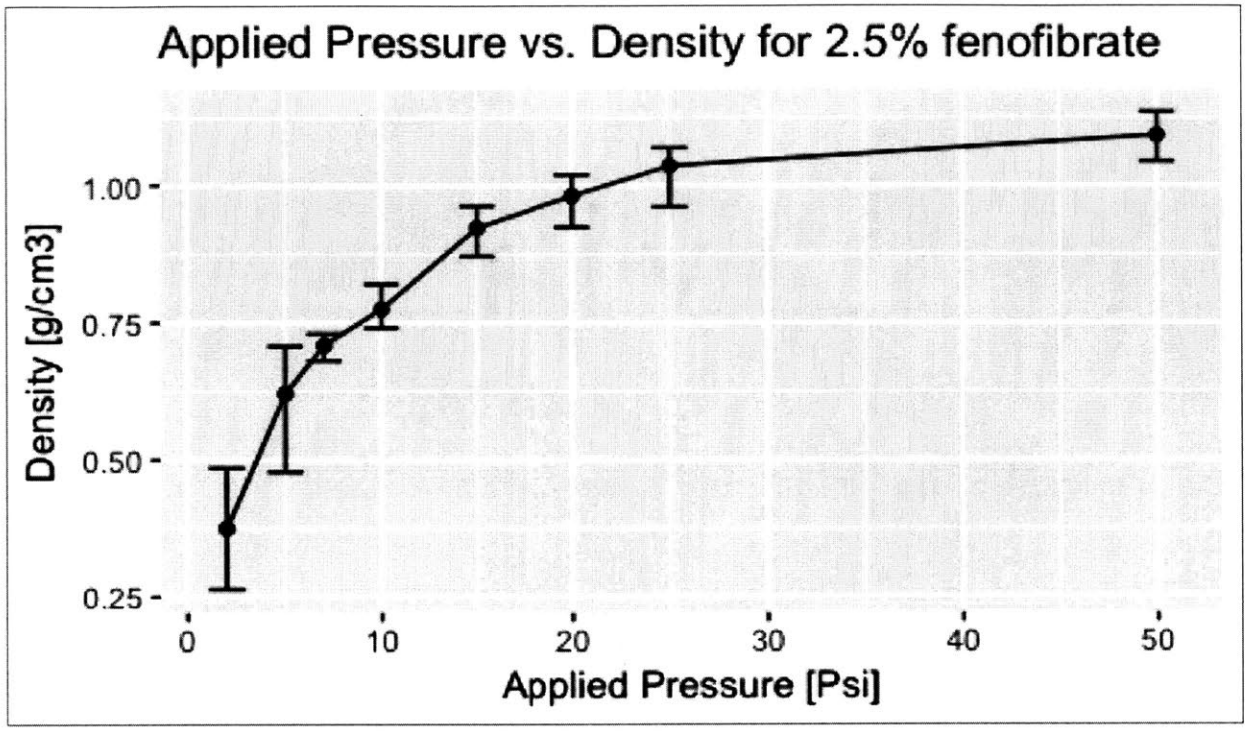

Figure 154: graph of applied pressure vs. density for 2.5% fenofibrate in PVA (the bars show minimum and maximum values)

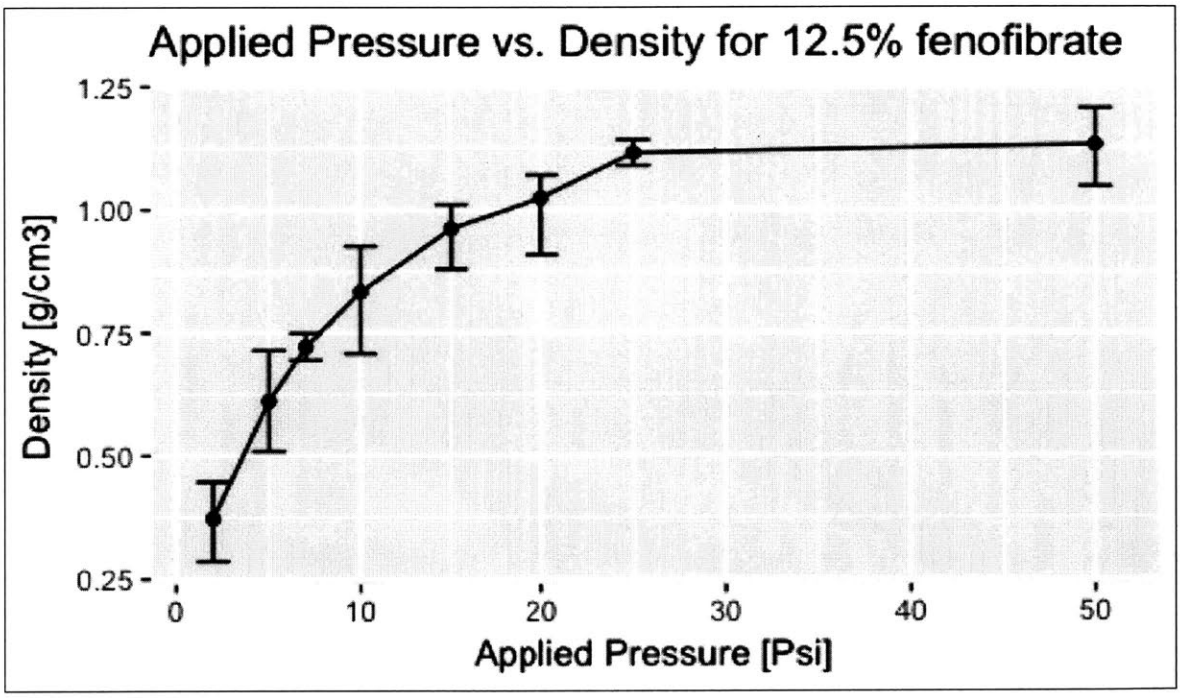

Figure 155: graph of applied pressure vs. density for 12.5% fenofibrate in PVA (the bars show minimum and maximum values)

The graphs in **Figure 153**, **Figure 154**, and **Figure 155** showed that the density increases at a decreasing rate until it became constant starting from 25 Psi. This data agrees with Riipi's

work showing that the density and the strength of tablets increased at low forces until it remained constant after a specific point [18].

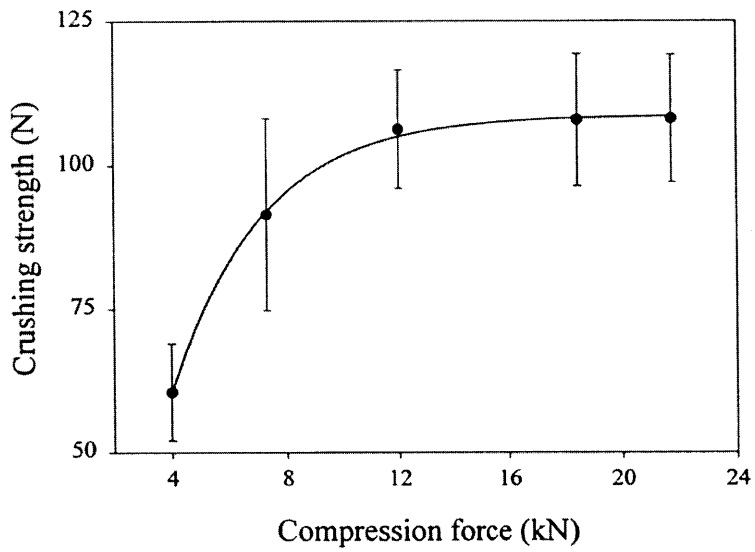

Figure 156: effect of compression force on the crushing strength of erythromycin acistrate tablets (18, Figure 1)

Noting that Riipi's work was done for different chemicals, his graph of the force versus strength showed the same shape as our pressure (directly proportional to the force) and density (directly proportional to the crushing strength).

5.4.3 Pressure and Solidity Relationships

After looking at the data with its error bars in Figure 153, Figure 154, and Figure 155. The average of each data point was calculated for further analysis:

Pressure [Psi]	Density [g/cm3]	Solidity
2	0.38	0.30
5	0.62	0.49
10	0.77	0.61
15	0.92	0.73
20	0.98	0.77
25	1.04	0.82
50	1.09	0.86

Table 71: average data for 2.5% fenofibrate pills

Pressure [Psi]	Density [g/cm3]	Solidity
2	0.37	0.30
5	0.61	0.49
10	0.83	0.66
15	0.96	0.76
20	1.02	0.81

25	1.12	0.89
50	1.13	0.90

Table 72: average data for 12.5% fenofibrate pills

Graphing the log values of the density versus the log values of the pressure looked as follows:

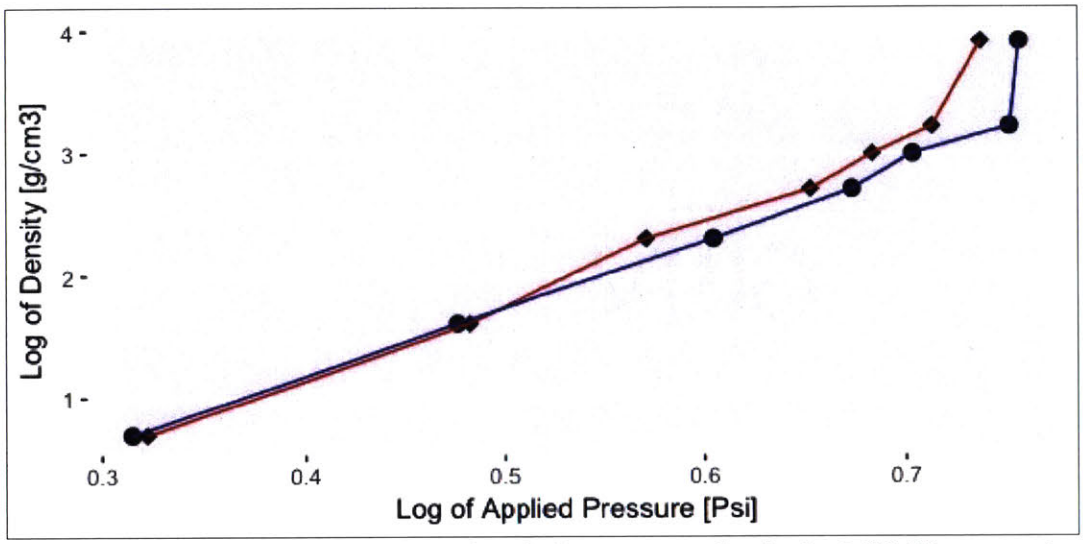

Figure 157: graph of logarithmic values of applied pressure vs. density for 2.5% (The square legend) and 12.5% (The circular legend) fenofibrate in PVA

A value of 1 was added to all the density log values in Figure 157 to make them positive. Figure 157 showed that the maximum density of the 2.5% mix was less than that of the 12.5%, which means that the 2.5% mix was less compressible, even though it had a higher theoretical density. Transforming these density values to solidity gave the following:

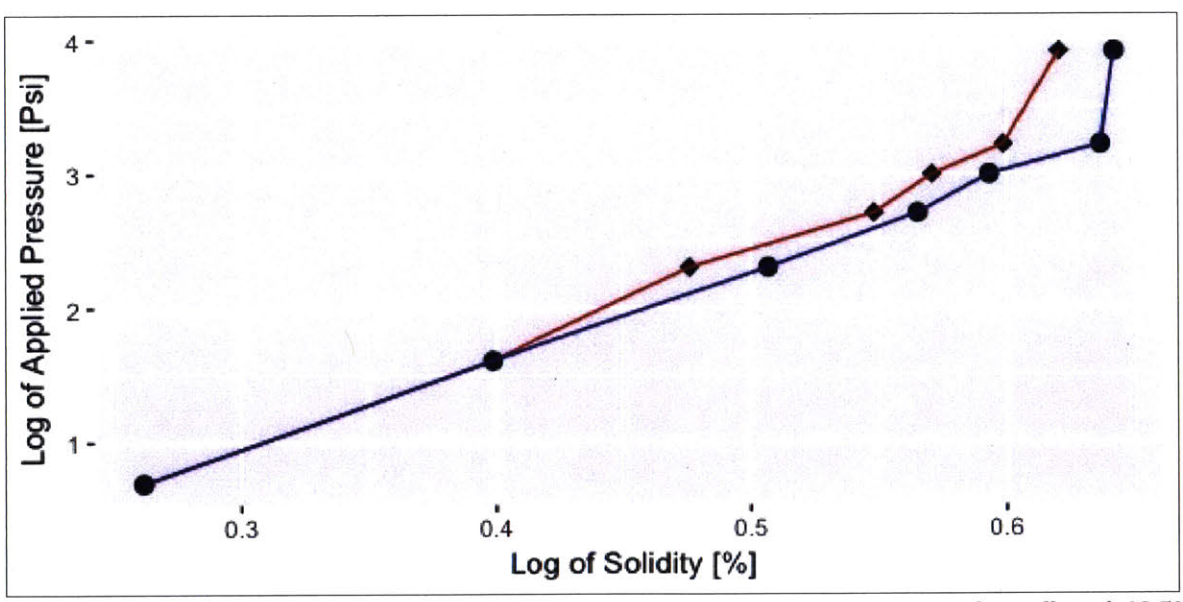

Figure 158: graph of log of the applied pressure vs. solidity for 2.5% (The square legend) and 12.5% (The circular legend) fenofibrate in PVA

Looking at the pressure versus solidity graph without log transformations:

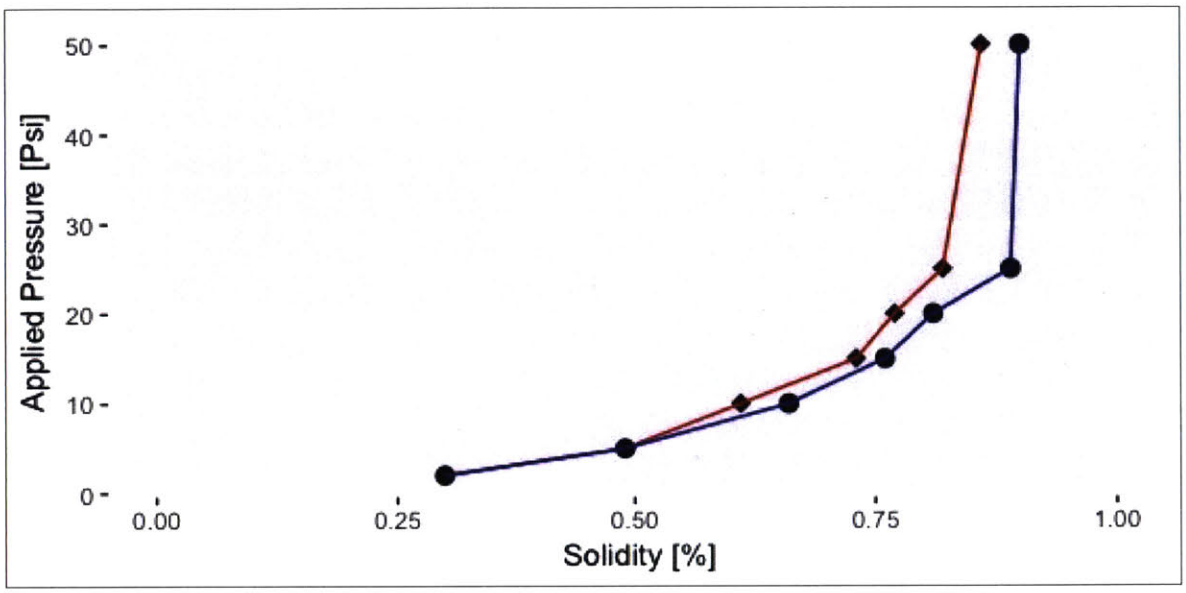

Figure 159: graph of the applied pressure vs. solidity for 2.5% (The square legend) and 12.5% (The circular legend) fenofibrate in PVA

Changing the scaling of the x-axis and the y- axis to a logarithmic scale gave:

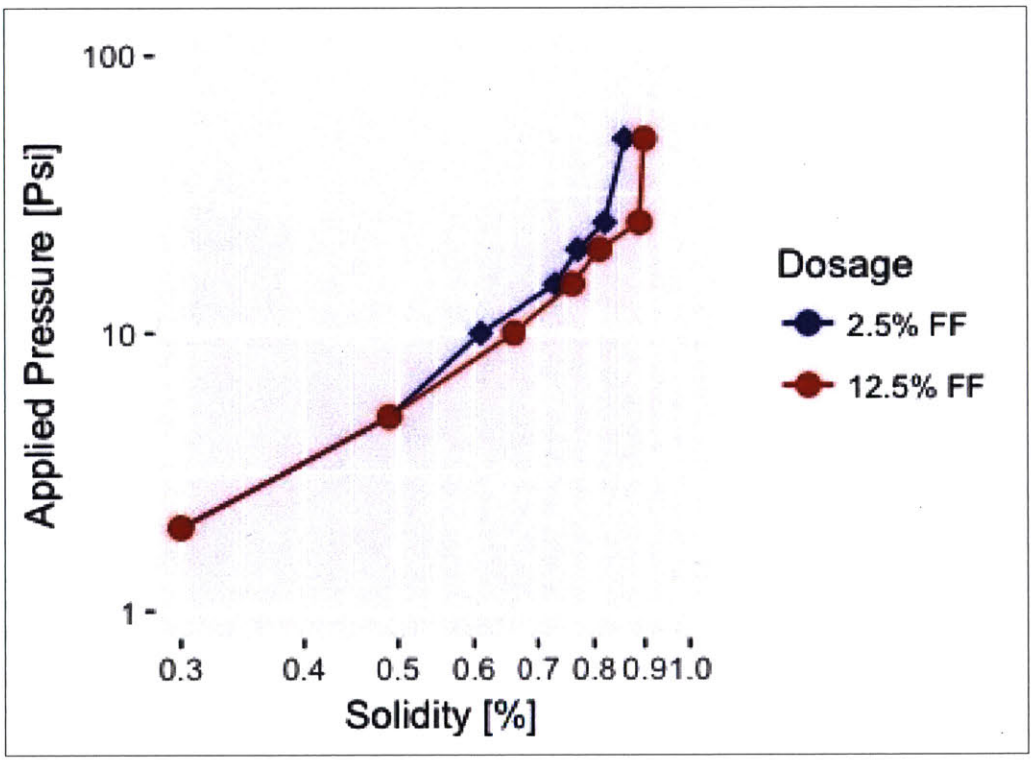

Figure 160: log scaled graph of the applied pressure vs. solidity for 2.5% (The square legend) and 12.5% (The circular legend) fenofibrate in PVA

It could be noted from Figure 158, Figure 159, and Figure 160 that the 12.5% always had higher density and solidity than the 2.5% dosage. The log scaled graph of the applied pressure versus the solidity, shown in Figure 160 could be compared to Choong's model [44], which looked as follows:

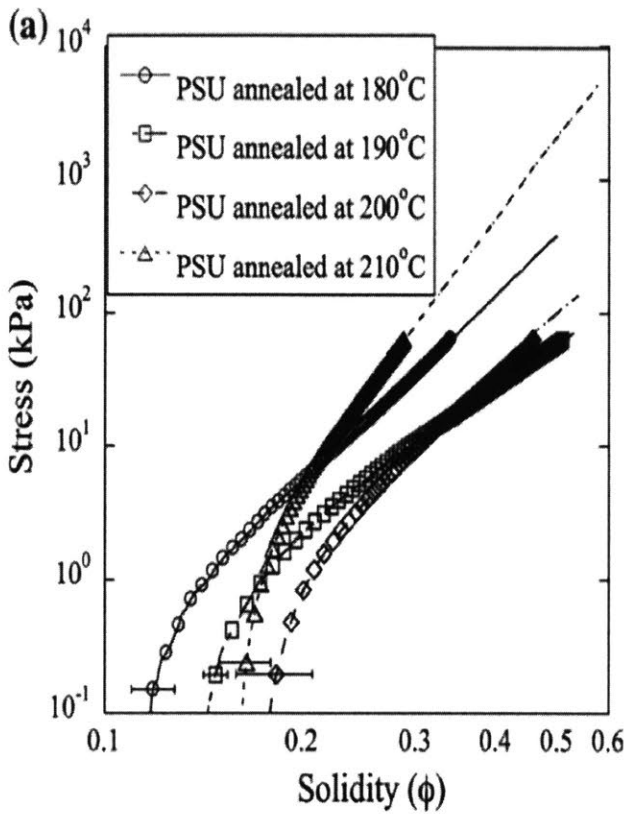

Figure 161: Choong's model of stress versus solidity [44, Figure 9]

Comparing the experimental graph in Figure 160 to Choong's graph in Figure 161 , it could be noted that they had the same trend[44]. The experimental data was fitted into a power law equation, which made it similar to Van Wyk's model [44] in Equation 28 below:

$$\sigma_{zz} = kE\left(\phi^3 - \phi_0^3\right)$$

Equation 28

where σ_{zz} is the relating transverse stress, and Φ is the solidity.

According to Choong, the power of the solidity (n) could have 2 different values; n=3 for 3D random fiber network and n=5 for planar random fiber network. Fitting the experimental data to a 3rd degree polynomial gave the following graph:

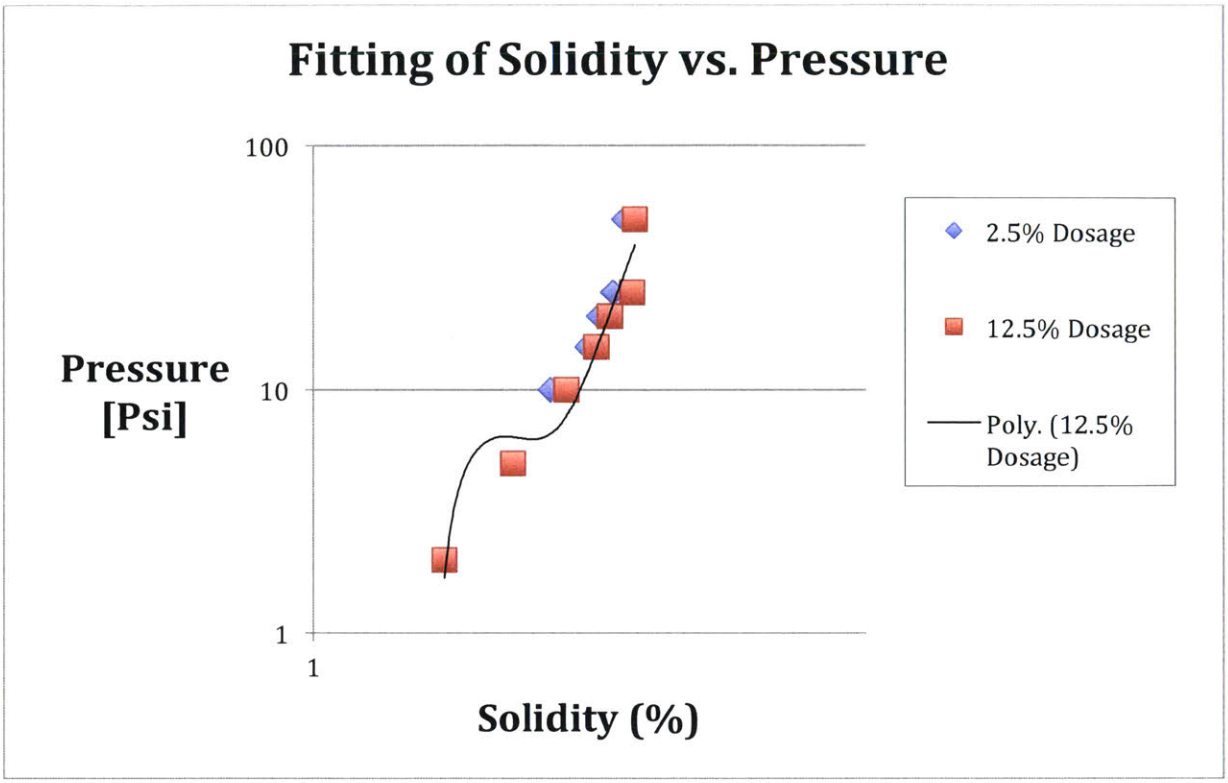

Figure 162: fitting the logarithmic scaled graph of solidity vs. pressure

Figure 162 showed that the experimental data is a good fit with a 3rd degree polynomial, following Van Wyk's model in Choong's work.

5.4.4 Density Correction Experiment

To get accurate density values of the pill, the mass of the metal contamination had to be subtracted from the total mass. To quantify the mass of this metal, a vacuum flask test was carried out, as seen in Figure 163:

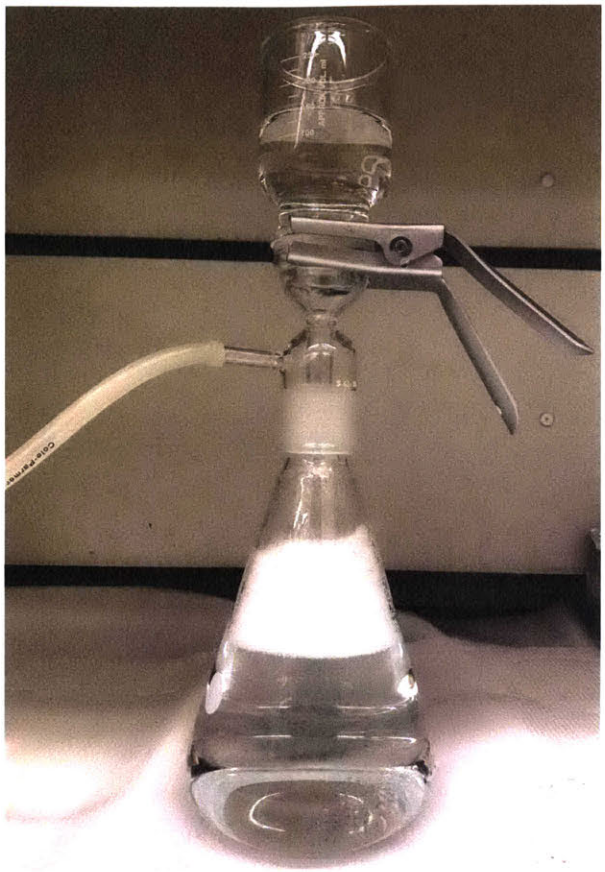

Figure 163: vacuum flask setup

During this test, five pills were firstly dissolved in water, because the polyvinyl alcohol dissolved and the metal contamination stayed as seen in Figure 164 below:

Figure 164: pill dissolves in water & metal contamination residues stay visible

This solution with metal contamination was then poured into the vacuum flask setup, and the weight of the filter paper, shown in Figure 165, was measured before and after the metal addition.

Figure 165: filter with metal contamination

The vacuum setup test showed that the mass of the metal (from 5 pills) was about 0.001 grams. This means that metal contamination in each pill weighted about 0.0002 grams. This was in the order of 0.2 milligrams, and our masses were around 100 milligrams. So it was decided that the mass difference due to metals contamination was negligible because it is about 0.2% of the total mass.

5.4.3 Friability test:

After preparing many pills, some of them were taken to the friability tester where the pills are rotated in the drum seen in Figure 166 to see how much powder mass is lost. The testing protocol performed by my colleague Bhattacharyya was exactly followed [40]. 5 pills were loaded to the ERWEKA friability tester TAR 220 and rotated 100 times at a speed of 25 rpm.

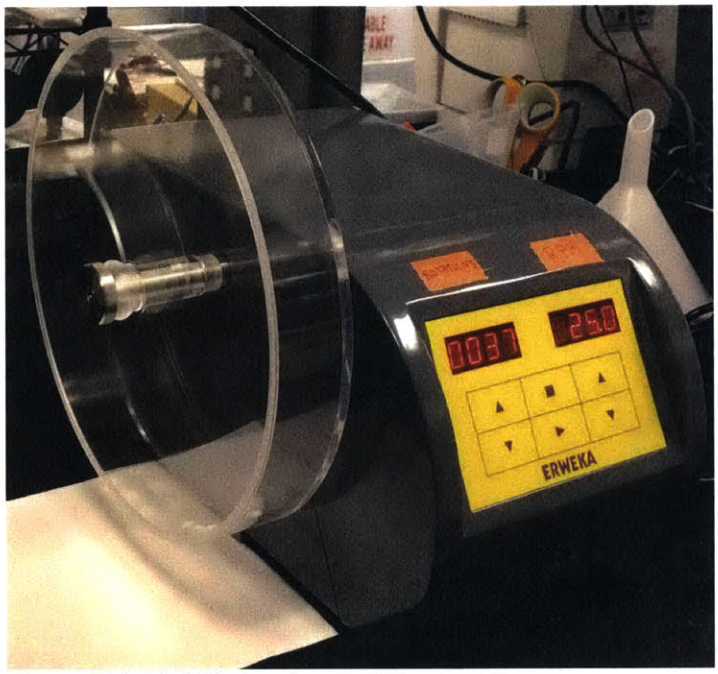

Figure 166: friability testing machine

The cycle looks as shown in Figure 167 and Figure 168. There is a lip in the rotating drum that cycles the pills up, as shown in Figure 167. When they reach the top of the drum, they fall down to the bottom of the drum, as shown in Figure 168. This drop is what tests the pill's capability of maintaining a long shelf life with no mass loss in transport. The results showed that there was zero mass lost during the experiment.

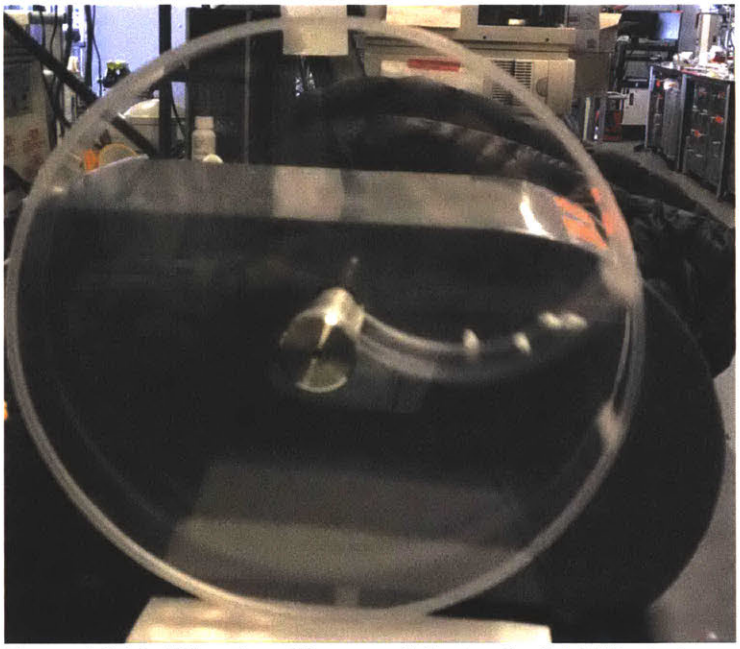

Figure 167: holding the pills upward during the friability test

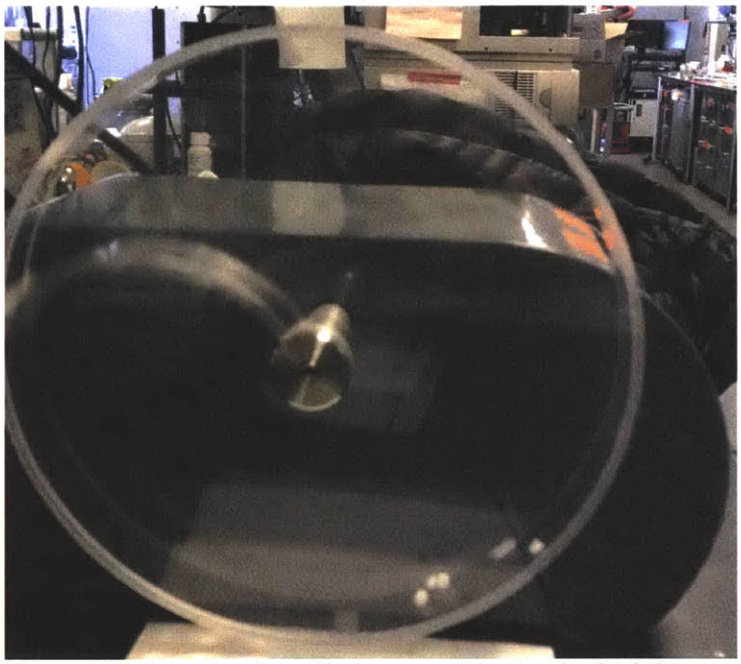

Figure 168: dropping the pills downward during the friability test

5.5 Dissolution profiles for various applied pressures

5.5.1 Dissolution Results

After making 120 pills and pressing them with different pressures, their dissolution profiles were analyzed using an Agilent Varian VK 7025 dissolution bath and a Cary 50 Bio UV spectrophotometer, seen in Figure 169.

Figure 169: dissolving the pills in the UV spectrophotometer

The analysis was performed according to the standard USP method for FEN using dissolution apparatus II filled with 1000 mL of 0.05M SDS. The paddle speed was 50 rpm and the solution temperature was maintained at 37□C. Measurements were made in situ for up to 6 hours using submersible probes, at 292nm, connected to the spectrophotometer by fiber optic cables, enabling measurement of UV-Vis spectra directly in the liquid media. Due to the low density of the tablets relative to the media, Japanese USP grade sinkers purchased from QLA, were used throughout the dissolution examination.

Figure 170: USP grade sinkers

Known standards of fenofibrate in the media were measured prior to the start of the experiment and fell within 5% of the claimed content. Only aesthetically acceptable tablets that were devoid of any visible defects were used for dissolution testing. A sample size of at least 5 tablets was measured for one dissolution profile, with the average being reported.

Figure 171: un-pressed mix and pills pressed at different pressures

The pressures by which the pills were pressed were: 0, 2, 5, 7, 10, 15, 20, 25, and 50 Psi. The time for 80% dissolution for both the 2.5% and the 12.5% fenofibrate looked as follows:

Pressure [Psi]	80% Dissolution Time [min]
0	22.5
2	64

5	68
7	71
10	83.5
15	95
20	97
25	99
50	99

Table 73: 80% dissolution times for 2.5% fenofibrate

Pressure [Psi]	80% Dissolution Time [min]
0	12
2	34
5	62
7	71
10	80
15	92
20	93
25	90
50	93

Table 74: 80% dissolution times for 12.5% fenofibrate

Plotting some of the dissolution profiles of the 2.5% fenofibrate:

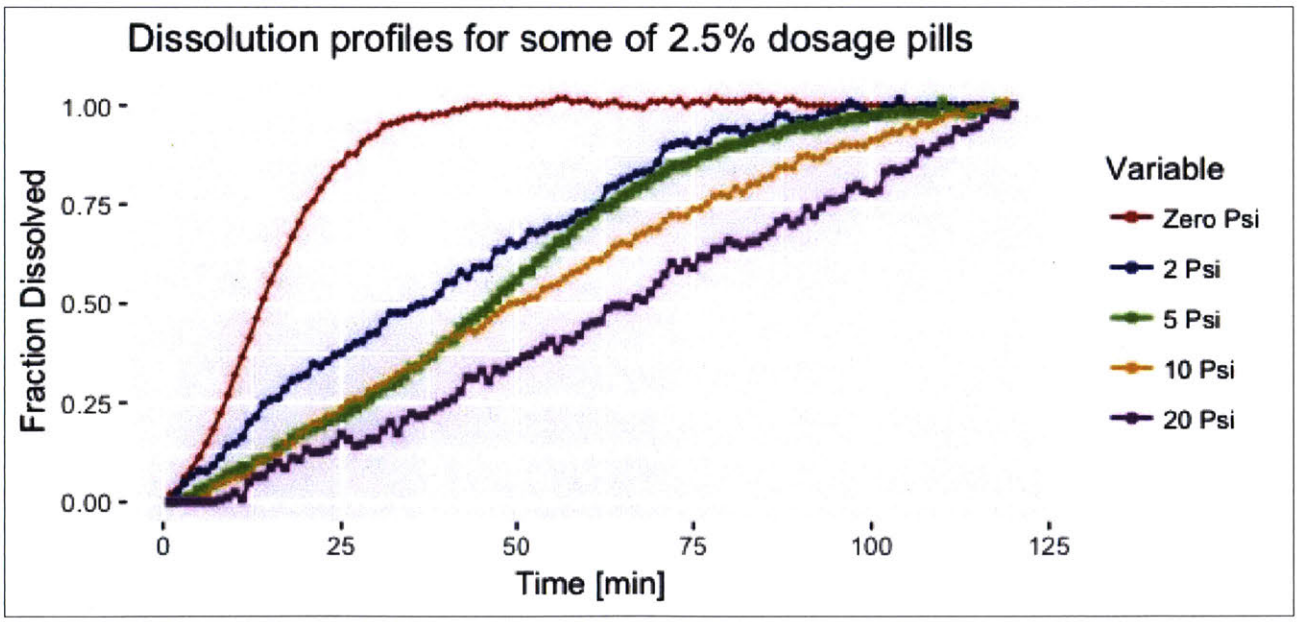

Figure 172: dissolution profiles of some of the 2.5% fenofibrate pills

Plotting all of the dissolution profiles of the 2.5% fenofibrate:

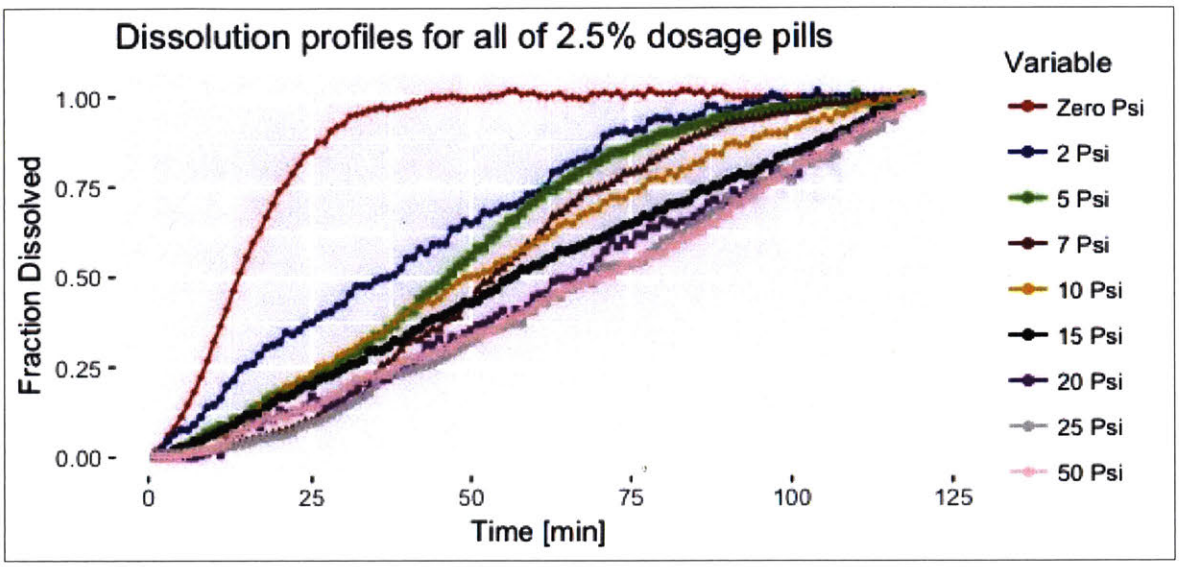

Figure 173: dissolution profiles of all of the 2.5% fenofibrate pills

Plotting some of the dissolution profiles of the 12.5% fenofibrate:

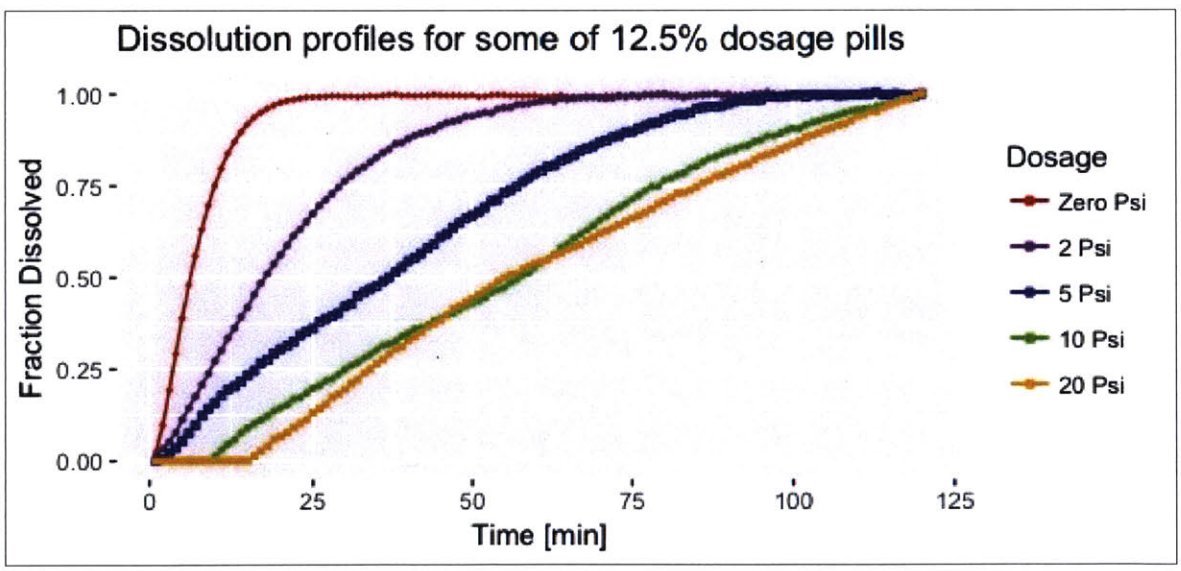

Figure 174: dissolution profiles of some of the 12.5% fenofibrate pills

Plotting all of the dissolution profiles of the 12.5% fenofibrate:

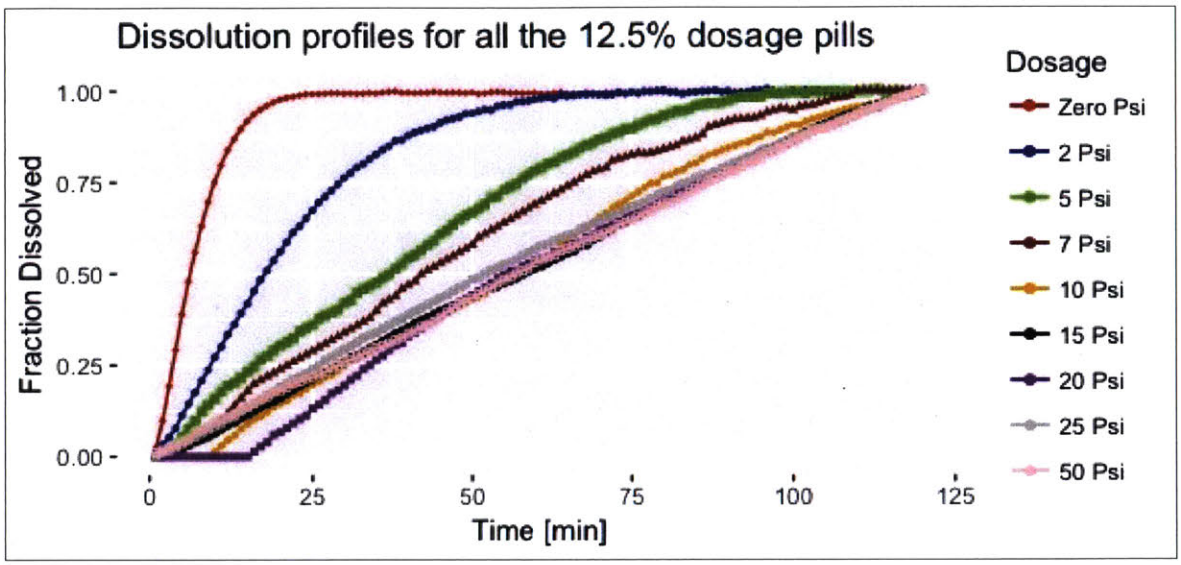

Figure 175: dissolution profiles of all of the 12.5% fenofibrate pills

Comparing the dissolution profiles of un-pressed 12.5% versus the 2.5% fenofibrate gave:

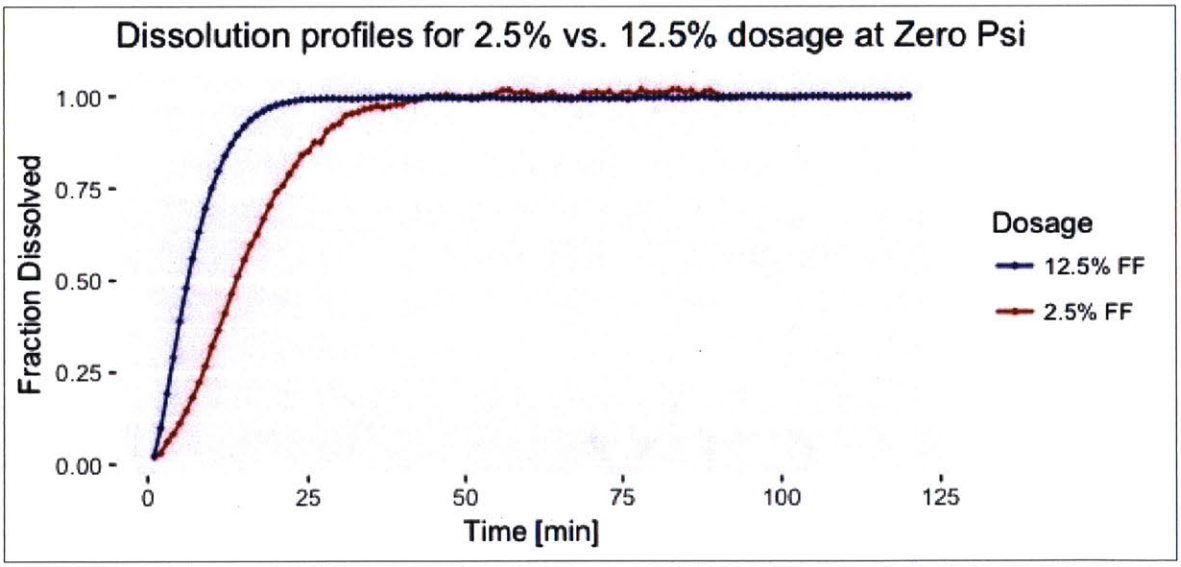

Figure 176: comparison of the dissolution profiles of un-pressed 12.5% versus 2.5% fenofibrate

Figure 176 above showed that the 12.5% dosage dissolved almost twice as fast as the 2.5% dosage did. 80% of the high dosage dissolved in almost 12 minutes and 80% of the low dosage dissolved in about 22.5 minutes. Comparing the dissolution profiles of 12.5% versus the 2.5% fenofibrate pressed at 5 Psi gave:

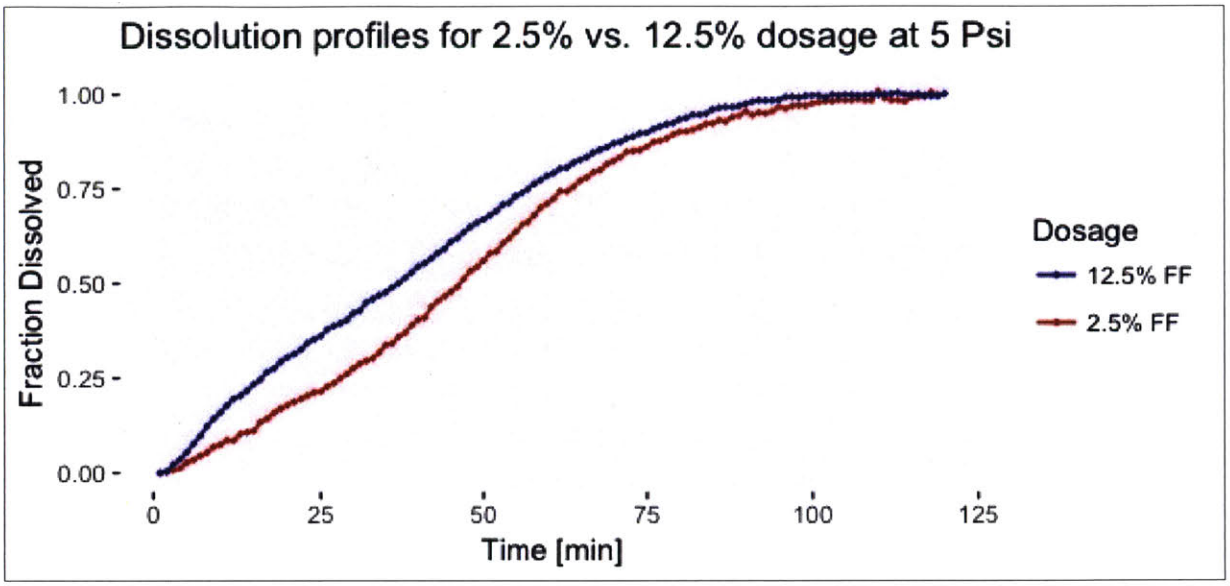

Figure 177: comparison of the dissolution profiles of 12.5% versus 2.5% fenofibrate pills pressed at 5 Psi

Comparing the dissolution profiles for pills pressed at 5 Psi showed that the 12.5% dosage dissolved faster than the 2.5% dosage, but the difference between their profiles was less. It took around 62 minutes to dissolve 80% of the high dosage, compared to around 68 minutes to dissolve 80% of the low dosage.

Plugging the time for 80% dissolution against different pressures applied would give:

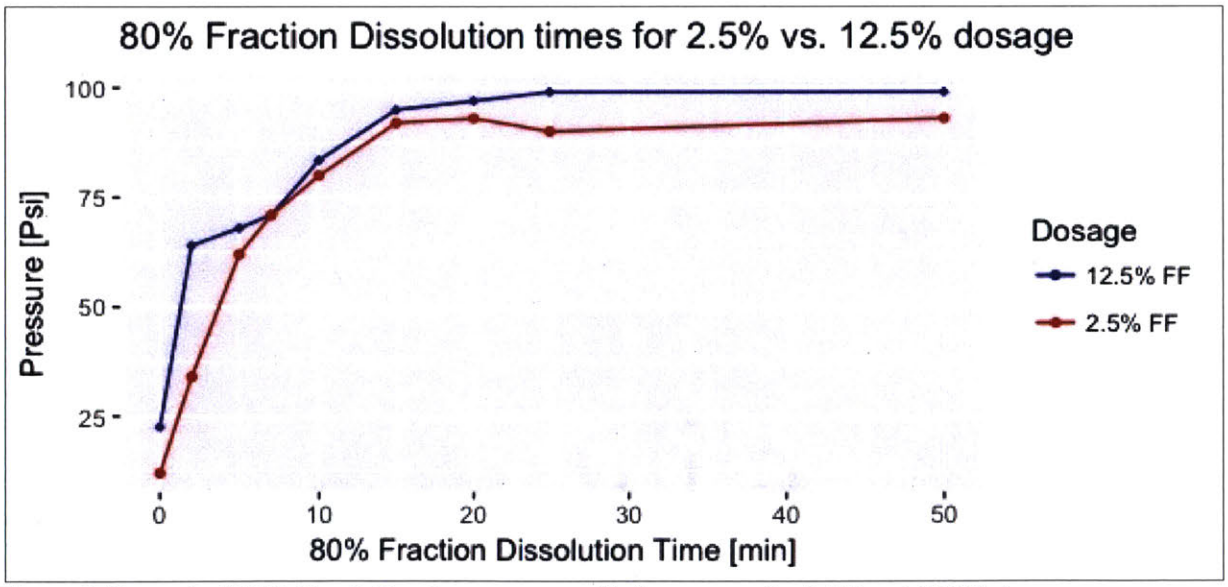

Figure 178: graph of 80% dissolution time versus applied pressures for 2.5% and 12.5% dosage

As seen in Figure 178 above, the dissolution time for 80% of the drug varies at low pressures; from zero to 10 Psi, then it becomes constant at higher pressures. This phenomenon is directly related to the density, as the density varies a lot at low pressures, then after 15 Psi, it becomes almost constant density, having a constant dissolution time. Also the 12.5% dosage had a

quicker dissolution than the 2.5% at all times, as observed in previous figures (Figure 176 and Figure 177) too.

5.5.2 Comparing the results above to the literature

The results above have shown that 80% of the mass of the un-compressed fibers dissolved in 10-20 minutes. If the fibers are compressed at 5 Psi, this 80 % dissolution times goes up to 60 minutes. If the fibers are further compressed with any pressure between 15 and 50 Psi, their density saturates at about 1.0 grams/cm^3 for the 2.5% and 1.1 grams/cm^3 for the 12.5% fenofibrate. Since the densities remained almost the same at this pressure range, the 80% dissolution times also remained the same, at approximately 90 minutes.

The previous work done by Indrani Bhattacharyya for 20% fenofibrate showed that the uncompressed fibers dissolved in about 7 minutes [40]. Comparing her previous data to the current data supports the conclusion that increasing the percentage of fenofibrate decreases the dissolution time. The current 2.5% fenofibrate mix dissolved in 22 minutes, the 12.5% dissolved in 12 minutes, and the previous 20% mix dissolved in only 7 minutes.

Chapter Six: Conclusions and Future Work

"If you don't see the book you want on the shelf, write it."
Beverly Cleary

Conclusions

On the mechanical side, we could conclude that this mechanism was successful in making nanofibrous pills, maintaining their small fibrous size, and high dissolution rate. This thesis has taken the project from the level of carrying out each of the three steps (spin, strip, and stomp) separately, to the level of transforming the material from a polymer solution to a tablet by pressing one button. The most important functional requirements and design parameters to build the machine were thoroughly studied. Some of these functional requirements were aligning the rod between the mechanisms, sliding it at the required speed, and spinning it with a safe grounded simple mechanism, among others. The anticipated risks versus the actual challenges were also discussed. Some of the anticipated ones were designing a bigger die cavity to avoid loosing any polymer, while the actual challenge was the exact opposite. The challenge was that the polymer was too sticky to strip off the rod, no material was ever lost, but it actually needed a bigger sliding motor to strip it off. This challenge among many others, like the pressure distribution and the dynamic grounding, were from the interesting findings in this project. These would be from the important factors to consider while taking this research further. It is hard to directly compare the output of this mechanism to the existing machinery like the rotary tablet press and the hot melt extrusion because it is very different and unique in its application for continuous manufacturing layouts.

On the chemical side, there were five main sections of findings: electrospinning parameter's studies, statistical quality control studies, fibers' microstructure studies, pressure and solidity studies, and dissolution profiles' studies. From the first study, it was found out that the parameters affecting the electrospinning's output were the applied voltage, distance between electrodes, and spinneret's rpm. The exact relationships between each parameter were plotted against productivity, and the collector's rpm was found to have no effect on output. From the second study, it was found that the process was under statistical control, but there were trends of increasing output when the solution was re-used, and trends of decreasing output if the machine was run under the exposure of sunlight. From the third study, it was found out the pressing the fibers maintained their nanosize of 0.2 to 0.3 micrometers. From the fourth study, it was found that the solidity increased when higher pressures were applied, following Choong's model [44], and It that the 12.5% fenofibrate was more compressible than the 2.5% fenofibrate in PVA at all conditions. From the fifth study, the dissolution profiles were graphed and it was found out that the low pressures of 2,5, and 7 Psi had the quickest dissolution, then after exceeding 15 Psi the dissolution profile was almost the same, also the 12.5% fenofibrate always had a faster dissolution than the 2.5% fenofibrate dosage.

Future Work

On the mechanical side, this machine has proven to be a successful mechanism for making nanofibrous pharmaceutical pills with few processing steps. However, it is still a prototype of the idea and some further modifications would be needed before industry could use it. The first modification would be making the die cavity, strippers, and the punch out of ceramic rather than aluminum, because the final batch of pills still had some metal remains in them. The second modification would be adding a mass measurement system to pull the rod collector once it has collected the required mass of the pill. Since electrospinning is a random process and fibers float around in the chamber attracting to all the surroundings, it is hard to have the 0.5% variability to meet the pharmaceutical standards [42]. Some suggestions for this mechanism might be adding a force sensor; whenever the mass is added to the rod, it would slightly deflect pushing this sensor with the specified mass/force. Another design suggestion is adding a laser sensor to pull the rod when a specific volume or thickness is accumulated it. Also the collected mass is usually in the range of 10 milligrams, so it needs high precision measurement devices to control it.

On the chemical side, a general study about the electrospinning parameters, pill's statistical control, nanofibrous microstructures, pressure/density relationships, and dissolution profiles was performed. But these results were hardly comparable to the literature because each electrospinning chamber runs at different conditions and gives different output. It could be comparable when more studies are performed on similar machineries in the future. The data in this study could be expanded by many ways: 1) Changing the materials (API percentage, and polymer mixtures), 2) Changing the setup (chamber shape and size), 3) Exploring different lengths, shapes, and materials for the collector surface, 4) Changing the range of parameters tested (expanding to more voltages or distances and compare their output, or narrowing down to a smaller pressure ranges and comparing their dissolution profiles), 5) Adding the mechanical control mechanisms suggested above and analyzing the differences in the output and productivity.

Works Cited

[1] Baronsky-Probst, J. , C. -V.Moltgen, W. Kessler, and R.W. Kessler. "Process design and control of a twin screw hot melt extrusion for continuous pharmaceutical tamper-resistant tablet production." *European Journal of Pharmaceutical Sciences* 87 (2016): 14-21. *ScienceDirect.* Web. 9 May 2016.

[2] Theron, S.A., A.L. Yarin, E. Zussman, and E. Kroll. "Multiple jets in electrospinning: experiment and modeling." *Polymer* 46 (2005): 2889-899. *ScienceDirect.* Web. 5 June 2016.

[3] Llorens, E., H. Ibanez, L.J. Del Valle, and J. Puiggali. "Biocompatibility and drug release behavior of scaffolds prepared by coaxial electrospinning of poly(butylene succinate) and polyethylene glycol." *Materials Science and Engineering* C 49 (2015): 472-84. *ScienceDirect.* Web. 15 June 2106.

[4] Balogh, Attila, Richard Cselko, Balazs Demuth, Geert Verreck, Jurge Mensch, Gyorgy Marosi, and Zsombor Kristof Nagy. "Alternating current electrospinning for preparation of fibrous drug delivery systems." *International Journal of Pharmaceutics* 495 (2015): 75-80. *S.* Web. 10 June 2016.

[5] Nagy, Zsombor Kristof, Attlia Balogh, Gabor Dravavolgyi, James Ferguson, and Hajnalka Pataki. "Solvent-Free Melt Electrospinning for Preparation of Fast Dissolving Drug Delivery System and Comparison with Solvent-Based Electrospun and Melt Extruded Systems." *The American Phamacists Association Journal of Pharmaceutical Science* 102 (2013): 508-17. *ScienceDirect.* Web. 1 June 2016.

[6] Hernandez-Navarro, Netzahualpille, Virgilio Gonzalez-Gonzalez, and Ivan E. Moreno-Cortez. "Electrospun polyvinylidene fluoride nanofibers by bubble electrospinning technique." *Materials Letters* 167 (2016): 34-37. *ScienceDirect.* Web. 8 June 2016.

[7] Jiang, Guojun, Sai Zhang, Yitao Wang, and Xiahong Qin. "An improved free surface electrospinning with micro-bubble solution system for massive production of nanofibers." *Materials Letters* 144 (2015): 22-25. *ScienceDirect.* Web. 5 June 2016.

[8] Forward, Keith M., and Gregory C. Rutledge. "Free surface electrospinning from a wire electrode." *Chemical Engineering Journal* 183 (2012): 492-503. *ScienceDirect.* Web. 3 June 2016.

[9] Sondej, Nicholas. "Direct Tablet Formation by Electrospinning and Compaction." Masters Thesis, Massachusetts Institute of Technology, 2015. Print.

[10] Sanchez-Serrano, Ibis. "A Brief Commercial History of the Biopharmaceutical Industry up to the Year 2000*." *The world's health care crisis: from the laboratory bench to the patient's bedside* (2011): 47-70. *Elsevier.* Web. 6 July 2016.

[11] Cora, Luciana A., Paulo R. Fonseca, Madileine F. Americo, Ricardo B. Oliviera, Oswaldo Baffa, and Jose Ricardo A. Miranda. "Influence of compression forces on tablets disintegration by AC Biosusceptometry." *European Journal of Pharamceutics and Biopharmaceutics* 69 (2008): 372-79. *ScienceDirect.* Web. 12 Sept. 2016.

[12] Samiei, Leila, Karen Kelly, Lisa Taylor, Ben Forbes, Elizabeth Collins, and Martin Rowland. "The influence of electrostatic properties on the punch sticking propensity of pharmaceutical blends." *Powder Technology* 305 (2017): 509-17. *ScienceDirect.* Web. 19 Sept. 2016.

[13] Sinka, I.C., F. Motazedian, A.C.F. Cocks, and K.G. Pitt. "The effect of processing parameters on pharmaceutical tablet properties ." *Powder Technology* 189 (2009): 276-84. *ScienceDirect.* Web. 4 Sept. 2016.

[14] Rybski, Christoffer, and Roland Jochem. "Benefits of a learning factory in the context of lean management for the pharmaceutical industry." *CIRP Conference on Learning Factories* 54 (2016): 31-34. *ScienceDirect.* Web. 20 Sept. 2016.

[15] Helm Instrument. "Shear Pin Load Cell in Tablet Press," www.helminstrument.com. 2016. Web. 20 Sept. 2016.

[16] Anbalagan, Pathiban, Srimanta Sarkar, Celine V. Liew, and Paul W.S. Heng. "Influence of the Punch Head Design on the Physical Quality of Tablets Produced in a Rotary Press." *Journal of Pharmaceutical Sciences* (2016): 1-10. *ScienceDirect.* Web. 20 Sept. 2016.

[17] Virtanen, Satu, Osmo Antikainen, and Jouko Yliruusi. "Determination of the crushing strength of intact tablets using Raman spectroscopy." *International Journal of Pharmaceutics* 360 (2008): 40-46. *ScienceDirect.* Web. 26 Sept. 2016.

[18] Riipi, Merja, Osmo Antikainen, Tapani Niskanen, and Jouko Yliruusi. "The effect of compression force on surface structure, crushing strength, friability and disintegration time of erythromycin acistrate tablets." *European Journal of Pharamceutics and Biopharmaceutics* 46 (1998): 339-45. *Elsevier.* Web. 12 Oct. 2016.

[19] Lahdenpaa, Esa, Mervi Niskanen, and Jouko Yliruusi. "Crushing strength, disintegration time and weight variation of tablets compressed from three Avicel® PH grades and their mixtures." *European Journal of Pharamceutics and Biopharmaceutics* 43 (1997): 315-22. *Elsevier.* Web. 5 Oct. 2016.

[20] Davies, Peter N., Harry E.C. Worthington, Fridrun Podczeck, and J. Michael Newton. "The determination of the mechanical strength of tablets of different shapes." *European Journal of Pharamceutics and Biopharmaceutics* 67 (2007): 268-76. *ScienceDirect.* Web. 5 Oct. 2016.

[20] "Hot Melt Extrusion." *Particle Sciences* 3 (2011). Web. 5 Oct. 2016.

[21] Tucker, Nick, Jonathan J. Stanger, Mark P. Staiger, Hussam Razzaq, and Kathleen Hofman. "The History of the Science and Technology of Electrospinning from 1600 to 1995." *Journal of Engineered Fibers and Fabrics* (2012): n. pag. *ScienceDirect.* Web. 12 Oct. 2016.

[22] Doshi, Jayesh, and Darrell H. Reneker. "Electrospinning Process and Applications of Electrospun Fibers." *Journal of Electrostatics* 35 (1995): 151-60. *Elsevier.* Web. 4 June 2016.

[23] Mohman, Moses M., Michael Shin, Gregory Rutledge, and Michael P. Brenner. "Electrospinning and electrically forced jets. I. Stability theory." *Physics of Fluids* 13.8 (2001): n. pag. *ScienceDirect.* Web. 10 Jan. 2017.

[24] Hohman, Moses M., Michael Shin, Gregory Rutledge, and Michael P. Brenner. "Electrospinning and electrically forced jets. II. Applications." *Physics of Fluids* 13.8 (2001): n. pag. *ScienceDirect*. Web. 16 Jan. 2017.

[25] Thompson, C.J., G.G. Chase, A.L. Yarin, and D.H. Reneker. "Effects of parameters on nanofiber diameter determined from electrospinning model." *Polymer* 48 (2007): 6913-922. *ScienceDirect*. Web. 18 Oct. 2016.

[26] Shenoy, Suresh L., W. Douglas Bates, Harry L. Frisch, and Gary E. Wnek. "Role of chain entanglements on fiber formation during electrospinning of polymer solutions: good solvent, non-specific polymer–polymer interaction limit." *Polymer* 46 (2005): 3372-384. *ScienceDirect*. Web. 4 Apr. 2016.

[27] Milner, Scott T. "Relating the shear-thinning curve to the molecular weight distribution in linear polymer melts." *Journal of Rheology* 40.2 (1996): n. pag. *ScienceDirect*. Web. 14 Apr. 2016.

[28] Pontrelli, Giuseppe, Daniele Gentili, Ivan Coluzza, Dario Pisignano, and Sauro Succi. "Effects of non-linear rheology on electrospinning process: A model study." *Mechanics Research Communications* 61 (2014): 41-46. *ScienceDirect*. Web. 4 Apr. 2016.

[29] Rutledge, Gregory C., and Sergey V. Fridrikh. "Formation of fibers by electrospinning." *Advanced Drug Delivery Reviews* 59 (2007): 1384-391. *ScienceDirect*. Web. 17 Apr. 2016.

[30] Palangetic, Ljiljana, Naveen Krishna Reddy, Siddarth Srinivasan, Robert E. Kohen, Gareth H. Mckinley, and Christian Clasen. "Dispersity and spinnability: Why highly polydisperse polymer solutions are desirable for electrospinning." (n.d.): n. pag. *ScienceDirect*. Web. 8 Apr. 2016.

[31] Chakraborty, Syandan, I-Chien Liao, Andrew Adler, and Kam W. Leong. "Electrohydrodynamics: A facile technique to fabricate drug delivery systems." *Advanced Drug Delivery Reviews* 61 (2009): 1043-054. *ScienceDirect*. Web. 2 Apr. 2016.

[32] Koski, A., K. Yim, and S. Shivkumar. "Effect of molecular weight on fibrous PVA produced by electrospinning." *Materials Letters* 58 (2004): 493-97. *ScienceDirect*. Web. 4 Mar. 2016.

[33] Bhattacharjee, P. K., and G. C. Rutledge. "Electrospinning and Polymer Nanofibers: Process Fundamentals." *Comprehensive Biomaterials* 1 (2011): 497-512. *Elsevier*. Web. 5 May 2016.

[34] Bhardwaj, Nandana, and Subhas C. Kundu. "Electrospinning: A fascinating fiber fabrication technique." *Biotechnology Advances* 28 (2010): 325-47. *ScienceDirect*. Web. 8 Apr. 2016.

[35] Basu, Sandip, Ashwini K. Agrawal, and Manjeet Jassal. "Concept of Minimum Electrospinning Voltage in Electrospinning of Polyacrylonitrile N,N-Dimethylformamide System." *Journal of Applied Polymer Science* 122 (2011): 856-66. *Wiley Online Library*. Web. 6 May 2016.

[36] Yarin, A.L., and E. Zussman. "Upward needleless electrospinning of multiple nanofibers." *Polymer* 45 (2004): 2977-980. *ScienceDirect*. Web. 19 May 2016.

[37] Dosunmu, O O, G C Chase, W. Kataphinan, and D H Reneker. "Electrospinning of polymer nanofibres from multiple jets on a porous tubular surface." *Nanotechnology* 17 (2006): 1123-127. *ScienceDirect.* Web. 18 June 2016.

[38] Brettmann, Blair K., Shirley Tsang, Keith M. Forward, Gregory C. Rutledge, Allan S. Myerson, and Bernhardt L. Trout. "Free Surface Electrospinning of Fibers Containing Microparticles." *American Chemical Society* 28 (2012): 9714-721. *Langmuir.* Web. 5 Feb. 2016.

[39] Forward, Keith M., Alexander Flores, and Gregory C. Rutledge. "Production of core/shell fibers by electrospinning from a free surface." *Chemical Engineering Science* 104 (2013): 250-59. *ScienceDirect.* Web. 9 Apr. 2016.

[40] Bhattacharyya, Indrani, Mark C. Molaro, Richard D. Braatz, and Gregory C. Rutledge. "Free surface electrospinning of aqueous polymer solutions from a wire electrode." *Chemical Engineering Journal* 289 (2016): 203-11. *ScienceDirect.* Web. 5 Apr. 2016.

[41] Jackson, S., I.C. Sinka, and A.C.F. Cocks. "The effect of suction during die fill on a rotary tablet press." *European Journal of Pharamceutics and Biopharmaceutics* 65 (2007): 253-56. *ScienceDirect.* Web. 5 Sept. 2016.

[42] " Guidance to the Industry of Power Blends and Finished Dosage Units." *U.S. Department of Health and Human Services. Food and Drug Administration. Center for Drug Evaluation and Research (CDER).* Oct. 2003. Web. 25 Sept. 2016.

[43] Theron, S.A., E. Zussman, and A.L. Yarin. "Experimental investigation of the governing parameters in the electrospinning of polymer solutions." *Polymer* 45 (2004): 2017-030. *ScienceDirect.* Web. 8 Oct. 2016.

[44] Choong, Looh Tchuin, Matthew M. Mannarino, Sandip Basu, and Gregory C. Rutledge. "Compressibility of electrospun fiber mats." *Journal of Materials Science* 48 (2013): 7827-836. Print.